Science of Climate Change

Volume 3.3
2023

https://scienceofclimatechange.org

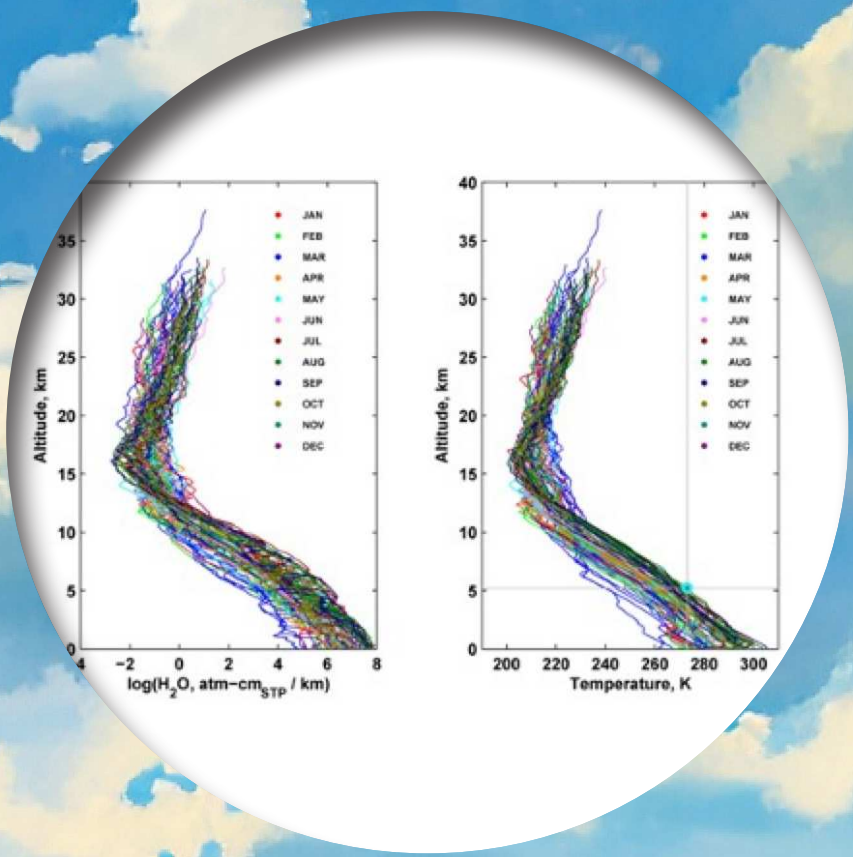

Published by: Klimarealistene (Org. no. 995 314 592)

ISSN 2703-9080 (print) ISNN 2703-9072 (online)

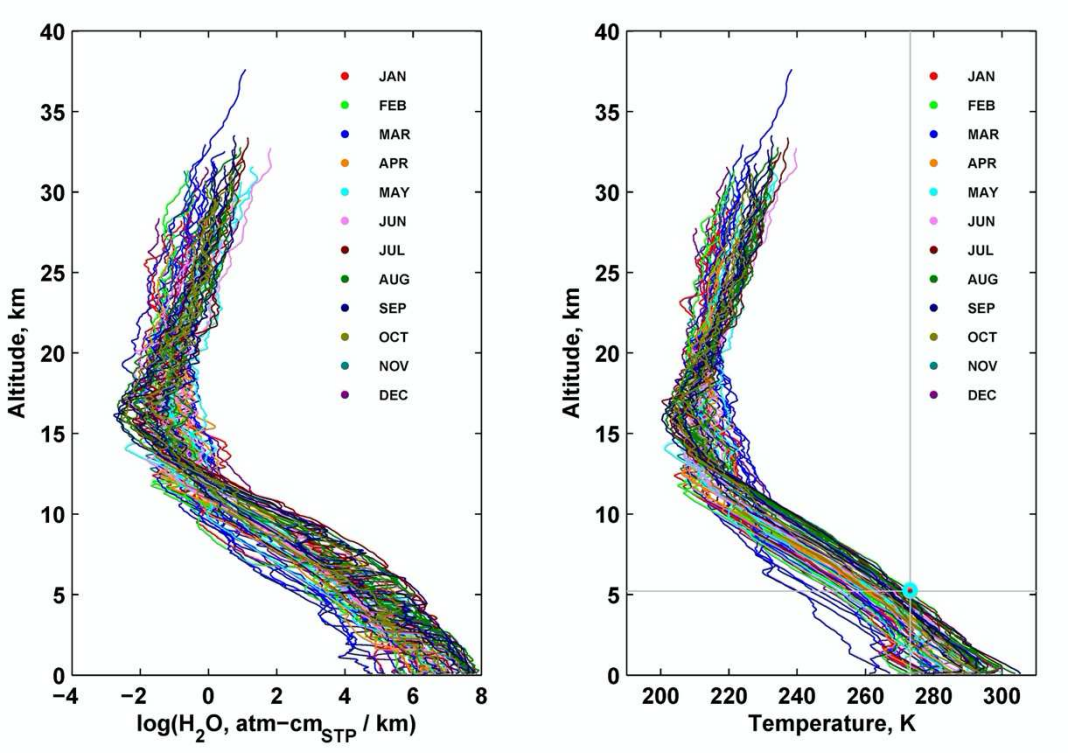

High resolution radiosonde observations from NOAA Sterling, Virginia. The left panel shows H_2O column density, and the right panel shows temperature. The temperatures and H_2O column density are highly correlated, and they follow the relevant theoretical relationships. The light blue dot around 5 km in the right panel is the observed maximum altitude of the H_2O condensation temperature at Sterling. Many climatologists mistakenly call this relationship as positive feedback. It must be clear that locally the temperature and water vapor content of the air parcels are alternative variables, and they are not connected by some ad-hoc positive or negative feedback parameter.

From an article by Ferenc Miskolczi: *Greenhouse Gas Theories and Observed Radiative Properties of the Earth's Atmosphere*.

Figure 25, page 264

SCIENCE OF CLIMATE CHANGE

Volume 3.3

September 2023

ISSN 2703-9072

Klimarealistene, P.O. Box 33, 3901 Porsgrunn, Norway

Table of Content

Editorial

In this issue we present three articles which all show that there is no dangerous warming created by antropogenic release of CO_2. The so called greenhouse effect is impossible or very small.

The first article is written by Ferenc Miskolczi presenting fundamental theoretical equations for understanding the observed global average radiative equilibrium. It is shown that this can be done from astrophysical considerations and some plausible assumptions of the composition of the Earth's atmosphere and surface. He shows that the greenhouse effect producing global warming is impossible and without any theoretical or empirical support.

Antero Olilla shows that natural climate drivers dominate in the current warming. He points to the cloud effect by cosmic radiation amplifying the solar irradiation, and the natural climate oscillations are the main drivers in a combined natural and antropogenic model for global warming (NAGW).

Finally, Raimund Müller estimates the e-time for CO_2 and finds that it is less than 4 years and has been fairly constant during the last 270 years. He finds that the human contribution to atmospheric CO2 is less than 7%. If he includes wood burning, it increases to 12%.

We are pleased to notice that we are able to publish scientific articles which have difficulties in other journals, because they don't support the current global warming doctrine.

Good reading

Jan-Erik Solheim
Editor

A digital version of this volume can be found here: https://doi.org/10.53234/SCC202304/xx

OPEN ACCESS

Klimarealistene
P.O. Box 33,
3901 Porsgrunn
Norway
ISSN: 2703-9072

Greenhouse Gas Theories and Observed Radiative Properties of the Earth's Atmosphere

Ferenc Miskolczi

Foreign Associate Member of the Hungarian Academy of Sciences, Budapest, Hungary

Correspondence: mis-kolczif@gmail.com

Vol. 3.3 (2023)

pp. 232-289

Abstract

In the last decade fundamental theoretical equations were developed for describing and understanding the global average radiative equilibrium state of the Earth-atmosphere system. It is shown that using the well-established laws of radiation physics the key climate parameters of the planet can be deduced theoretically, from purely astrophysical considerations and some plausible assumptions on the material composition of the planetary surface and the structure of the atmosphere. It is also shown, that the Earth-atmosphere system is in radiative equilibrium with a theoretical solar constant, and all global mean flux density components satisfy the theoretical expectations. The greenhouse effect predicted by the Arrhenius greenhouse theory is inconsistent with the existence of this radiative equilibrium. Hence, the CO_2 greenhouse effect as used in the current global warming hypothesis is impossible. The greenhouse effect itself and the CO_2 greenhouse effect based global warming hypothesis is a politically motivated dangerous artifact without any theoretical or empirical footing. Planet Earth obeys the most fundamental laws of radiation physics.

Keywords: Greenhouse effect theory; radiative equilibrium; climate change

Submitted 2023-03-09; Accepted 2023-07-08; https://doi.org/10.53234scc202304/99

1. Introduction

All planets in our solar system are isolated celestial objects orbiting around the Sun. Isolated objects can only exchange energy with other objects and the surrounding space environment by mains of radiation (Peixoto & Oort (1992) [64], page 104: *"all exchange of energy between the Earth and outer space is through radiative transfer"*). The exchange of *shortwave* (SW) and *infrared* (IR) − or *long-wave* (LW) − radiant energy happens through the *active planetary surface* (APS). By definition, APS is the sum of the identifiable clear and cloudy (solid or liquid) surface areas which contributes to the exchange of radiant energy with the atmosphere above and, − in case of semi-transparent atmospheres − directly with the Sun and the space environment. The atmosphere above the APS has its own SW and LW upward contribution to the total radiation leaving the planet.

The APS may receive inward radiation from the full 4π solid angle, and emits and reflects (or scatters) radiation into the full 4π solid angle. Planets with semi-transparent condensing *greenhouse gas* (GHG) atmospheres usually have complex multi-layer adaptive APS which must be able to configure itself to the planetary *radiative equilibrium* (RE) state. Some GHGs (CO_2, CH_4) are practically uniformly mixed in the atmosphere, others (H_2O, O_3) have vertical structures and diverse geographical patterns.

Further on, we shall use the concept of a *passive* planet. A passive planet has negligible internal source of thermal energy (from non-radiative processes) propagating through the APS and the atmosphere above and will contribute to the *top of the atmosphere* (TOA) net radiation.

Compared to the magnitude of the flux densities involved in the planetary radiative processes, the combined effect of the thermal energy released by geothermal flux, tidal friction, plate tectonics, surface erosion, volcanism, forest fires, human energy production, or other natural and non-natural sources is far too small to give a reasonable estimate of their role in the long-term climate change, Kandel & Viollier (2005) [1].

In this study any power dissipation in the system that is *unrelated* to the incoming solar radiation will be disregarded partly because it cannot be accurately quantified, and partly because later, when the observational evidence of their global scale net contributions will be available, it may be considered (as part of the net heat conduction, or the net dissipation due to latent heat transfer among the geological reservoirs).

Due to the stochastic dynamical nature of the climate it is impossible to quantitatively decompose the thermal structure (and in fact the GHG structure) of the atmosphere showing the individual contributions of the processes mentioned above. For example, the 0.06 – 0.086 Wm^{-2} heat flow from the planetary interior in [1] can never be associated with the global mean thermal structure or the surface temperature.

However, one must acknowledge, that the real (empirically observed) atmospheric thermal structure implicitly involves all the power dissipation in the system independently of the origin. In other words, working with real radiosonde data one must be sure, that the nature knows very well how to establish the global average thermal structure as the function of the power dissipation from any source. For better understanding let us quote the following statement from the Science magazine, Lacis et al. (2010) [13]:

"Because the solar-thermal energy balance of Earth [at the top of the atmosphere (TOA)] is maintained by radiative processes only, and because all the global net advective energy transports must equal zero, it follows that the global average surface temperature must be determined in full by the radiative fluxes arising from the patterns of temperature and absorption of radiation. This then is the basic underlying physics that explains the close coupling that exists between TOA radiative fluxes, the greenhouse effect, and the global mean surface temperature."

From practical point of view working with the concept of a passive planet at the end of the complete flux density simulations the planetary radiative balance will clearly show if there is a need for a correction term (attributed to unaccounted power dissipations in the system) to establish the Sun-Earth radiative equilibrium. Planets or Moons without atmosphere have limited capabilities to regulate their radiative budget and their equilibrium state is not discussed here. In the steady-state RE (at the TOA of an isolated passive planet) the long term global mean radiation field must satisfy the next two requirements:

- The energy conservation principle dictates that the sum of the reflected and absorbed parts of the effective available (or intercepted) solar flux at the TOA must be equal.
- According to the flux form of the Kirchhoff law at the TOA the total outgoing LW radiation and the absorbed SW solar radiation must be equal.

Expressed in analytic equations we may write:

$$F_0 / 4 = F_E = F_A + F_R = F_E(1-\alpha_B) + \alpha_B F_E\,, \tag{1}$$

$$OLR^A = F_A = F_E(1-\alpha_B)\,, \tag{2}$$

where F_0 is the local solar constant, $F_E = F_0 / 4$ is the *effective available solar flux* over a unit area on the Earth (at the TOA), F_A and F_R are the absorbed and reflected SW flux density components of F_E, $\alpha_B = F_R / F_E$ is the Bond albedo (by definition), and OLR^A is the total outgoing LW radiation. The ¼ scaling factor of F_0 in (1) converts the intercepted solar flux to flux density available over a unit surface area of a planet (or any spherical celestial object). Such a planet will obey the energy and momentum conservation principles of the radiation field in its simplest form where all planetary LW flux density components are scaled with the solar luminosity. These are the top-level constraints imposed on the radiation field of the Sun-planet system, and assures, that an isolated passive planet cannot change the local solar constant. Obviously, such a planet is an abstraction, but observations show that it is not an unrealistic one.

It is quite reasonable to assume that after the formation and during the billions of years of planetary evolution planets have always sufficient time to maintain the average quasi-static state of the *Chandrasekhar-type radiative equilibrium* (CRE), Chandrasekhar (1960) [2], page 200. Equations (1,2) are not a kind of wish-list, they are the direct consequences of the energy and momentum conservation, energy minimum (or entropy maximum) principles of nature.

Climate change (the observed, as opposed to declared) are to be investigated either as a consequence of mere fluctuations between regions (which upsets at localities what was earlier regarded as normal) or due to external perturbations of the total energy input to the Earth-atmosphere system. Here climate change will be regarded as deviations of the basic (radiative and thermodynamic) global mean climate parameters from their long-term average value, due to possible internal (natural or random) fluctuations, or external perturbations of the total energy input to the Earth-atmosphere system (through the upper and lower boundaries). Internal fluctuations are due to the chaotic nature of the dissipative dynamic climate system, and they do not alter the long-term radiative balance. Regarding the large variety of time scales of the possible internal fluctuations and external perturbations that may occur one has to be careful with selecting the length of a characteristic averaging time interval, over which the radiative equilibrium is established, Scafetta (2010) [3], Scafetta et al. (2018) [51].

In Figure 1 the exponential increase of the atmospheric CO_2 concentration in the last 75 years is an empirical fact, Andrews (2023) [6]. However, it is an open question how these changes in the GHG content of the atmosphere may alter the radiative equilibrium state of the planet, i.e. the validity of (1,2). The light blue regression function was established between the time differences from the reference year of 1948 and the Mauna Loa 63 annual mean data between 1959 and 2021. Although the relationship between the thermal history of the Earth and the composition of the atmosphere on evolutionary time scale is an interesting subject, the man-made CO_2 greenhouse problem is only relevant to the last century.

Planets with large amount of latent heat storage (in geological reservoirs) may moderate the internal and external fluctuations by phase pinning (Maxwell rule). In the Earth's atmosphere the *water vapor* (WV) is the only condensing GHG, therefore the triple point temperature (we call it phase temperature) of the H_2O at $t_P = 273.16\,\mathrm{K}$ (0 °C) has a unique role in the climate system. Notice, that in the Kelvin scale the reference temperature $t_{ZERO} = -273.16\,^{\circ}\mathrm{C}$, that is, t_P in K practically equal to $-t_{ZERO}$ in °C.

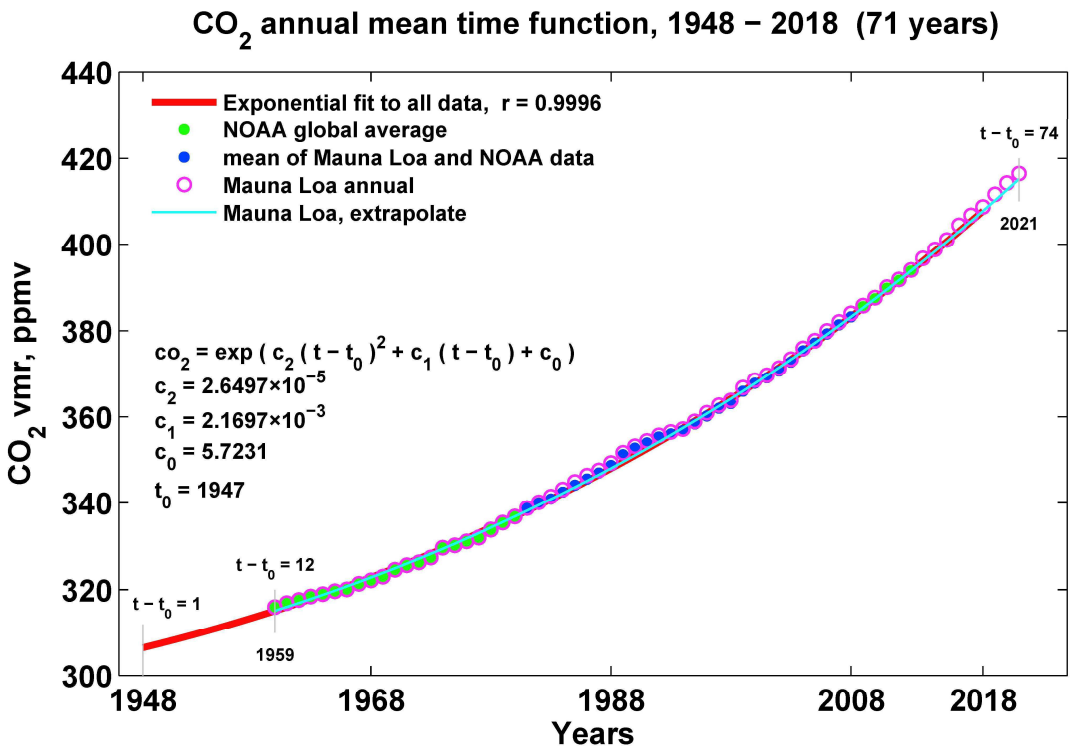

Figure 1: Time dependence of the CO_2 volume mixing ratio in the last 75 years. Our empirical exponential fit was based on the publicly available numerical annual mean data in the NOAA NCEP/NCAR Reanalysis data time series. The origin of the observed ~35 % increase is not yet identified. The Mauna Loa weekly data shows significant seasonal fluctuation, probably related to the seasonal changes of the SW radiation input.

The purpose of this paper is to answer two greenhouse effect related fundamental questions:

- Do greenhouse gas theories contradict energy balance equations?
- Is the proposed greenhouse effect due to anthropogenic carbon dioxide emissions supported by observed atmospheric thermal and humidity structures and global scale simulations of the infrared absorption properties of the Earth's atmosphere?

In 2017 these two questions were explicitly raised by the *Supreme Court of British Columbia* in the libel cases of Michael Mann vs. Timothy Ball and Andrew Waver vs. Timothy Ball. This paper was built on the testimony presented to the Court in the above cases, Miskolczi (2016) [4]. Further on we shall also address some problems of recent global radiative budget schemes and present a realistic planetary radiative budget by establishing new theoretical approach to the greenhouse effect.

We also wish to demonstrate that the theoretical expectations are fully consistent with the observations. The special orbit of the Earth, the unique GHG composition of the atmosphere, the huge amount of water (in all three phases), the partial cloud cover, and the existence of the biosphere make our planet a very distinguished member of the solar system. Although the general constraint of the energy conservation principle (1) and Kirchhoff law (2) is valid for any isolated passive celestial object, other planets or moons have entirely different physical environments therefore, we shall not discuss (in details) the *relevance* of our new greenhouse effect related theoretical considerations here.

In what follows, we shall introduce some definitions and present observed empirical facts on the radiative structure of the Earth-atmosphere system (section **2**); discuss the methodology of the greenhouse effect validations (section **3**); present relevant recently developed radiative transfer background information (section **4**); summarize the new results (section **5**); and state the conclusions (section **6**).

In the Appendix the Planck radiation laws and the new (theoretical) *law of radiation-temperature duality* – a relationship between the flux density and temperature – are discussed in some detail.

2. Greenhouse gas theories and radiative balance equations

Although the use of the radiative *greenhouse effect* (GE) terminology associated with the Earth's climate goes back about two centuries, the physically meaningful definition, and the structured theoretical foundation of the planetary GHG GE is still missing.

The root of the problem is in the difficulties of characterizing the planetary climate with a single, properly chosen (scalar) physical quantity. It is no wonder, that humans living on the Earth's surface are very much interested in the average surface temperature of their immediate environment. The variability of ground surface temperature on different time scales and geographical locations affect people's every day's life.

In case of the *local thermodynamic equilibrium* (LTE), the isotropic source function at the lower boundary of the atmosphere and the isotropic upward flux density from a perfectly black surface (in direct contact with the atmosphere above) are equal, Mihalas & Mihalas (1984) [48], page 328. Accordingly, there is no discontinuity or jump in the temperature at surface, and the boundary layer can be characterized with a single radiative temperature t_S from the source function, Manabe & Wetherald (1967) [5], Van Wijngaarden & Happer (2020) [57].

The extrapolation of the average local or regional surface temperature to global scale and longer periods of time leads to the concepts of global climate change, and ultimately to the CO_2 related *anthropogenic global warming* (AGW). We believe the temporal and areal averages of any single physical quantity should be meaningful. However, in the greenhouse effect literature one may find articles stating (without proof) that the assumption of uniform temperature for the whole global surface is inadequate, le Pair & de Lange (2022) [7], Kramm & Dlugi (2011) [8].

2.1 Definitions of basic greenhouse parameters

In climate science the GHG GE is arbitrarily defined as the Δt_A temperature difference between the ground surface *radiative temperature* t_S and the planetary SW *absorption temperature* t_A:

$$\Delta t_A = t_S - t_A, \tag{3}$$

where $t_A = (F_A / \sigma)^{1/4}$, $t_S = (S_U / \sigma)^{1/4}$, S_U is the isotropic ground surface upward flux density, and $\sigma = 5.6699833 \times 10^{-8}$ $\mathrm{Wm^{-2}K^{-4}}$ is our adopted *Stefan-Boltzmann* (SB) constant. Unless specified otherwise, all physical constants were taken from the *National Institute of Standards and Technology* (NIST), Mohr et al. (2007) [9]. Using the SB law, any flux density may be converted to *equivalent blackbody temperature* (EBT), which facilitates the convenient comparison of temperatures (instead of fluxes) without referencing to any real radiating surface. Associated with the local solar constant, it is customary to define the $t_0 = (F_0 / \sigma)^{1/4} = 394.117$ K effective temperature which is the EBT for our adopted $F_0 = 1367.95$ $\mathrm{Wm^{-2}}$ solar constant, (see paragraph *4.2*). In addition to (3), GE may also be expressed by the greenhouse factor G_A, which is the difference of the respective flux densities from the SB law:

$$G_A = \sigma t_S^4 - \sigma t_A^4 = S_U - F_A . \quad (4)$$

Raval & Ramanathan (1989) [10] introduced the normalized greenhouse factor which is the ratio of G_A to S_U:

$$g_A = (S_U - F_A)/S_U . \quad (5)$$

For real − not perfectly black − ground surfaces one may also define a t_G *hypothetical* EBT via the $\varepsilon_B S_G = \varepsilon_B \sigma t_G^4 = \sigma t_S^4 = S_U$ equation, where ε_B is the LW flux emissivity. Perfectly black surfaces will have ε_B equal to 1.0 , $t_G = t_S$, and $S_U = S_G$. Here S_G is the surface upward blackbody radiation associated with the change of thermal energy due to processes of non-radiative origin (evaporation, condensation, sublimation, heat conduction, etc.).

Apparently, F_A from (2) depends only on the long term means of F_0, and α_B. Therefore, t_A may be written as:

$$t_A = ((1-\alpha_B)F_E/\sigma)^{1/4} = ((1-\alpha_B)F_0/(4\sigma))^{1/4} . \quad (6)$$

Since in (6) t_A does not depend on the LW absorption and emission properties of the system, the arbitrarily defined Δt_A, G_A, and g_A cannot be related to the GHG content of the atmosphere. They are only dependent on the choice of the global mean t_S, consequently, the planetary greenhouse effect is not a GHG dependent observed global radiative phenomenon.

In astrophysics textbooks the t_{APS} *effective (equivalent) planetary surface temperature* of the APS used to be defined by the SB law and the F_E effective available SW solar flux. t_{APS} may be expressed with different astronomical quantities, Ahren (2004) [11]:

$$t_{APS} = (L_0/(\pi\sigma))^{1/4}/(2d_E^{1/2}) = (E_0 A_{SUN}/(\pi\sigma))^{1/4}/(2d_E^{1/2}) = (F_E/\sigma)^{1/4} , \quad (7)$$

where L_0 is the solar *luminosity*, E_0 is the solar *surface emission*, d_E is the *semi-major axis of the Earth's orbit*, $A_{SUN} = 4\pi r_0^2$ is the *solar surface area*, and r_0 is the solar radius. The right side of (7) is the definition of t_{APS} by the F_E *effective available solar flux*, as it was given in (1). Using F_R one may also define the t_R *equivalent reflection temperature* by the SB law: $t_R = (F_R/\sigma)^{1/4}$. Similarly to the definitions of the climatological Δt_A, G_A, and g_A, the APS and reflection greenhouse parameters are:

$$\Delta t_{APS} = t_S - t_{APS}, \quad G_{APS} = \sigma t_S^4 - \sigma t_{APS}^4, \quad g_{APS} = G_{APS}/S_U , \quad (8)$$

and

$$\Delta t_R = t_S - t_R, \quad G_R = \sigma t_S^4 - \sigma t_R^4, \quad g_R = G_R/S_U . \quad (9)$$

The important fact is that t_A and G_A in (3,4) are constrained by the conservation principles of radiation energy and momentum, and by the SB law:

$$G_A = G_{APS} + F_R , t_A = (t_{APS}^4 - t_R^4)^{1/4} . \quad (10)$$

These constraints tell us that t_A is not a free parameter, but the sole function of F_0, and α_B. Based on (2) F_A and OLR^A must be equal, which implies the $F_A = OLR^A(S_U^A, \tau)$ functional relationship. Here τ is the *flux optical thickness* representing the all-sky LW absorption properties of a global average atmospheric air column, computed from the all-sky global average atmospheric structure. This quantity can only be accessed by extremely complex *radiative transfer* (RT) computations.

Since in definition (3) $t_S = (S_U / \sigma)^{1/4}$ is the ground surface radiative temperature, the assumed equilibrium relationship is:

$$F_A(F_0, \alpha_B) = OLR^A(S_U, \tau), \tag{11}$$

which obviously violates the (1,2) RE conditions. That is, keeping the left-hand side of (11) constant (no change in F_0 and α_B) the reduced OLR^A (due to increased GHG) cannot be restored to the original value simply by adjusting S_U, without adding thermal energy to the system (from somewhere). Remember, that the APS of a planet with condensing GHGs (clouds) is the sum of the clear and cloudy areas, which is a physically (and practically) identifiable mixture of solid and liquid surfaces. Applying definitions (3-5) for the whole planet, S_U must be the S_U^A (scaled to the TOA), and OLR^A must be the all-sky TOA LW radiation.

It is well known from mathematics that (11) type of equations hold only if the left and right sides are independent identical constants. The fate of the terrestrial greenhouse effect entirely depends on the existence of the long term radiative equilibrium state of the Earth. If the radiative equilibrium (independently of the GHG content) holds, then the GHG greenhouse effect does not exist, and definitions (3-5) are artifacts. Since the ground surface temperature is governed by CRE state of the planet, from the point of view of the CO_2 based AGW, the (3-5) GE parameters may be calculated, but they are useless, and physically meaningless quantities.

To determine Δt_A one needs to know t_S, F_0, α_B, and OLR^A. All these quantities can routinely be measured by ground based and satellite observing systems. The most quoted textbook data of t_S, F_0, α_B, and OLR^A are: 288 K, 1368 Wm^{-2}, 0.3, and 239 Wm^{-2}, subsequently, Schmidt et al. (2010) [12], Lacis et al. (2010) [13]. These numerical data show that the greenhouse temperature, and the flux density differences are about 33 K, and 151 Wm^{-2}. In this example the planetary RE condition is explicitly assumed, and no surprise that the imbalance at the TOA is close to zero.

There are several problems with the estimates above. It should be known that the assumed 288 K surface temperature is not an empirically measured quantity, but it is based on an international agreement dated back to 1924, (*International Commission for Air Navigation*, NOAA (1976) [14], therefore the real meaning of the 33 K is questionable. In fact, there is no standard, widely accepted definition of an empirically verified global mean surface temperature. Another serious mistake is the simultaneous use of t_A and OLR^A with t_S and ground surface upward flux S_U. Because of the permanent presence of the global average cloud cover, the radiation field of S_U and OLR^A are decoupled. Physically meaningful GHG GE may only be defined for clear-sky conditions, that is, GHG GE only exists over clear and above-cloud air columns, or perhaps above the whole APS, [10]. For the fluxes from the whole APS, (and similarly for t_{APS}), one cannot assign a definite physical altitude, but using the known source function profile, an effective altitude maybe attributed by the SB law.

The spectral aspects of the greenhouse effect are presented in Figure 2. In this simplified view the *Planck equivalent blackbody spectral flux densities* (EBFs) are plotted for the assumed 288 K surface temperature (green curve) and the 255 K SW absorption temperatures (red curve). Notice that in the wavenumber domain the areas under each curve are proportional with the spectrally integrated flux densities. The $\Delta t_A = 288 - 255 = 33$ K and $G_A = S_U - F_A = 151$ Wm^{-2} quantities are just arbitrary definitions used by the climatologists to indicate that the surface emits more IR radiation than the absorbed SW solar radiation. The light blue curve of the $G_{A,\nu}$ spectral greenhouse factor is the EBF at $t = (G_A / \sigma)^{1/4} = ((S_U - F_A) / \sigma)^{1/4} = 227$ K temperature.

According to the conservation of radiative energy the area under $G_{A,\nu}$ must be equal to the dark blue shaded area, that is, $\sigma t_s^4 - \sigma t_A^4 = G_A = \sigma t^4 = 151\,\mathrm{Wm^{-2}}$. Since $G_{A,\nu}$ does not depend on any GHG absorption, therefore the statement that the $\Delta t_A = 33\,\mathrm{K}$ is caused by the GHG absorption is not justified. The signatures of the spectral absorption of any GHG are not present in this figure. Although the maximum of the spectral greenhouse factor is close to the center of a strong CO_2 IR absorption band (black dot on the light blue curve), this figure does not have any useful information on the relationship between the surface temperature and the amount of the GHGs.

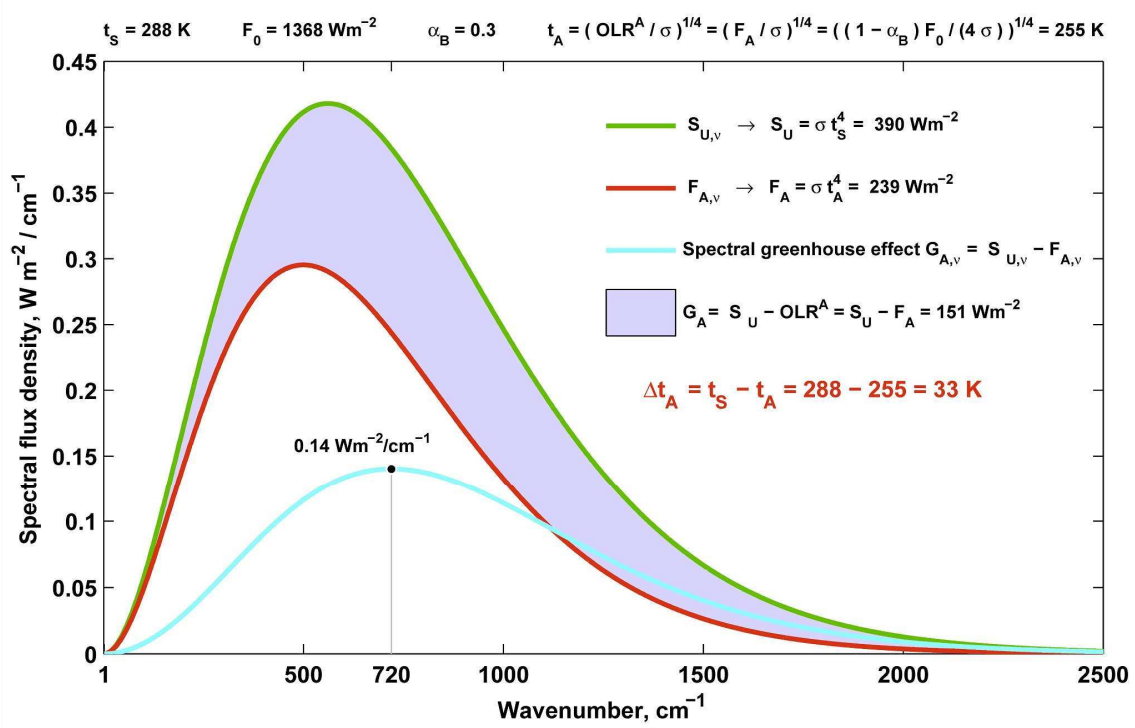

Figure 2: Spectral greenhouse effect. The curves are the Planck spectral flux density distributions belonging to the equivalent blackbody temperatures. In this view the ground surface is assumed to be perfectly black, $t_G = t_S$.

2.2 Violation of the energy conservation principle

Beside the empirical knowledge of the material composition of an average atmospheric structure, RT computation of the GE requires a theoretically founded functional relationship between the clear-sky S_U, OLR, and the amount of atmospheric GHGs. All of the different GHG column amounts must be explicitly and simultaneously involved in the computations of flux transmittance, absorption, and optical thickness of a semi-transparent global average air column.

Here we define some frequently used RT quantities and relationships. Trivially, $S_U = S_T + A_A$ where S_T and A_A are the transmitted and absorbed part of S_U. The flux transmittance T, flux absorption A, and flux optical thickness τ are defined as: $T = S_T / S_U$, $A = (S_U - S_T)/S_U$, and $\tau = -\ln(S_T / S_U)$. Further on, parameters referenced to the air column above an optional cloud-top are marked by an upper index 'c'.

In the classic radiative transfer and greenhouse effect literature a general $OLR(S_U,\tau)$ function for semi-transparent planetary atmospheres does not exist. The first published relationship of this kind appeared about 20 years ago in Miskolczi & Mlynczak (2004) [15]. Later it was shown with sufficient mathematical rigor that the clear-sky OLR and the surface upward LW radiation S_U in clear-sky radiative equilibrium are related by the next analytical equations:

$$OLR = S_U f(\tau) = S_U \frac{2}{1+\tau+\exp(-\tau)}, \tag{12}$$

where $f(\tau)$ is the newly introduced *transfer function* (and, by definition, $g(\tau)=1-f(\tau)$ is the *greenhouse function*), Miskolczi, (2007) [16]. The theoretical derivation of (12) was the missing link, which − through the transfer function and flux optical thickness − connects the surface temperature to the GHG content of the atmosphere. Here we should note, that in practice (12) is not a general requirement for an atmospheric air column. The instantaneous local or global mean atmospheric structures may or may not be in exact radiative balance. However, a realistic time-averaged structure should have a τ close to the planetary equilibrium value, which is the solution of the $OLR/S_U = f(\tau_E) = f_E$ equation. As an example, for the *global average TIGR2* (GAT) atmosphere (Scott (2009) [31]) : $\tau = 1.8691$, $\tau_E = 1.8602$, (they are close). For the *US Standard Atmosphere 1976* (USST76) atmosphere (NOAA, 1976 [14]): $\tau = 1.5092$ and $\tau_E = 1.8672$, and, evidently, the USST76 structure *is badly out of radiative balance*, and should not be used in radiative budget studies. Similarly to (12), the radiative equilibrium requirement above the cloud top is:

$$OLR^C = S_U^C f^C(\tau^C) = S_U^C \frac{2}{1+\tau^C+\exp(-\tau^C)}, \tag{13}$$

where S_U^C is the upward flux from the cloud top, τ^C is the flux optical thickness of the air column above the cloud top. While (12) is closely satisfied for the clear-sky portion of the atmosphere, (13) does not hold, indicating that the radiative structure above the cloud top is affected by other dynamical processes. In particular, instead of (13) the $OLR - OLR^C = A_A - E_D$ equation holds, where A_A is the absorbed isotropic surface upward flux and E_D is the anisotropic downward flux from the clear atmosphere. For more details on the theoretical RT functions see paragraph *3.3*. We shall see later, that the radiative equilibrium condition above the cloud top may be expressed by the $OLR^C = E_D^C$ relationship, where E_D^C is the atmospheric downward flux density arriving at the cloud top. As we have already mentioned, in the stochastic dissipative climate system locally and regionally the RE is not a constraint, τ and S_U in (12) can take any value. However, for an isolated planet, and on global scale the radiative equilibrium is a strict constraint. For planets with partial cloud cover − instead of (11) − the correct relationship between OLR^A and F_A must have the functional form of

$$OLR^A(\tau, S_U, \beta, S_U^C) = F_A(F_0, \alpha_B), \tag{14}$$

where β is the cloud cover, $S_U^C = S_U^C(h^C)$ is the upward flux density from the cloud top, and h^C is the equilibrium cloud top altitude. Evidently α_B will also depend on the cloud cover and cloud altitude: $\alpha_B = \alpha_B(\beta, h^C)$. Shortly, the practical derivation of the equilibrium cloud cover is based on the empirical fact that the clear air column above a characteristic h^C is in a special dynamical equilibrium which assures the $OLR^C = E_D^C$ equality (black circle, shown in Figure 6). The cloud top at this altitude is in thermal and radiative equilibrium with the local source function. More detail is given in paragraph *4.4*, or in Miskolczi (2014) [17].

The principle of the conservation of the radiant energy dictates that the true all-sky TOA OLR^A must be a strictly linear function of the cloud cover, it has to be the weighted sum of the clear-sky OLR and cloudy sky OLR^C by the fractional clear and cloudy areas of the APS:

$$OLR^A = sc((1-\beta)OLR + \beta OLR^C), \tag{15}$$

where sc is a spherical correction factor, necessary for the conversion of the fluxes from any reference altitude to TOA fluxes. Similar equation holds for the upward flux from the APS:

$$S_U^A = sc((1-\beta)S_U + \beta S_U^C). \tag{16}$$

From (16) immediately follows the analytical relationship between the t_S ground surface radiative temperature, and the F_0, sc, β, and S_U^C parameters:

$$t_S = ((F_0/(4sc) - \beta S_U^C)/(1-\beta)/\sigma)^{1/4}. \tag{17}$$

Obviously t_S in (17) does not depend directly on any amount of non-condensing GHGs. In a two-level radiating system (cloud-free surface and cloud top) the Δt_A, G_A, and g_A can never be directly associated with the GHG content of the atmosphere. So far GE theories are not capable to predict a-priori the observed equilibrium t_S. The reason is that the definition (3) completely ignores the radiative effect of the cloud cover, and consequently, the radiative constraint on dependence of S_U^C on the GHGs cannot be asked. Ignoring the radiative balance requirements represented by (12-17), discussion on the GE and the related global climate change does not have much merit. Without any theoretical or experimental proofs, in the GE literature Δt_A is simply attributed to the absorption and re-emission of the surface upward radiation by the IR active atmospheric gases. In 1896 Svante Arrhenius put forward the question:

"*Is the mean temperature of the ground in any way influenced by the presence of heat-absorbing gases in the atmosphere?*",

and he tried to quantify the effect of the CO_2 and associate it with the ice-ages in the planetary climate history, Arrhenius (1896) [18]. The official − *Intergovernmental Panel on Climate Change* (IPCC) approved − CO_2 greenhouse effect hypothesis states that:

increasing CO_2 content of the atmosphere will increase the absorbed upwelling LW radiation from the surface, will reduce the outgoing LW radiation, and will increase the downward LW radiation received by the surface. As a result, the surface will warm up until the top of the atmosphere radiative balance is restored,

Pierrehumbert (2011) [19], Lindzen (2007) [20], Nurse & Cicerone (2014) [21], Smith (2008) [22]. Of course, this is not a greenhouse theory but an unproven hypothesis which poses deliberate constraint on the atmospheric response to increased GHG content.

The key information badly missing here are the theoretical radiation laws governing the radiation climate and the long time theoretical and empirical RE state of the atmosphere. To talk about planetary GE is not very smart without having the slightest idea of both the governing theoretical constraints, and the quasi-static equilibrium state of the system. In this article we shall not waste the time to critically evaluate the tons of supporting literature of the (climate model based) AGW theory, we shall quote only some (frequently referenced) representative examples from the well-known, world famous radiative transfer giants mentioned above.

Climate modelers generally assume a hypothetical positive feedback process which amplifies the initial warming: higher surface and atmospheric temperatures will increase the water vapor content of the atmosphere, and the increased water vapor absorption will further increase the warming effect.

Since the magnitude and quantitative constraint of this effect is unknown, *global climate models* (GCMs) are stabilized with diverse ad-hoc H_2O feedback parameterizations, aimed to fit model outputs to some expected climate scenarios, to real world empirical data, or just to set a desired (acceptable) GHG climate sensitivity.

The unphysical assumption of positive feedback (known as the Simpson paradox) stems from the Schwarzschild solution of the RE state in stellar atmospheres, which predicts unconstrained temperature grows with increasing optical depth, see for example Schwarzschild (1906) [23] (page 28, equation 11), or in the semi-gray treatment of the runaway GE in Shaviv (2012) [37]. The Schwarzschild solution also predicts a large (never observed) surface temperature jump at the lower boundary, and at the small optical thickness limit it violates the law of conservation of radiant energy (an airless planet should have a surface radiative temperature equal to the temperature of the APS).

3. Quantitative validation of the CO_2 greenhouse effect

There is an on-going debate on the origin and the cause of the increase in the atmospheric CO_2 concentration shown in Figure 1. Several publications suggesting that most of the sources of the atmospheric CO_2 are unrelated to human activity, Harde (2019) [62]; Berry (2021) [63]. Recent estimate of the man-made contribution to the observed ~35 % changes is only about 6 %, Poyet (2022) [24]. From our point of view this problem is irrelevant, and in fact we try to focus on the real problem of establishing the theoretical relationships between the atmospheric GHG content and the surface radiative temperature. It is not our purpose discuss the GE definition of (3) and the pretty much useless $\Delta t_A \approx 33$ K temperature difference. To properly attribute the increase of GHGs to the AGW hypothesis one needs a sound physical theory, and one has to relay on relevant empirical facts for validation.

3.1. The global mean picture

The practical approach to the validation effort is to collect long term geographically diverse global radiosonde data sets containing information about the state of the surface and the atmosphere and perform high quality radiative transfer computations to obtain the true long time global average radiative structure of the system. Once the reliable global mean flux density components of the system are known, then the simple task is to compare the global mean observed surface temperature to the predicted one by the RT theory, that is, by validating the key parameters (t_S, F_0, sc, β, and S_U^C) in (17).

The first obvious requirement to conduct such studies are the availability of global scale primary radiosonde observations. Readily available sources of the vertical temperature, water vapor and ozone structures are the world climate data centers and the national meteorological data archives. In our validation efforts we frequently used the following radiosonde data sets: two archives − known as TIGR2 and TIGR2000 sets − of global radiosonde observations between 1976 and 1989, Scott (2009) [31]; 61 annual global mean soundings for years 1948-2008 from the NOAA-R1 archive *National Oceanic and Atmospheric Administration* (NOAA) NCEP (2012) [32]; one full year of high resolution (6 second) morning and evening soundings from the former NOAA *testing facility in Sterling Virginia* (NOAA-S). Several simulations were also performed for the different versions of the USST76 atmosphere, and for some research grade (1 second) soundings from special locations and purposes. Raw radiosonde observations in their original structures are not suitable for direct radiative transfer computations. They must be cleaned of any thermodynamical inconsistencies, sensor errors, and the altitude levels should be optimized for the purpose of the particular applications. In Figure 3 a radiosonde observation from Barrow (Alaska) is shown with cleaned and re-layered structure needed for flux density computations.

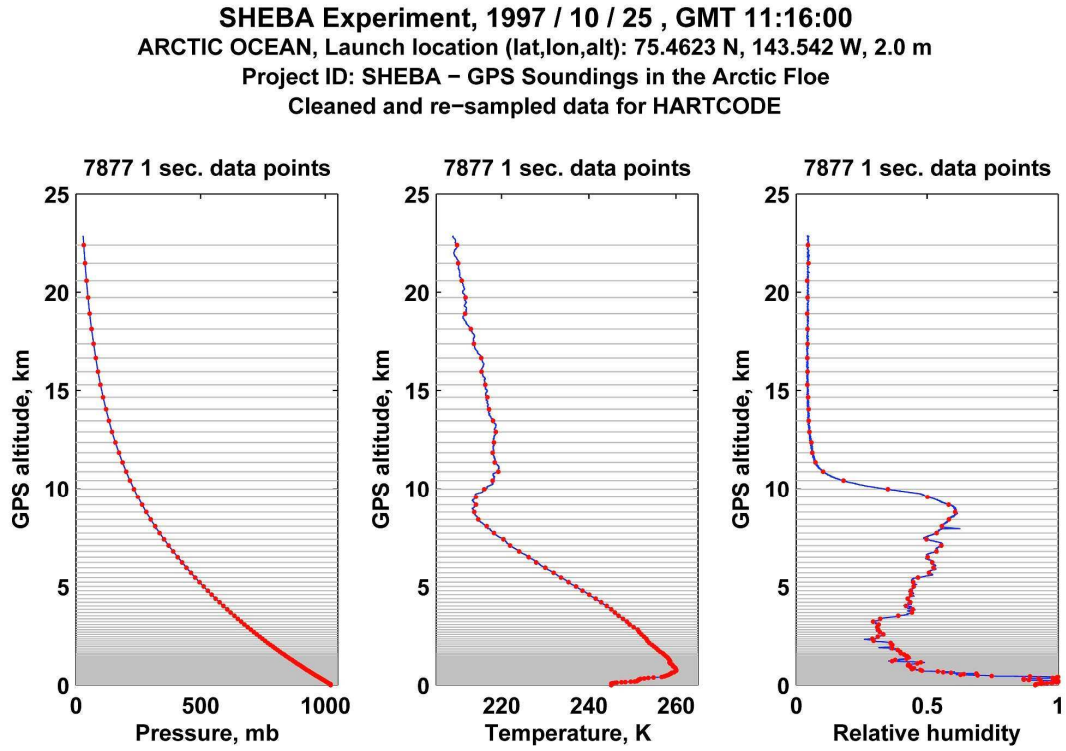

Figure 3: Radiosonde observation taken at Barrow (Alaska). The raw data has to be re-shaped to make it suitable for RT computations. The 140 exponentially spaced gray lines are the levels where the RT code computes the upward and downward fluxes. Between the lines the atmosphere assumed to be homogeneous.

In Figure 4 comparisons of the thermal and water vapor structures of the GAT [31], and the USST76 atmospheres are presented. Both of them are frequently used in radiative budget studies. Compared to the USST76 atmosphere the significant differences in the vertical temperature and H_2O structures are obvious. It is not shown here, but the GAT vertical ozone structure and the global mean column amount of ozone are also different, the USST76 ozone amount is about 10 % higher.

Notice that the USST76 tropospheric lapse rate is much higher, the isothermal stratosphere does not exist, and the H_2O column amount is about half of the global average. Unfortunately, on the top of the inherent uncertainties, global climatological data sets are also subject to deliberate data manipulations, therefore extreme care is needed to identify a suitable clean archive.

The second obvious requirement is adequate high quality RT software. It must be quite clear that the accuracy of a research *line-by-line* (LBL) RT code should not be restricted by speed requirements, vertical resolution, or absorption band selections common in radiative transfer modules in climate models. Our choice was the *High-resolution Atmospheric Radiative Transfer Code* (HARTCODE) which was explicitly developed for extreme numerical accuracy, Miskolczi (1989) [25], Rizzi et al. (2002) [26].

Test computations show that HARTCODE adequately responds to extremely small changes of the most important input parameters, for example, 1.0 ppm increase in the CO_2 volume mixing ratio, Miskolczi (2010) [27]. Routine comparisons of RT codes from different authors and their empirical validations may be found in Kratz et al. (2005) [28], and Saunders et al. (2007) [29].

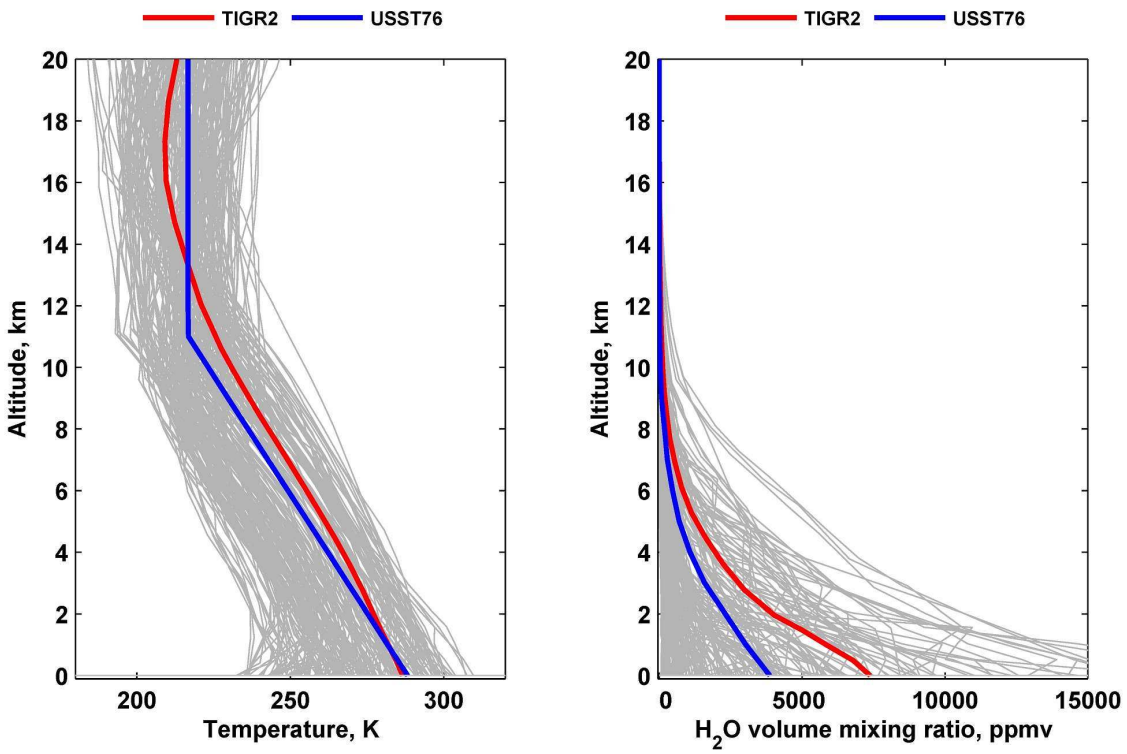

Figure 4: Comparisons of the vertical thermal and humidity profiles of the global average TIGR2 (GAT) and theUSST76 atmospheres. Thin gray lines are the individual radiosonde data as it was observed by the TIGR2 global radiosonde archive. One has to notice the significant differences between the averages in both the thermal and humidity profiles (blue and red lines). Such differences adversely affect the flux density simulations.

Further unique features of HARTCODE are the strict preservation of the monochromatic Beer-Lambert law, the Helmholtz reciprocity principle, and the spherical refractive computation of the directional transmittances through every optical path segment. The spectroscopic details of the IR flux transmittance and optical depth computations are presented in Miskolczi (2011) [30], and in [17].

Befor using an RT software designed for directional radiance computations several other test requirements shoud be met. Such requirements are routinly checked through international validation campaigns. The ultimate test is the empirical proof, that under controlled experiments the simulated directional spectral radiances agree with satellite and ground based observations.

The Helmholtz reciprocity principle is demonstrated for vertical and horizontal viewing geometries in Figure 5. It is essential to observe this principle when computing hemispheric transmittances from directional path transmittances. Any RT code is supposed to be able to compute the same directional path transmittance for the reverse trajectory (independently of the viewing geometry).

3.2. Flux density components

To gain knowledge of the radiative structure of the atmosphere first, we need to compute the vertical distribution of all the upward and downward flux density components of a cloud-free air column for altitudes of sufficient vertical resolution.

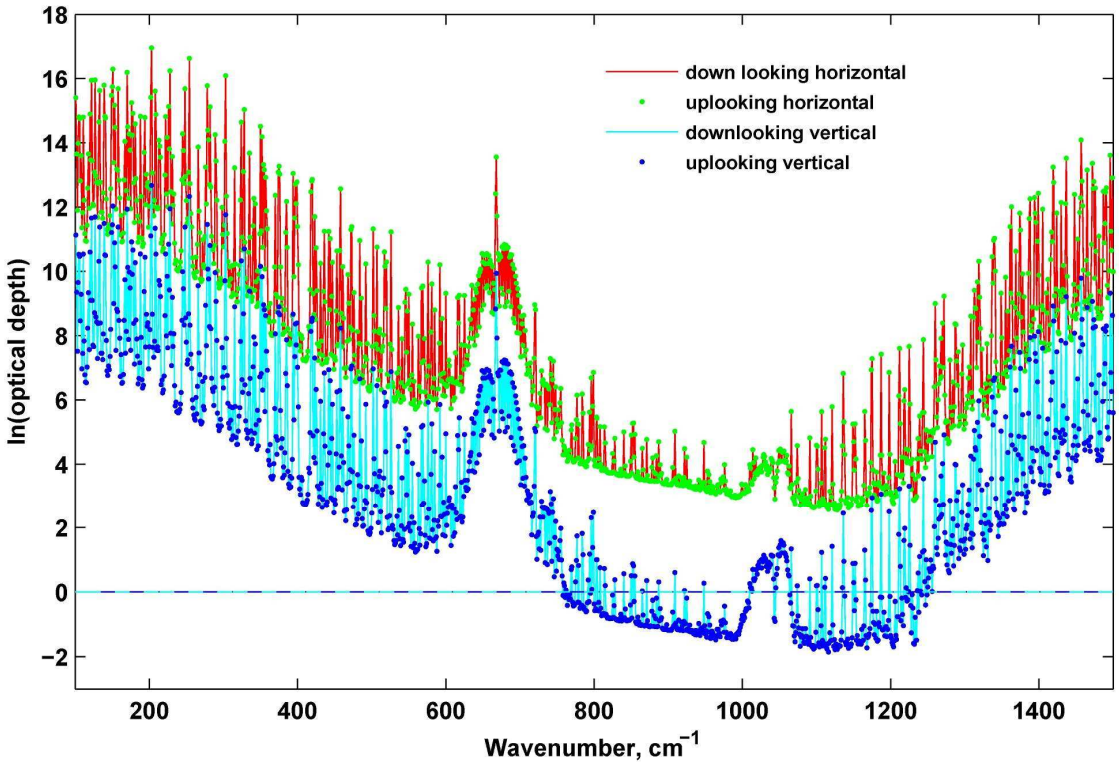

Figure 5: Helmholtz reciprocity principle requires the equal line of sight optical thickness (and path transmittance) for every slanted atmospheric optical paths. In this test vertical and horizontal viewing were considered. High resolution HARTCODE spectral optical thickness computations perfectly reproduce the principle. Note that the Helmholtz principle is not valid for spherically integrated (hemispheric) flux optical thickness.

In vertically inhomogeneous atmosphere showing cylindrical symmetry flux density computations at any altitude (depending on the vertical discretization shown in Figure 3) require angular integration of the path radiances over both the upper and lower hemispheres, and also the altitude integration (both upward and downward direction) of the parts of the atmosphere above and below the given altitudes.

Such computations are presented for the GAT atmospheric structure in Figure 6. Here it is assumed, that at any z altitude a solid or liquid surface discontinuity (cloud layer) is present, emitting isotropic radiation according to the local source function (pink line). The continuous lines are the upward and downward boundary fluxes from the regions bounded by z km and $z_{TOP}=70$ km, (these fluxes are marked in black letters in the legend). The dashed lines are the upward and downward boundary fluxes from the regions bounded by $z=0$ km and z km (these fluxes are marked in red letters at the top of the figure). The upper thin (light blue) horizontal line indicates the altitude where the source function $S_U(z)$ (pink curve) is equal to the $OLR(z)$ (black curve). The lower horizontal line indicates the altitude where $E_U(z)$ and $E_D(z)$ are equal. The small black circle at about $h^C=1.92$ km altitude marks the interception of the $OLR(z)$ and $E_D(z)$ functions where $OLR(h^C)=E_D(h^C)$. At this h^C the global average cloud cover could be in radiative equilibrium with the OLR^C, and in thermal equilibrium with the local source function S_U^C. Of course, the accurate h^C cannot be determined graphically from this figure. In section *4.4* the quantitative procedure of the computation of the accurate h^C, α_B, and S_U^C is discussed.

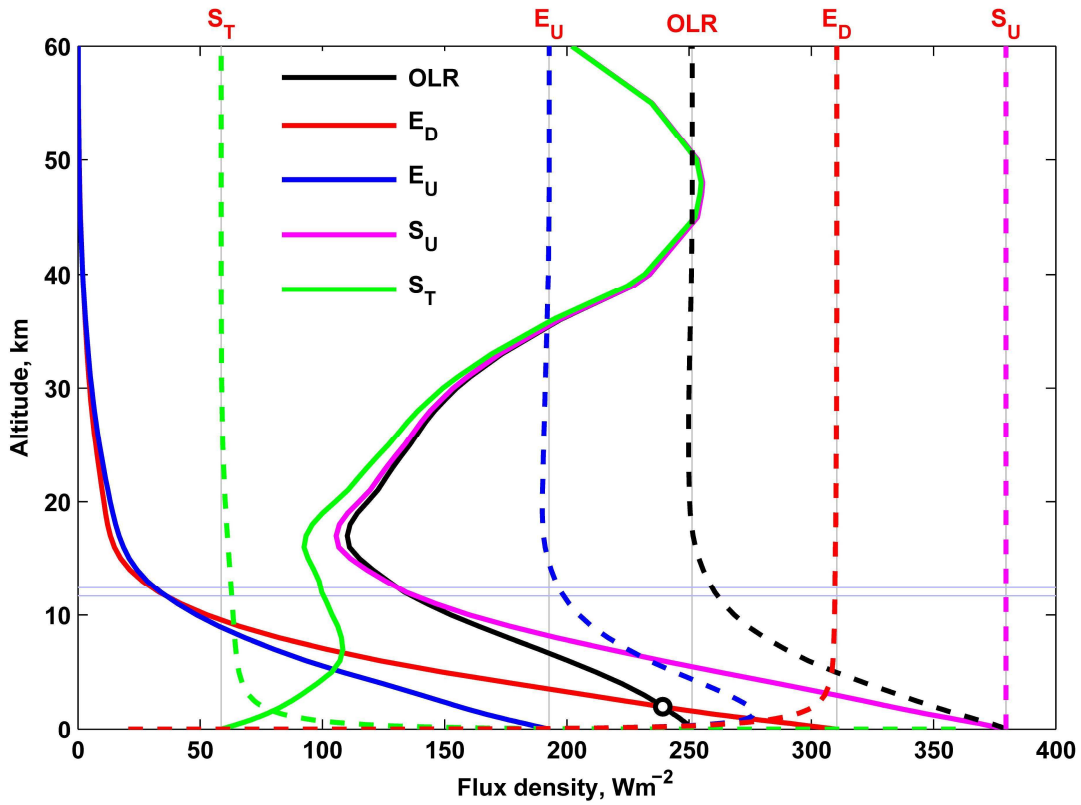

Figure 6: Layer boundary fluxes for the GAT atmosphere. Solid lines are the cumulative upward and downward layer contributions from the regions bounded by the TOA and a given altitude z. Dashed lines are the cumulative layer contributions from the regions bounded by the surface and a given altitude z .

There are many other interceptions of the flux curves which may increase the degree of freedom of the system's response to establish its overall radiative equilibrium. The numerical details of the (surface referenced) flux components of the whole clear air column and the two segments of the same air column divided by the h^C altitude is shown in Figure 7. This figure shows the very first result which revealed some numerical relationships relevant to the global average radiative flux and cloud structure. At h^C altitude the source function is $S_U^C = S_U(h^C) = 333.82\ \mathrm{Wm^{-2}}$ and a global average cloud layer at this altitude should be in radiative equilibrium with $E_D^C = OLR^C = 240.142\ \mathrm{Wm^{-2}}$. It is also shown, that the A_A^C absorbed part of S_U^C (in the blue region) can only leave the system as the clear-sky OLR.

Radiosonde observations show that $t_S = 286.06\,\mathrm{K}$ and the physically meaningful (surface referenced) Δt clear-sky greenhouse effect and the G greenhouse factor are: $\Delta t = 27.9\,\mathrm{K}$, and $G = S_U - OLR = 127.9\ \mathrm{Wm^{-2}}$. The greenhouse effect over the cloud cover is somewhat smaller: $\Delta t^C = 21.89\ \mathrm{K}$, and $G^C = S_U^C - OLR^C = 93.68\ \mathrm{Wm^{-2}}$.

We have seen that the average planetary radiation climate − as a set of scalar climate radiation parameters − assumes an extensive *global average cloud cover* β , at a characteristic *global average cloud altitude* h^C , which breaks up the planetary radiation field into three (not necessarily continuous) major regions.

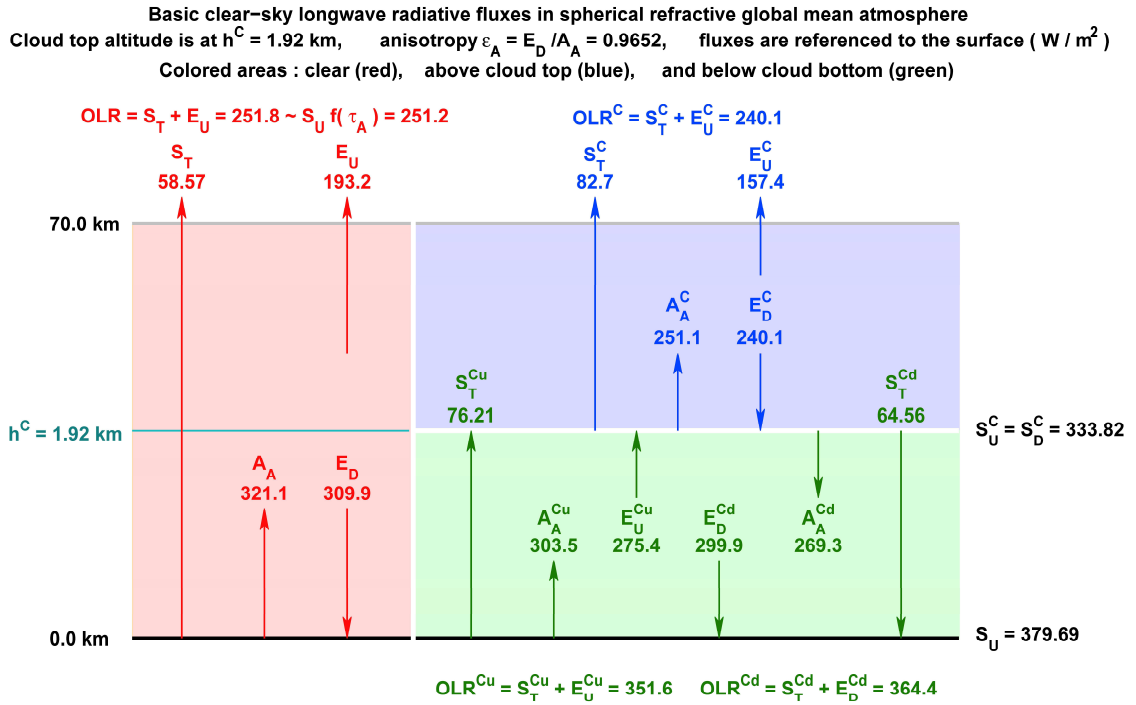

Figure 7: Boundary upward and downward fluxes in the whole average clear air column (red), in the above $h^C = 1.92$ km altitude (blue) and in the below h^C (green) vertical regions. Without the knowledge of the cloud cover the full global mean radiative structure cannot be established.

In Figure 8 the SW and IR as well as the clear and cloudy flux density components are summarized. Here the definitions and the flux density components of interest are displayed together with their numerical value in Wm^{-2}. This figure is based on Figure 7, but here the flux density components are weighted with the cloud cover, and the LW TOA fluxes are referenced to 70 km. altitude. (For example to obtain correct clear-sky transmitted LW flux at the TOA the S_T in Figure 7 must be multiplied by the $(1-\beta)$ clear-sky fraction and the sc spherical correction: $58.57(1-0.6618)0.9789 = 19.39\ Wm^{-2}$.)

The SW components (F_0 and F_E) are in the top line. In the second line F_E is partitioned by the Bond albedo into F_A absorbed, and F_R reflected parts. In the third line they are further partitioned to clear (F and R) and cloudy (F^C and R^C) components. Remember, that the Bond albedo is not the true reflection properties of the sunlit side of the planet, but – as the ratio of the reflected and absorbed parts of the incoming SW radiation – it is the characteristic of the planetary radiation budget. For further partition of the reflected components into surface and atmospheric origin one must deal with the diurnal cycle and multiple scattering problems, which is not an easy task, and for our purpose it is not needed. After depositing the momentum in the system anywhere, eventually, all scattered SW radiation will leave the system. GE by definition is a LW radiative phenomenon, and more important for us the knowledge of the accurate IR flux density components, which can be directly related to the surface temperature and the TOA net LW flux. It should be emphasized, that this view is not a kind of simplified model, the LW flux density arrows are real global mean fluxes of the GAT atmosphere, they were derived by LBL simulations using first principles, *without any assumptions on the thermal structure and the radiation field*. Even the choices of β and h^C were based on empirical facts shown in Figure 6.

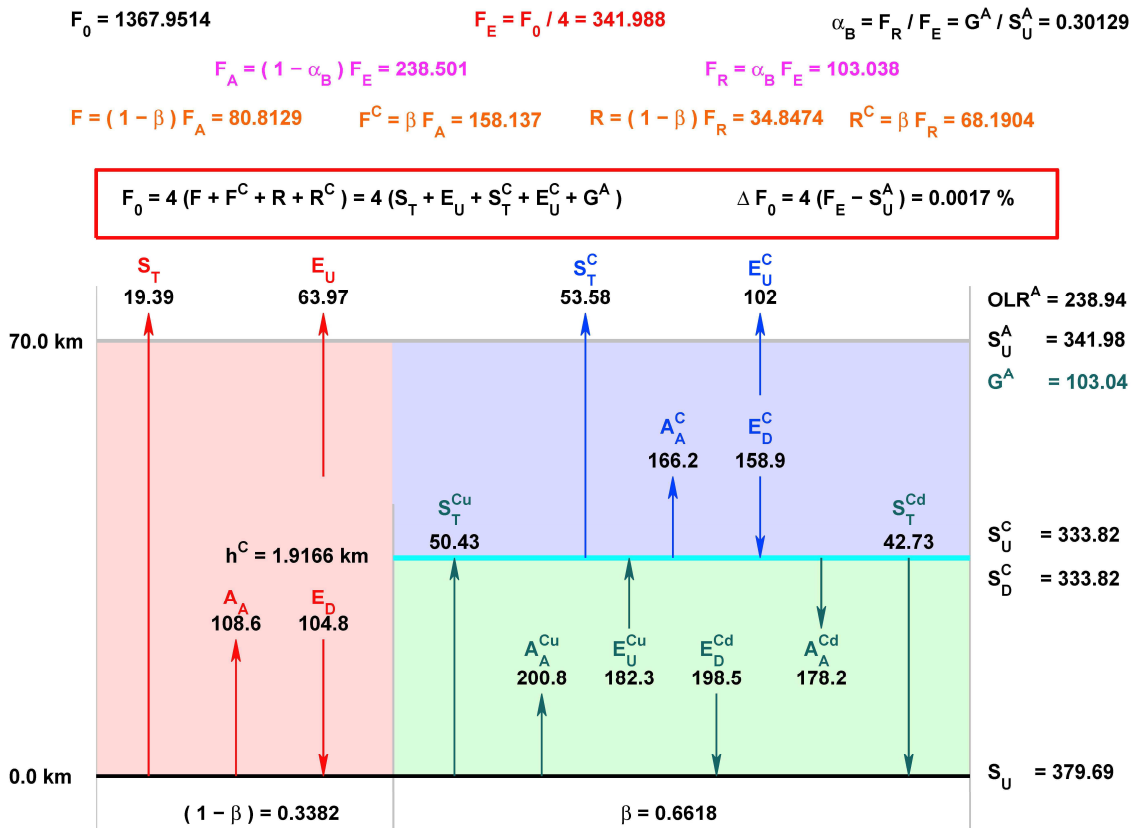

Figure 8: All-sky SW and LW radiative flux components (Wm^{-2}). The red, blue and green regions represent the sum of the clear, above cloud and below cloud portions (spherical shell sectors) of the atmosphere. The equations in the middle show that the F_0 solar constant obtained from the SW and LW flux components agree, therefore the Chandrasekhar-type radiative equilibrium state of the planet is empirically proven.

The IR flux density components are in and around the colored areas at the lower part of the figure. TOA fluxes are referenced to $z_{TOP} = 70$ km altitude; all other fluxes are referenced to the ground surface. The flux absorption of an air column between 70 and 120 km altitudes is less than 0.0005, therefore the flux density contribution from above 70 km is negligible. The numerical accuracy of the flux density components are five significant digits.

The downward upper boundary fluxes at the clear, and above cloud regions are zero. As it was already mentioned, surface fluxes may be referenced to the TOA by applying a spherical correction: $sc = R_E^2 / (R_E + z_{TOP})^2$, where $R_E = 6371 \times 10^3$ m is the volumetric radius of the Earth. Due to refraction, the accurate computation of sc is far more complex and results in an $sc = 0.978918$ (0.0547 % larger) value, which corresponds to an effective altitude of ~ 68.236 km.

In cloud-free areas the ground surface (having a global average radiative temperature t_S) and the semi-transparent atmosphere (with an average GHG and thermal structure) above can directly and freely cool to space. The same is true above an average planetary cloud cover, but with different lower boundary conditions.

The cloud top and cloud bottom altitudes are stochastic variables, the global means of them were set to the same 1.9166 km altitude. Of course, this does not mean that the average cloud cover has zero geometrical thickness.

Remember, the combined lower boundaries of the red and blue areas constitute the APS. From the green area (below the cloud cover) the IR radiation cannot escape (to the atmosphere above the cloud cover, or to the space), and cannot contribute directly to the planetary RE.

Among the flux density components the following trivial relationships must hold (by definitions): $OLR = S_T + E_U$, $OLR^C = S_T^C + E_U^C$, $OLR^{Cu} = S_T^{Cu} + E_U^{Cu}$, and $OLR^{Cd} = S_T^{Cd} + E_D^{Cd}$. Here OLR is the clear sky, OLR^C is the cloudy sky, OLR^{Cu} and OLR^{Cd} are the upward and downward LW boundary fluxes below the cloud layer, respectively.

The *equilibrium equation* (in a red box in the middle of Figure 8) shows that the CRE state of the planet holds, the relative difference of F_0 from the SW and LW components is $\Delta F_0 = 0.0017\,\%$. The TOA flux difference between the SW F_E and the LW $OLR^A + G_E = S_U^A$ (planetary net flux) is 0.00584 Wm^{-2}, indicating that the combined effect of all the computationally ignored planetary thermal flux contributions from non-radiative origin has to be very small indeed. It appears, that the net non-radiative power dissipation in the system is compensated within the system and has no long term observable effect on the planetary radiative equilibrium state of the Earth.

According to the long-term steady state requirement there cannot be any accumulating direct radiant energy in any of the three regions, however, unlimited transfers of thermal energy to-and-from the global latent heat reservoirs are permitted (as it happens in the real environment through the phase boundaries).

The most important conclusion of our computations is the solid empirical proof of the existence of the assumed steady state planetary RE. In Figure 8 the key planetary IR fluxes from the APS are:

$$OLR^A = sc((1-\beta)(S_T + E_U) + \beta)(S_T^C + E_U^C)) = 238.94\,\mathrm{Wm^{-2}}, \tag{18}$$

and

$$S_U^A = sc(S_U(1-\beta) + S_U^C\beta) = 341.98\,\mathrm{Wm^{-2}}. \tag{19}$$

The APS-referenced greenhouse factor is just equal to the all-sky reflected SW flux density $G^A = S_U^A - OLR^A = F_R = 103.04\,\mathrm{Wm^{-2}}$. The astrophysical textbook value for the radiative temperature of the APS (see [11]) $t_{APS} = (16\pi\sigma d_E^2 / L_0)^{-1/4} = 278.68\,\mathrm{K}$ is in perfect agreement with simulated mean all-sky surface temperature of $t_{APS}^S = (S_U^A / \sigma)^{1/4} = 278.68\,\mathrm{K}$ from (19). Here $L_0 = 3.847\times10^{26}$ J/s is the solar luminosity, $d_E = 1.4959789\times10^{11}$ m is the semi-major axis of the Earth's orbit, NASA (2012) [47], and $r_0 = 6.96\times10^8$ m is the solar radius, NASA (2012) [46].

For further consistency check, from the fluxes from (18) and (19) the simulated β^S cloud cover, α_B^S Bond albedo, and F_0^S solar constant were computed and compared, showing reasonably good agreement:

$$\beta^S = \frac{S_U^A / sc - S_U}{S_U^C - S_U} = 0.6615\,, \tag{20a}$$

$$\alpha_B^S = 1 - \frac{OLR^A}{S_U^A} = 0.3013\,, \tag{20b}$$

$$F_0^S = 4S_U^A = 1367.93\,. \tag{20c}$$

3.3. Radiative transfer functions and flux optical thickness

Radiative transfer functions (RTFs)are simple algebraic functions of the flux optical thickness of a semi-transparent planetary atmosphere. In section *2.2* we have already defined the flux optical thickness as $\tau = -\ln(S_T / S_U)$. One can see that the transmission, absorption, transfer and greenhouse functions are explicit functions of this τ. In Figure 9 the fundamental radiative transfer functions and the normalized upward atmospheric emissions $E = E_U / S_U$ for about a thousand weather balloon observations are displayed. The black dots in the yellow-shaded area are clear indication of theoretical constraints exposed by the RT functions. The light grey vertical line is the *annual global average* τ of all the data points.

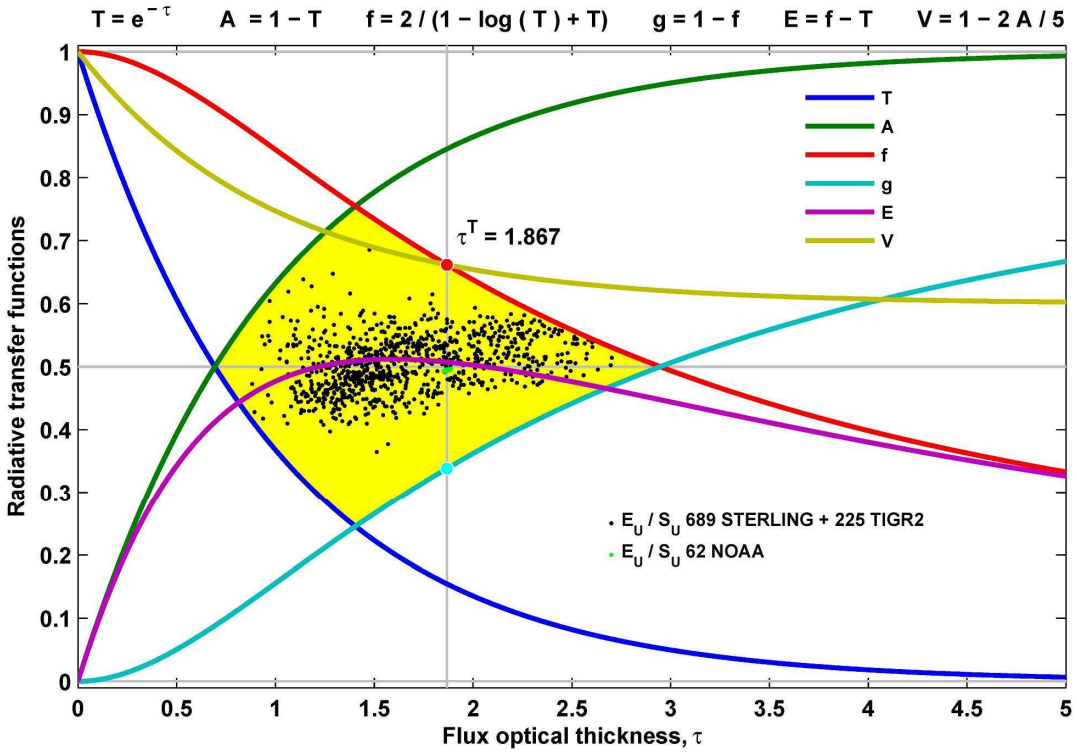

Figure 9: Basic radiative transfer functions. T, A, f, g, E, *and* V *are the transmission, absorption, transfer, greenhouse, emission and virial functions respectively. By definition, the clear-sky* T *and* τ *of an air column are:* $T = S_T / S_U = \exp(-\tau)$ *and* $\tau = -\ln(T)$.

From extended flux density simulations (using diverse radiosonde data) we gained enough confidence to conclude that the Earth's long time global mean flux optical thickness is equal to a theoretically predictable mathematical constant $\tau^T : \tau = \tau^T = 1.86756$. The theoretical τ^T may be computed either from the $f(\tau^T) = V(\tau^T)$ (red dot) or from the $g(\tau^T) = 2A(\tau^T)/5$ (light blue dot) transcendental equations.

The definition of the $V(\tau)$ virial function: $V(\tau) = 1 - 2A(\tau)/5$. This theoretical function takes care of two theoretical requirements (they are empirical facts as well). One is the $S_U = 2E_U$ equality (stems from the Clausius virial theorem), and the other is the constraint known as the transparent limit (without atmosphere *OLR* must be equal to S_U).

In the Earth's atmosphere the theoretical equilibrium optical thickness is the natural constraint on the equilibrium mass of the WV in the atmosphere (the WV column amount in precipitable cm). The average τ of the NOAA-R1 annual global means (green dots) and τ of the GAT atmosphere are equal to τ^T.

The stability of the planetary radiation climate is controlled by the derivatives of T, f, g, E, and V functions: $dT/d\tau = -T$, $df/d\tau = -f^2 A/2$, $dE/d\tau = -f^2 A/2 + T$, $dV/d\tau = -2T/5$. Notice that all the signs of the derivatives are negative, implying a strong tendency of the system to return to its equilibrium state (Braun-LeChatelier principle). Considering the permanent changes of the state of the H_2O in the system it is anticipated that the RE state of the atmosphere will also be affected by dynamical processes related to the condensation and evaporation, permanently present in a global average air column. Our explicit definition of the τ_D dynamical optical thickness is: $\tau_D E_U = OLR(1+\tau_D)/2$. Remember, condensation will reduce, evaporation will increase τ_D, and what actually happens will depend on the sign of the $\tau - \tau_D$ difference. Unfortunately, in this article we cannot discuss further interesting and important theoretical questions related to the changes in τ_D.

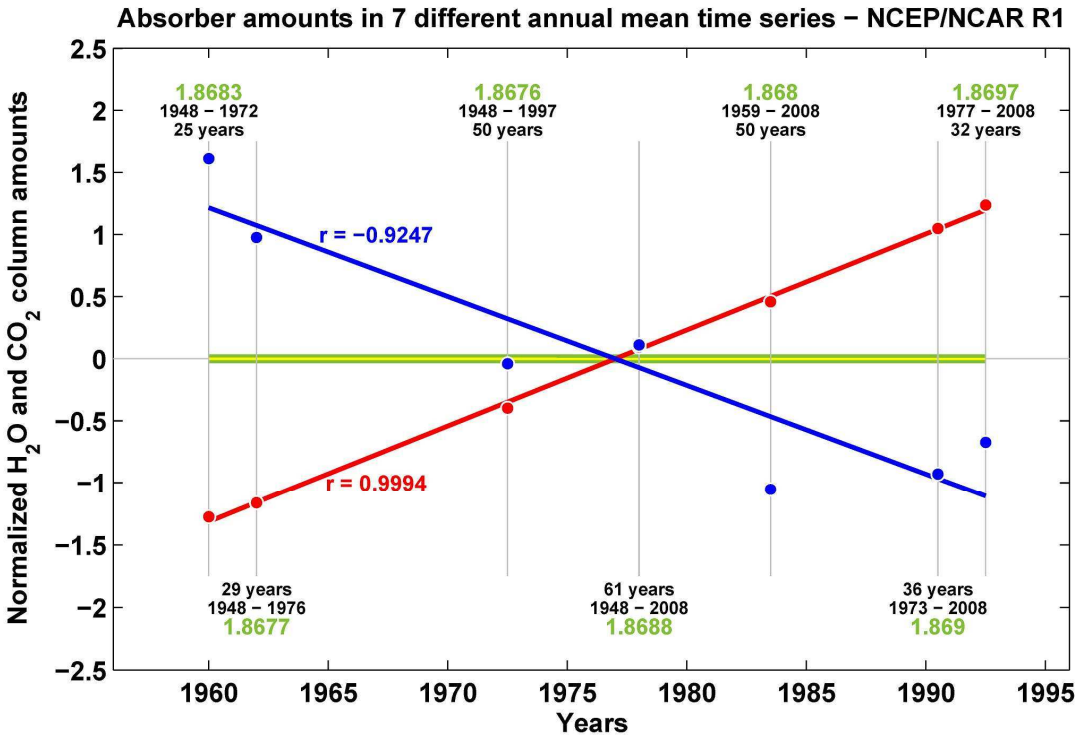

Figure 10: Changes of H_2O (blue) and CO_2 (red) column amounts in 7 different time series. Atmospheric structures are from the NOAA-R1 radiosonde archive. The green and yellow trend lines (deviations from the sample mean and deviations from the τ^T theoretical value show no tendency.

In Figure 10 the constancy of the IR flux optical thickness (light green numbers) is maintained in each randomly selected subset of different length from a 61-year long NOAA-R1 time series. Here the CO_2 (red line) and H_2O (blue line) normalized column amounts are plotted for the 1948-2008-time interval. The sign of the H_2Ocorrelation coefficient (blue number) is a clear indication of the climate stabilizing role of the water vapor. The increase of the atmospheric carbon dioxide is apparently coupled with the decrease of the atmospheric water vapor column amount. The time-averaged CO_2 column amounts − unlike concentrations − increase linearly.

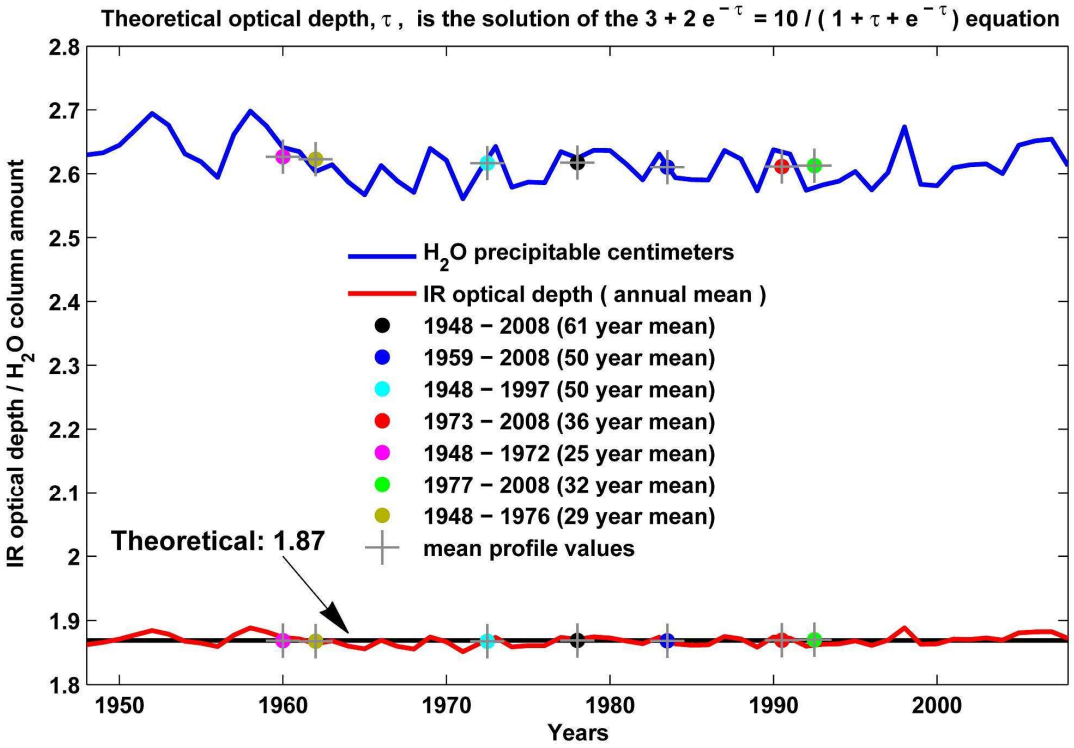

Figure 11: The constancy of the annual mean flux optical thickness in 7-time series of different length (NOAA-R1 radiosonde archive). H_2O column amounts are in prcm.

Time period	Centre	Years	Altitude	Temperature	H_2O	CO_2	Tau
1948−2008	1978	61	0.7931	0.8183	−0.2841	0.9839	0.06488
1959−2008	1983.5	50	0.8059	0.8349	0.04499	0.9937	0.2976
1948−1997	1972.5	50	0.6621	0.6625	−0.4843	0.9827	−0.2284
1973−2008	1990.5	36	0.6947	0.7987	0.1148	0.9974	0.3491
1948−1972	1960	25	−0.005748	0.1731	−0.5907	0.983	−0.4184
1977−2008	1992.5	32	0.58	0.7424	0.03992	0.9973	0.267
1948−1976	1962	29	0.001769	0.0584	−0.6048	0.9804	−0.4396

Figure 12: Trend line correlation summary of seven NOAA-R1 time series. The last five columns on the right are linear regression coefficients for the top altitude of the air column, surface temperature, water vapor and carbon dioxide column amounts, and the flux optical thickness. The IR flux optical thickness has no correlation with time and the strong signal of increasing atmospheric CO_2 content in any time series is not present in the IR flux optical thickness data. Consequently, the atmospheric CO_2 increase cannot be the reason of global warming.

In Figure 11 the changes in the flux optical thicknesses and the H_2O column amounts are also demonstrated. Notice that the random fluctuation in the IR optical thickness (red line) correlate well with the H_2O column amounts (blue line). Again, the constancy of the flux optical thickness is coupled with the constancy of the water vapor content of the air column. The sample means (colored dots) are practically equal to the mean profile values (+ gray symbols) which is an indication that a single column average atmospheric structure can safely be used instead of the global average fluxes from a large data set.

Detailed numerical data of the regression analysis of the key variables − altitude, temperature, H_2O, CO_2, and flux optical thickness − are given in Figure 12. According to Figures 10, 11, and 12 the long-term global mean OLR and S_U cannot change independently, they are linked analytically to the changes in the flux optical thickness by (12) .

The IR flux optical depth has no correlation with time and the strong signal of increasing atmospheric CO_2 content in any time series is not present in the IR flux optical thickness data. Consequently, the atmospheric CO_2 increase cannot be the reason for global warming. It is interesting to note, that in the individual time series the H_2O does not correlate with the time, while in the mean values the negative correlation is quite obvious (in Figure 10).

Based on the NOAA-R1 soundings and simulations Figure 13 shows the no-feedback response and the true observed changes of the OLR in the 200-1500 cm^{-1} spectral range. The real atmosphere does not follow the GHG GE hypothesis of the IPCC. The observed true change in the OLR is positive and the atmosphere and the whole system do not resume the initial state. The fictitious no-feedback response is unrelated to climate change.

More details are presented in Figure 14 where the no-feedback responses of some other GHGs are also displayed. The observed 23.6 % increase in CO_2 causes -0.75 Wm^{-2} radiative imbalance (red dot). In the same time period, based on the NOAA-R1 archive the real change is 3.02 Wm^{-2} (blue dot). There is no such thing that the OLR remains constant and the surface warms up due to some incorrect GHG GE hypothesis, or because of the outcomes of CO_2 doubling experiments conducted with never validated GCMs.

The changes of OLR due to the pressure induced continuum absorption of N_2 and O_2 are negligible. The contribution to the changes of OLR from the changes of IR absorption of CH_4 (red line) does not seems to be significant either.

IPCC scientists ignore the fact that the clear sky OLR is governed by the unpredictable stochastic nature of the upper tropospheric humidity field (and also the global cloudiness and wind field) which cannot be modelled by any deterministic global climate model. The theoretical constraints governing the global mean radiation flux components are also not part of the GCMs.

In Figure 15 the chaotic nature (in space and time) of the upper tropospheric humidity field is presented, McIDAS (2008) [33]. Evidently, it is impossible to give a reasonable long-term estimate of the OLR^A and t_S, therefore the long-term prediction of climate change is not an appropriate task for GCMs.

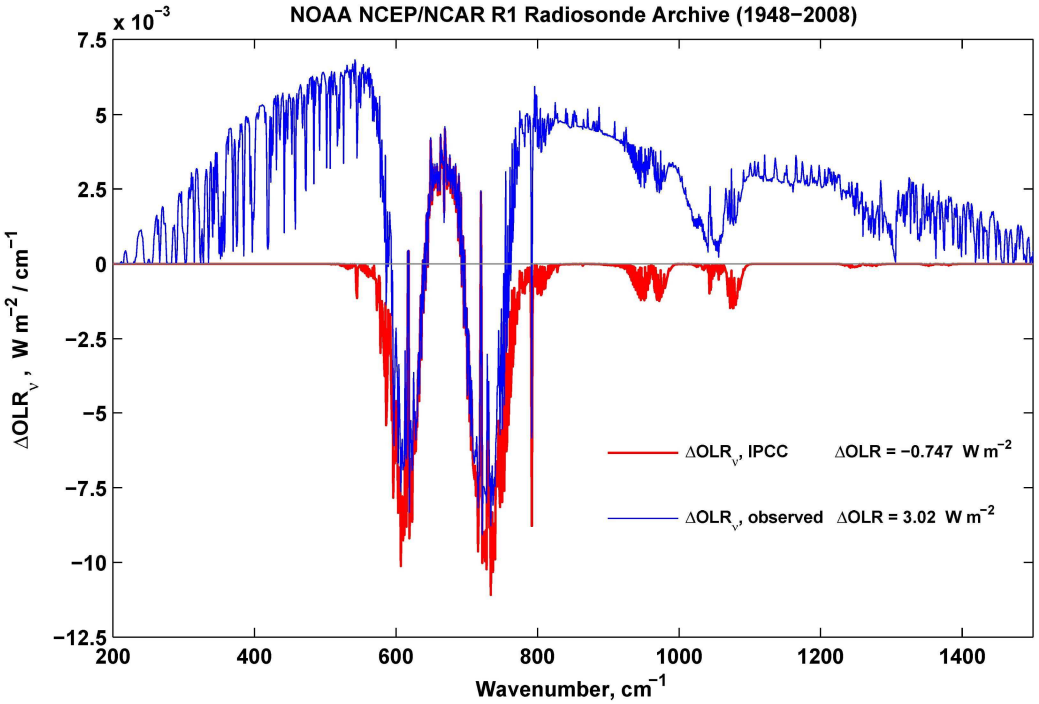

Figure 13: Comparison of the observed and expected changes in the clear-sky spectral OLR . The IPCC type no-feedback response to 23.56 % increase in carbon dioxide is negative, while the true observed changes are definitely positive.

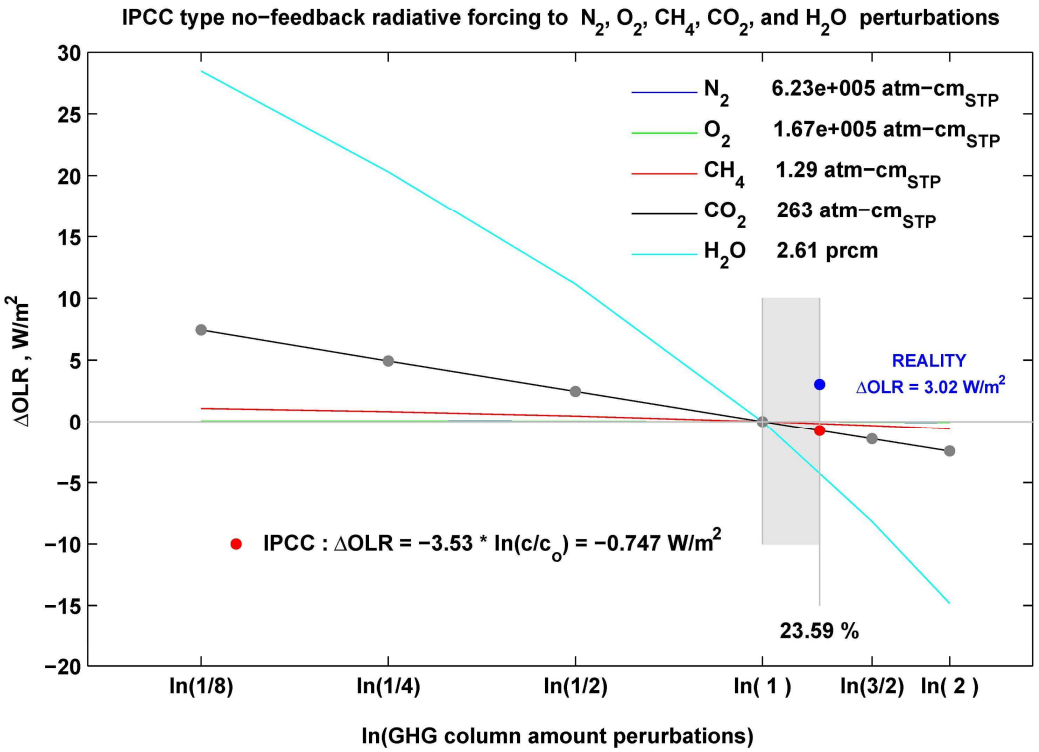

Figure 14: HARTCODE GHG perturbation study shows that at the TOA the no-feedback response of increased atmospheric CO_2 is negative (red dot). CO_2 doubling studies are not consistent with observations.

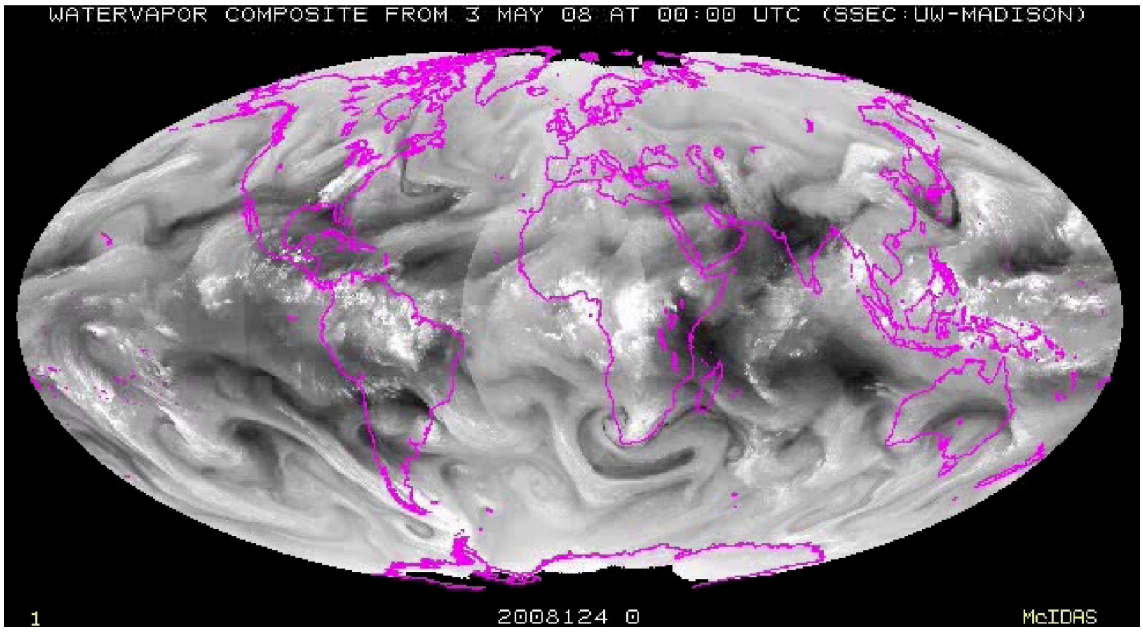

Figure 15: Satellite view of the changes in the upper tropospheric humidity field.

4. The scientific background

In this section some GE related fine details are discussed. Let us list some fundamental IR flux density relationships and the simplest RT functions characteristics of the global mean clear atmosphere:

- Atmospheric Kirchhoff law: $E_D = \varepsilon_A A_A$ (ε_A is the anisotropy factor – discussed later)
- Law of radiative equilibrium: $OLR / S_U = f = 2/(1+\tau+T)$
- Virial function: $OLR / S_U = V = (3+2T)/5$
- Greenhouse identity: $G = S_U - OLR = A_A - E_U$
- Schwarzschild-Milne equation: $OLR = (E_D + E_U)/2$

Based on the equations above, formally, infinite number of valid RT functions may be created by simple (linear) combinations. The new combined functions will all satisfy the clear-sky global RE constraints, but the interpretation of the new equations might not be that simple. In case of the $f = V$ equality and the $\tau^T \cong \tau$ close match the interpretation came relatively easy, but for example to relate the global mean w water vapor column amount to τ, is not that straightforward: $w = w_0 / (1 - 4\exp(-\tau)) = 2.61$ prcm, where $w_0 = 1.0$ prcm.

4.1. Radiative equilibrium at the surface

To establish the radiative equilibrium between the ground surface and the atmosphere above, the ε_A spherical emissivity (or the anisotropy) of the inhomogeneous IR radiation field of the atmosphere has to be considered. The anisotropy of the downward LW radiation is the $\varepsilon_A = E_D / E_{D,I}$ ratio, where E_D is the downward radiation from the real atmosphere, and $E_{D,I}$ is the downward radiation from the isotropic radiation field of temperature t_S (present in the atmosphere).

Because of the $E_{D,I} = S_U(1-\exp(-\tau)) = S_U A = A_A$ mathematical identity, ε_A may easily be expressed as $\varepsilon_A = E_D / A_A = 0.96515341$, where S_U, τ, and $E_{D,I}$ are from GAT LBL simulations. We shall reference this new fundamental relationship as the *atmospheric Kirchhoff law*. The ε_A dimensionless quantity turned out to be one of the most important astronomical parameters of the Earth's radiation climate. In the literature the $\varepsilon_0 = E_D / S_U$ ratio is often termed as sky emissivity, which is not an independent parameter, but related to the ε_A anisotropy factor by the $\varepsilon_0 = \varepsilon_A A$ relationship. Large scale simulations showed that for local atmospheric structures $\varepsilon_0 < 1.0$ always holds, therefore heating of the surface by E_D is impossible. To interpret the theoretical equilibrium global average surface temperature, the following three issues should be taken care of: anisotropy of IR radiation reaching the surface from above; non-radiative energy transport processes at the surface; surface reflection of the downward IR radiation. In a clear atmosphere, the three processes may be easily considered in terms of three parameters ε_A, ε_B, and E_D:

$$E_D / A = \varepsilon_A S_U = \varepsilon_B S_U + (1-\varepsilon_B) E_D, \tag{21}$$

where $\varepsilon_B = E_D S_T / A_A / (S_U - E_D)$ – expressed from (21) – is the *true emissivity* of the surface, taking into account only the non-radiative processes and ignoring the IR surface reflection of E_D. The EBT computed from the $\varepsilon_B S_U$ product defines the t_T *true emissivity temperature* of the surface: $t_T = (\varepsilon_B S_U / \sigma)^{1/4} = 271.43$ K. Obviously, the identity of $1 \equiv \varepsilon_A A + (\varepsilon_A / \varepsilon_B) T$ must also hold. For the S_U isotropic radiation and the t_S EBT there are plenty of exact relationships similar to equations (21) which all satisfy the law of conservation of radiative energy. For example, we may simply write that

$$S_U = A_A \varepsilon_A (1-\varepsilon_B) / (\varepsilon_A - \varepsilon_B), \tag{22}$$

which may suggest that S_U (or t_S) will increase with increasing A_A (due to increased CO_2). This is not the case. Using the definition of A_A, (22) will be reduced to an identity expressing the constancy of the flux optical thickness: $\tau = \ln(\varepsilon_A(1-\varepsilon_B) / (\varepsilon_B(1-\varepsilon_A)))$. We conclude, that once the surface temperature t_S from (17) is physically defined, the equations (21,22) links this t_S to other conservative climate parameters associated with the three most important clear-sky IR radiative processes discussed above.

4.2 The Sun

It should be recognized that the Sun is a very complex object, and the solar constant has its own natural fluctuations. Depending on the state of the Sun F_0 may vary (on different time scales) between $F_0^{\min} = 1359.7$ and $F_0^{\max} = 1376.2$ Wm^{-2} introducing 1.2% (quasi-periodic) changes in the short term averages, Berk et al. (2008) [43]. From $F_0^{\min}$ and $F_0^{\max}$ the F_0^{av} arithmetic average is $F_0 = F_0^{\text{av}} = 1367.95$ Wm^{-2}, which is very close to the established long term average ground based observations of 1368 Wm^{-2}. It is not very wise to declare an official solar constant and continuously upgrade it according to the relatively short-term satellite observations. Even NASA warns that their data in the factsheets, NASA (2016) [44] are approximations and they are not appropriate for scientific use. The data are usually given in three or four significant digits and they cannot be consistent with the known physical laws of nature where the key astronomical information and the most fundamental constants of the theoretical physics are given with 10-50 ppm relative accuracy.

To construct a long-term continuous satellite solar constant data base considerable effort has been devoted to reviewing the calibration algorithms of the radiometers involved in different satellite missions. In Scafetta & Willson (2013) [49] one can see largely different composite series from different authors which are the clear sign that the *satellite solar constant problem* is not yet resolved. Once the actual solar constant cannot be known to better than ~0.3 % relative accuracy, (see [49] Fig.15) climate modelers must acknowledge this fact and refer to the reason of their choice of the solar constant.

Sun is the source of the observable radiative and not directly observable entropy flux densities and their specific intensity, radiance, or brightness counterparts. We have found that a theoretical solar constant may be derived from the next equation:

$$F(d)=(\pi/\sigma)^{1/3}d_E^{8/3}r_0^{-2/3}d^{-2}/10, \tag{23}$$

where $F(d)$ is the flux density in $\mathrm{Wm^{-2}}$, and d is the distance from the centre of the Sun in meters. In this universal function d may vary from inside the Sun to anywhere in the solar system. This equation stems from the temperature-flux density duality principle which rests on an intrinsic mathematical property of the Planck distribution, Miskolczi & Héjjas (2021) [45]. This analytical form of $F(d)$ is discussed in more details in the Appendix.

Knowing the solar surface area the theoretical solar luminosity, solar surface emission, solar constant and the available SW flux density may easily be computed from the $F(d)$ function: $L_0^T=4\pi^{4/3}\sigma^{-1/3}d_E^{8/3}r_0^{-2/3}/10$, $E_0^T=(\pi/\sigma)^{1/3}(d_E/r_0)^{8/3}/10$, $F_0^T=(\pi/\sigma)^{1/3}(d_E/r_0)^{2/3}/10$, and $F_E^T=F_0^T/4$. The theoretical solar constant and the available SW radiation over a unit area at the TOA are: $F_0^T=1367.95145\,\mathrm{Wm^{-2}}$, and $F_E^T=341.98785\,\mathrm{Wm^{-2}}$. The diluted theoretical solar entropy flux density is $J_0=(4/3)\sigma t_{SUN}^3(r_0/d_E)^2=(4/3)\pi^{1/4}\times10^{-3/4}=0.31566483\,\mathrm{Wm^{-2}\,K^{-1}}$, which is a mathematical constant. The $t_{SUN}^T=(E_0^T/\sigma)^{1/4}=5778.0754$ theoretical solar surface EBT is practically equal to $t_{SUN}=(F_0/d_F/\sigma)^{1/4}=5778.0738\,\mathrm{K}$. The very important point here is the fact that the $F(d)$ theoretical function depends only on geometrical factors (the solar radius and the semi-major axis of the orbit of the Earth) and of course, independent of any short term or long-term satellite or ground based radiation measurements. Consequently, debate on the theoretical F_0^T solar constant should be restricted to the debate on the accuracy of r_0, and d_E. Of course, the barycenter of the solar system and the steady state center of the Sun (as a fixed geometrical point) do not exist. Sun is not a fixed perfect sphere but a rotating and pulsating gas globe which is subject to gravitational perturbations from other members of the solar system. This physical reality reflected in the singularity of the $F(d)$ function at $d\equiv0$ where $F(d)=\infty$.

The reference solar constant F_0^T is mathematically consistent with the radiation laws and the known accuracies of the Planck and Boltzmann constants from NIST. It is also consistent with the recent values of r_0, d_E, and the spectral solar constant in Chance & Kurucz (2010) [34]. The existence of the theoretical solar constant does not support the idea of introducing a kind of new standard solar constant (and the backward correction of previous standards) based on purely the newest satellite observations. The accuracy of flux density or radiance measurements will never conquer the accuracy of the measurements of distance, linear size or time. It looks that the extreme stability of the climate over millions of years is linked to the existence of the F_0^T theoretical solar constant.

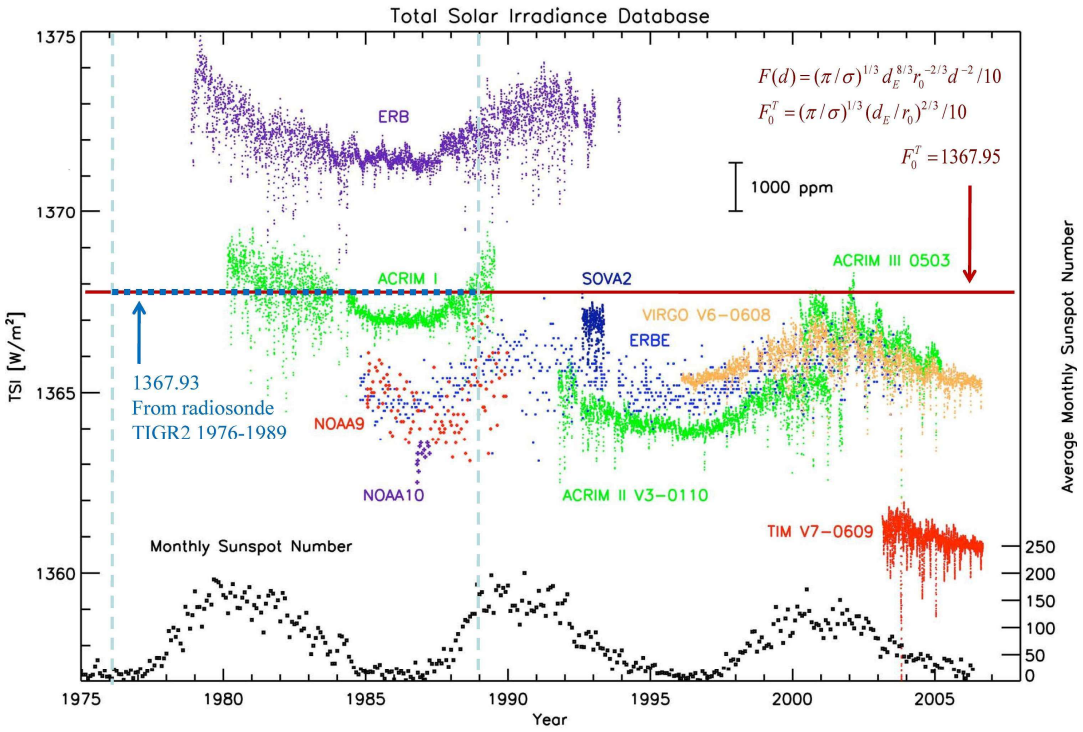

Figure 16: Comparisons of the F_0^T theoretical solar constant with direct satellite observations, and with LW flux density simulations from the TIGR2 archive. The blue dotted line is at $F_0^{obs}=4S_U^A$ and S_U^A is the all-sky global mean surface upward flux density from the APS. The $F_0^{obs}=F_0^T=F_0$ is the indication of planetary radiative equilibrium. All fluxes are in Wm^{-2}.

In Figure 16 F_0^T is compared to the observed F_0^{obs} (quoted under paragraph *2.3*), and the satellite observations from Kopp and Lean (2011) [35]. The $F_0^T=F_0^{obs}=F_0$ equality means that the planet is in strict radiative equilibrium with the theoretical solar constant, where in (23) F_0 mathematically locked to σ, r_0, and d_E.

4.3 Greenhouse gas greenhouse effect

Recently there is a serious problem with the use of the classic definition of the GHG GE. The ambiguity arises from the fact that some scientists recognized that the classic GHG greenhouse effect cannot be discussed without the presence of the global cloud cover and started to use the greenhouse effect terminology in a generalized way, including the cloud effect. For example, in [12] and [13] the authors attribute about ~50 % of the total GE to the H_2O, only 25 % is the contribution of all non-condensing GHGs, and the remaining 25 % is the cloud effect This confusion should be avoided, CO_2 is a greenhouse gas and not a solid or liquid substance. If there is no cloud cover present in an air column one has to talk about the clear-sky GHG greenhouse effect, and in fact, that is what we are interested in.

To answer the question what is the contribution of the individual atmospheric layers to the total greenhouse effect in Figure 17 the vertical distribution of the clear sky greenhouse factor is demonstrated.

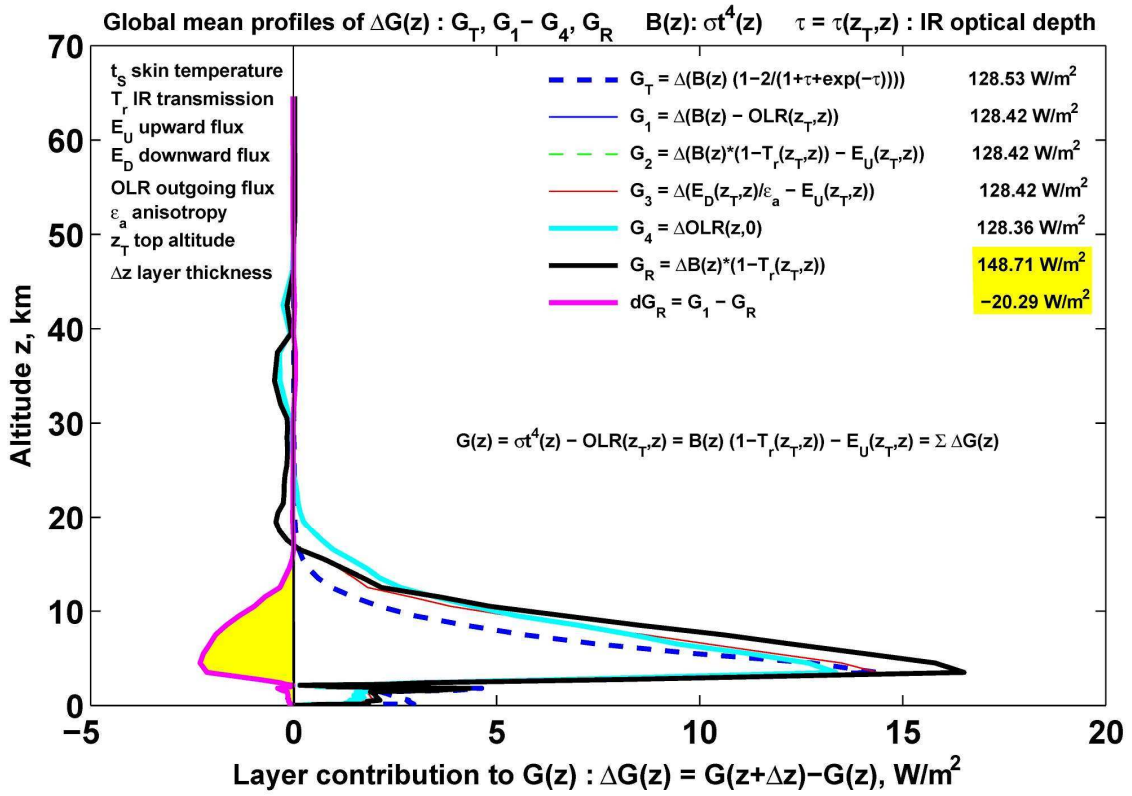

Figure 17: Except G_R the different greenhouse factors (G_T, G_1, G_2, G_3, G_4) are in good agreement. In case of the GAT atmosphere the maximum contribution comes from about 4-5 km altitude.

Apparently, the different numerical computations of the G factors (on the right side) gives consistent results. However, G_R from [10] or from Ramanathan & Inamdar (2006) [36] shows large discrepancy (about 20 Wm^{-2} overestimate). The cause is the incorrect mathematical representation of GF, (see for example equations 1 and 2 in the Nature article [10]). Unfortunately, despite our direct attempt to communicate with the authors, this serious mistake was never acknowledged or corrected, however, this error could effectively invalidate the whole H_2O positive feedback argument in [10].

4..4 Cloud effect

Celestial objects in the Solar system may have no atmosphere at all (Moon), they may have GHG atmosphere which is condensing on the planetary surface (Mars), they may have GHG atmospheres condensing on both the surface and within the atmosphere (Earth), and they may have GHG atmospheres condensing only in the atmosphere (Venus).

Planets may also have diverse set of surface materials which is generally not expected to produce a Bond albedo needed for the planetary radiative equilibrium, see (1,2). It is quite plausible to assume that condensing GHGs in the atmosphere will form an opaque layer of liquid and solid particles (disrupting the propagation of the IR radiation), and will change the Bond albedo in a way that the planetary radiative equilibrium will be established. Theoretically steady state RE of non-condensing semi-transparent GHG atmosphere of a passive planet cannot exist, since the ground surface of such planet would cool down freely to the astronomical limiting temperature depending partly on the local solar constant and Bond albedo, and partly on the outward diffusion of thermal energy from the planetary interior.

In the special case of Earth, the astronomical limiting temperature is practically equal to the temperature of the triple point of H_2O. In other words, at some (sufficiently low) temperature any gas will become a condensing GHG, therefore, without the presence of condensing GHGs in the system there is no atmosphere at all.

The above concept is fully consistent with observations of atmospheres of comets and planets in the solar system. A comet starts to build up atmosphere when getting closer to the Sun and the surface materials start to evaporate. On the reverse trajectory when getting farther from the Sun the atmosphere condenses back to the surface and disappears.

Atmospheres with condensing GHGs might have several internal boundaries (cloud layers) at different altitudes which instantly disrupt the propagation of the electromagnetic radiation, consequently, the global mean cloud cover is the major factor in establishing and maintaining the planetary radiative balance. Note that in gas phase the spectral gas absorption is restricted to certain spectral ranges characteristic of the molecular structure of a particular GHG.

In the interesting case of the thin Martian CO_2 atmosphere − due to the lack of cloud cover − we can only speak of clear-sky GE. The Martian atmosphere contains 33.3 times more CO_2 but the GE is only about ~3 K, indicating that the amount of atmospheric CO_2 is not a major factor in creating the Martian GE. Compared to the ~2.61 prcm of water vapor in the Earth's atmosphere, the Martian atmosphere contains a negligible amount of water vapor (approximately 0.00155 prcm) which is insufficient to form extensive cloud cover and significantly increase GE and GF. In the Martian carbon dioxide atmosphere, the planetary RE is maintained by the diurnal changes of the mass of the GHG atmosphere and the heat (released or received) at the lower boundary by the phase changes of the CO_2. One must conclude that the Earth's clear-sky GE cannot be explained by the CO_2 content of the atmosphere. GE are closely related to the amount of condensing greenhouse gases and their physical state.

In the hot and thick atmosphere of Venus the complex, fully closed multi-layer cloud structure completely decouples the IR radiation field of the ground surface from the *outgoing long wave radiation* (OLR). Below the closed cloud layers, the IR radiation field is a type of cavity radiation in RE. The planetary RE is maintained solely by the radiation from the cloud top (at an effective cloud top altitude) and the atmosphere above. Due to the dramatically different roles of the atmospheric composition, clouds and surface characteristics, the formation and functioning of the greenhouse effect are quite different on the three planets. In Figure 18 the GE of the Martian atmosphere is compared to the GE in the Earth's atmosphere.

In the Earth's atmosphere (14) shows that the planetary radiative equilibrium cannot be established without involving the cloud cover in the greenhouse problem. The concept of the numerical evaluation of the equilibrium cloud cover is presented in Figures 19 and 20.

As a first step we define the $\beta^A(F_A, h^C)$ and $\beta^E(F_E, h^C)$ global mean cloud covers relevant to the TOA and APS radiative balance requirements. From a set of β^A and β^E (computed for large number of different α_B and h^C) and using a multi-parameter optimization algorithm the global average α_B and h^C can be calculated. In the two-dimensional optimization problem, only one global average cloud layer is assumed, and the norm of $\| \beta^A - \beta^E \|$ is to be minimized. As a computational detail, the accuracy of our global average cloud cover largely depends on the vertical resolution of the LBL code used. In our case around 2 km altitude the layer thickness was set to 40 m.

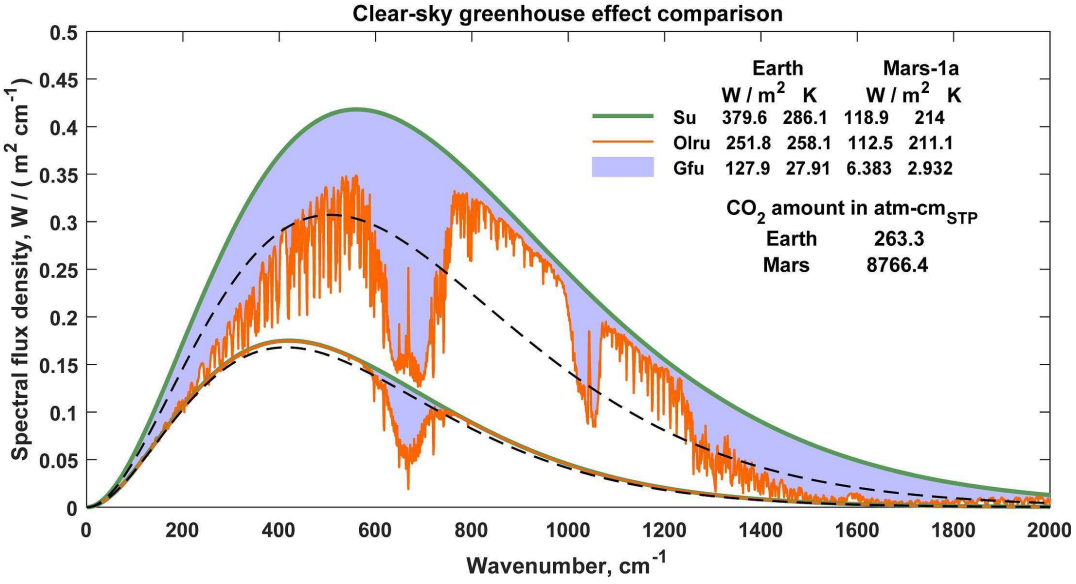

Figure 18: Comparison of the greenhouse effect on Earth and Mars. The clear sky GE, $(S_U/\sigma)^{1/4}-(OLR/\sigma)^{1/4}$ and GF, S_U-OLR are not controlled by the CO_2 content of the atmosphere. The black dashed lines are the EBFs of the two planets.

$$F_A = (1-\beta^A)\,OLR + \beta^A\,OLR^C$$

$$F_E = (1-\beta^E)\,S_U + \beta^E S_U^C$$

$$\beta^A(F_A, h^C) = (F_A - OLR)/(OLR^C(h^C) - OLR)$$

$$\beta^E(F_E, h^C) = (F_E - S_U)/(S_U^C(h^C) - S_U)$$

$$F_A = (1-\alpha_B)F_E$$

$$\min(\,\|\,\beta^A(h^C,\alpha_B) - \beta^E(h^C,\alpha_B)\,\|^2\,)$$

Figure 19: Radiative equilibrium cloud cover constraints. At the TOA LW fluxes from the APS must be equal to F_E, the all-sky outgoing LW radiation must be equal to F_A, and the cloud covers from the two constraints must be equal.

From a 20-year long time series data of ISCCP−D2 in Van Andel 2010 [61] a global mean of 66.38 +/− 1.48 % was reported. In Figure 21 satellite cloud climatology data are in excellent agreement with our theoretical cloud cover of $\beta = 0.6618$. The equilibrium cloud cover must be equal to the theoretical transfer function: $\beta = 2/(1+\tau^T+\exp(-\tau^T))$, where $\tau^T = 1.8676$ is the theoretical equilibrium flux optical thickness. In the case of Earth the CRE situation holds and from the equilibrium equation in Figure 8 follows the $\alpha_B = g^A$ equality. Knowing the accurate β, S_U, and S_U^C the g^A can be checked against the next theoretical equation in [17]:

$$g^A = g/(1+\beta S_U^C/(1-\beta S_U)) + g^C/(1+(1-\beta)S_U/(\beta S_U^C)) = 0.30129061. \qquad (24)$$

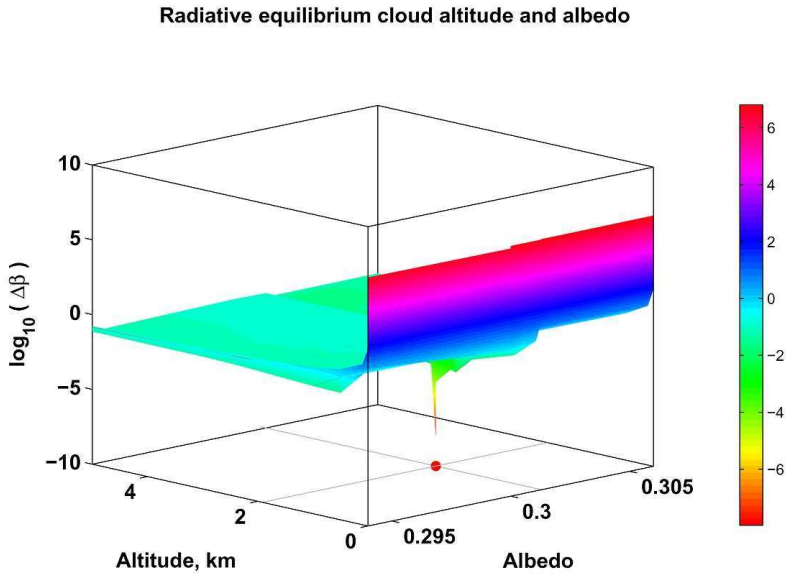

Figure 20: The multi-parameter optimization algorithm. Sharp minimum of the $\| \beta^A - \beta^E \|$ *norm found at* $\alpha_B = 0.30129$ *and* $h^C = 1.9166\,km$.

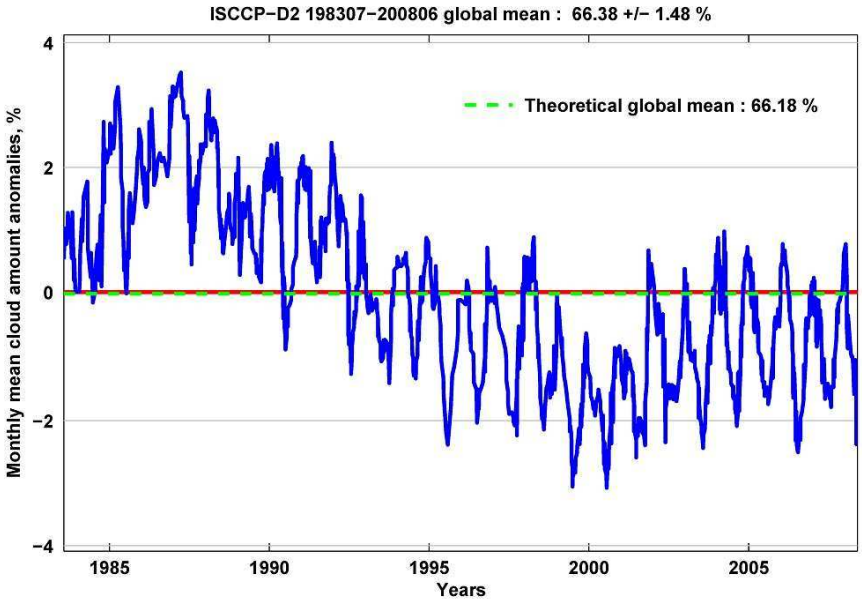

Figure 21: The theoretical cloud cover (green dashed line) is compared with satellite observations in the 1983-2008-time interval (red line). The agreement is well within the uncertainty of the satellite observations.

The $\alpha_B = F_R / F_E = (S_U^A - OLR^A) / S_U^A = g^A = 0.30129061$ equality is evident, therefore, the use of (17) with the S_U^C and β above is quite justified: $t_S = ((F_0 / (4sc) - \beta S_U^C) / (1-\beta) / \sigma)^{1/4} = 286.075\,\mathrm{K}$. This t_S is practically equal to the global average surface radiative temperature from radiosonde observations.

4.5 Water vapor

Compared to Mars and Venus on Earth the planetary RE situation is far more complex. Since the phase changes of the H_2O may happen at any time and anywhere in the system the Earth has an extremely variable cloud, surface ice and snow cover. The combined surfaces where the water vapor is in direct contact with liquid water, snow, and ice will be termed as the phase boundary. Through this hypothetical complex surface the total amount of water vapor in the atmosphere will change by the release or buildup of the latent heat by evaporation, condensation or sublimation. In steady state the net condensation and evaporation associated with rain droplets (within the atmosphere) must be zero and the mass balance of the atmosphere is maintained by the evaporation or sublimation from the ground surface and precipitation or deposition to the ground surface. These processes will result in a decrease or increase of the flux optical thickness which is coupled with the mass exchange trough the lower boundary.

The total mass (or the potential energy) of the atmosphere and the flux optical thickness are controlled by the virial theorem, (see [17]). The mass conservation in the hydrological cycle expresses indirectly the conservation of the flux optical thickness.

The observed and theoretically predicted constant flux optical thickness (see [27]) is plain proof of the climate control by the water cycle. In other words, increasing or decreasing the energy input to the system will result in the release or storage of the required amount of radiant or thermal energy through the phase boundary to assure the radiative equilibrium while keeping the temperature of the phase boundary unchanged.

To clarify further the water vapor feedback problem, from the NOAA-S archive 689 high quality all-sky radiosonde observations were processed to show the relationship between the local mean layer temperature and water vapor column density. During 1992-1993 from the high resolution (6 second) data 654130 individual layer mean temperature and water vapor column density pairs were collected.

In Figure 22 the primary measured relative humidity and the computed H_2O column density profiles are plotted showing no correlation. The H_2O column density directly enters to the LBL computation of the layer flux transmittance and optical thickness.

In Figure 23 the linear correlation coefficient between the temperature and natural logarithms of the column density is 0.99, which − considering the relevant quantitative theoretical relationships − is not a surprise. The light blue dot around 5 km (in the right plot) is the observed maximum altitude of the H_2O condensation temperature at Sterling. Many climatologists mistakenly call this relationship as positive feedback. It must be clear that locally the temperature and water vapor content of the air parcels are alternative variables, and they are not connected by some ad-hoc positive or negative feedback parameter.

According to thermodynamics phase transitions are controlled by the changes in the molar free energy and entropy. In view of the known analytical dependence of the ambient temperature on the water vapor content (of an individual air parcel) the whole positive H_2O feedback hypothesis seems to be nonsense.

In Figure 24 we show the dependence of the CO_2 and H_2O column amounts in 7 different NOAA-R1 time series. The column amounts were computed in two sections: the lower part (green dots), the upper part (red dots), and also for the total air column (blue dots). While below about 2 km both the H_2O and CO_2 increased, above 2 km the relationship reversed. The net effect for the whole air column is decreasing H_2O with increasing CO_2 (with a sufficiently large linear correlation coefficient).

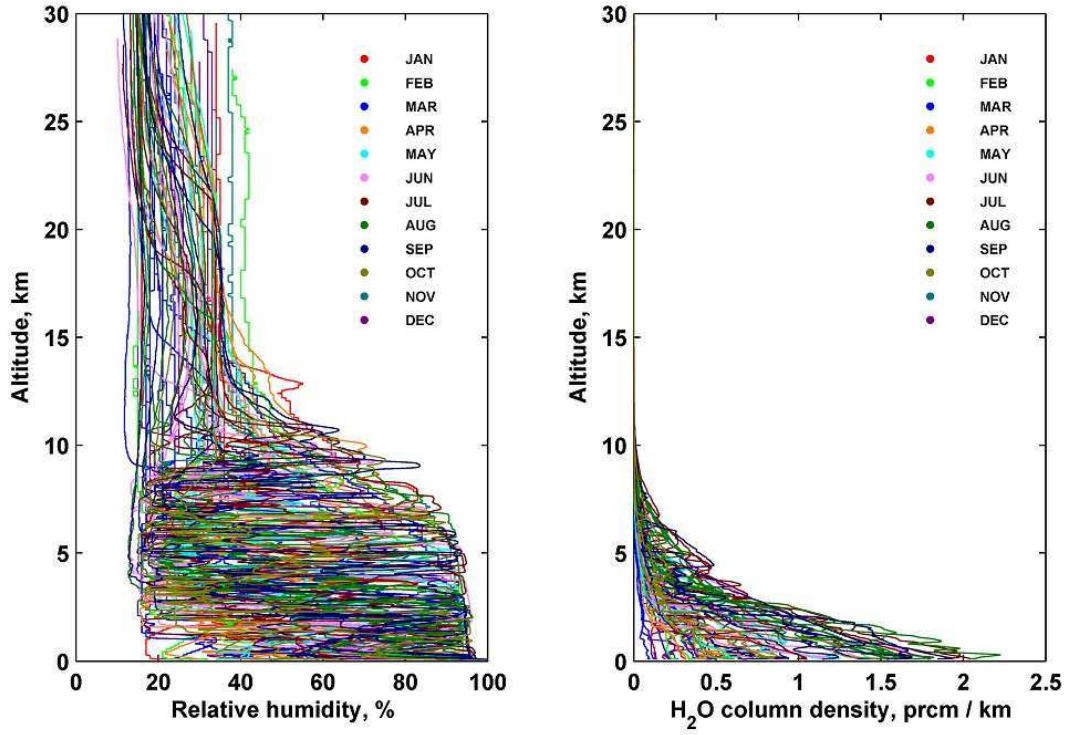

Figure 22: High resolution radiosonde observations from NOAA Sterling, Virginia. The left panel shows, that the tropospheric relative humidity is a true stochastic component of the climate system.

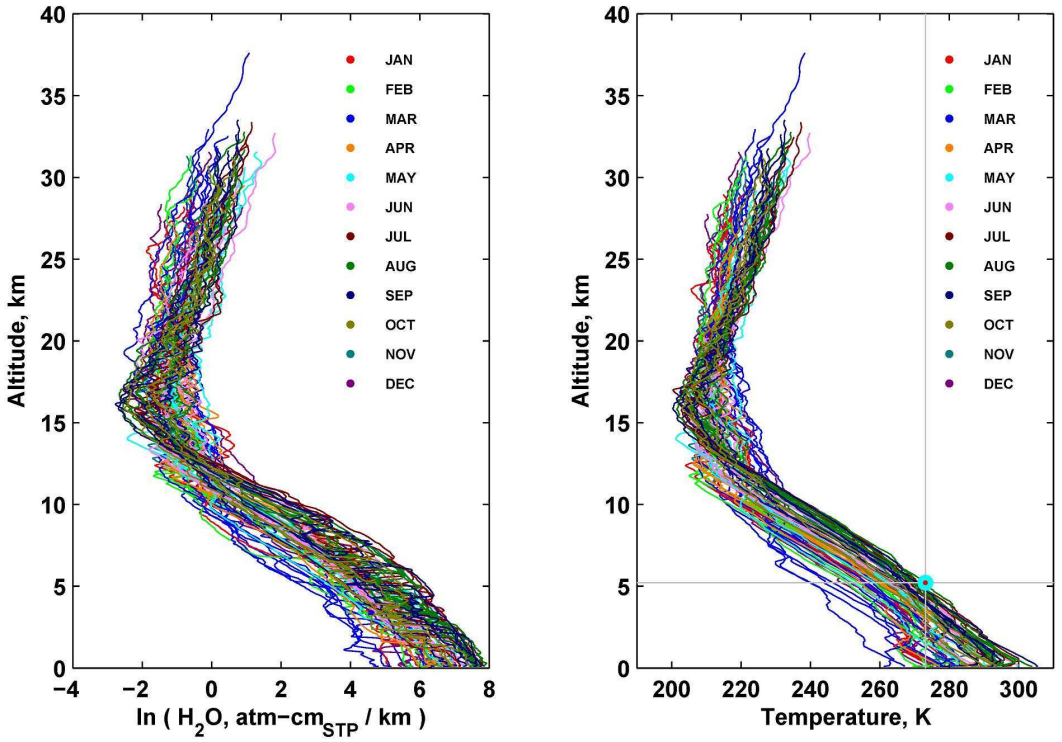

Figure 23: High resolution radiosonde observations from NOAA Sterling, Virginia. The temperatures and H_2O column density are highly correlated, and they follow the relevant theoretical relationships.

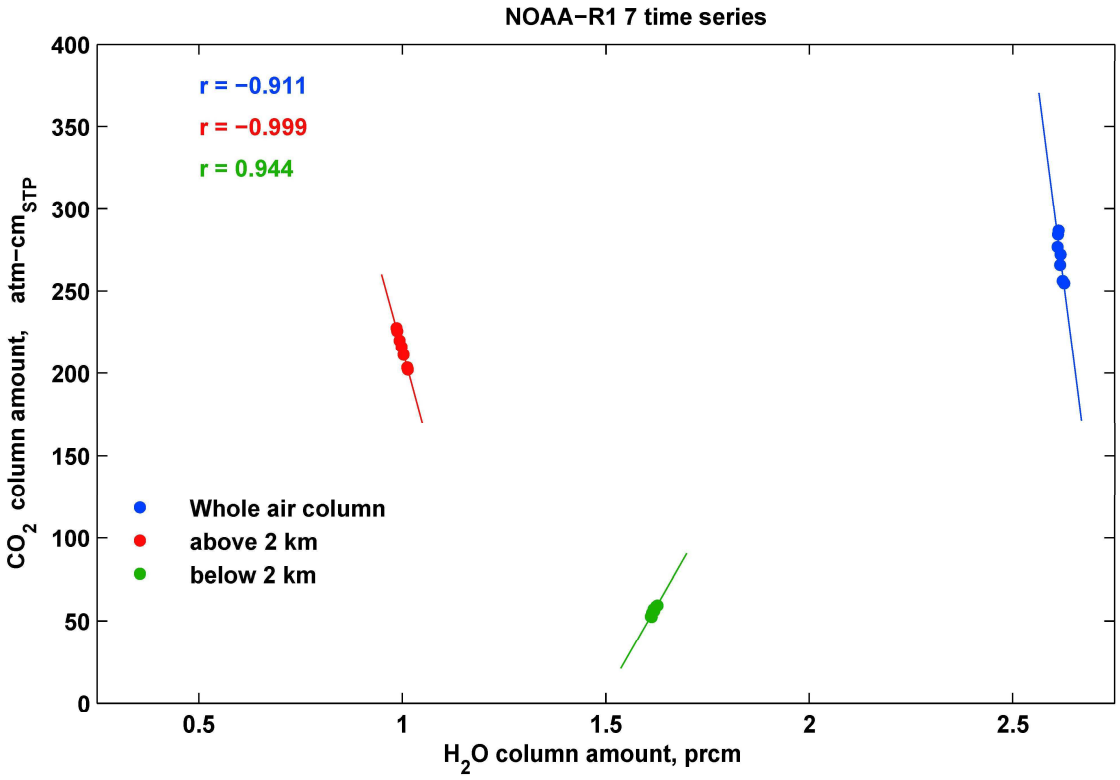

Figure 24: Changes in the CO_2 and H_2O column amounts in the 7 NOAA-R1 time series (presented in Figures 10, 11, and 12).

The blunt statement of the IPCC on the positive water vapor feedback mechanism is probably based on the increasing H_2O in the lower atmosphere with increasing CO_2 (green dots). However, the response of the dynamical system evidently coupled with reduced H_2O in the upper levels, in such a way, that the net change of H_2O in the total air column is negative. One should not forget that this figure is not proof that increasing CO_2 concentration will decrease the water vapor. Rather, it is proof that the system may adjust its IR absorption properties to the actual CRE requirements by restructuring the vertical water vapor distribution.

4.6 Energy budget cartoons

The usual way to support the idea of the classic greenhouse effect is to present planetary energy budget schemes where the global radiative flux density components as well as the sensible and latent heat fluxes in the system are estimated either from direct measurements or from radiative transfer computations.

The most well-known is the Kiehl & Trenberth (1997) [39] energy budget. In Miskolczi (2014) [17], based on 13 years of radiosonde observations, it was first shown with high degree of accuracy that the Earth-atmosphere system is in the state of radiative equilibrium. The *radiative imbalances* at the upper and lower boundaries of the atmosphere that appear in peer-reviewed radiative budget cartoons (Trenberth et al., (2009) [40]; Stephens et al. (2012) [41]; Wild et al. (2012) [42]; NASA (2010) [38]) do not exist. The radiative equilibrium stems from energy conservation and energy minimum principles and it is the natural state of the Earth-atmosphere system. So far none of the published planetary energy budgets give any bearing to the origin and physics of the atmospheric greenhouse effect and unfortunately, almost all of them suffer from serious errors in the methodology and evaluation. Some of them are listed below.

1. Quantitative discussion of the greenhouse effect should be based on the strict, detailed, clear, and physically meaningful definition of the phenomenon. For example, in Schmidt et al. (2010) [12] and Lacis et al. (2010) [13], we see published totally misleading quantitative results about how the share of the present-day global GE is distributed between GHGs. They state that the contributions of H_2O and CO_2 are 50 % and 20 % subsequently. In common understanding these data means that the CO_2 absorption in the 15μm band is about half of the absorption of the H_2O in the whole IR, which is sheer nonsense.

2. Due to the heavily overlapping nature of the terrestrial spectral radiation field it is mathematically impossible to decompose the flux optical thickness into the contributions of the individual molecular species, (see [16], Appendix A). The LBL computational technique was developed to remove the uncertainties due to the spectral overlaps of the absorption coefficients of different GHGs.

3. Clouds (or any kind of solid or liquid particles in the atmosphere) radiate continuous IR spectra and have nothing to do with the IR spectral absorption of the greenhouse gases. The cloud forcing approach to the greenhouse problem does not help to clarify and quantify the planetary radiative budget. The $F_E = S_U^A$ and $F_A = OLR^A$ equalities show clearly that the global average atmosphere is in radiative equilibrium with a well-defined t_S surface temperature, β cloud cover and the equilibrium cloud top temperature.

4. From the confirmed $G^A = S_U^A - OLR^A = F_R$ and $F_E = S_U^A$ equalities follow the conservation of radiant energy, radiative equilibrium, and they give solid empirical support to the theoretically introduced equivalent blackbody temperature. Because of the two-layer structure of the global average atmosphere the ground surface referenced GE cannot contain any dependences on the albedo, cloud cover, radiative temperature, LW absorption, or flux optical thickness, rendering the GE to observations of t_S, and OLR^A, and leaving the greenhouse problem entirely to the mercy of the GCMs and their unphysical assumptions and countless ad-hoc tuning parameters.

5. No quantitative constraints on the shortwave system albedo, cloud cover and cloud altitude are established. These are key climate parameters, and some kind of theoretical expectation must be referenced or developed. The steady state planetary radiative balance is abandoned in favor of a hypothetical man-made greenhouse warming. In science the quantitative estimate of 0.6 ± 17 Wm^{-2} missing heat in Stephens, 2012 [41] means that climatologists have no idea why and how the hidden (thermal and radiant) energy is distributed among the different latent heat reservoirs.

6. In the budgets the global mean thermal and GHG structure of the atmosphere is not specified. Generally, the LW fluxes relevant only to the USST76 are used as the global average. The most recent [38] budget (presented in Figure 25) adopted the flux density components from the [39] radiative budget which is obviously wrong. Transmitted flux densities from the surface (40 Wm^{-2}) in [39] were computed for the USST76 atmosphere and its 390 Wm^{-2} surface upward flux. 15 years later, in the NASA picture the corresponding fluxes are 40.1 and 398.2 Wm^{-2} which is nonsense. About ~10 Wm^{-2} increase in surface upward flux and practically unchanged surface transmitted flux density deserves some explanations. Another problem is the net non-radiative flux density into the atmosphere which supposed to be zero for an isolated planet.

7. Due to the fatal mistake of using the USST76 atmospheric model, not even one flux density component is close to the ones from the GAT structure. The 0.6 Wm^{-2} fictitious missing heat (white number) is meaningless and violates energy conservation principles (atmospheric Kirchhoff law). For reference, our simulated flux density terms are inserted (black numbers). In the blue and red squares are the top of the atmosphere and the surface referenced flux components.

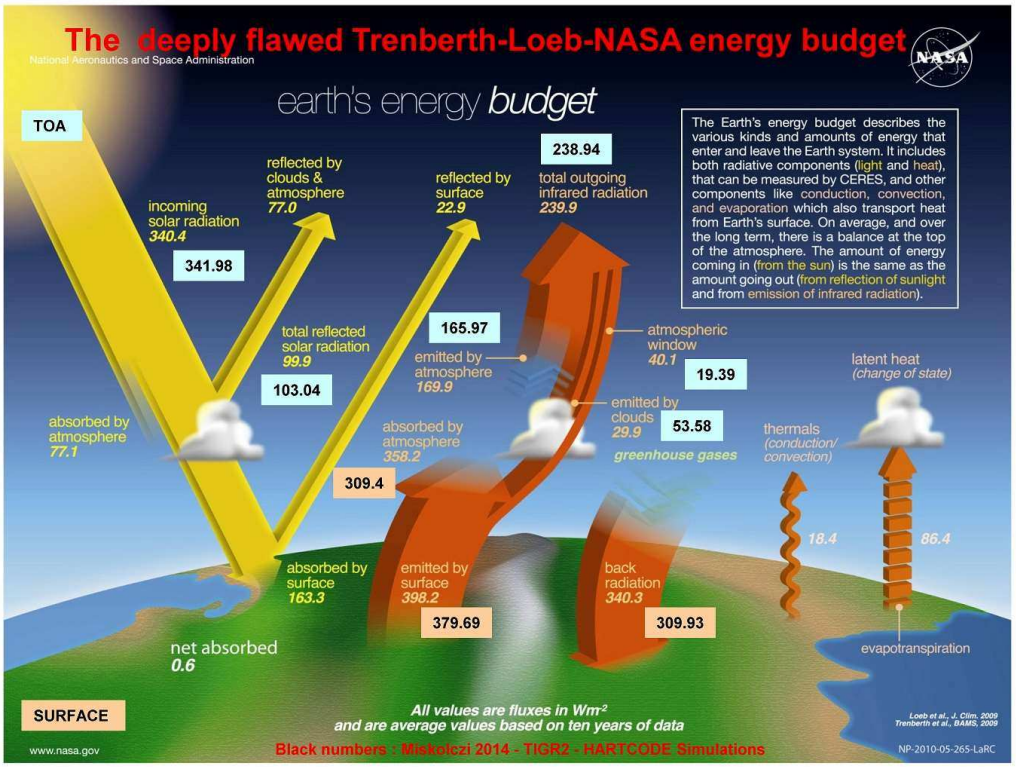

Figure 25: All-sky energy budget of the Earth-atmosphere system, adopted from NASA.

8. The most serious problem with the cartoons is the ignorance of a long line of well-known fundamental concepts and principles of theoretical physics. Some of them are: energy and momentum conservation principles of the radiation field, Wien's law, virial theorem, energy minimum principle, Maxwell rule, Kirchhoff law, Helmholtz reciprocity principle, Vogt-Russel theorem, Braun-LeChatelier principle. Apart from the ignorance of the newest laws of atmospheric radiative transfer, one has to observe that the complexity of the climate system is not a free ticket for violating the first principles of physics.

Further on, it is not apparent that climatologists have access to an accurate RT software for the calculation of correct atmospheric flux densities. Note, that remote sensing applications use high accuracy inter-calibrated LBL radiance codes developed for special applications. However, there is a long way to go to arrive at a correct LBL flux density software from simple directional LBL radiance-transmittance codes.

4.7 Deliberate data manipulation of climatological data

We have discovered that vital climatological data sets were deliberately manipulated. The verification of the planetary energy budget and radiative balance require high quality primary information from global scale radiosonde observations. If the radiosonde observations are wrong then no one will trust in the satellite retrievals of the temperature, humidity or ozone structures. Satellite products depend on the calibration and tuning (of the instruments and retrieval algorithms) based on the ground truth information.

The common mistake of the climatologists is to assume that satellite information is always correct, no matter what. This is not true; satellite information cannot ever be more accurate than the ground truth.

It should be kept in mind that most of the vital flux density components cannot theoretically be measured by any instrument. For example, the so called windows radiation (usually defined in the 721-1260 cm^{-1} spectral range) is not a good representation of the true S_T surface transmitted flux density. That is, the S_T (or S_T^C) flux density component can never be accurately measured even by broad-band or ideal Fourier spectrometers.

Scientists must also be aware that government research institutions may deliberately manipulate their databases to reflect their wild imagination on how the GE works. A good example is the NOAA-R1 archive which was used in our trend analysis study in Miskolczi, 2010 [27]. This global archive shows consistently that between 1948 and 2008 the flux optical thicknesses from the profiles are equal to the theoretical τ^T of 1.867 (see Figure 9).

However, the true equilibrium optical thickness of the NOAA-R1 time series is $\tau_E = 1.937$ and it is far off from τ^T, which is a sign that none of the annual mean profiles are close to the radiative equilibrium. The $\tau_E - \tau^T = 0.06$ optical thickness difference corresponds to about 250 % increase in CO_2 concentration. This is of course impossible; the Earth cannot be out of radiative balance by about 4 Wm^{-2} at the TOA for 61 years.

Such a situation can only happen by altering the thermal structure (especially the close to surface temperature field). Much more serious is the problem with the USST76 atmosphere and the [39] budget, where due to the unrealistic temperature and humidity structure the imbalance in the OLR at the TOA is about 29.38 Wm^{-2}. The NOAA-R1 archive may be used for trend analysis, but − because it violates the energy conservation principle − it is useless for global energy budget research.

Other examples are the TIGR2 and the updated TIGR2000 archives. A closer look at the TIGR2000 revealed that more than half (915 out of 1761) profiles are coincidental, and they are included in both archives. The humidity and ozone structures in those coincidental profiles were poorly modified in an obvious way that the original thermal structures were preserved.

The authors of the database should have known that the H_2O, O_3, and the thermal structures in real atmospheres are highly correlated, which property is widely used in water vapor and ozone statistical retrievals from satellite spectral measurements.

In Figure 26 we present one sample (out of the 915 manipulated profiles) where the increased H_2O and ozone content resulted in increased flux optical thickness (to a value corresponding to CO_2 doubling). The left plot shows the unchanged temperature profile, the right two plots show the manipulated H_2O and O_3 profiles respectively.

As a result of the data manipulation the TIGR2000 archive now contains 915 unrealistic atmospheric structures (mostly with increased upper tropospheric humidity and ozone amounts) which makes the database useless for both remote sensing and radiative budget applications. Creating fake radiosonde observations to support the belief in CO_2 GE based global warming is not a scientific approach.

The upper tropospheric humidity problem (if there is any) will not be resolved by artificial increase of the humidity data in the raw radiosonde observations. Unfortunately, there is evidence of extended data manipulations in other climate data sets that renders the whole climate science to a hiding game, and largely reduces the chances to obtain scientifically sound answers to the role of the GHGs in the global warming.

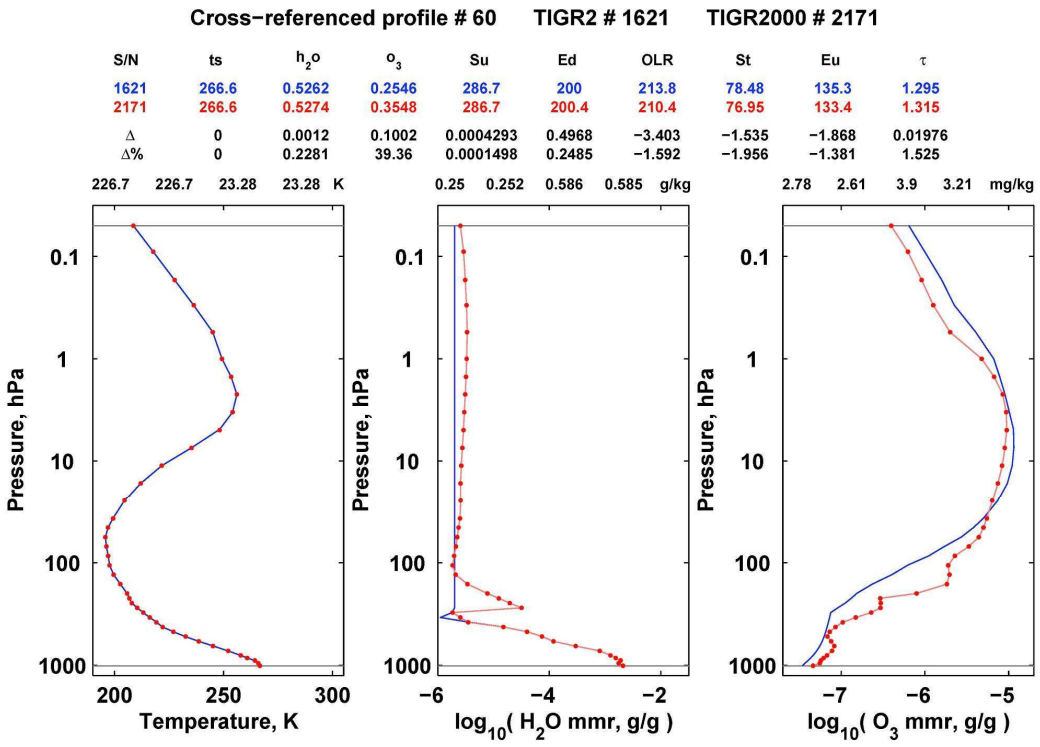

Figure 26: Evidences of large scale data manipulation in radiosonde observations. Comparing the two versions of the TIGR database shows that in more than 50 % of the profiles the upper tropospheric H_2O and O_3 mass mixing ratio were increased (red dots). In this example the changes resulted in 3.4 Wm^{-2} decrease in OLR and significant increase in the flux optical thickness.

4.8 Overview of spectral flux density components

Summarizing our quantitative results in Figures 27, 28, and 29 the spectral distributions of the most important flux density components are presented. The spectrally integrated fluxes are accurate up to 4-5 significant digits. In these figures the meaning of the subscript 'A' (in t_A and t_A^{NASA}) refers to the global mean emission temperature of the Earth for the GAT atmosphere, and for the NASA (computed from the EBTs of the all-sky OLRs).

In Figure 27 the $B(t_A) = B(t_A^{NASA})$ and $B(t_S) = B(t_S^{NASA})$ equalities are indications that the GAT atmosphere is very close to the real global average atmospheric structure. The black dotted line(over the yellow line) is the Planck blackbody curve of the GAT t_e^{bt} mean color temperature showing the maximum entropy of the OLR^A.

While the surface referenced equilibrium clear sky GF ($\sigma t_S^4 / \varepsilon_A - OLR = 154.5$ Wm^{-2}) has no clear physical meaning, in Figure 28 the APS referenced GF can easily be associated with the deposited momentum by the reflected radiation: $G_{APS} = S_U^A - OLR^A = F_0 \alpha_B / 4 = 103.04$ Wm^{-2}. In the figure G_{APS}^e (black curve) is the Planck blackbody function of the EBT of the G_{APS} (206.47 K). This temperature is apparently equal to the SW effective equivalent reflection temperature: $t_R = (F_R / \sigma)^{1/4} = 206.469$ K.

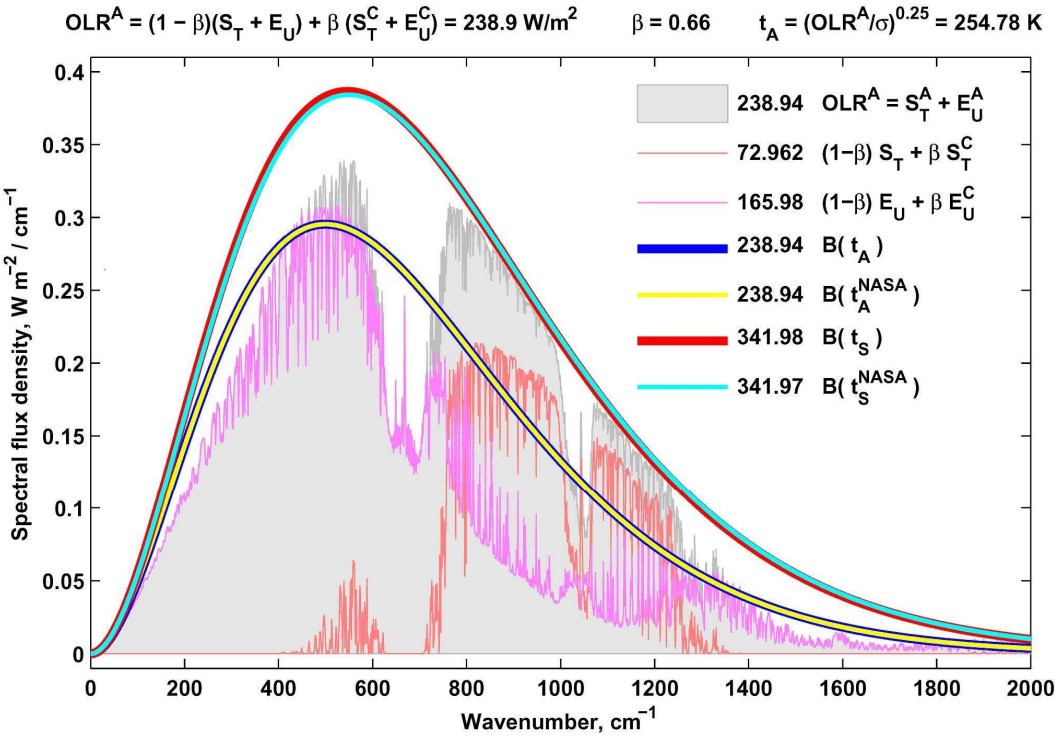

Figure 27: Flux density spectra of the all-sky GAT atmosphere. The equivalent blackbody spectra $B(t_A)$ *and* $B(t_S)$ *from GAT are equal to the equivalent spectra from* $B(t_A^{NASA})$ *and* $B(t_S^{NASA})$.

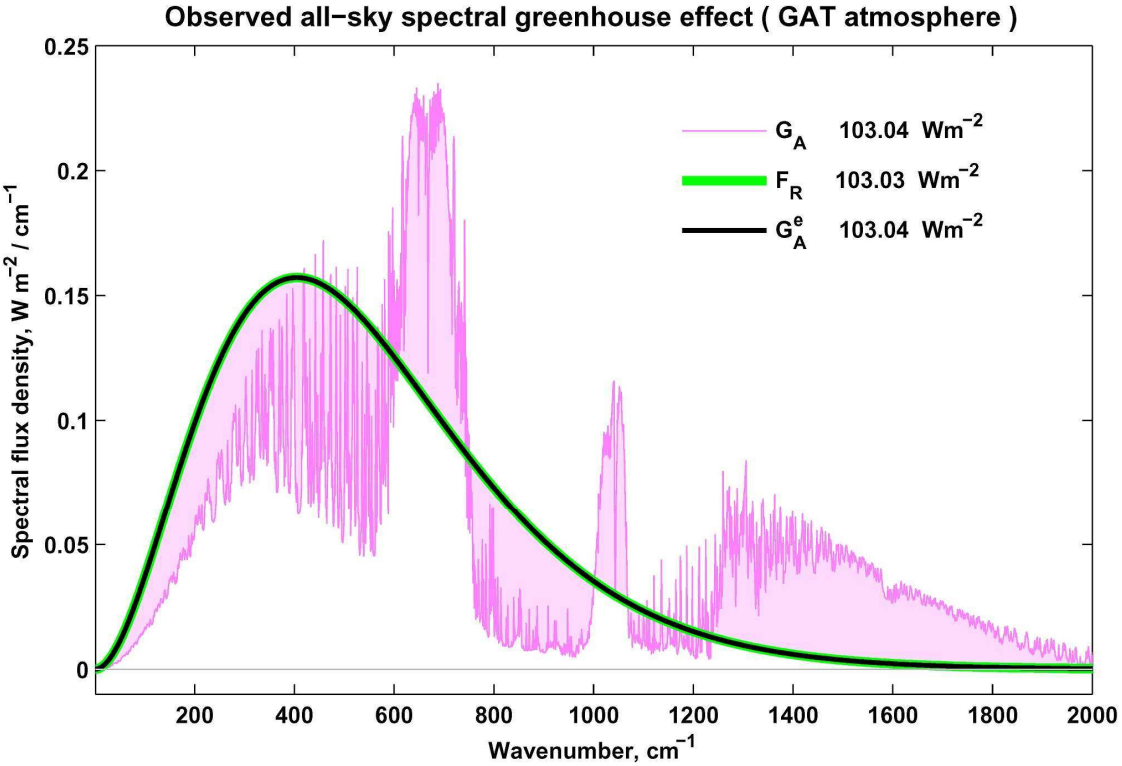

Figure 28: Spectral all-sky greenhouse effect referenced to the APS. The integrated flux densities from the G_{APS}^{e} *and* F_R *curves agree quite well.*

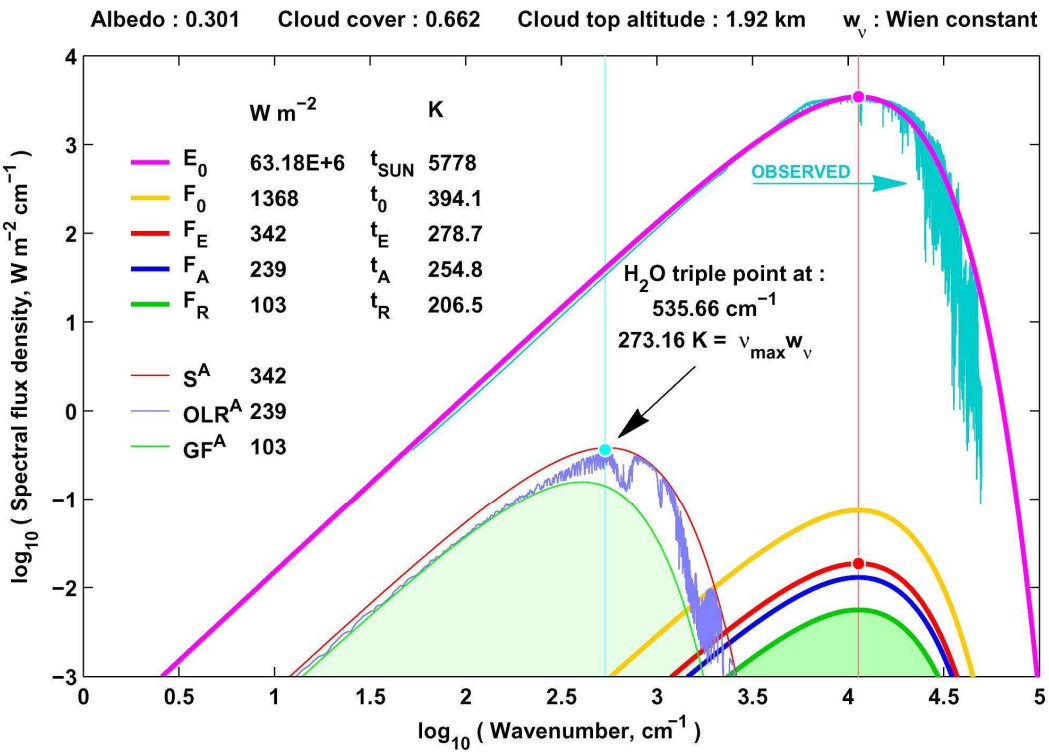

Figure29: Solar and terrestrial equilibrium blackbody spectra. The observed solar reference spectrum (dark cyan line) is from the Chance and Kurucz, 2010. The light blue line is the observed TOA OLR_ν^A *from the TIGR2 radiosonde archive.*

In Figure 29 all the SW and LW equivalent effective blackbody fluxes of the Sun-Earth system are presented. One must recognize, that at large, the Earth-atmosphere system is nothing but a converter of the low entropy SW solar radiation to maximum entropy terrestrial radiation. Theoretically the J^A entropy flux density of OLR^A may be expressed by the maximum of the spectral flux density of OLR^A: $J^A = c_e OLR^A_{\max,\nu}$, where $c_e = 4.2337344\,\mathrm{cm^{-1}K^{-1}}$, and $OLR^A_{\max,\nu} \approx 0.338\,\mathrm{Wm^{-2}/cm^{-1}}$ (at $\nu_{\max} \approx 535\,\mathrm{cm^{-1}}$). The light blue dot shows that the Earth has a special orbit where the Wien temperature is equal to the t_P phase temperature of the H_2O. Obviously the empirical spectral OLR^A has the maximum entropy flux density. The Wien constant in wavenumber representation is $w = 0.50994751\ \mathrm{K/cm^{-1}}$.

4.9 Comments on the new view of greenhouse effect

Almost all attempts to publish the results presented in this paper failed. Articles were routinely rejected by the mainstream scientific journals − Science, Astrophysical Journal, Tellus, Journal of Quantitative Spectroscopy and Radiative Transfer, Journal of Geophysical Researches etc. − mostly without sending for review. For example, the review of the Hungarian Science magazine (Magyar Tudomány) rejected the publication of the above results saying that it should be published first in some elite journals. Probably this is the reason why it is hard to find any useful critical comments on the presented quantitative results in the peer reviewed literature.

However, the blogosphere is flooded with academically illiterate comments from self-declared experts. As an example, it is worth reading the comments of A. Lacis (moderated by J. Curry at her Climate Etc. blog) on the Miskolczi's article [17].

The whole comment is just an ad hominem attack, probably motivated by the lack of his knowledge of basic radiative transfer concepts. There is a number of posts and comments on various websites like J. Curry, Science of Dooms and Real Climate etc. They don't deserve to be repeated in this journal.

They do not sound very scientific. Let us have a closer look into the *best* rebuttal. In Spencer 2010 [59] he wrote an *executive summary* on my [27] E&E article. Spencer simply ignored the important fact that in the whole article I dealt with clear sky conditions only. Since the clear and all sky fluxes are not directly (and quantitatively) comparable, his numerical comparisons with the [39] radiative budget is totally meaningless.

He is also, in my opinion, confused in a series of radiative transfer details: does not comprehend what anisotropy means and how to compute it (he called the spherical emissivity a *fudge factor*), what is the flux density form of the Kirchhoff-Planck relationship, what is the Virial theorem and how to apply it, what is directional and flux optical thickness.

If the blog comment above − without correct quantitative references to my well documented computational results − represent the matured opinion of the global warming community on the greenhouse science, then certainly the open scientific discussion must be improved on this topic.

One should remember that real science cannot ever be settled. Planetary climate science is not an exception; it will eventually make its progress with or without the 'consensus' of the politically oriented IPCC. The various hypotheses and approximations must be scientifically evaluated and eventually rejected, accepted or improved.

It is worth to look at what the consensus science means regarding the global mean surface radiative temperature. In Figure 30 we compare theoretical and empirical temperatures (in ºC) of the GAT atmosphere and some published temperatures in the mainstream literature in the last 30 years.

The title of the figure shows the theoretical equations (17) and (21), and there are other 20 numbered equations (inside the figure) giving the surface upward flux density S_U as the function of different flux density components and other RT parameters. The black dots are temperatures computed from the 20 equations via the SB law, the average is 12.93 ºC, and the standard deviation is 0.87 % (of the mean).

The red line is the GAT radiosonde observations which perfectly agrees with the (17,21) theoretical expectations. The magenta line with the black '+' symbols are the temperatures of the APS computed form F_E and S_U^A (5.53 ºC) apparently agreeing very well.

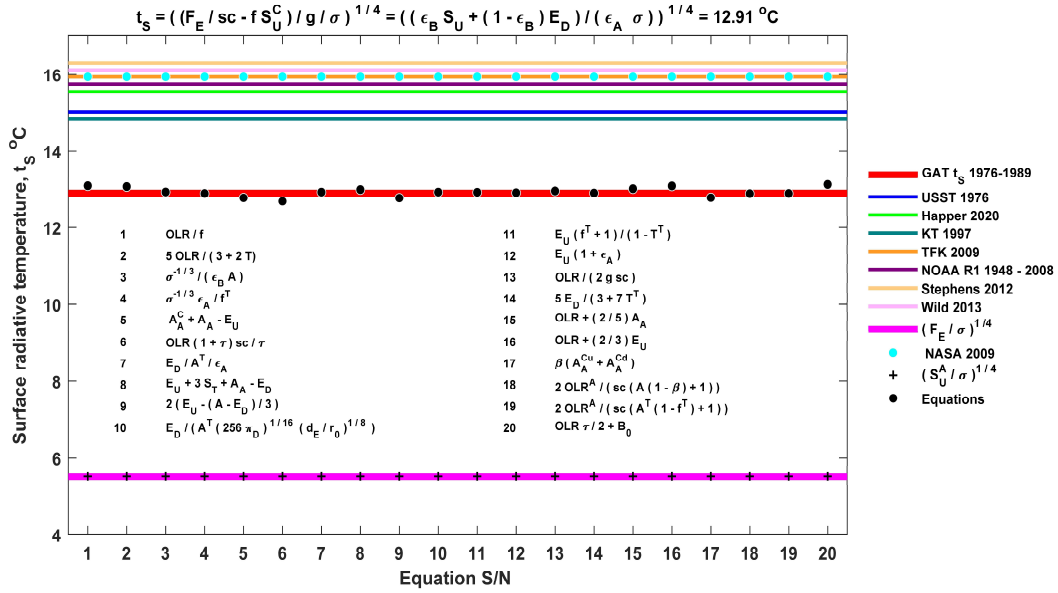

Figure 30: The global mean surface temperature from real science and from IPCC consensus. The published surface temperatures above 15 °C (in the upper part of the plot) are all erratic, they are more than 2 °C warmer than the real observed and theoretically expected ~ 13 °C. The public may deserve to know this information.

The upper part of the figure shows the diverse surface temperatures published in the peer-reviewed elite journals by the IPCC followers. None of them are anywhere close to the observed reality therefore they are useless for any climate study. No one may seriously expect to quantify a hypothetical small GHG surface warming effect if the initial surface temperature has an error of a magnitude larger.

5. Summary

The classic GH effect hypothesis is not a theory and it is unable to establish the required quantitative relationship between the GHG content of the atmosphere and the planetary surface temperature. In climate science the arbitrary definition of the GE is not suitable to associate the heat absorption properties of the atmosphere with the amount of GHGs present in the atmosphere. The reason it is invalid is the two-level radiative structure of the atmosphere and the unlimited supply of the water vapor in its three phases.

In addition to this the strongly stochastic nature of the humidity field makes the tracking of the phase changes of the H_2O impossible therefore the quantitative knowledge on the changes of the dynamical optical thickness (that is related to the phase transitions of the H_2O) is unknown. The large number of new physical relationships − and new universal constants of radiation physics − converging to form a coherent picture of the planetary IR radiative processes which ultimately establishes the correct radiative budget of the Earth-atmosphere system. Compared to surface and satellite flux density observations the rigorous numerical testing of the new equations has not produced any contradictory results. The new equations and constants were presented in a series of published papers, open conference presentations, and in NASA science team meetings. So far neither the equations nor the numerical results were openly challenged by radiative transfer experts or wider climate science community.

The theoretically constant equilibrium flux absorption coefficient of the Earth's atmosphere negates the existence of the Arrhenius type greenhouse gas greenhouse effect. If there are no changes in the greenhouse effect, then there is no climate sensitivity to man-made increase of the atmospheric CO_2. The excess optical thickness from increased CO_2 will condense into water droplets and will rain out from the atmosphere without the IPCC or government permission. Alternatively, structural variations in the global wind and humidity field, or the cloud cover may easily restore the equilibrium flux optical thickness. Evaluating the global average flux density components from ground truth observations it is evident, that the Earth-atmosphere system is in CRE with a theoretical solar constant. Some simple empirical manifestations of this equilibrium include:

1. equality of the Bond albedo and the empirical normalized all-sky greenhouse factor referenced to the APS:
   $g^A = G^A / S_U^A = \alpha_B = 0.3013$;
2. equivalence of the APS referenced greenhouse factor and reflected solar flux:
   $G^A = (S_U^A - OLR^A) = F_R = \alpha_B F_0 = 103.04\ \mathrm{Wm^{-2}}$;
3. equality of the sum of the radiative fluxes from the cloud top and cloud base and the total infrared radiation absorbed in the three regions of the atmosphere:
   $S_U^C + S_D^C = A_A + A_A^C + A_A^{Cu} + A_A^{Cd} = 653.8\ \mathrm{Wm^{-2}}$;
4. constancy of the global average atmospheric equilibrium infrared flux optical thickness:
   $\tau^T = \tau = \ln(S_U / S_T) = 1.86756$;
5. constancy of the radiative equilibrium water vapor column amount:
   $w = w^0 / (1 - 4T) = w^0 / (1 - 4T^T) = 2.612$ prcm;
6. theoretical and empirical equivalence of the cloud cover, transfer, and virial functions:
   $\beta = f = V = f^T = 0.661$;
7. equivalence of the theoretical intercepted absorbed available solar flux density from astronomical parameters and the empirical all-sky planetary TOA IR fluxes from the APS:
   $F_A = F_0(1 - \alpha_B) = OLR^A = S_T^A + E_U^A = 238.95\ \mathrm{Wm^{-2}}$;
8. equality of EBT of the intercepted available solar radiation over a unit area and the empirical EBT temperature of the APS:
   $(F_E / \sigma)^{1/4} = (S_U^A / \sigma)^{1/4} = 278.68$ K;
9. equality of the theoretical solar constant, empirical solar constant, and the long term observed average solar constant:
   $F_0^T = F_0^{OBS} = F_0 = 1367.95\ \mathrm{Wm^{-2}}$;
10. equality of the above cloud downward flux and the above cloud OLR:
    $E_D^C = OLR^C = 155.58\ \mathrm{Wm^{-2}}$;
11. equality of the simulated phase temperature and the H_2O triple point temperature:
    $t_P = (\sigma^{-1/3} + \varepsilon_A^{1/4} t_S) / 2 = 273.18$ K.;
12. equality of the SW and IR anisotropy factors:
    $\varepsilon_A = E_D / A_A = \varepsilon_A^T = 2^{-1/2} t_0 / (t_0 / \sigma)^{1/4} = 0.965153$;
13 equality of the surface radiative temperature from the Kirchhoff law, the solar constant, and from radiosonde:
    $t_S = (E_D / (A\varepsilon_A \sigma))^{1/4} = ((F_E / sc - \beta S_U^C / (1 - \beta)) / \sigma)^{1/4} = 286.06$ K;
14 equality of the SW virtual temperature and the empirical virtual temperature:
    $\hat{t}_0 = (t_0 / \sigma)^{1/4} = ((2(S_U^A + OLR^A / (1 - g^A)) / \sigma)^{1/4} / \sigma)^{1/4} = 288.744$ K;
15 equality of the SB constant from fundamental physical constants and from astronomical parameters:
    $\sigma = 10^{-4}(2/3)\pi^5 \mathrm{c}_2 / \mathrm{c}_1^4 = (d_E / (r_0 F_0^{3/2}))^2 \pi_D = 5.669833697 \times 10^{-8}\ \mathrm{Wm^{-2}K^{-4}}$

Science is not a talk-show, all arguments and critiques against the new view of the greenhouse effect must be quantitative. If this situation remains for long, then the system of new equations will be upgraded to the *only greenhouse theory* which explains the observed facts and obeys the fundamental principles of physics. The easily verifiable numerical facts mentioned above are only a fraction of the infinite number of possible quantitative relationships that all ensure the stability of the Earth's climate.

Scientific facts are stubborn things, they cannot be changed by fraud, misinformation, manipulation of climate data, censorship or democratic voting. Unfortunately, understanding the greenhouse effect phenomenon requires detailed knowledge of radiation physics, which can only be expressed in complex mathematical relationships, equations and formulae. Basic principles of radiation physics are not expected to be known by the general public, nor by climatologists, environmentalists and politicians who are boldly making statements on the subject but are not familiar even with the simplest physical concepts.

A good example is the most recent public announcement of a Hungarian politician Orsolya Ferencz who recently declared in a TV show that the Miskolczi Greenhouse Theory (MGT) is *officially invalid*, Ferencz (2022) [58]. It is clear, that the only purpose of her politically motivated statement is the misinformation of the people and, as such, it has no scientific value. Obviously, her scientific background information on the atmospheric radiative transfer is missing, and unfortunately, she has no idea about the falsification protocol of a scientific theory. One should remember that in the Middle Ages there was an official, government-approved view of the structure of solar system and how the inquisition worked to suppress new ideas. I hope climate science will proceed in a better way.

6. Conclusions

In this article all the arguments are focused on the theoretical and observational issues of the greenhouse effect and not on the question whether the global surface temperature is changing or not. The most valuable result of this research is the theoretical foundation of the observed radiative structure of the Earth's atmosphere. A long line of new radiation laws and their empirical validation together constitute the backbone of the physics of the greenhouse effect. Our planet enjoys the stable climate because the hydrological cycle forces the climate system to maintain the chaotic upper tropospheric humidity and wind field, the equilibrium cloud cover and precipitation, and moves the latent heat among the different geological reservoirs – as required by the planetary energetics. The role of the non-condensing GHGs stems from the fact that they do not participate in the hydrological cycle, they cannot contribute to the entropy production, but they can regulate the transmitted flux density to the level required by the Milne-Eddington equations. The greenhouse effect terminology of the climatologists refers to the steady state temperature difference between t_S and t_A. However, the $\Delta t_A \approx 28$ K, and the related $G_A \approx 128$ Wm^{-2} clear-sky temperature and flux density differences are constants, they cannot violate the planetary radiative equilibrium and energy conservation principles. One should admit that Δt_A and G_A are practically meaningless parameters and they cannot be related to the IR atmospheric absorption of the CO_2. Any perturbations to the flux optical thickness by non-condensing GHGs will force the hydrological cycle to restore the theoretical equilibrium state. The greenhouse effect predicted by the Arrhenius greenhouse theory is inconsistent with the existence of the CRE. Hence, the CO_2 greenhouse effect as used in the current global warming hypothesis is impossible. Let us emphasize the overall conclusion:

The Arrhenius type greenhouse effect of the CO_2 and other non-condensing GHGs is an incorrect hypothesis and the CO_2 greenhouse effect based global warming hypothesis is also an artifact without any theoretical or empirical footing.

Without scientific proof the debate on the CO_2 GE based catastrophic AGW should be abandoned and policymakers should focus on the more urgent environmental and social issues of humanity. The recent worldwide energy crisis is a warning sign that the promotion of the so-called green energy is neither solving energy shortages nor helping to protect the environment from pollution. The climate does not need protection, but the clean environment does.

Funding: This work did not receive any funding.

Guest-Editor: Ole Henrik Ellestad; Reviewers: anonymous.

List of acronyms with the page numbers of first occurrences

SW	shortwave (1)
IR	infrared (1)
LW	long-wave (1)
APS	active planetary surface (1)
GHG	greenhouse gas (2)
RE	radiative equilibrium (2)
TOA	top of the atmosphere (2)
CRE	Chandrasekhar-type radiative equilibrium (2)
WV	water vapor (3)
GE	greenhouse effect (4)
LTE	local thermodynamic equilibrium (4)
AGW	anthropogenic global warming (4)
SB	Stefan-Boltzmann (5)
NIST	National Institute of Standards and Technology (5)
EBT	equivalent blackbody temperature (5)
RT	radiative transfer (6)
EBF	Planck equivalent blackbody spectral flux density (7)
GAT	global average TIGR2 atmospheric structure (9)
IPCC	Intergovernmental Panel on Climate Change (9)
GCM	global climate models (10)
NOAA	National Oceanic and Atmospheric Administration (11)
NOAA-S	testing facility in Sterling Virginia (11)
LBL	line-by-line (12)
HARTCODE	High-resolution Atmospheric Radiative Transfer Code (12)
RTF	Radiative transfer function (15)
OLR	outgoing longwave radiation (28)
MGT	Miskolczi Greenhouse Theory (44)
MCT	mean color temperature (48)
ECS	equilibrium climate sensitivity (51)

Acknowledgements

I am indebted to A. Rörsch, C. Wiese, E. Berry, A. Harvey, D. Hagen, S. Welcenbach, C. Game, K. Gregory, and N. Van Andel, for their substantive professional discussions. Also, thanks are due to K. Sifrin, K. Vinnikov, I. Wilson, J. Pompe, R. Tscheuschner, D. Brooks, W. Guang, Y. Shao-min, R. Tattersall, L. Szarka, E. Petz, I. Héjjas, I. Kalmár, Z. Korényi, L. Livo, F. Tompa, S. Nagy, Z. Kolláth, S. Kenyeres, E. Fuggerth, A. Bazso-Dombi, S. Balogh, and all those who have followed my many years of research and contributed with their useful advices to clarify numerous theoretical problems that have arisen in the course of my work. I am very grateful to D. Lawson, and the editors and reviewers for their comments and the help with the technical preparation of the manuscript.

References

[1] Kandel, R., and Viollier, M., 2004: *Planetary radiation budgets*, Space Science Reviews (2005) 120: 1–26DOI: 10.1007/s11214-005-6482-6, pp. 4

[2] Chandrasekhar, S., 1960: *Radiative Transfer*. © 1960 by Dover Publications, Inc.

[3] Scafetta, N., 2010: *Empirical evidence for a celestial origin of the climate oscillations and its implications.* Journal of Atmospheric and Solar-Terrestrial Physics 72 (2010) 951

[4] Miskolczi, F., 2016: *Expert opinion on the greenhouse gas theories and the observed infrared absorption properties of the Earth's atmosphere.* https://climatecite.com/ferenc-miskolczi-testimony-in-mann-vs-ball-libel-case/

[5] Manabe, S. and Wetherald, R. T., 1967: *Thermal Equilibrium of the Atmosphere with a Given Distribution of Relative Humidity.* Vol. 24, No. 3 JAS, (1967) 242

[6] Andrews, D. E., 2023: *Clear Thinking about Atmospheric CO2.*Science of Climate Change, Vol. 3.1 (2003), pp. 1-13, https://doi.org/10.53234/scc202301/13

[7] le Pair C. and de Lange C.A., 2022: *On the Theory of the Earth's Physical Parameters, Distributed in Space and Time. Science of Climate Change*. Vol. 2.3 (2022) pp. 302-309

[8] Kramm, G., and Dlugi, R., 2011: *Scrutinizing the atmospheric greenhouse effect and its climatic impact*. Natural Science, Vol.3, No.12, 971-998 (2011), http://dx.doi.org/10.4236/ns.2011.312124

[9] Mohr P. J., Taylor B. N. and Newell D. B., 2007: *CODATA Recommended Values of the Fundamental Physical Constants: 2006*. National Institute of Standards and Technology, Gaithersburg, Maryland 20899-8420, USA

[10] Raval, A., and Ramanathan, V., 1989: *Observational determination of the greenhouse effect*. NATURE 342 (1989) 758-761

[11] Ahren, J. L., 2004: *Planets*. http://zebu.uoregon.edu/~js/glossary/albedo.html, © 2004, Judson L. Ahern

[12] Schmidt, G., A., Ruedy, R., A., Ron L. Miller, R., L., Lacis, A. A., 2010: *Attribution of the present-day total greenhouse effect*. JGR, Vol. 115, D20106, doi:10.1029/2010JD014287, 2010, pp. 3

[13] Lacis, A., Schmidt, G.A., Rind, D., Ruedy, R., A., 2010: *Atmospheric CO_2: Principal Control Knob Governing Earth's Temperature*. Science 330 (2010) 356-359

[14] NOAA, 1976:*US Standard Atmosphere 1976*. NOAA, NASA, USAF, Washington, D.C. October1976, NOAA-S/T 76-1562

[15] Miskolczi, F. and Mlynczak M., 2004: *The greenhouse effect and the spectral decomposition of the clear-sky terrestrial radiation*. Időjárás, 108, 4, 209–251, Corpus ID: 44927545, https://www.met.hu/en/ismeret-tar/kiadvanyok/idojaras/index.php?id=261

[16] Miskolczi, F. M., 2007: *Greenhouse effect in semi-transparent planetary atmospheres*. IDŐJÁRÁS, Quarterly Journal of the Hungarian Meteorological Service, Vol. 111, No. 1, January–March 2007, pp. 1– 40

[17] Miskolczi, F. M., 2014: *The Greenhouse Effect and the Infrared Radiative Structure of the Earth's Atmosphere*. Development in Earth Science Vol. 2, 2014, http://www.seipub.org/des, https://www.researchgate.net/publication/268507883

[18] Arrhenius, S.,1896: *On the Influence of Carbonic Acid in the Air upon the Temperature of the Ground*. Philosophical Magazine and Journal of Science Series 5, Vol. 41, April 1896, 237-276.

[19] Pierrehumbert, R. T., 2011: *Infrared radiation and planetary temperature*. © 2011 American Institute of Physics, 8·0031·9228·1101·010-6, Jan. 2011, Physics Today, 33-38

[20] Lindzen, R. S., 2007: *Taking Greenhouse Warming Seriously*. E&E, Vol. 18, No. 7+8, 2007, 937–950

[21] Nurse, P. and Cicerone, R. J., 2014: Climate Change, Evidence & Causes. An overview from the Royal Society and the US National Academy of Sciences, RS & NAS Feb. 27th 2014

[22] Smith, A. P., 2008: *Proof of the Atmospheric Greenhouse Effect*. American Physical Society, 1 Research Road, Ridge NY, 11961, PACS numbers: 92.60. Vb,05, 90. +m, (2008) http://arxiv.org/abs/0802.4324v1

[23] Schwarzschild, K., 1906: *On the equilibrium of the Sun's atmosphere*. Nachr. v. d. Königlichen Ges. d. Wissenscaften zu Göttingen. Math-Phys. Klasse, Vol. **195,** 41-53.

[24] Poyet, P., 2022: *The Rational Climate e-Book*. The Extended 2nd Edition https://patricepoyet.org/

[25] Miskolczi, F., 1989: *High resolution atmospheric radiative transfer code (HARTCODE)*.https://www.researchgate.net/publication/287994595DOI: 10.13140/RG.2.1.2319.6240

[26] Rizzi, R., Matricardi, M., and Miskolczi, F., 2002: *Simulation of up-looking and down-looking high-resolution radiance spectra with two different radiative transfer models*. Applied Optics, Vol. 41, No. 6, 20 Feb. 2002, 940-956

[27] Miskolczi F. M., 2010: *The stable steady-state value of the earth's global average atmospheric Planck-weighted greenhouse gas optical thickness*. Energy & Environment 21, 4 (2010) 243-262

[28] Kratz, D. P., Mlynczak, M. G., Mertens, C. J., Brindley, H., Gordley, L. L., Martin-Torres, J., Miskolczi, F. M., and Turner, D. D., 2005: *An inter-comparison of far-infrared line-by-line radiative transfer models*. Journal of Quantitative Spectroscopy & Radiative Transfer 90 (2005) 323–341

[29] Saunders, R., Rayer, P., Brunel, P., von Engeln, A., Bormann, N., Strow, L., Hannon, S., Heilliette, S., Liu, X., Miskolczi, F., Han, Y., Masiello, G., Moncet, J.-L., Uymin, G., Sherlock, V., and Turner, D. S., 2007: *A comparison of radiative transfer models for simulating Atmospheric Infrared Sounder (AIRS) radiance*s. JGR-Atmosphere, Vol. 112, D01S90, 2007, 1-17, http://onlinelibrary.wiley.com/doi/10.1029/2006JD007088/epdf

[30] Miskolczi, F. M., 2011: *The stable stationary value of the Earth's global average atmospheric infrared optical thickness*. European Geophysical Union, EGU 2011, Vienna, 13662, 1-20, http://presentations.copernicus.org/ EGU2011-13622_presentation.pdf

[31] Scott, N., 2009: *TIGR, Thermodynamic Initial Guess Retrieval 2000*. http://ara.lmd. polytechnique.fr/htdocs-public/products/TIGR/TIGR.html

[32] NOAA NCEP, NOAA Earth System Research Laboratory, 2012: *Time series*. http://www.cdc.noaa.gov/cgi-bin/Timeseries/timeseries1.pl

[33] McIDAS Water Vapor Composit_2008: http://www.ssec.wisc.edu/data/composites.html

[34] Chance, K., and Kurucz, R., L., 2010: *An improved high-resolution solar reference spectrum for earth's atmosphere measurements in the ultraviolet, visible, and near infrared*. Journal of Quantitative Spectroscopy & Radiative Transfer 111 (2010) 1289–1295

[35] Kopp, G., and Lean, J., L., 2011: *A new, lower value of total solar irradiance: Evidence and climate significance*. Geophysical Research Letters, Vol. 38, L01706, doi:10.1029/2010GL045777

[36] Ramanathan, V., and Inamdar A. K., 2006: *The radiative forcing due to clouds and water vapor*. In Frontiers of Climate Modeling, Cambridge University Press, 2006, 119-151

[37] Shaviv, N., J., Shaviv, G., and Wehrse, R. 2012: *The Maximal Runaway Temperature of Earth-like Planets*. 2011, Icarus, 216, 2, 403-414

[38] NASA, 2010: *Earth's energy budget.* http://www.nasa.gov, Document: NP-2010-05-265-LARC, http://scienceedu.larc.nasa.gov/energy_budget

[39] Kiehl, J., T., and Trenberth, K., E., 1997: *Earth's Annual Global Mean Energy Budget.* AMS, BAMS, Vol. 78, No. 2, 1997, pp.199

[40] Trenberth, K., E., Fasullo, J., T., and Kiehl J., 2009: *Earth's Global Energy Budget.* AMS, BAMS, March 2009 pp. 311-323

[41] Stephens, G., L., et al., 2012: *An update on Earth's energy balance in light of the latest global observations.* Nature. Geo-science. 5 (2012) 691–696, doi:10.1038/ngeo1580

[42] Wild, M., Folini, D., Schar, C., Loeb, N., Dutton, E. G., Konig-Langlo, G., 2012: *The global energy balance from a surface perspective.* Climate Dynamics (2013) 40:3107–3134, DOI 10.1007/s00382-012-1569-8

[43] Berk, A., Anderson, G., P., Acharya, P., K., Shettle, E., P., 2008: *MODTRAN5.2.0.0 User's Manual*. ftp://ftp.pmodwrc.ch/pub/Claus/Vorlesung2009/ModtranDaten_etc/ MODTRAN(R) 5.2.0.0.pdf

[44] NASA, 2016: *Notes on the Fact Sheets.* NASA Official: Ed Grayzeck, edwin.j.grayzeck@nasa.gov, Last Updated: 29 February 2016, DRW

[45] Miskolczi, F. & Héjjas, I., 2021: *The self-regulation of climate*. *Ferenc Miskolczi's climate theory with comments by István Héjjas.* In Hungarian: *Az Éghajlat Önszabályozása. Miskolczi Ferenc klímaelmélete Héjjas István magyarázataival.* Püski 2021, [ISBN 978-963-302-328-0]

[46] NASA, 2012: *Sun Fact Sheet*.nssdc.gsfc.nasa.gov/planetary/factsheet/sunfact.html

[47] NASA, 2012: *Earth Fact Sheet*. nssdc.gsfc.nasa.gov/planetary/factsheet/earthfact.html

[48] Mihalas, D. & Mihalas, B. W., 1984: *Foundations of radiation hydrodynamics*. Oxford University Press, 1984, pp. 328

[49] Scafetta, N. & Willson, R. C., 2014: *ACRIM total solar irradiance satellite composite validation versus TSI proxy models*. Astrophysics and Space Science. DOI 10.1007/s10509-013-1775-9

[50] Wu, W. and Liu Y., 2010: *Radiation entropy flux and entropy production of the Earth system*. Rev. Geophysics. 48, RG2003, doi:10.1029/2008RG000275.

[51] Scafetta, N., Milani, F., Bianchini, A., Ortolani, S., 2016: *On the astronomical origin of the Hallstatt oscillation found in radiocarbon and climate records throughout the Holocene.* Earth-Science Reviews162, 24–43, 2016. http://dx.doi.org/10.1016/j.earscirev.2016.09.004

[52] Scafetta, N., 2022: *CMIP6 GCM ensemble members versus global surface temperatures.* Climate Dynamics, https://doi.org/10.1007/s00382-022-06493-w

[53] NIST, 2018: *Fundamental Physical Constants—Extensive Listing* http://physics.nist.gov/constants

[54] NASA, 2016: *Jupiter Fact Sheet*. nssdc.gsfc.nasa.gov/planetary/factsheet/earthfact.html NASA Official: Ed Grayzeck, edwin.j.grayzeck@nasa.gov, Last Updated: 19 April 2016,dave.williams@nasa.govNIST

[55] Willman, A., J., 2012: *Planetary System Data.* Copyright © 1996 A. J. Willman, Jr. All rights reserved. http://www.princeton.edu/~willman/planetary_systems/,This page was last updated: 2012 September 20

[57] VanWijngaarden, W. A. and Happer, W., 2020: *Dependence of Earth's Thermal Radiation on Five Most Abundant Greenhouse Gases*. arXiv:2006.03098v1 [physics.ao-ph] 4 Jun 2020

[58] Ferencz, O., 2022: https://hirtv.hu/video/261689

[59] Spencer, R., W., 2010: *Comments on Miskolczi's (2010) Controversial Greenhouse Theory.* https://www.drroyspencer.com/2010/08/comments-on-miskolczi%E2%80%99s-2010-controversial-greenhouse-theory/

[60] Shaviv, N., 2006: *On Climate Sensitivity and why it is probably small.* http://www.sciencebits.com/OnClimateSensitivity

[61] VanAndel, N., 2010: *Note on the Miskolczi Theory*. E&E, Vol. 21, No. 4, 2010, pp.277-292

[62] Harde, H., 2019: *What Humans Contribute to Atmospheric CO2: Comparison of Carbon Cycle Models with Observations*. International Journal of Earth Sciences. Vol. 8, No. 3, pp. 139-159.

[63] Berry, E., X., 2021: *The Impact of Human CO2 on Atmospheric CO2*. Science of Climate Change, Vol. 1.2 (2021) pp. 213-249

[64] Peixoto, J., P., Oort, A., H., 1992: *Physics of Climate*. American Institute of Physics, New York, Printed in the United States of America. Third printing, 1993

Appendix

Duality of flux density and radiation temperature

1. Planck radiation laws

Let us recall the most fundamental equations of the Planck radiation laws. The wavenumber, wavelength, and frequency representations are all suitable for spectral characterization of radiative processes. Further on we use the wavenumber representation, usually found in IR spectroscopy, where the $b_\nu(t_\nu)$ spectral radiances are expressed in units of mW/(m^{2}cm^{-1}sr):

$$b_\nu(t_\nu) = c_2\nu^3(\exp(c_1\nu / t_\nu) - 1)^{-1}, \tag{a1}$$

where c_1 and c_2 are the radiation constants appropriate for the wavenumber domain, and the t_ν color temperatures are expressed in K. In case of isotropic radiation field $t_\nu \equiv t$ is a constant, the Kirchhoff-Planck relationship holds and $b_\nu(t)$ is called the Planck (spectral) distribution of blackbody radiance. From (a1) follows the definition of the color (or brightness) temperature, commonly used in remote sensing applications:

$$t_\nu(b_\nu) = c_1\nu / \ln(c_2\nu^3 / b_\nu + 1). \tag{a2}$$

In case of gaseous materials, the spectral structure of t_ν may be very complex, and the $\overline{t}_\nu$ average may not be equal to EBT. We have seen that, the *mean color temperature* (MCT) of the Sun is about 292.71 K smaller: $t_{SUN} = 5778.075$, $\overline{t}_{\nu,SUN} = 5485.362$ K. In isotropic case $t = t_\nu = \overline{t}_\nu$. In Table 1 some characteristic parameters of the SW solar radiation are presented. Detailed explanations of the symbols are given in section *2*.

Table 1: Radiative parameters of the Sun.

EBT and *MCT* are the equivalent blackbody, and mean color temperatures

Parameters	*EBT*	*MCT*	Units	Symbols
1 *temperatures*	5778.0758	5485.36	K	$\tilde{t} = \overline{t}_\nu$
2 *Wien's law*	5778.0623	5485.3524	K	$W_\nu\nu_{\max}$
3 *SB law*	63197970	51332316	Wm^{-2}	$\sigma\tilde{t}^4$
4 *flux density*	63197967	51332316	Wm^{-2}	$B(\tilde{t})$
5 *MCT*	5778.0754	5485.36	K	$\tilde{t}$
6 *virtual temperatures*	565.00621	557.71036	K	$\hat{t}$
7 *dual flux density*	5778.0754	5485.36	Wm^{-2}	$\tilde{B}(\hat{t})$
8 *maximum of* $B_\nu(\tilde{t})$	3444.5702	2947.1405	Wm^{-2}/cm^{-1}	$B_{\max,\nu}$
9 *maximum wave number*	11330.7	10756.7	cm^{-1}	$\nu_{\max}$
10 *entropy flux density*	14583.396	12477.415	Wm^{-2}/K	J

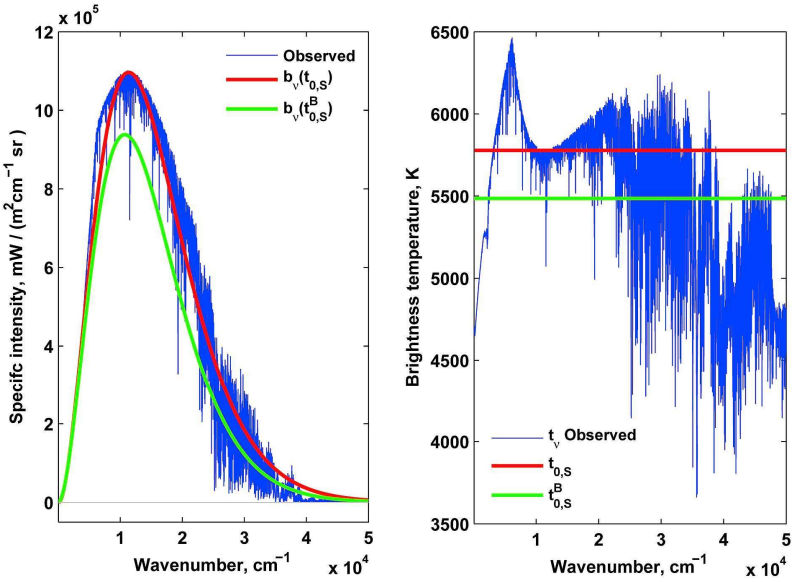

Figure 31: Spectral characteristic of the observed solar specific intensity (left plot) and brightness temperature spectra (right plot). The Sun is definitely not a blackbody radiator.

In Figure 31 the solar spectral radiance and color temperature spectra are shown. From the $b_\nu(t_{0,S})$ and $b_\nu(t^B_{0,S})$ specific intensity spectra – in the left plot – the solar constant could be ~18 % (257 Wm^{-2}) less if computed from $b_\nu(t^B_{0,S})$ instead. See also row 4 and 5 in Table 1. This figure actually is a proof, that the solar radiation is not blackbody radiation, therefore, any *equilibrium climate sensitivity* (ECS) study of GCMs – related to the variations in the solar constant – cannot be based on the SB law or the Planck response, Shaviv (2015) [60].

The form of the Kirchhoff-Planck relation for radiative flux densities is obtained by integrating (a1) by solid angle and wavenumber. The conversion of spectral radiances from units of $mW/(m^2cm^{-1}sr)$ into $B_\nu(t)$ spectral flux densities in $W/(m^2cm^{-1})$ means a multiplication by the $\pi_D = \pi \times 10^{-3}$ factor. Spectrally integrated $B_\nu(t)$ will result in the $B(t)$ flux density function in Wm^{-2}, which depends only on the temperature. The wavenumber and solid angle integral of (a1) yields the Stefan-Boltzmann (SB) law:

$$B(t) = \sigma t^4 . \qquad \text{(a3)}$$

In the wavenumber domain the SB constant may be expressed with the c_1 and c_2 radiation constants: $\sigma = 10^{-4}(2/3)\pi^5 c_2 / c_1^4 = 5.669833697 \times 10^{-8}\ Wm^{-2}K^{-4}$, where $c_1 = 1.438786\ K/cm^{-1}$, and $c_2 = 1.1909596 \times 10^{-5}\ mWm^{-2}cm^{-4}sr^{-1}$. By definition, the t temperature obtained from (a3) is the $t = (B/\sigma)^{1/4}$ EBT, (for the Earth $t_0 = (F_0/\sigma)^{1/4} = 394.101649\ K$). Specifically for the Earth, the $\sigma \equiv \pi_D E_0 / F_0^4 \equiv \pi_D (d_E / r_0)^2 / F_0^3$ relationships numerically also holds exactly. (In double-precision arithmetic '*exact*' means a numerical accuracy up to 15 significant decimal digits.)

The form of the SB law for the $U(t)$ energy density of the radiation field: $U(t) = at^4\ Jm^{-3}$, where $a = 4\sigma / c\ Jm^{-3}K^{-4}$, and c is the speed of the light in vacuum. Differentiation of (a1) by wavenumber yields Wien's displacement law:

$$t / \nu_{\max} = W_{\nu}, \tag{a4}$$

where $W_{\nu} = 0.50994751$ K/cm^{-1} is the Wien constant in the wavenumber representation, and $\nu_{\max}$ is the wavenumber of the maximum of the $B_{\nu}(t)$ function. The radiation entropy flux density may be expressed in different forms, Wu & Liu (2010) [50]:

$$J = cat^3 / 3 = (4/3)\sigma t^3 = (4/3)\sigma^{1/4} B^{3/4} = (4/3)B/t\,. \tag{a5}$$

At a unique temperature of $t_M = \sigma^{-1/3}$ K, and unique flux density of $B_M = \sigma^{-1/3}$ Wm^{-2} (a3) reduces to a mathematical identity of $t_M \equiv B_M = \sigma^{-1/3} = 260.301$, and the temperature and flux density cannot be numerically distinguished. At t_M and B_M the entropy flux density – from (a5) – is exactly 4/3 Wm^{-2}/K.

At this point we did not pay much attention to the numerical value of $\sigma^{-1/3}$, and we just introduced the $\sigma_M = \sigma^{-1/3}$ and $c_M = \pi_D^{1/3}\sigma_M = 38.123536778$ notions, where σ_M and c_M quantities can equally have dimensions of K or Wm^{-2}, and called this strange situation to temperature-flux density duality. We may call t_M and B_M *mixing temperature* and *mixing flux density*, and refer to the c_M parameter as *dual entropy constant*.

However, empirical evidence shows that σ_M cannot be discarded as a physically meaningless quantity. Radiosonde observations showed that $2t_P - t_S \cong \sigma_M$, indicating that σ_M, (or c_M) is quantitatively associated with the phase temperature of the H_2O and the global mean surface temperature, (see [17]). Flux density simulations show that the $t_T + E_D - A_A \cong \sigma_M$ empirical relationship also holds, indicating that mixed (temperature and flux density) mathematical expressions of physical quantities are also associated with σ_M.

Using astronomical parameters of the Earth and Sun ($E_0, t_{SUN}, F_0, r_0, d_E, d_F$) and the SB law, later we were running into several mathematical identities where the dimensions of the involved quantities did not match:

$$F_0 = \pi_D t_{SUN}, \quad \sigma F_0^4 = \pi_D E_0, \quad (4/3)\sigma F_0^3 = (4/3)\pi_D d_F\,. \tag{a6}$$

In the 1st equation of (a6) the left side is flux density in Wm^{-2},the right side is temperature in K. In the equivalent form of this equation $F_0 \equiv (\pi_D E_0 / \sigma)^{1/4}$, where the E_0 flux density virtually has the dimension of radiance. Taking the 4th power of this equation and multiplying with σ we get the 2nd equation, where both sides are flux densities but on the left side F_0 must be temperature in K, as required by the SB law. In the 3rd equation the right side is a dimensionless quantity, while the left side (assuming that F_0 is temperature in K) may be taken as entropy flux density in Wm^{-2}/K, see the second equation of (a5) . Perhaps the $\pi_D^{1/4} t_{SUN} = 1367.9514$ K quantity may be called as the t_{π}K *entropy temperature* of the Sun.

Rearranging the 3rd equation of (a6) and using the $d_F = (r_0 / d_F)^2 = F_0 / E_0$ definitions of the dilution factor, the solar constant equation (23) in *4.2* may easily be derived: $F(d) = c_M d_E^{8/3} r_0^{-2/3} d^{-2}$. Obviously, for the Earth $d = d_F$, $F(d_E) = c_M d_F^{-1/3}$ and here c_M is Wm^{-2}. Notice, that because of the $d_E^{8/3}$ term in (23), the $\sigma = \pi_D E_0 / F(d)^4$ relationship – from the 2nd equationof (a6) – cannot be valid for any other planets.

Further interesting fact is, that the radiation entropy flux density from (a5) for the t_π entropy temperature is 193.51 Wm^{-2}/K, which is numerically very close to the GAT clear-sky emission of $E_U = 193.24\,Wm^{-2}$, (see Figure 7). Similar coincidences, without straightforward physical explanations, used to be termed as tele-connections. Such surprising numerical relationships are the $F_0 = (15/(\pi^4 c_2 d_F))^{1/3} c_1^{4/3}$, or $\sigma = \pi_D E_0 / F_0^4$ expressions, where c_2, c_1, and σ are known functions of the fundamental physical constants.

All of the strange relationships just mentioned point to a hidden mathematical property of the Planck radiation laws, and also to the very special astronomical parameters of the Sun and the Earth's orbit. Because of the mixed dimensions (a3) may not be a unique relationship between flux densities and temperatures. Looks like (a3) structurally represents physically meaningful relationships among long lines of different RT quantities.

2. Law of radiation-temperature duality

Let $\tilde{t} = \overline{t_\nu}$ be the MCT of the spectral t_ν over the whole wavenumber domain. Let us also define the $\hat{t} = (\tilde{t} / \sigma)^{1/4}$ *virtual temperature* as the EBT from the flux density being numerically exactly equal to $\tilde{t}$. The virtual notation indicates that $\hat{t}$ is a mixed physical quantity, meaning that $\tilde{t}$ in K may formally enter into the SB law as flux density in Wm^{-2}.

A very important mathematical property of equations (a1-a5) is the exact mathematical equivalence of the $\tilde{B}(\hat{t})\,Wm^{-2}$ integrated $\tilde{B}_\nu(\hat{t})$ spectral flux density, and the average color(or brightness) temperature $\tilde{t}$ K:

$$\tilde{t} \equiv \tilde{B}(\hat{t}) = \pi_D \int_0^\infty c_2 \nu^3 / (\exp(c_1 \nu / (\overline{t_\nu} / \sigma)^{1/4}) - 1) d\nu \,. \qquad \text{(a7)}$$

Equation (a7) is a new insight not found in the literature and will be referred to hereafter as the *law of radiation-temperature duality*. Further on, $\tilde{B}(\hat{t})$ and $\tilde{t}$ will be termed as *dual flux density* and *dual temperature*. Remember, that for ideal blackbody radiation $\tilde{t}$ is the t temperature itself. To prove that the law of duality holds for temperature t_M is relatively simple. Using (a1) one has to show quantitatively that (a7) is true:

$$t_M = \pi_D \int_0^\infty b_\nu(t) d\nu = \pi_D c_2 \int_0^\infty \nu^3 (\exp(c_1 \nu / t_M) - 1)^{-1} d\nu \,, \qquad \text{(a8)}$$

where $t_M = \sigma^{-1/3} = (\pi_C c_2)^{-1/3} c_1^{4/3}$, and $\pi_C = \pi^5 / 15000$. Substituting ν with the $x = \nu c_2 \pi_C / c_1$ new variable we arrive at the next equation:

$$(\pi_C\, c_{2,\nu})^{-1/3} c_{1,\nu}^{4/3} = \pi_D c_{2,\nu} (c_{2,\nu} \pi_C / c_{1,\nu})^{-4/3} \int_0^\infty x^3 (\exp(x) - 1)^{-1} dx \,, \qquad \text{(a9)}$$

where the Riemann sum of the right integral is $\pi^4 / 15$, which reduces (a9) to an identity, independent of t_M. Since any t temperature can be expressed (scaled) by t_M with a constant of proportionality, our statement holds for any t temperature.

In Figure 32 HARTCODE GAT simulations of the all-sky OLR_ν^A and the relevant t_ν brightness temperature spectra are presented. On the contrary to the solar spectra in Figure 31, the terrestrial radiation is a fair approximation of the maximum entropy blackbody radiation.

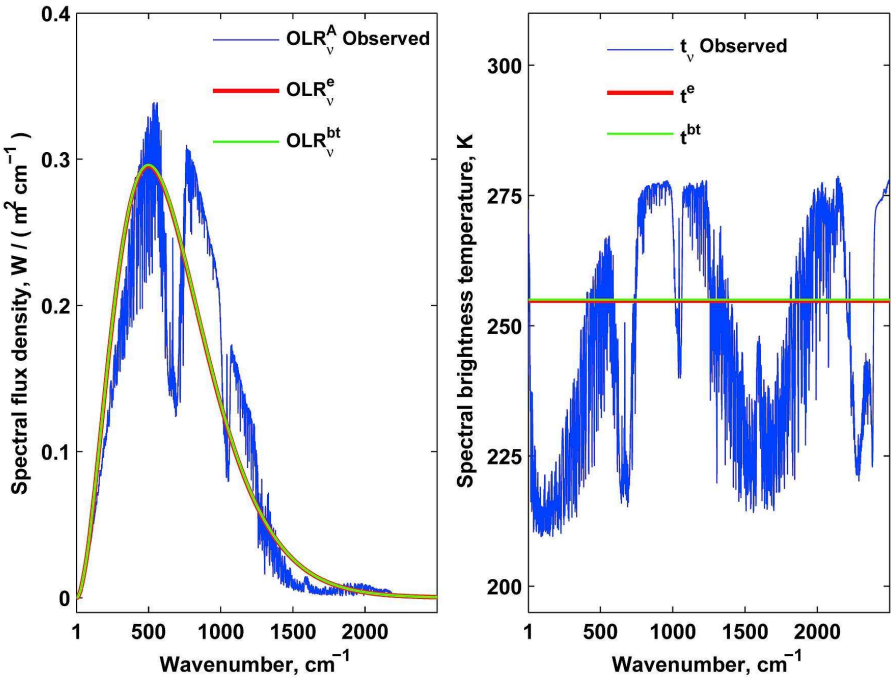

Figure 32: Spectral OLR^A_ν *and* t_ν *(thin blue lines) of the GAT atmosphere. In the right plot the* t^{bt} *mean brightness temperature and the* t^e *EBT are practically equal. In the left plot* OLR^e_ν *EBF, and* OLR^{bt}_ν *flux density from* t^{bt} *are also equal. The IR radiation leaving the Earth is close to ideal blackbody radiation.*

The integral flux densities of OLR^e_ν and OLR^{bt}_ν are about equal, and the SB law for ECS estimations in CO_2 doubling studies theoretically may safely be applied. Based on the SB law and GCM simulations without feedback processes, the ECS in Scafetta (2022) [52] would result in ~1 K surface temperature rise.

Of course, this is a plain nonsense, the stochastic climate system is not controlled by the SB law, but by the random combination of the most diverse physical processes, laws, and principles of nature, which is ultimately able to produce the OLR^A_ν maximum entropy IR radiation of the Earth-atmosphere system. On the other hand, popular CO_2 doubling studies in GCM simulations are based on artificial atmospheric structures, therefore producing quite unrealistic results which are violating the Schwarzschild-Milne equations.

The means of conversion of the incoming SW solar to outgoing LW terrestrial radiation are based on the stochastic processes in the global hydrological cycle, which is – using the infinite supply of water from the oceans – creating the global average equilibrium cloud cover.

The duality of flux density and temperature is independent of the spectral structure of the radiation field, should therefore be regarded as an intrinsic mathematical property of the Planck distribution.

In the context of the Planck distribution, this fact is probably not of great novelty to mathematicians working on theory of the distribution functions, but it may be of some interest to physicists,

astrophysicists or astronomers. The duality of flux density and temperature provides the theoretical background for number of unexplained tele-connections.

The SW solar radiation field must obey the law of duality. At d_E distance from the Sun a virtual $\hat{t}_0 = (t_0 / \sigma)^{1/4} = 288.74448$ K temperature can be computed, which will be consistent with the t_0 EBT, and the numerical identity of $B_0 = \sigma \hat{t}_0^4 \equiv (F_0 / \sigma)^{1/4} = t_0 = 394.11692$ Wm^{-2} or K. Just like t_0, $\hat{t}_0$ is an astronomical parameter and has nothing to do directly with the t_S global mean surface radiative temperature (from (17) in paragraph *2.2*). By definition, the $\varepsilon_A^T = t_E / \hat{t}_0$ dimensionless ratio is the *theoretical anisotropy factor of the incoming directional SW radiation field* at the d_E distance from the Sun. The numerical value of $\varepsilon_A^T = 0.9651535$ may be expressed by several mathematical identity:

$$\varepsilon_A^T = t_E / \hat{t}_0 = 2^{-1/2} t_0 / \hat{t}_0 = 2^{-1/2} (F_0 / \sigma_M)^{3/16} = \pi_N / d_F^{1/16} = \pi_N (d_E / r_0)^{1/8}, \qquad \text{(a10)}$$

where $\pi_N = (\pi_D / 256)^{1/16}$. To establish the relationship between t_S and t_0 the anisotropy of the solar and terrestrial radiation fields has to be evaluated. It was shown in paragraph *4.1* that the ε_A IR clear-sky anisotropy factor of the GAT atmosphere practically equal to ε_A^T: $\varepsilon_A^T \cong \varepsilon_A = E_D / E_{D,I} = 0.96515341$. The close agreement of ε_A and ε_A^T is a proof that the structure of the global mean atmosphere is such, that the SW and IR anisotropy factors are exactly the same.

As a prominent example, the $\hat{t}_0^{obs}$ empirical virtual temperature from GAT simulation is in very good agreement with the true $\hat{t}_0$: $\hat{t}_0^{obs} = ((2(S_U^A + OLR^A / (1 - g^A)) / \sigma)^{1/4} / \sigma)^{1/4} = 288.74395$ K. The relative deviation of $\hat{t}_0$ and $\hat{t}_0^{obs}$ is ~1.83×10^{-4}%. As expected, the atmospheric Kirchhoff law also gives a perfect match with t_S: $t_S = (E_D / (\varepsilon_A A \sigma))^{1/4} = 286.06469$ K.

Assuming constant E_0 and F_0, we can easily determine the local $F(d)$ theoretical solar constant as a function of d distance from the Sun to any point in the solar system. Let $(r_0 / d)^2$ be the local dilution factor associated with the distance d, and let us use the next duality of the solar surface emission $E_0 = c_M d_F^{-4/3} = c_M (r_0 / d_E)^{-8/3}$.

By multiplying both sides with $(r_0 / d)^2$, the left hand side will define the $F(d) = (r_0 / d)^2 E_0$ function, and the right hand side will be transformed to the next mathematical identity: $c_M (r_0 / d_E)^{-8/3} (r_0 / d)^2 = c_M r_0^{-2/3} d_E^{8/3} d^{-2}$. The final form of $F(d)$:

$$F(d) = c_M r_0^{-2/3} d_E^{8/3} d^{-2}, \qquad \text{(a11)}$$

where r_0 and d_E are the proper *time averages* of the Sun's radius and the semi major axis of the Earth's orbit. Using the $F_0 = c_M d_F^{-1/3}$ duality, and the $r_0^{-2/3} d_E^{8/3} = d_F^{-1/3} d_E^2$ identity, $F(d)$ may be expressed in $d_a = d / d_E$ astronomical units:

$$F(d_a) = F_0 d_a^{-2}. \qquad \text{(a12)}$$

The precise determination of the relevant r_0 and d_E is the subject of solar physics, and perturba-

tion calculations in celestial mechanics. The EBT temperature expressed from (a11) may be written as: $t(d) = c_M 10^{3/4} \pi^{-1/4} d_E^{2/3} r_0^{-1/6} d^{-1/2}$. The effective surface temperature of the planets in astrophysical sense is $t_0(d) = 2^{-1/2} t(d)$ K.

Outside the Sun, using Kepler's third law, $F(d)$ can also be expressed in terms of the orbital periods of the planets:

$$F(\mathrm{P}) = c_M \kappa_E^{-2/9} \mathrm{P}_E^{16/9} r_0^{2/3} \mathrm{P}^{4/3}, \qquad \text{(a13)}$$

where P is the orbital period in seconds of any planet, $\mathrm{P}_E = 3.155941209 \times 10^7$ s is the orbital period of the Earth, and $\kappa_E = 2.97496184 \times 10^{-19}$ s^{-3}m^2 is the Kepler constant for the Earth.

Equation (a11) has a singularity at $d = 0$ – at the center of the Sun or the barycenter of the solar system – which would physically imply an infinitely high temperature and an infinitely large flux density, which of course cannot exist. In principle, the solar system is in constant motion and a static geometrical center representing its center of gravity cannot be assigned. Using (a11) at $d = d_E$ we may formally define the $F_0^T = c_M r_0^{-2/3} d_E^{8/3} d_E^{-2} = 1367.954$ Wm^{-2} theoretical solar constant, which is agreeing well with F_0 and F_0^{obs}.

Apart from the singularity at $d = 0$, the distance d can vary from the Sun's interior to any point in the solar system. As already mentioned, the accuracy of (a11-a13) depends solely on the accuracy of measured geometric distances and times, and therefore it is free from the calibration problems often encountered in radiation measurements which makes F_0^T a real good candidate for a reference solar constant.

Based on model calculations the temperature at the center of the Sun is 1.571×10^7 K, NASA (2012) [46]. If we wonder what equation (a11) considers to be the Sun's center, we gradually decrease the distance d to the hypothetical center of the Sun in our equation and find when the resulting flux density of the radiation temperature calculated from the SB law equals the temperature of NASA's above. Our result shows that at 94.15 m from a hypothetical solar center the temperature is 1.5710053×10^7 K. This distance (in terms of astronomical distances) is a good approximation to the solar center, so our equation practically confirms the NASA complex model calculations. Further reducing the distance from a hypothetical solar center (d in (a11)), the radiative temperature increases rapidly, reaching 1.52436097×10^8 K degrees at a distance of 1 meter. At extremely small distances, such as the unit Planck length ($l_P = 1.61622938 \times 10^{-35}$ m, CODATA (2018) [53]), the temperature is 379.17×10^{23} K, which is of course still far from infinity.

It is also worth examining the accuracy of (a11) for much larger values of d. Again, referring to NASA data, Jupiter has a solar constant of 50.26 Wm^{-2}, a Bond albedo of 0.343, a distance d of 778.57×10^9 m, and an equilibrium absorption temperature of 109.9 K, NASA (2016) [54]. Similar data can be found in the planetary database of Willman (2012) [55]. From (a11), the theoretical solar constant of Jupiter is $F(d) = 50.504$ Wm^{-2}, which is about equal to the NASA data. The equilibrium absorption temperature of Jupiter is $(F(d)(1-0.343)/(4\sigma))^{1/4} = 109.9804$ K, which is also equal to the NASA data. The above examples show that (a11) does indeed accurately reproduce the wide range of solar constants in the solar system.

The point of our equation is not to show the trivial dependence of the flux density on distance d

, but rather to show that the solar constant of any planet depends specifically on the semi-major axis of the Earth's orbit. Consequently, the Earth plays a very special role in the energetics of our solar system. It may even be that we should reconsider our ideas about the origin and formation of the solar system and our heliocentric worldview.

The law of duality interconnected the F_0 solar constant, the σ Stefan-Boltzmann constant and the r_0 solar radius into an accurate mathematical expression for the d_E semi-major axis of the Earth's orbit, where the working hydrological cycle assures the maximum radiation entropy of the OLR while maintaining a stable planetary climate: $d_E = (\sigma\pi_D)^{1/2} F_0^{3/2} r_0 = 1459789$ m. To answer the question why it is so needs further studies of planetary evolution.

To show the distinguished characteristics of the Earth's orbital position in the solar system in Figure 33 and 34 we compare planetary solar constants and anisotropy factors of the five inner planets. In these figures the black dots mark the unique orbital position of the Earth where the duality based F_0, $F_P(d)$ and $\varepsilon_P(d)$ parameters exactly reproduce the empirical data.

In Figure 33 the F_0^T and F_0^{obs} are equal and they numerically agree with the t_π entropy temperature. The maximum and minimum relative differences of F_0^T and the satellite records between 1978 and 2018 (in Scafetta [49], figure 1) are 0.44 % and -0.58 %, corresponding to about 1.0 K change in t_0.

In Figure 34 the SW ε_P were computed from the $\varepsilon_P = t_E / \hat{t}_0$ using the $\hat{t}_0$ (red dots), and from the $\varepsilon_P = \pi_N d_F^{-1/16}$ using d_F (green dots). The black dot marks the unique orbital position of the Earth where the empirical IR $\varepsilon_A = E_D / E_{D,I}$ and both SW ε_P are equal.

Finally, returning to our prominent example, using the $t_S = (E_D / (\varepsilon_A A\sigma))^{1/4}$ atmospheric Kirchhoff law, the $\varepsilon_A^T = \pi_N (d_E / r_0)^{1/8}$ anisotropy, and the $\varepsilon_A \cong \varepsilon_A^T$ close agreement, the E_D^T theoretical equilibrium downward atmospheric emission of the global average atmosphere will depend only on the ε_A^T astronomical parameter, and the τ^T theoretical IR equilibrium global mean flux optical thickness: $E_D^T = \varepsilon_0^T S_U$, where $\varepsilon_0^T = \varepsilon_A^T (1 - \exp(-\tau^T))$, and ε_0^T is the theoretical equilibrium clear-sky emissivity. The relative differences of $E_D - E_D^T$ and $\varepsilon_0 - \varepsilon_0^T$ are 0.0286 %.

Our planetary mean climate is particularly fond of the constants ε_A^T and τ^T, and leaves no room for any greenhouse gas perturbations. The message of our equations is quite clear and does not require the official approval of the Hungarian Academy of Sciences, or the academically illiterate politicians and their IPCC.

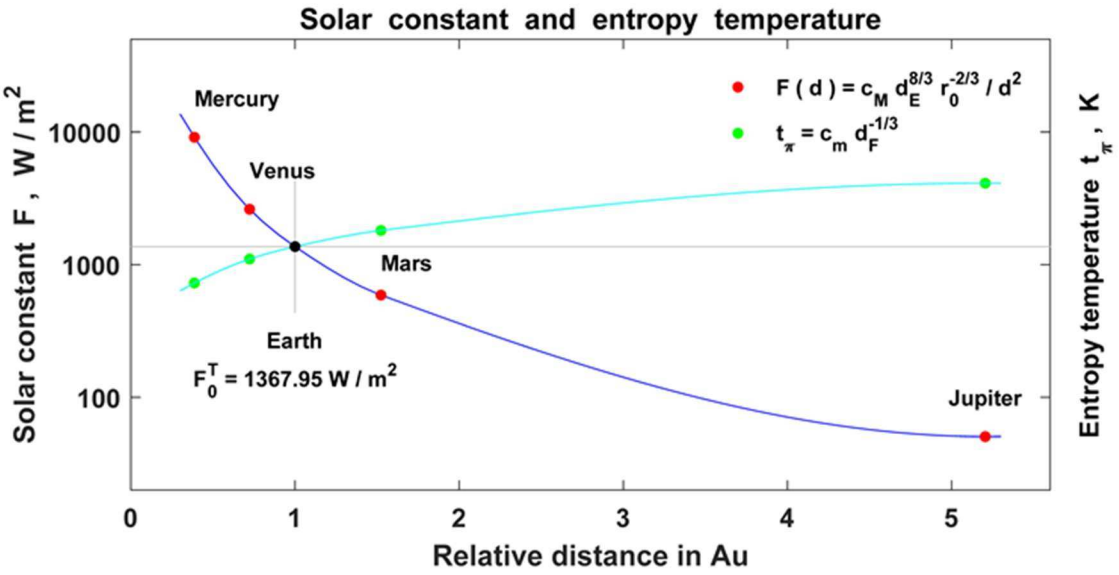

Figure 33: Numerical comparisons of the planetary solar constants from the $F(d)$ function (red dots) with the entropy temperatures from $t_\pi = \pi_D^{1/4} t_{SUN} = c_M d_F^{-1/3}$ dualities (green dots). The empirical F_0^{obs} (black dot) from GAT simulations perfectly agrees with F_0^T.

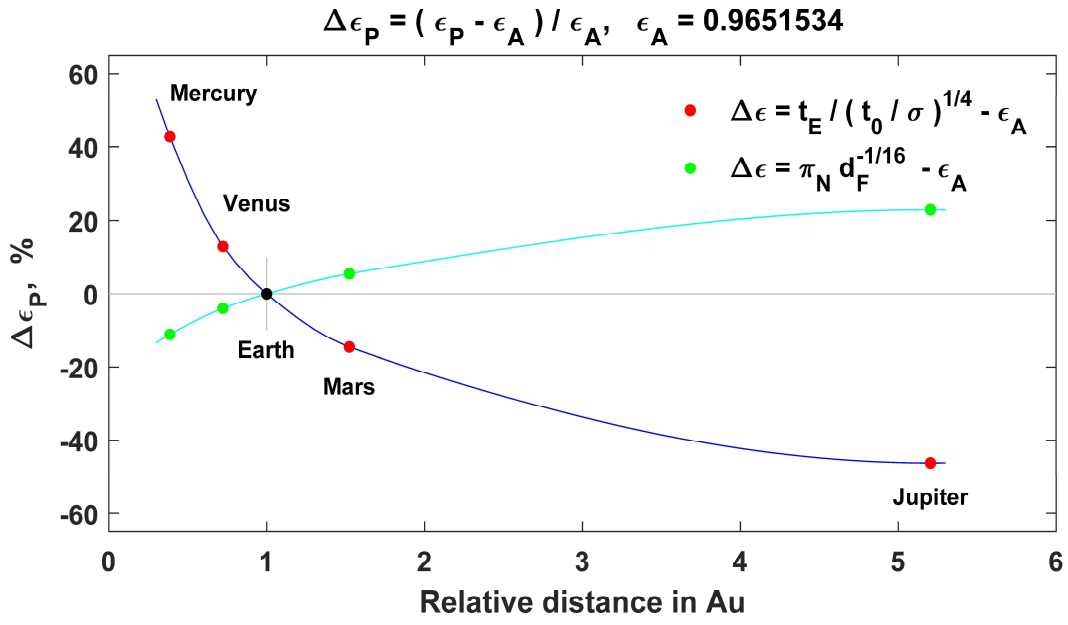

Figure 34: Comparisons of the ε_P SW anisotropy factors of the planets from the law of duality with the ε_A IR anisotropy factor of the GAT atmosphere from the atmospheric Kirchhoff law.

Natural Climate Drivers Dominate in the Current Warming

Antero Ollila

School of Engineering (Emer.)
Aalto University, Espoo, Finland

OPEN ACCESS
Klimarealistene
P.O. Box 33,
3901 Porsgrunn
Norway
ISSN: 2703-9072

Correspondence to
aveollila@yahoo.com

Vol. 3.3 (2023)
pp. 290-327

Abstract

Anthropogenic global warming (AGW) is the prevailing theory of the IPCC for global warming. Greenhouse (GH) gases are the major drivers, whereas albedo, aerosols, and clouds have had cooling effects, and natural drivers have an insignificant role (<0.8 %). According to Assessment Report 6 (AR6), these radiative forcings (RF) have been a total of 2.70 Wm^{-2} causing a temperature increase of 1.27 °C in 2019. Many research studies are showing significantly lower RF and climate sensitivity values for anthropogenic climate drivers. Research studies offering natural climate drivers as the partial or total solution for global warming have gradually emerged like solar radiation changes, cosmic forces, and multidecadal, century- and millennial-scale oscillations. The cloud effects are still a major concern in General Circulation Models (GCMs). The cloudiness changes have a major role in cosmic effects like magnifying the warming effect of the Total Solar Irradiation (TSI). The 60- and 88-year oscillations are the best-known oscillations, which are commonly known as AMO (Atlantic Multidecadal Oscillation) and the Gleissberg cycle explaining the ups and downs of the global temperature in the 1900s. Mechanisms of long-term climate oscillations are still under debate. There are also essential differences between carbon cycle models and GH effect magnitude specifications. The synthesis of these natural climate drivers together with anthropogenic drivers constitutes an alternative theory called Natural Anthropogenic Global Warming (NAGW), in which natural drivers have a major role in dominating the warming during the current warm period. These results mean that there is no climate crisis and a need for prompt CO_2 reduction programs.

Keywords: *anthropogenic climate drivers; natural climate drivers; climate sensitivity; radiative forcing; positive water feedback; climate oscillations; carbon circulation; SW radiation anomaly*

Submitted 2023-02-09, Accepted 2023-07-31, Updated 2023-12-26,

https://doi.org/10.53234/scc202304/03

1. Introduction

The results of the IPCC are prevailing perceptions of global warming or more commonly climate change. According to AR6 (IPCC, 2021), the contribution of the anthropogenic climate drivers is 99.2 % of the global warming from 1750 to 2019. The model-calculated temperature anomaly according to AR6 in 2019 was 1.27 °C and the estimate of the global observed temperature anomaly in 2019 was 1.29 °C (IPCC, 2021, Fig. 7-51). The main indicator of global warming is the

surface temperature Ts, and according to IPCC, there is practically no error between the observations and the GCMs in 2019. At first sight, it looks like there is a perfect match between the AGW and the observations. A prompt analysis reveals contradictions.

There is a significant improvement in the model calculated Ts values if compared to the same figures reported in AR5 (IPCC, 2013). The total Radiative Forcing (RF) was 2.34 Wm^{-2} in 2011. Using the Climate Sensitivity Parameter (λ) value of 0.5 $K/(Wm^{-2})$, the model calculated temperature Ts increase was 1.17 ºC. This figure is 37.6 % greater than the observed temperature anomaly of 0.85 ºC in 2011. This temperature amomaly has increased to 1.29 °C in 2019. The reasons for this abrupt temperature increase should be identified since GH gases are not able to cause such an increase according to the IPCC.

The testimony of Christy (2017) in the U.S. House Committee on Science 2017 contains the description of the scientific test between the 102 CMIP5 climate model runs (CMIP5 means Coupled Model Intercomparison Project Phase 5 experiment design) and the tropical mid-tropospheric temperature from 1979 to 2016. The observed temperatures consist of satellites, balloons, and model-computed temperatures called reanalyze. In the test was applied the F-Test method of Vogelsang-Franses designed to determine whether the trends of the two time series are equivalent or significantly different. The test values showed that all three observational temperature trends were highly significantly different (99 % confidence level) than the average of 102 CMIP5 models. The error between the average 102 CMIP5 models and the satellite temperature was about 0.55 ºC during the period from 2010 to 2015.

Together, 16 scientists have published an article (Santer et al., 2017) in which they realize that "*Over most of the early twenty-first century, however, model tropospheric warming is substantially larger than observed; warming rate differences are generally outside the range of trends arising from internal variability.*"

One of the objectives of this paper is to challenge the IPCC's climate change science. The most important issues of global warming are the RF magnitude of CO_2, the positive water feedback, transient climate response (TCR), and the relative strengths of greenhouse (GH) gases. The first objective of this review study is to find out and analyze the anthropogenic contributions according to the competing research studies not applied by the IPCC. Since these issues are the most important, the theoretical aspects will be analyzed thoroughly.

The second objective is to analyze the anthropogenic carbon amount in the atmosphere and its residence time, which are the basis for the scenario calculations during this century. The third objective is to analyze the GH effect specification of the IPCC, which is "IPCC-made" and conflicts with the IPCC policy to apply only reviewed research results. There are alternative specifications not considered by the IPCC. The GH effect specification of the IPCC does not affect global warming calculations, but it creates a strong GH gas image for CO_2.

The contributions of alternative research studies of anthropogenic climate drivers are usually much lower than those of the IPCC. Therefore, natural climate drivers are needed for filling up the gap. The IPCC omits almost totally the long-term solar radiation changes, cosmic forces, and multidecadal, century- and millennial-scale oscillations as drivers of global warming. The fourth objective is to summarize and analyze the differences between AGW and NAGW.

2. Materials and methods

The material and data applied to the IPCC reports and mainly the newest AR6 (IPCC, 2021) constitute the reference basis for analyses. The scientific papers, which may not have been referred to by the IPCC, constitute another source of results and data. The approach of this review study is to analyze critically the results of the IPCC and to compare them to the alternative research papers, which we could call research studies of contrarians. The RF value of CO_2 and the positive water

feedback have decisive roles in the IPCC science and therefore these issues have been analyzed thoroughly.

3. Results

3.1 The strength of carbon dioxide (CO_2) as a GH gas

The RF value calculated at the tropopause was called instantaneous radiative forcing (IRF) in the AR5, and at the top of the atmosphere (TOA), the IPCC (2013) used the term Effective Radiative Forcing (ERF). The IPCC changed the terminology and the specifications of RF terms in the AR6 (IPCC, 2021). The Instantaneous Radiative Forcing (IRF) was defined now as the change in the net TOA (Top of the Atmosphere) radiative flux following a perturbation, excluding any adjustments. The Stratospheric Temperature-adjusted Radiative Forcing (SARF) was defined as the change in the net radiative flux at the TOA following a perturbation, including the response to stratospheric temperature adjustments.

The ERF is the final RF at the TOA for a particular forcing agent, and it is the sum of the IRF and the adjustments. The AR6 refers to four RF studies, which have practically the same ERF results but essential differences in calculation methods. The RF value of CO_2 caused the concentration increase from 280 ppm to 560 ppm has been marked as $2*CO_2$ and it is needed in calculating climate sensitivity values as temperature changes. The $2*CO_2$ of Myhre et al. (1998) is 3.71 Wm^{-2}, and it is based on spectral calculations at the tropopause with stratospheric adjustments. This value has been used by the IPCC in three previous Assessment Reports, namely TAR (IPCC, 2001), AR4 (IPCC, 2007), and AR5 (IPCC, 2011). In 2010 Schmidt et al. (2010) called this value a canonical estimate as it seemed to be unchallenged. In AR6 the IPCC writers introduced a higher $2*CO_2$ on questionable rationale. In the AR6 three other $2*CO_2$ values have been referred namely the 3.75 Wm^{-2} of Etminan et al. (2016) and the 3.75 Wm^{-2} of Meinshausen et al. (2020) are based on spectral calculations at the TOA by using the Oslo LBL code (Myhre et al., 2016). The $2*CO_2$ of Smith et al. (2018) the 3.70 Wm^{-2} and is based on the simulation of 11 GCMs applying the average IRF values at the TOA and the adjustments.

Finally, the IPCC (2021) formulated a new presentation not found in these referred scientific papers, since they replaced IRF with SARF. The IPCC formulated a new paradigm, and the ERF of 3.93 Wm^{-2} is 5.3 % greater than in the three referred studies above from 3.7 Wm^{-2} to 3.75 Wm^{-2}.

A simple mathematical formula is available for calculating RF values for other concentration values. The original equation of Myhre et al. (1998) for calculating the RF value of CO_2 was

$$RF = k * \ln(C/560) \ [Wm^{-2}] \quad (1)$$

where k = 5.35, and C is the concentration of CO_2 (ppm). It should be noticed that RF is radiative forcing change due to the external climate driver changes, which may have happened since 1750. The values of this equation are a little bit lower than that of the official RF values of AR6 (IPCC, 2021), but the IPPC does not introduce the equation giving a $2*CO_2$ value of 3.93 Wm^{-2}. Eq. (1) gives the RF value of 2.06 Wm^{-2} for CO_2 concentration 411.7 ppm in 2019, and the same value in AR6 (IPCC, 2021, Fig. 7.6)) is 2.16 Wm^{-2}, which is 4.9 % greater being in line with the $2*CO_2$ values.

There are different $2*CO_2$ values, which are not referred to in the AR6 (IPCC, 2021). Barrett et al. (2006) and Schildknecht (2020) have applied LBL (line-by-line) calculations and their values are

3.1 Wm^{-2} and 3.0 Wm^{-2}. Wijngaarden and Happer (2020) achieved a 2*CO_2 value of 3.0 Wm^{-2} based on their LBL calculations using the HITRAN database (2021). Their RF value for 2*CO_2 (from 400 ppm to 800 ppm) of 3.0 Wm^{-2} is at the altitude of 86 km, and the same value at 11 km is 5.5 Wm^{-2}, which has not been explained.

Harde (2013) also applied his own LBL calculations and his two-layer atmospheric model. His 2*CO_2 value is 2.4 Wm^{-2}. Miskolczi and Mlynczak (2004) carried out extensive LBL calculations with different atmospheric compositions, and their 2*CO_2 value is 2.53 Wm^{-2}.

Ollila (2014) has reported a 2*CO_2 of 2.16 Wm^{-2} utilizing LBL calculations with the Spectral Calculator tool (GATS, 2021) by using the HITRAN (2021) database and water-continuum model. Ollila's calculations are in line with Ohmura (2001) that 98 % of total LW absorption happens in the troposphere, and therefore the CO_2 absorption does not increase in the stratosphere, but it is saturated before the altitude of 1 km. The IRF value (the RF at the troposphere) of Smith et al. (2018) is 2.6 Wm^2.

3.2 Positive water feedback

Positive water feedback is a cornerstone in any GCM and the simple model of IPCC. IPCC (2007) writes in AR4 that *"The positive water feedback doubles the radiative forcing of any GH gas."* The AR5 (IPCC, 2013, p. 667) writes *"Therefore, although CO_2 is the main control knob on climate, water vapour is a strong and fast feedback that amplifies any initial forcing by a typical factor between two and three."* Because it is a big difference between factors two and three, IPCC should show at least a few references to the proper research studies.

The theoretical justification of positive water feedback is based on the equation of Clausius–Clapeyron. This equation represents the pressure-temperature relationship in a saturated water vapor atmosphere. The real atmosphere is not saturated by water vapor, and therefore the theoretical basis is weak. Because the atmosphere's saturation is around 70% on average, it could possible that the positive water feedback relationship would follow the Clausius–Clapeyron equation. The direct humidity and temperature measurements from 1980 onward show no positive water feedback in the long run.

The encompassing satellite temperature measurements were introduced in 1979 (UAH, 2017). In the same year, a new humidity semiconductor sensor technology Humicap® was introduced by the leading humidity measurement company Vaisala. Reliable empirical conclusions about the water feedback can be drawn from the behavior of the climate since 1979. Global humidity data is available from 1948 but its accuracy is not at the same level as data after 1979.

The temperature according to the UAH satellite data set of the lower troposphere (UAH, 2022) and absolute humidity as Total Precipitable Water (TPW) values from NOAA's NCEP/NCAR Reanalysis dataset (2022) are depicted in Fig. 1. The short-term temperature changes are distinctly related to the El Niño and La Niña events, which are caused by the regional changes of the ocean currents and winds in the tropical central and eastern Pacific Ocean. They initiate the temperature change, and the strong change in absolute humidity amplifies the change by a factor of about 100 percent (Ollila, 2020a). It is practically the same as the positive feedback used by IPCC, but can it be found in the long-term trends?

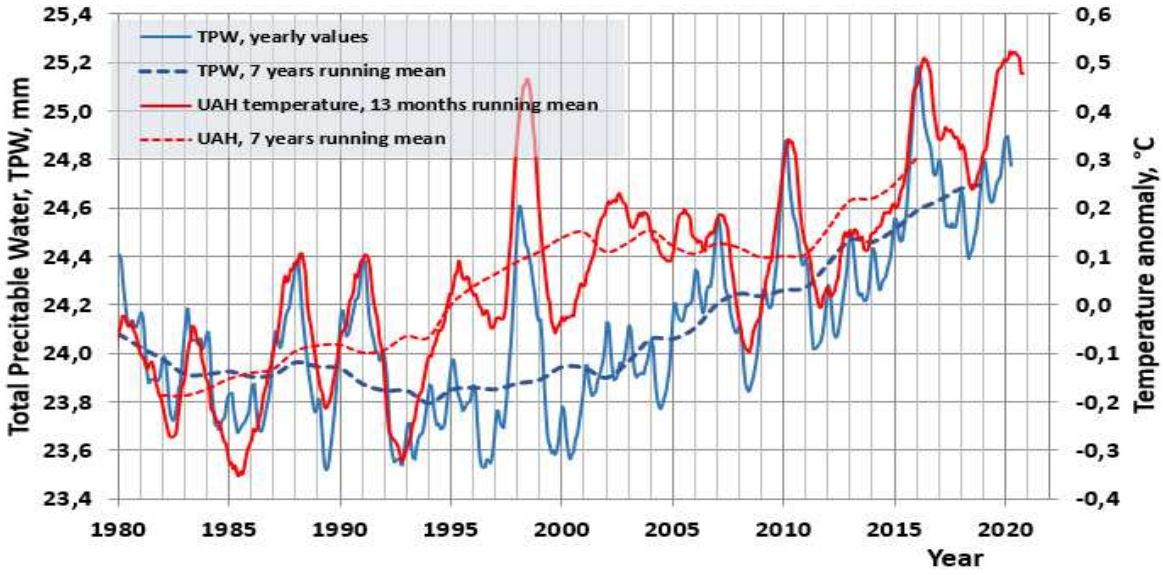

Figure 1. The temperature trend and TPW (Total Precipitable Water) trends from 1980 to 2020.

There are essential features in the long-term trends of temperature and TPW, which are calculated and depicted as yearly and 11-year running mean values. The long-term value of temperature has increased by about 0.4 ºC from 1979 to 2000 but the TPW values show a negative trend. During the temperature pause from 2000 to 2015, the TPW values show a positive trend. This behavior of TPW conflicts with the positive water feedback theory.

The surface temperature values can be calculated using a simple equation, as defined by the IPCC (2013, p. 664):

$$dTs = \lambda * RF\ [°C] \quad (2)$$

where dTs is the global mean surface temperature change, and λ is the "climate sensitivity parameter". The IPCC reported in TAR (2001) that "*λ is the nearly invariant parameter (typically about 0.5 K/(Wm^{-2}).*" This λ value was taken from the study of Ramanathan et al. (1985), based on eight research papers varying from 0.47 K/(Wm^{-2}) to 0.53 K/(Wm^{-2}). When Syuruko Manabe was awarded the Nobel Prize for Physics in 2021, one of Manabe's main credits was that he was the first to introduce positive water feedback in 1967 (Manabe, 1967). He concluded that water feedback doubles the original RF of CO_2, and his λ value was 0.53 K/(Wm^{-2}). This feature became one of the essential features of GCMs as early as the 1980s but in his original paper, Manabe did not conclude if positive water feedback should be used or not in warming calculations.

In AR6 (IPCC, 2021) the IPCC changed its nomenclature and used the term "climate feedback parameter" α, which is the reciprocal of λ = 1/α. The feedback parameter α can be decomposed into different types of feedback, and the sum of feedback parameters is the direct relationship between the ERF and the global equilibrium surface temperature change.

Even though the IPCC did not report a λ value for ERF in AR6, it can be calculated from the data in Fig. 7.6 and Fig. 7.7 of AR6 (IPCC, 2021), which are based on the GCM calculations. The ERF value of 2.70 Wm^{-2} results in a warming of 1.27 °C, meaning the λ value of 1.27 °C / 2.70 Wm^{-2} = 0.47 °C/(Wm^{-2}), which is applicable in TCR calculations since the λ value of CO_2 is the same.

This λ value means that water feedback has been applied in the GCMs used for calculating warming values in Fig. 7.7.

It is possible to calculate the value of λ using different methods. The simplest method is based on the total energy balance of the Earth by equalizing the absorbed and emitted radiation fluxes (Schlesinger, 1986; Ollila, 2014)

$$SC(1-\alpha) * (\pi r^2) = sT^4 * (4\pi r^2)\ [W] \quad (3)$$

where SC is the solar constant (~1360 Wm^{-2}), α is the total albedo of the Earth, s is the Stefan-Boltzmann constant ($5.6704*10^{-8}$ $[Wm^{-2}K^{-4}]$, and T is the temperature (K). The term SC(1-α)/4 is the same as the net radiative forcing (RF) and therefore Eq. (3) can be written in the form $RF = sT^4$. When this equation is derived, it will be $d(RF)/dT = 4sT^3 = 4(RF)/T$. The ratio d(RF)/dT can be inverted, transforming it into λ:

$$dT/(d(RF)) = \lambda = T/(4RF) = T/(SC(1-\alpha))\ [K/Wm^{-2}] \quad (4)$$

Using the average radiation CERES (2021) flux values for the period 2008–2014, λ = 255.294 K /(1360.04*(1-0.2916) Wm^{-2}) = 0.265 K/(Wm^{-2}). Temperature 255.294 corresponds to the Stefan-Boltzmann temperature for radiation 240 Wm^{-2}. Since λ gives the slope of a very nonlinear expression, there might be doubts if temperature change depends linearly closely enough on the RF in the range of about +10 Wm^{-2} as needed in the Shared Socioeconomic Pathways (SSP) scenario calculations of the IPCC. In Fig. 2, the emission temperature is depicted as a function of the Stefan–Boltzmann law and according to Eq. (1), using the λ value of 0.265 Wm^{-2}. The deviation between these two curves is insignificant, and the numerical values show that in the RF range from 230 Wm^{-2} to 250 Wm^{-2}, the error with these two equations is only 0.05 °C. This means that the linear Eq. (1) using a constant λ value is sound when calculating the dT values of different RF forcings.

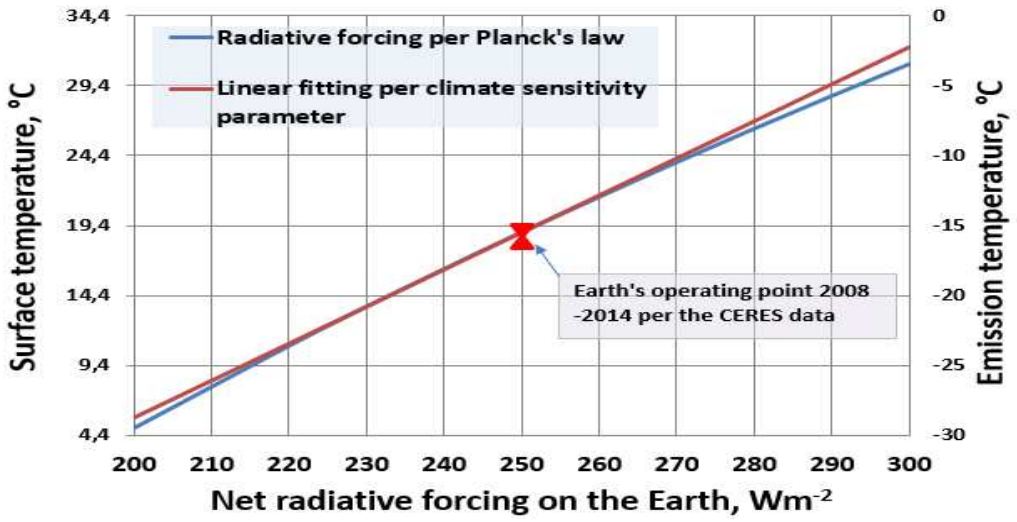

Figure 2. Emission temperature dependency according to Stefan-Boltzmann law and according to linear dependency per Eq. (4).

The difference between the λ values of 0.47 K/(Wm^{-2}) and 0.265 K/(Wm^{-2}) is due to the positive water feedback.

3.3 Climate sensitivity

Climate sensitivity (CS) is a useful measure, telling us how much the Earth's surface temperature Ts would increase driven if CO_2 concentration would increase from 280 ppm to 560 ppm (=2*CO_2). There are two types of climate sensitivity, namely Transient Climate Response (TCR) which was called earlier Transient Climate Sensitivity (TCS), and Equilibrium Climate Sensitivity (ECS) (IPCC, 2013). According to AR6 (IPCC, 2021) the "*TCR is a surface temperature response for the hypothetical scenario in which atmospheric carbon dioxide (CO_2) increases at 1% yr^{-1} from pre-industrial to the time of a doubling of atmospheric CO_2 concentration (year 70)"*. The TAR of the IPCC (2001) defines TCR as a transition of the surface-troposphere system from one equilibrium state to another.

In the ECS calculations, the climate system must reach the equilibrium, which takes a longer amount of time, because the deep oceans are included and they have a long time to heat up and not all feedbacks are developed into full effects, like albedo changes of the surface for example. IPCC (2013, p. 1112) also states that *"TCR is a more informative indicator of future climate than ECS"*. Therefore, the analyses of this study have been carried out only for TCR values.

Applying Eq. (2) gives the TCR value of 1.85 °C (= 0.47 °C/(Wm^{-2}) *3.93 Wm^{-2}), while the best estimate of AR6 (IPCC, 2021) is 1.8 °C. For example, the Ts for the worst-case scenario SSP5-8.5 determined according to Eq. (1) would be: dTs = 0.47 K/(Wm^{-2}) * 8.5 Wm^{-2} = 4.0 °C using the λ value of the AR6. Ts would be 4.5 °C using the λ value of 0.5 K/(Wm^{-2}), which is practically the same as the average value of 4.4 °C of the AR6 calculated by GCMs. These examples show that the average warming values calculated using Eq. (1) are the same as the results calculated by complicated GCMs applicable for the present-day warming, TCR calculations, and scenarios according to SSP (Shared Socioeconomic Pathways) calculations.

This fact is not easily accepted by those researchers who think that these calculations can be correctly carried out only by GCMs. What is the relationship between the λ and the TCR, and are the TCR values calculated using λ close enough to TCR values as defined by the IPCC?

It is a question about the dynamic delays in Ts calculations. The TCR specification (IPCC, 2021) defines that CO_2 increases at 1% yr^{-1}, from pre-industrial levels to double the atmospheric CO_2 concentration. Since the CO_2 growth rate has been smaller than 1 % yr^{-1}, the dT effects from 1750 to 2019 in Figure 7.7 of AR6 can be simply calculated according to the equation T = λ * RF. This means that the results are the same when using Eq. (1) compared to the average results of several GCM simulations. The same applies to TCR calculations, as shown above: 1.85 °C using λ versus 1.8 °C using GCMs. If there were time delays in response longer than one year, the equation dT = λ * RF would give different results.

One could expect, that the TCR values calculated by GCMs are more accurate than those calculated by using Eq. (1). In fact, there is quite a significant uncertainty range by using GCMs as can be found in the AR6 (IPCC, 2021): "*The best estimate of TCR is 1.8°C, the likely range is 1.4°C to 2.2°C"*. This uncertainty comes from the GCMs, which use different modeling methods and especially different amounts of various feedback. It means that GCMs do not improve the accuracy of TCR calculations but increase uncertainty for the reasons commented above.

Using Eq. (1) for calculating the warming values is correct since the dynamical time constant for the ocean is 2.74 months, and for land, 1.04 months (Stine et al., 2009). These values mean that for a stepwise RF change, Ts has reached its new equilibrium value in one year, since the settling (relaxation) time is about four times longer (98.3 % of the final change achieved) than the

residence time (4 * 2.74 = 11 months) according to a first-order process dynamic system having a single time constant.

The literature survey of non-IPCC TCR values can be divided into three major categories based on the research method, namely A) using the 2*CO_2 values of the IPCC, B) using the 2*CO_2 by applying researchers own LBL analysis calculations, C) using observed Ts values and other climate data.

The survey of research studies of category C reveals that the TCR values vary from 0.0 °C of Fleming (2018) to 1.2 °C of Otto et al. (2013). The results of this category are not reliable enough since they are too heavily dependent on other climate drivers like solar irradiation variations, volcanic impacts, surface albedo changes, etc. Kissin (2015). Usually, the elimination of these effects has not been considered at all.

The TCR values of category A are very consistent since they are very close to each other: 1.15 °C from Bengtson and Schwartz (2012), 1.2 °C from Schlesinger (1986), and 1.33 °C from Lewis and Curry (2015). Even though these research studies apply 3.7 Wm^{-2} as the RF value, they have not found positive water feedback in the climate explaining the deviations from the IPCC's value of 1.8 °C. These results are fully in line with the IPCC (2007), which writes in section 8.6.2.3 of AR4 that *"with any feedback operating, the global warming from GCMs would be around 1.2 °C."* Ollila (2020b) has carried out warming calculations by applying only feedback from the atmosphere, which is called Planck's response. Using an RF value of 3.7 Wm^{-2} gives the warming value of 1.12 °C, which is also very close to the values above.

The results of category B vary considerably little: 0.6 °C by Barrett et al. (2006), 0.48 °C by Miskolczi and Mlynczak (2004), 0.51 °C by Ollila (2012), 0.6 °C by Ollila (2014), 0.5 – 0.7 °C by Kissin (2015), 0.4 °C by Smirnov (2017), 0.7 °C by Harde (2017), and 0.5 °C by Schildknecht (2020). The only explanation is that these researchers have found a smaller 2*CO_2 value than 3.7 Wm^{-2} and they have not found positive water feedback. The differences cannot be explained by the identified flaws in calculation methods.

It should be noticed that the survey of this study does not cover all research studies showing lower CS values than IPCC. Gervais (2021) has listed 109 studies that conclude that CS is from 0.0 to 1°C. The most common result of these studies is that the TCR/ECS value is negligible or close to zero, and they are usually based on the analysis of empirical climate data. The studies of Miskolczi (2014) and Drotos et al. (2020) have proposed a feedback mechanism in the climate that will drive the long-term temperature effect of 2*CO_2 to zero, which means that the GH effect would be constant and not depend on the CO_2 concentration; so far, these proposals have not received any common acceptance.

3.4 Relative strengths of major GH gases

The global warming potential (GWP) definition means how much a GH gas can absorb infrared energy if 1 kg has been released into the atmosphere over a specified period (normally 100 years) when compared to the same amount of CO_2 gas (IPCC, 2007). The 100-year GWP value of methane is 27.9 and the same value of nitrogen oxide is 273 (IPCC, 2021). The GPW value definition is highly theoretical, and it is not applicable in warming calculations, because only the actual GH gas concentration has a warming impact and not the future concentrations.

A more realistic analysis can be carried out to find out the relative strengths in the climate of this century by increasing the GH gas concentration in question by 10 % from its concentration in the present atmospheric conditions and calculating the absorption for the altitude of 120 km (Ollila, 2017a). When CO_2 acts as a reference having a strength of 1, the relative strengths of other GH

gases are water 11.8, ozone 0.78, nitrogen oxide 0.14, and methane 0.11,

The simplest method for comparing the relative strengths of GH gases is to compare their RF values from 1750 to 2019 as shown in Table 1.

Table 1. Relative strengths of carbon dioxide, methane, and nitrogen oxide according to AR6 (IPCC, 2021, Fig. 7.6) based on the concentration changes from 1750 to 2019.

GH gas	RF in 2019, Wm^{-2}	Concentration change, %	RF/1% change	Relative strength
CO_2	2.16	40.36	5.35	1
CH_4	0.54	159.17	0.34	0.11
N_2O	0.21	20.00	1.05	0.25

These two calculation methods show that the GWP values give wrong images about the strengths, and they do not represent the warming impacts of GH gas on a certain year during this century. The warming impact of water is almost linearly dependent on the water vapor content in the atmosphere, and it explains why water is such a strong GH gas.

The physical explanations for these relative strengths can be noticed in Fig. 3, where the absorption peaks of major GH gases have been depicted.

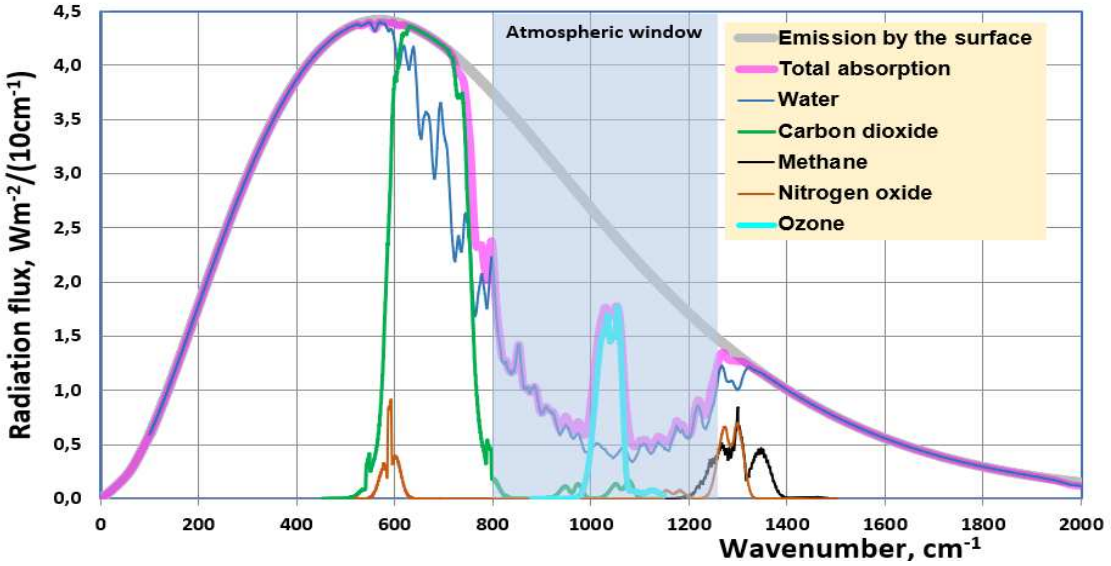

Figure 3. The absorption areas of GH gases in clear sky conditions.

The absorption peaks of methane and nitrogen oxide are badly overlapping with the absorption effects of water and carbon dioxide explaining their weak RF impacts. On the other hand, the absorption peak of ozone is relatively strong since its absorption wavenumber zone from 1000 to 1100 water has the minimum absorption effect.

3.5 Carbon dioxide circulation and time delays in the atmosphere

In calculating the future warming impacts of CO_2, it is important to know in which way fossil emissions would change the atmospheric CO_2 concentration. The only way to find out this behavior is to build a model simulating the carbon cycle between the atmosphere, the ocean, and the land. About 25 % of the atmospheric CO_2 changes every year, because the oceans absolve and dissolve CO_2, and in the same way land plants (later land) photosynthesize and respire CO_2. The present-day anthropogenic emission of about 10 GtC per year (gigatons of carbon) is only 4.5 % of the annual CO_2 flux of about 220 GtC circulating through the atmosphere.

Since 1960, CO_2 circulation has behaved practically the same way that about 55 % of annual emissions have been taken up by the two sinks. During the last 10 years, the atmospheric CO_2 amount has increased yearly with the amount corresponding to about 4.5 GtC, which is 45 % of the annual fossil fuel emissions but it does not mean that this increase is totally anthropogenic as the IPCC assumes. Yearly fossil emissions mix with the existing atmospheric CO_2. From this almost evenly mixed CO_2, the ocean, and the land uptake CO_2 according to their atmospheric composition, and simultaneously CO_2 flows into the atmosphere from the ocean and the land having different compositions. A comprehensive isotope measurement study of the dissolved CO_2 in the ocean (Sabine et al., 2004) shows that the ocean is a sink for anthropogenic CO_2, but the sink of the total CO_2 (total CO_2 is the mixture of anthropogenic and natural CO_2) between the ocean and the land is not clear. The ocean used to be the main sink for the total CO_2 (IPCC, 2013; Ollila, 2020c) before 1960. According to the AR6 (IPCC, 2021) during 2010-2019 the average yearly sink anthropogenic CO_2 value of 5.9 GtC yr^{-1} was divided 42 % versus 58 % between the ocean and the land. This means that if the recycling system of CO_2 works in the same way also during this century, the atmospheric CO_2 concentration will increase steadily.

Two permanent isotopes of carbon molecules exist. The most common is ^{12}C, having 6 positrons and 6 neutrons; however, ^{13}C has one extra neutron. Isotope ^{12}C is the most common, being 98.9 % of all carbon; the rest is ^{13}C. An exceedingly small concentration of unstable isotope ^{14}C, which is radioactive, also exists.

The measurement unit of ^{13}C (marked as $\delta^{13}C$) is a fraction of carbon isotope ^{13}C expressed as ‰, and it has been called permille. This unit is linearly dependent (Srivastava et al., 2018) on the relationship $^{13}C/^{12}C$*:*

$$\delta^{13}C = (S/N-1) * 1000\ [‰] \quad (5)$$

where $S = {}^{13}C/{}^{12}C$ being a sample and $N = ({}^{13}C/{}^{12}C)_{standard} = 0{,}0112372$. The value of the standard comes from a sea fossil "Belemnitella Americana." Many climate researchers have never heard about this measurement unit. It looks like the IPCC does not want to report on permille values since in the AR6 (IPCC, 2021) is only one figure namely Fig. 5-6 and its panel c, where is a short permille trend of the atmospheric CO_2. The same applies to the main referred research study (Friedlingstein et al., 2020), which is the basis of the carbon cycle description in the AR6: no reference to the permille values.

Anthropogenic CO_2 means CO_2 originating from fossil fuels and land use (NOAA, 2018). Fossil fuels have the same permille value as plants from the Carboniferous era (359 – 299 million years ago); this value is -28 ‰. The typical $\delta^{13}C$ values in the present day are the atmosphere about -8.6 ‰, the ocean surface from -8.0 ‰ to -10 ‰, the land -26 ‰, and the fossil fuels -28 ‰ (Quay et al., 2003; NOAA, 2020c).

The permille unit is odd because most values of carbon dioxide (CO_2) mixtures are negative. The atmosphere is the mixture of natural CO_2 from the ocean and plants and the fraction of anthropogenic emissions remaining there. The term "total CO_2" has been used for the mixture of natural and anthropogenic CO_2 flux or amount. The Suess Effect shifts continuously the isotopic ratio of both ^{13}C and ^{14}C in the atmosphere and the ocean because of anthropogenic CO_2 emissions. The change in $\delta^{13}C$ value is mainly due to the combustion of fossil fuels and the circulation of CO_2. Because the permille values of anthropogenic CO_2 differ so much from the atmospheric values today (-8.6 ‰), it can be used to calculate the fraction of anthropogenic CO_2 in the atmosphere by applying carbon circulation models.

Carbon cycle models referred to by the IPCC are all-encompassing and they apply several sub-models designed for special tasks like CO_2 exchange with plants. In this section, the approach is to analyze critically the IPCC's carbon cycle model, which refers to the yearly published article "Global Carbon Budget" by Friedlingstein et al (2020), and to compare its key figures to the results of the 1DAOBM-3 model of Ollila (2020c), and Berry (2021).

In AR5, the IPCC (2013a, p. 467–469) writes: "*About half of the emissions remained in the atmosphere 240 PgC±10 PgC since 1750.*" In the same way in AR6 (2021), the increased mass of the atmosphere originates from the emissions. The total CO_2 mass in 2019 was 876 GtC; in 1750, the same was 591 GtC (IPCC, 2021). Two simple tests can be carried out to check the numbers of the AR6. If all the CO_2 increase were anthropogenic CO_2 as IPCC reports (2021), its amount would be 285 GtC in 2019, meaning a fraction of 32.5 %. The rest (67.5 %) would be assumed to be natural CO_2 having a $\delta^{13}C$ value of -6.35‰, which is the permille value of the atmospheric CO_2 in 1750. The $\delta^{13}C$ of this atmospheric CO_2 mixture would be

$$\delta^{13}C = 0.324 * (-28) + 0.676 * (-6.35) = -13.4 \text{ [‰]} \quad (6)$$

If eq. (6) would give the permille value of -8.6 ‰, the permille value of the natural CO_2 in the atmosphere should be about +1.0 ‰. Since the plants have not been sink according to AR6 (IPCC, 2021, p. 5-22), the land has not changed the atmospheric permille value. The ocean has been the major sink but the fractionation from air to sea and from sea to air are so close to each other that the recycling fluxes have not been able to change the natural CO_2 value significantly. This analysis shows that the increased atmospheric mass from 1750 cannot be totally anthropogenic since the currently observed $\delta^{13}C$ is about -8.6‰.

Another test can be carried out to test the correctness of the carbon cycle figures of the IPCC (2021). There is a fractionation phenomenon from air to sea, from sea to air, and vegetation CO_2 exchange. However, about 99 % of anthropogenic CO_2 is a carbon isotope of ^{12}C; therefore, its recycling happens similarly to natural CO_2. Although the ^{13}C fraction would differ in recycling anthropogenic carbon fluxes, over 99 % is the same material, which must still be labeled anthropogenic if it originates from human actions. Table 2 has enlisted the carbon cycle fluxes (CCFs) of the IPCC (2021) from Fig. 5.12 since it is the only presentation of this kind in the AR6.

Table 2. The average CCFs (GtC yr^{-1}) from 2010 to 2017, according to IPPC (2021, Fig. 5.12), and the percentage fraction of the anthropogenic CO_2 from the total oceanic or terrestrial CCF.

Total carbon cycle flux from the atmosphere, GtC yr^{-1}	Anthropogenic CO_2 and percentage from the CCF
Total CO_2 in the atmosphere, 870 GtC	279 GtC, 32.1 %
From the atmosphere to the ocean, anthropogenic, 79.5	25.5 GtC yr^{-1}, 32.0 %
From the atmosphere to land plants, anthropogenic, 142.0	29.0 GtC yr^{-1}, 20.4 %

The key figures in Table 2 mean that the ocean-atmosphere flux would not discriminate the atmosphere's anthropogenic fraction since it contains the same 32.0 % of this fraction because in the atmosphere this fraction is the same of 32.1 %. Surprisingly enough, the gross photosynthesis flux has only 20.4 % of anthropogenic CO_2. Does a physical explanation for this land discrimination exist? No. Instead, the plants prefer anthropogenic CO_2 for its higher ^{12}C isotope concentration. The ocean's euphotic layer (max. depth of about 200 m) also favors anthropogenic CO_2 since phytoplankton and plants prefer the ^{12}C.

According to the IPCC (2021), when there is an annual emission of anthropogenic CO_2 increase,

only the anthropogenic molecules will be sequestrated by the sea and the land plants, and on average 44-45 % is removed from the atmosphere annually (IPCC, 2021). Both anthropogenic and natural CO_2 has about 98.9 % carbon isotopes ^{12}C, but there is no natural process that could identify the origin of ^{12}C and select only ^{12}C molecules with the anthropogenic origin, which would be sequestrated and not a single one with a natural origin. In reality, sequestration of ^{12}C must happen according to the relative amounts of these molecules: if the concentration of ^{12}C with the natural origin is double in comparison to anthropogenic ^{12}C molecules, the double amounts will be sequestrated.

The fractionation phenomenon between the reservoirs changes the relative amounts of ^{13}C molecules (amount only about 1.1 %) and it affects the permille number of the CO_2 amount sequestrated by a reservoir. But fractionation does not control the sequestration process since it is only a consequence.

According to AR6 (IPCC, 2021), "*The ocean uptake of anthropogenic carbon is a two-step set of abiotic processes that involves the exchange of CO_2, first across the air-sea boundary into the surface mixed layer, followed by its transport into the ocean interior where it is stored for decades to millennia, depending on the depth of storage (Gruber et al., 2019)*." This adiabatic process means that the atmospheric CO_2 dissolves in the surface ocean according to Henry's law, which leads to the equilibrium between the atmospheric and the dissolved CO_2. The study of Humlum et al. (2013) reveals that the time lag between CO_2 concentration changes and the ocean's surface temperature is 11-12 months globally.

The AR6 (IPCC, 2021) does not report, in which way the anthropogenic CO_2 is divided between the ocean mixing layer and the intermediate & deep ocean. Gruber et al. (2019) reported that 50 % of the anthropogenic CO_2 is in the layer above 400 meters depth. The total anthropogenic CO_2 in the ocean was 160 GtC in 2019 (IPCC, 2021). Since the surface mixed layer depth is 75-100 meters, the anthropogenic CO_2 in this layer can be estimated to be about 0.3*0.5*160 = 25 GtC. According to IPCC (2021), the annual average recycle 2008-2017 flux of anthropogenic CO_2 was 25.5 GtC. These figures would mean that the ocean recycle flux would return yearly into the atmosphere practically all the anthropogenic CO_2, which was absorbed by the surface mixed layer. This would mean zero sequestration rate by the ocean. This is another example of the physical contradictions of the IPCC model.

The main differences in carbon cycle representations between the AR6 of the IPCC (2021), which is based on the research report of Friedlingstein et al. (2020), Ollila (2020c), and Berry (2021) have been tabulated in Table 3.

Table 3. The key figures of anthropogenic CO_2 according to Friedlingstein et al. (2020) from 2010 to 2019, Ollila (2020c) for the year 2019, and the same of Berry for the year 2020.

Reservoir	Cumulative 1750-2019			Yearly net fluxes	
Amount (GtC) or flux (GtC yr^{-1})	IPCC	Ollila	Berry	IPCC	Ollila
Anthropogenic CO_2 in/to the atmosph.	285	70	71	5.1	0.3
Anthropogenic CO_2 in/to the ocean	170	250	206	2.5	5.8
Anthropogenic CO_2 in/to land plants	230	166	71	3.4	3.2
Total anthropogenic amount, GtC	685	486	452		

The total amount of anthropogenic CO_2 of Ollila includes 32 GtC of land-use CO_2 emissions, and the same of the IPCC is 240 GtC (imbalance in terrestrial sink 10 GtC). The anthropogenic CO_2 amounts of Berry and Ollila are very close to each other, and the main difference is due to the land-

use emissions applied by Ollila. This result is very interesting since the calculation basis of Ollila is a complicated model of CO_2 recycling between different reservoirs considering the fractionation between reservoirs and Berry's approach is simpler.

The ocean absorbs anthropogenic CO_2 yearly at 5.8 GtC according to Ollila (2020c) but in the IPCC's model, it is only 2.6 GtC. The anthropogenic flux 5.8 GtC yr^{-1} is not the net absorption rate of total CO_2, since there is a natural CO_2 flux of 3.6 GtC yr^{-1} back into the atmosphere keeping the net sequestration rate in 2.2 GtC, which is less than in buffer-factor models (2.6 GtC yr^{-1}). This is the reason for the composition of the total atmospheric CO_2 increase of 265 GtC since 1750: 195 GtC of natural CO_2 and 70 GtC of anthropogenic CO_2.

According to Friendlingstein et al. (2020) and the IPCC (2021), the amount of 265 GtC is totally anthropogenic by nature. This is an assumption, which has not been supported by any figures or analyses. In AR4 the IPCC (2007, p. 948) says that the turnover time for natural CO_2 is about four years. It is in line with the definition of the turnover time, which is calculated by diving the total CO_2 mass of the atmosphere mass of 880 GtC with a total CCF of 220 GtC yr^{-1}, which gives the same figure. In AR5 the IPCC (2013, p.469) writes: "*The removal of human-emitted CO2 from the atmosphere by natural processes will take a few hundred thousand years (high confidence). Depending on the RCP scenario considered, about 15 to 40% of emitted CO2 will remain in the atmosphere longer than 1,000 years."* This is again an example of the physical contradictions of the IPCC carbon cycle model.

In tracer testing, which is commonly used in scientific studies, a very small amount of a chemical or a radioactive compound is used to detect flows, delays, and other dynamic properties of a fluid system under scrutiny. For estimating the residence time of the anthropogenic CO_2 in the atmosphere, the results of the only full-scale test carried out by humanity with the climate are now available. The nuclear bomb tests in the atmosphere from 1945 to 1964 accidentally created this kind of tracer test situation.

The decay curve of the ^{14}C can be combined with some of the worldwide measurements (Levin et al., 2010; Utrecht, 2016; LLNL, 2016) carried out since the 1950s and this is illustrated in Fig. 4. The simulated decay rate of the first order dynamic system with a residence time of 16 years gives an excellent fit.

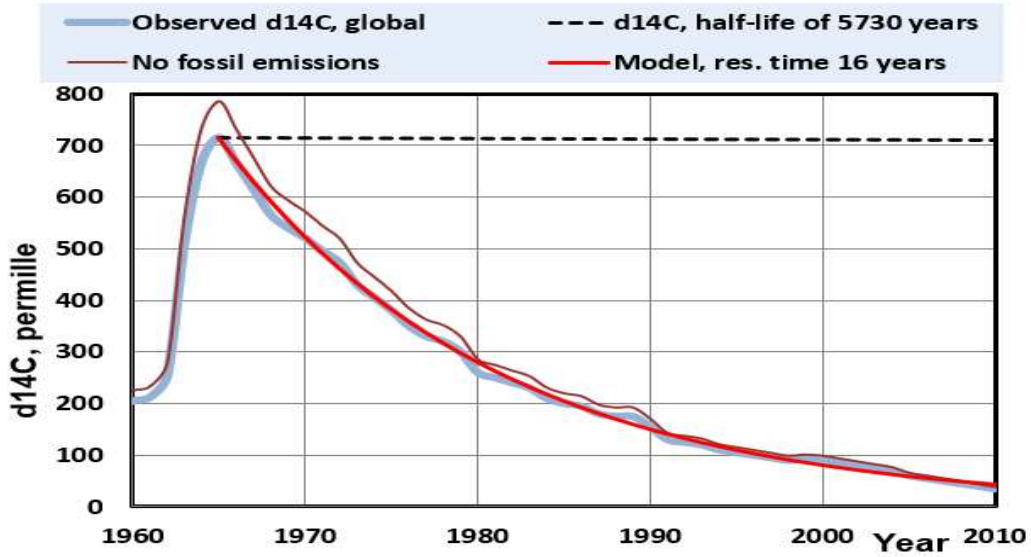

Figure 4. The observed global decaying rate of ^{14}C (blue curve), the simulation result by 1DAOBM-3 (red curve), the theoretical decaying rate of ^{14}C without recycling fluxes in the carbon circulation system (black dashed curve), and the estimated decaying rate in the climate system without fossil fuel emissions (brown curve).

This tracer test by the ^{14}C corresponds perfectly to the behavior of anthropogenic CO_2. In both cases, the concentration change of a new CO_2 flux into the atmosphere starts from zero. The nuclear bomb test can be used to validate any CO_2 circulation model.

If a model gives a shorter residence time of 16 years for anthropogenic CO_2 in the atmosphere, it is probably wrongly composed. This is true for early research studies showing residence times from 2 to 15 years, which gives an average residence time is 7.6 years, which was identified by Segalstad (1998) when he surveyed 34 residence time studies from 1957 to 1990. A common feature of these studies is that they have used a model, where is one mixing tank (the atmosphere) and the total CCF flows through this tank. This process model is flawed since in reality, the carbon cycle encompasses three reservoirs with recycling fluxes.

Revelle and Suess (1956) estimated that "the exchange time" for an atmospheric CO_2 molecule to be absorbed by the sea is "the order of magnitude of 10 years". In this case "the exchange time" T_e was defined to be the half-life time since T_e was marked to be 1/k, where k is the time constant of the first-order dynamic system. A half-time means the time when 50 % of the change has happened. For the first order system a half time = ln2/k = 0.693/k. Residence time T (also called turn-over time) is 1/k. Therefore, in the first order system $T_e = 0.693 * T$.

The value of 10 years of T_e by Suess and Revelle corresponds to 14.4 years of residence time. This value calculated from cosmogenic ^{14}C data is surprisingly close to 16 years of T confirmed by the empirical nuclear bomb tracer test years later.

Another useful timescale is relaxation time or adjustment time (marked with T_{adj}), which means the time needed for a perturbed system to return to equilibrium or a steady state. Because theoretically, T_{adj} would be infinitely long, in practice T_{adj} is approximated by multiplying the residence time by four: $T_{adj} = 4$ T. At this time moment, a step change has reached the level of 98.3 % from the final equilibrium value. The IPCC uses T_{adj} values in reporting how long it takes the anthropogenic CO_2 to leave the atmosphere if anthropogenic emissions would stop.

The conclusion about IPCC's adjustment time for anthropogenic CO_2 is that it is in direct conflict with the tracer test results with radiocarbon. The relaxation time of 1DAOBM-3 is 64 years is the same as the radiocarbon relaxation time.

The simulation results applying 1DAOBM-3 (Ollila, 2020c) and Berry (2021) show that the amount of the anthropogenic CO_2 in the atmosphere in 2019 is only 70 GtC, corresponding to the portion of 8 % because natural CO_2 flows into the atmosphere from the ocean and the vegetation. According to Ollila (2020c), this amount is concordant with the $\delta^{13}C$ measurement in 2017 (Locean, 2016) being -8.6 ‰. Any permille value observation or presentation and how it should be calculated cannot be found in the AR6 (IPCC, 2021) or Friedlingstein et al. (2020). The conclusion could be that the division between natural and anthropogenic atmospheric CO_2 amounts does not support the observed $\delta^{13}C$ value.

Harde and Salby (2021) have concluded that the residence times of atmospheric natural and anthropogenic CO_2 are the same since the CO_2 molecules are similar. They use the term "absorption time", which seems to be according to graphical presentations the same as the residence time of 16 years of bomb carbon.

A simple test can be carried out if the adjustment time of 64 years could be possible for the total CO_2 increase of 285 GtC from 1750 to 2019. How long it would take that the extra 285 GtC in the atmosphere would decrease to zero if the anthropogenic emissions (about 10 GtC yr^{-1}) were stopped totally? If the yearly decrease is the same as the present-day sequestration rate of about 5.5 GtC each year, it would take 52 years. But as the decay curve of ^{14}C shows in Fig. 4, the decay rate will decrease continually according to the first-order dynamic model, which time constant is

16 years. The atmospheric anthropogenic amount of 70 GtC can decrease to almost zero in 64 years as has happened but it is impossible to the total CO_2 amount of 285 GtC due to the restricted sequestration capacity of the ocean and the land plants.

The only way to find an answer is a model simulating carbon recycling between the three reservoirs. Ollila has simulated the decrease rate of the total atmospheric CO_2 when anthropogenic emissions stop by applying his model 1DAOBM-3 and the simplified dynamic models of Bern2.5CC (Joos et al., 2001) and Joos2013 by Joos et al. (2013). Bern2.5CC has been also the selection of the IPCC. The results have been depicted in Fig. 5.

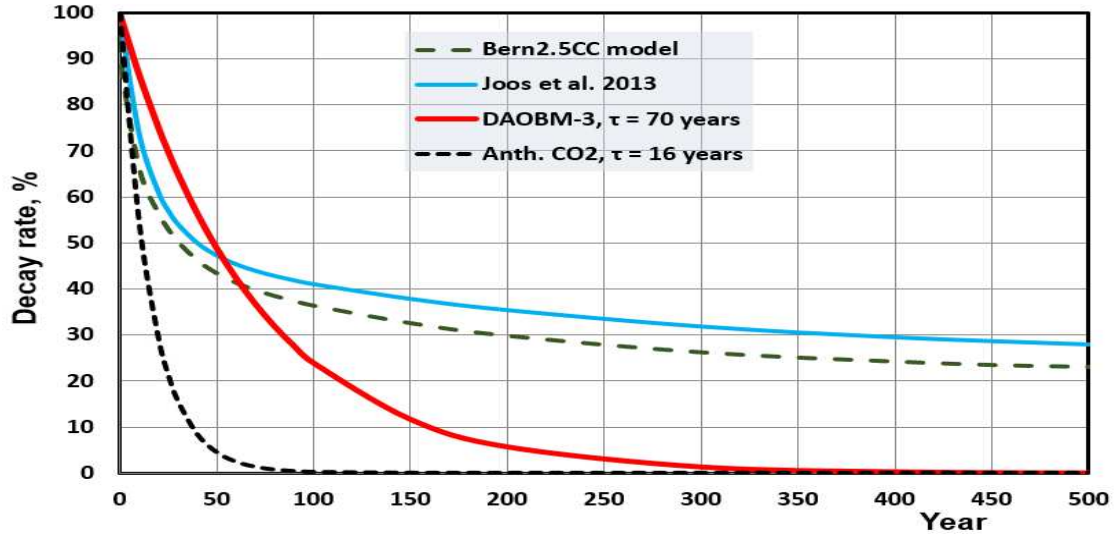

Figure 5. Decay rates of total atmospheric CO_2 concentration using different carbon cycle models, and the anthropogenic CO_2.

The dynamic models of Bern2.5CC and Joos2013 are combinations of four first-order dynamic models with different residence times from 1.189 years to 393.4 years and a constant, which means that CO_2 would never decrease to zero level but stay at the level of about 20 % from the original starting level. There is no physical reason for this assumption.

The fitting of the 1DAOBM-3 simulation shows that a residence time of about 70 years is a reasonable compromise. It is not very good fitting since recycling fluxes, especially from the land, increases on yearly basis more and more CO_2 into the atmosphere. It means that the adjustment time would be 4*70 = 280 years before the atmospheric CO_2 level would have returned to about the same level as 1750. It is not probably a coincidence that the present CO_2 concentration increase has happened during the last 270 years. The surface temperature after 2010 in this simulation has been constant.

A common feature among the IPCC contrarians is that the increase in atmospheric CO_2 cannot be totally anthropogenic since they find several faults and violations of physical laws in the IPCC's carbon cycle modeling. There are still different results among the contrarian research studies but they are closing each other.

3.6 The decadal climate oscillations

The first observational evidence for about 60- to 80-year temperature oscillations in the North Atlantic basin was identified during the 1980s (Folland et al., 1984; Folland et al., 1986), and they

were followed by Schlesinger and Ramankutty (1994), and Klyashtorin et al. (2009). This phenomenon was termed the Atlantic Multidecadal Oscillation (AMO) by Kerr (2000). Chen et al. (2018) identified the same kind of oscillation in the northern part of the Pacific, and it has been termed the Pacific Multidecadal Oscillation (PMO).

Researchers of astrophysics have studied the cyclic behavior of solar magnetic activity since 1843 when it was discovered by Schwabe (1843) to have about an 11-year duration. Hale (1908) discovered the magnetic nature of sunspots and that the complete magnetic cycle spans two solar cycles (22 years). Gleissberg found in 1958 that the solar cycles weaken and strengthen in the period of about 80 years by applying a lowpass filter to the sunspot number records. The periodicity of the 88-year Gleissberg cycle like the 220-year Suess (1980) cycle is related to the Schwabe cycle.

The same periodicities of about 60- to 90-year have been found in regional and global measurements during the thousands of years like the global temperature (HadCRUT5, 2021), Indian monsoons (Agnihotri et al., 2002), NE Pacific coast sediments (Patterson et al., 2004), cosmogenic isotope concentrations of ^{14}C and ^{10}Be (Attolini et al., 1987; Cini Castagnoli et al., 1992), auroral records (Feynman and Fougere, 1984), and tree-ring analyses (Lin et al., 1975; Peristykh and Damon, 2003; Ollila and Timonen, 2022). Scafetta (2010) and Ollila (2017b) have introduced and analyzed the planetary oscillation called Astronomic Harmonic Resonances (AHR), which creates a 60-year oscillation pattern. These different 60-oscillations have been depicted in Fig. 6.

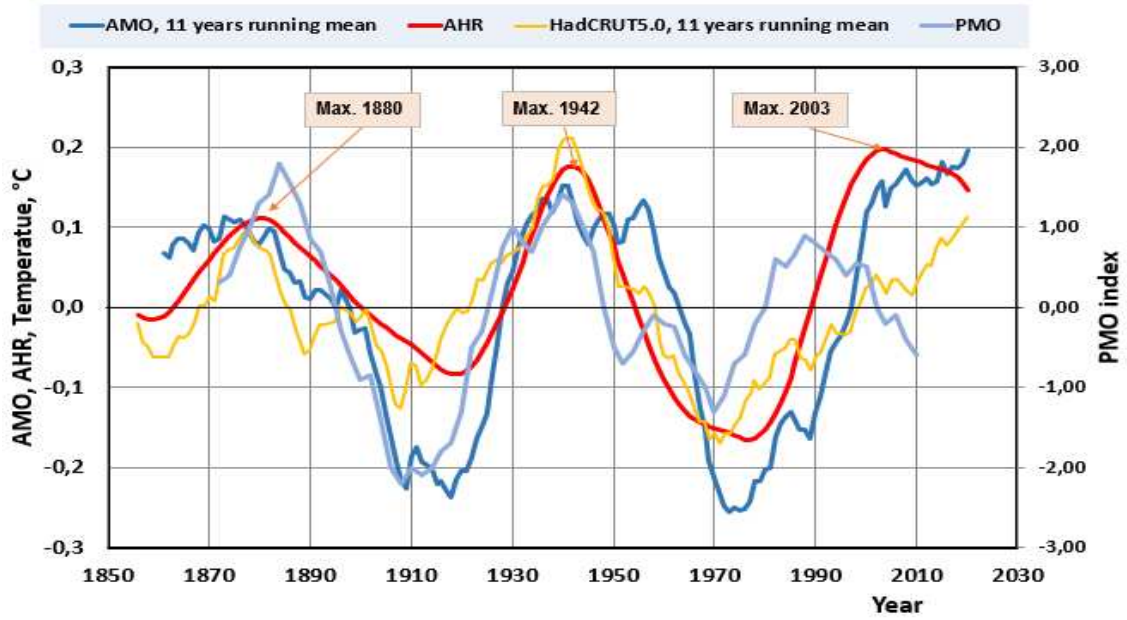

Figure 6. The 60-year fluctuations of AMO (NOAA, 2022), PMO, AHR, and temperature trends. The AHR trend is from the study of Ollila (2017b), and the PMO has been digitized from Fig. 5 of Chen et al. (2016) with 2-year steps.

As Fig. 6 indicates, the AMO and PMO are probably connected to global-scale multidecadal oscillation (GSMO), also called Global-Scale Multidecadal Variability of about 50 to 70 years as observed in the temperature behavior. The trends also illustrate the fact that the NH oscillations are stronger than global oscillation amplitudes.

Internal and external forces have been proposed to cause oscillations. Ermakov et al., (2009) were

the first to introduce that the cosmic dust variations may cause temperature oscillations. Scafetta (2010) and Ollila (2017b) have analyzed that the orbital periods of Jupiter and Saturn can create temperature variations of 60 years by moving the solar system barycentre, which causes variations in the cosmic dust amount entering the atmosphere. The temperature effect happens through cloudiness variations.

Ollila and Timonen (2022) analyzed the year-accurate tree-ring data series called the Finnish Timberline Pine Chronology (FTPC) from the year 1000 onward. They found that the tree-ring variations can be explained with two oscillation periods of 60- and 88-years. The 60-year period matches the AHR phenomenon, and the longer oscillation is a well-known 88-year oscillation, which was first discovered by Gleissberg (1958). This oscillation can be connected to the repetitive occurrence of the basic solar Schwabe cycle of 11 years (varying from 10 to 14 years) as well as the Hale 22-year cycle. In Fig. 6 the 60- and 88-year cycles have been combined and the periodicity of the combined signal correlates very well with the FTPC tree-ring signal, Fig. 7.

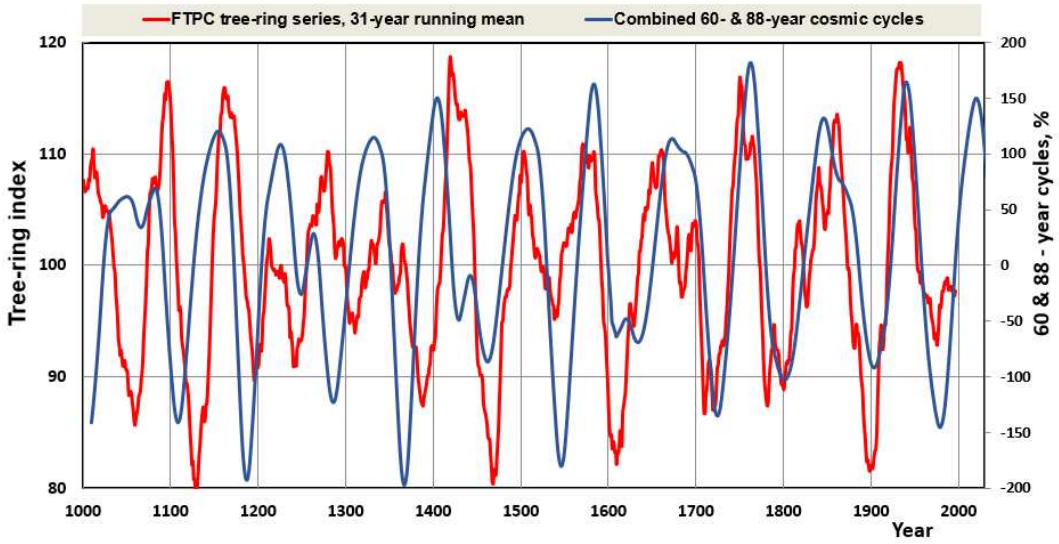

Figure 7. FTPC 31-year running mean signal and combined AHR & Gleissberg signal.

The temperature effect of the 60- & 88-year signal on the temperature change from 1750 to 2019 is minimal since there are grand maximums (simultaneous maximums) during these years. On the other hand, this oscillation can explain the cyclic behavior of the global temperature from 1750 to 2020.

The 60- to 88-year oscillations had their simultaneous maximums in 1940. When the oscillation phases changed to negative phases, the cooling effect of the 60- & 88- year oscillations became dominant over the greenhouse gas effects and caused global temperature to decrease, which happened from 1940 to 1975. Similarly, when the 60- & 88 oscillations turned from a negative to a positive phase, global warming accelerated, as it did after 1975 and finally increased the global temperature by about 0.25 °C (Fig. 6) till 2000. The IPCC has not recognized this temperature behavior in its temperature reconstruction during the 1900s.

3.7 Century- and millennial-scale climate oscillations

Century- and millennial-oscillations have a major role in explaining long-term variations thinking the anthropogenic period from 1750 to the present. If there are longer periodicities than about 250 years, they are possible explanations for the present-time warming at least partially. The first step is to find out research studies analyzing these periods and the second step is to analyze the

proposed mechanisms.

Century- and near-millennium scale research studies have used typically ice-core drilling samples of Antarctica and Greenland, and the other group of studies has used cosmogenic analyses of ^{14}C and ^{10}Be samples from other sources like marine and lake sediment records, and $\delta^{18}O$ records of speleothems (geological formations of mineral deposits in natural caves).

The analyses (Davis et al., 2017; Davis et al., 2018; Davis et al., 2019) of Antarctica drill hole samples have revealed a dominating periodicity of about 143-146 years during the last 446 millennium years, which has been coined to Antarctic Centennial Oscillation (ACO) and Antarctic Oscillation (AAO). The analyses show also millennial-scale oscillations from 800 to 1500 years.

The temperature and CO_2 variations are smaller in Antarctica than in Greenland, and therefore same oscillations should be easily found also on the Northern Hemisphere. Dansgaard et al. (1984) and Dansgaard et al., (1993) concluded from the ice-core records of Greenland for the period of 250 000 years that climate has been unstable during glaciation periods, and these climate periods were named Dansgaard – Oeschger (D-O) oscillations. The periodicities of Greenland's ice-core records according to Vinther et al. (2010) have been 1270, 1470, and 2550 years. In the later article of Vinther (2011), a dominant period is about 1000 years peaking at 1000 and 2000 years. Bond (1997) has found the same 1470±500 years periodicity in the North Atlantic Sea sediments during the Holocene.

Davis et al. (2019) have named external forces of the Earth like periodic variations in solar insolation and natural perturbations of Earth's orbital cycles to be probable reasons for variations.

Also, Bond (1997) thinks that oscillations found in the North Atlantic area are caused by solar insolation changes.

3.8 The Sun's activity changes

The Earth receives about 99.97 % of its energy from the Sun. The Sun's radiated energy measure is Total Solar Irradiance (TSI), which has both long-term variations in the millennium scale and short-term variations like Schwabe's 11-year cycle and Gleissberg's 88-year cycle. Solar magnetic field variations are responsible for solar irradiation changes. There are two main categories of methods in evaluating historical TSI values, which are sunspot records starting from 1610 and cosmogenic isotopes of ^{10}Be and ^{14}C applicable for millennial periods.

Hoyt and Schatten (1993) have used the indices of the equatorial solar rotation rate, sunspot structure, decay rates of sunspots, the number of sunspots without umbrae, and the decay rate of sunspots and sunspot cycle, and developing a model for TSI calculation. Lean (1995, 2004, 2010) has reconstructed the TSI trend from 1610 onward by using revised sunspot activity records and the correlation between sunspot darkening and faculae brightening (bright areas between sunspots data). Bard et al. (2000) have used the cosmogenic isotope measurements of ice cores samples of the South Pole. Shapiro et al. (2011) and Steinhilber et al. (2012) have found that solar irradiancy and cosmic radiation variations have caused large historical solar forcings. These TSI constructions have been depicted in Fig. 8.

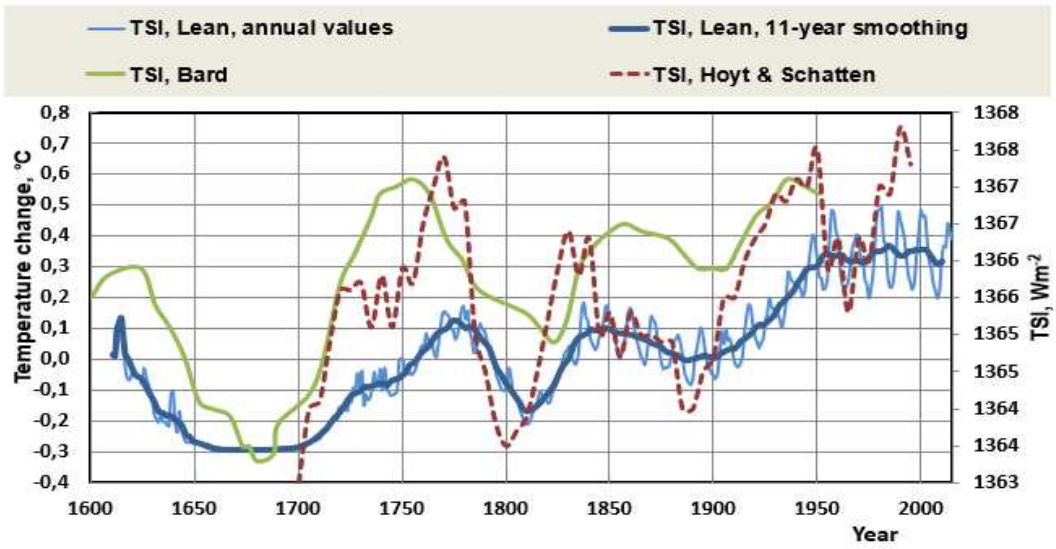

Figure 8. TSI reconstructions of Lean (2004), Hoyt and Schatten (1993), and Bard et al. (1997). The temperature scale applies only to Lean (2004).

According to the data of Lean (2004), the estimated TSI change from 1750 to 2000 has been about 1.1 Wm^{-2}. Based on the latest TSI observations, Lean (2010) has also modified her original TSI estimate of 1366 Wm^{-2} for the 2000s to the modern TSI level of 1361 Wm^{-2} but her estimate for the TSI change is the same 1.1 Wm^{-2}. This TSI change means an RF value of 1.1/4 = 0.275 Wm^{-2}. Connolly et al. (2021) have carried out a comprehensive review study about Sun effects on the Northern Hemisphere temperature trends. Its results show a common feature in all TSI reconstruction studies that around 1900 the TSI value was about -2 Wm^{-2} lower, in the 1930's about +1 Wm^{-2} higher, and from 1990 onward about 1.5 Wm^{-2} higher than the reference level. The TSI reconstruction of Velasco Herrera et al. (2015) shows the same general TSI trends as above and they also predict that the TSI trend has a minimum around the 2050s.

A general conclusion can be drawn that the TSI has varied from 1600 onward including low TSI values during the Little Ice Age (LIA, Maunder minimum) and Dalton minimum. The Sun's activity seems to be now at the maximum level starting from 1990 and the TSI value has varied thereafter relatively little according to the Sun's cycle phase of about 11 years (Schwabe cycle).

Kauppinen et al. (2010) and Ollila (2013) have found out from satellite cloudiness observations that a 1 % cloudiness change causes a 0.1 °C temperature change. Ollila (2017b) has introduced that the TSI impacts cause cloudiness changes and due to this effect, an RF change should be multiplied by a factor of 4.2. By applying this factor, the temperature impact of the TSI change of 1.1 Wm^{-2} from 1750 to 2020 would be 0.32 °C.

3.9 Tree-ring analyses covering the last millennium

Climatic variations leave their mark on the annual rings of trees making it possible to study climate variations. Their thickness growth (tree-ring width) is regulated by the average summer temperature in cool areas and precipitation in arid regions. With the development of dendrochronological methods and the global expansion of research data, the time perspective of research covers the Holocene climate retrospectively. The tree rings are in a special position, as they are the only representative of the year-accurate proxies. In Fig. 9 the results of four tree-ring analyses have been depicted.

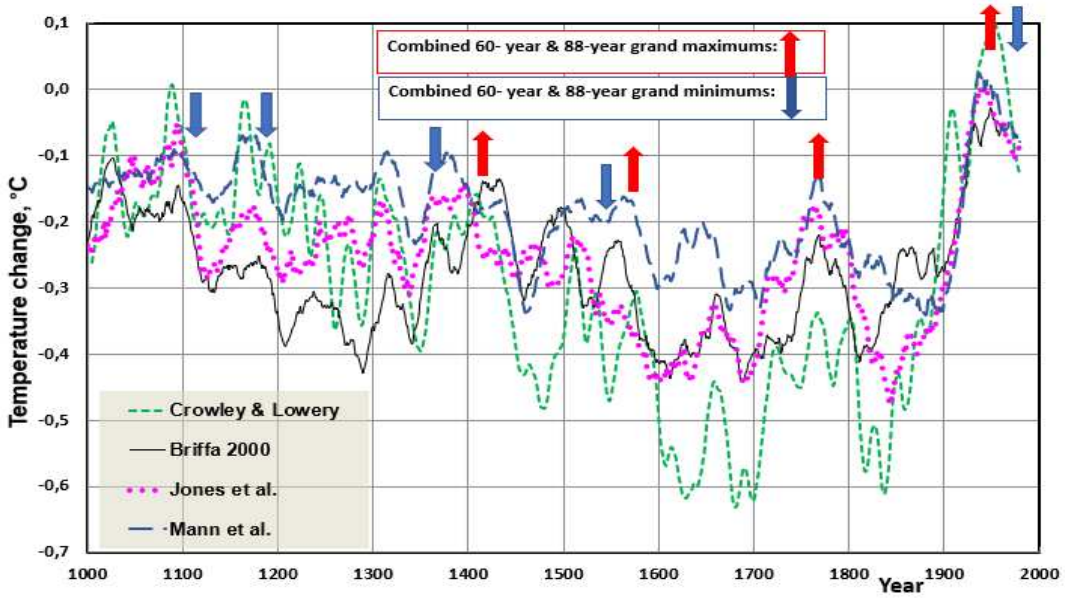

Figure 9. The proxy temperature results of tree-ring analyses of Crowley and Lowery (2000), Briffa (2000), Jones et al. (1998), and Mann et al. (1999). The grand maximums and minimums of 60- and 88-year oscillations have been marked (Ollila and Timonen, 2022).

There are differences in the trends of different tree-ring analyses. Anyway, there is a common tendency that temperatures to start to decline after the beginning of the millennium, there is a minimum during the LIA in the 15th century, and the temperature starts to increase thereafter.

3.10 Summary of temperature proxies of the last millennium

In Fig. 10 three different types of temperature-related proxies have been depicted.

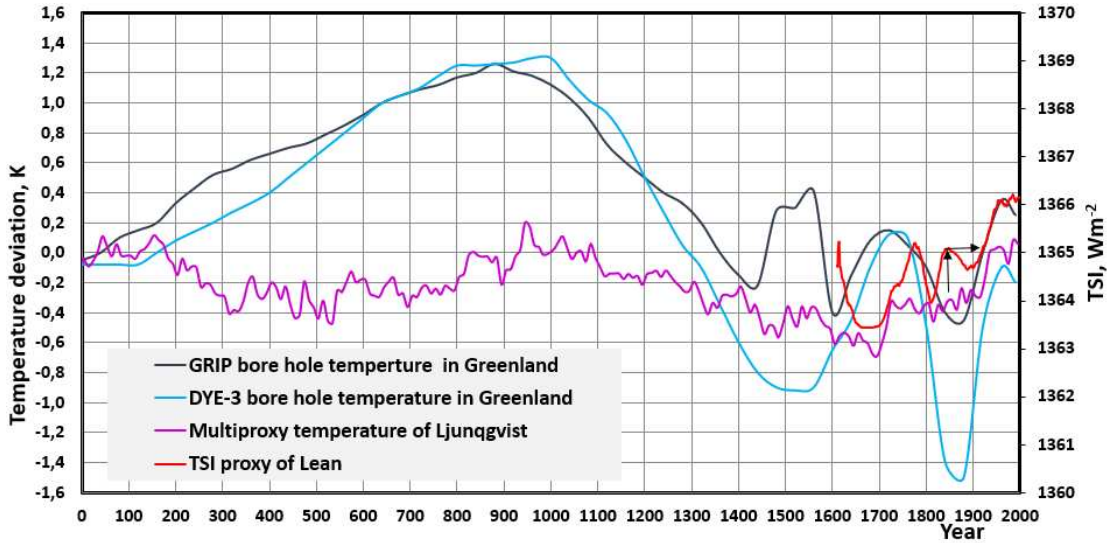

Figure 10. Two proxy temperatures of Greenland's borehole data (Vinther et al, 2011), the multiproxy temperature proxy of Ljungqvist (2010), and the TSI proxy of Lean (1995).

Borehole temperature proxies smooth out short-term variations but they indicate a period of about 1000 years having maximum peaks in about 1000 and the present maximum in 2000 (Hughes et al., 2020; Vinther et al., 2010). The temperature variations seem to be much greater in Greenland than globally, which has also been noticed during the last 50 years.

The temperature data of Ljungqvist (2010) include nine types of temperature data, namely two historical documentary records, three marine sediment records, five lake sediment records, three speleothems $\delta^{18}O$ records, two ice-core $\delta^{18}O$ records, four varved thickness sediment records, five tree-ring width records, five tree-ring maximum latewood density records, and one $\delta^{13}C$ tree-ring record. Because of the combination of different trends, this proxy is rather heavily averaged.

All these proxies show the same kind of temperature trend that during the last millennium, there have been about 1000 yearlong climate oscillations, which is caused by solar activity variations. The Earth is recovering from the LIA and is now at a new maximum.

The IPCC has concluded that the present high temperatures of the 2000s are unprecedented (IPCC, 2013). If the scrutiny period is 2000 years backward, we need not rely on temperature proxy methods only, which show two warm periods (Ljungqvist, 2010) namely the Roman warm period from 250 BC to AD 450 and the Middle Ages warm period from AD 950 to 1250. These well-known warm periods have not happened only in Europe and in North America. Li et al. (2023) have found that during the last 3500 years, the maximum precipitation and temperatures from May to October occurred on the northeastern Tibetan Plateau during the period of 800 – 1400 rather than during the current warm period.

There is also concrete evidence of warmer periods other than temperature proxies. The Lendbreen glacier in Norway is melting and it revealed a well-preserved fabric, which was made according to radiocarbon dating between AD 230 to 390 (Vedeler and Jorgensen, 2013). Retreating Mendenhall glaciers in Alaska has exposed forest remnants growing from 700 to 1000 based on the radiocarbon method according to the statement of Professor Connor (2013). These examples show that these warm periods have been long and at least as warm as the present ones.

3.11 Shortwave radiation anomaly of the 2000s

A significant shortwave (SW) radiation anomaly (later SW_{net}) has been observed by the CERES (2021) satellite measurements from 2001 onward. This trend has been depicted in Fig. 2(a) of Loeb et al. (2021) and in Fig. 7.3 of AR6 (IPCC, 2021). Loeb et al. (2021) concluded that the SW anomaly is probably due to the changes in low-level clouds, and the reasons for these changes may be natural and not known by climate researchers. It should be noted that Marsh and Svensmark (2000) have shown in their study that cosmic rays influence low cloud properties. The SW_{net}, varies according to yearly values of CERES (2021) from 240.36 Wm^{-2} in 2001 to 241.97 Wm^{-2} in 2019, which means an increase of 1,61 Wm^{-2}.

The significant SW anomaly of the 2000s (depicted as shortwave radiation downwelling in Fig. 11) is a reality but its warming impact has not been generally acknowledged in climate science since it challenges the basis of GCMs.

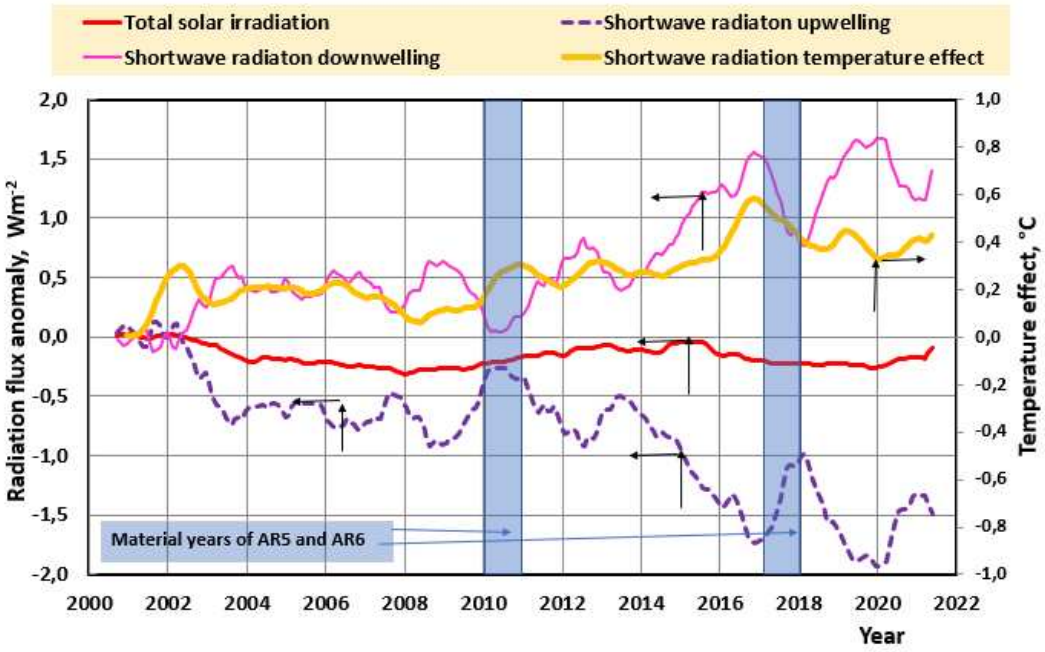

Figure 11. SW and LW radiation changes at the TOA from 2001 to 2020 (Ollila, 2021). The SW_{net} change is the same as the Shortwave radiation downwelling.

The most important issues in climate change are the RF value of CO_2 and the positive water feedback. The SW radiation anomaly of the 2000s created a unique opportunity to test the accuracies of the GCMs applied by the IPCC and a challenging model of Ollila (2021). According to the glossary of AR5 (IPCC, 2013), the portion of any top-of-atmosphere radiative effect that is due to anthropogenic or other external influences, such as changes in the Sun, is termed instantaneous radiative forcing (IRF).

Ollila (2021) simulated the temperature effects during SW radiation anomaly from 2001 to 2019 using both the IPCC's simple climate model and his simple climate model by starting temperature changes from zero in 2001, Fig. 12. In the IPCC model, a λ value of 0.47 Wm^{-2} was applied, and the CO_2 impact was calculated using Eq. (1) and (2), but the other GH gas effects were omitted due to their insignificant impact in the 20-year simulation period. Also, long-term (from 60 to 1000 years) temperature oscillation effects were omitted. For this study, the earlier simulations of the Ollila model were repeated using Eq. (2), with the λ value of 0.265 Wm^{-2}, and the RF value of CO_2 was calculated using Eq. (1). The temperature impact dT of the ENSO effect has been calculated from the Oceanic Nino Index (ONI, 2021), dT = 0.1 * ONI with 6 months delay (Trenberth and Fasullo, 2013; Ollila (2021). The dynamical time constants for the ocean were 2.74 months, and for land, 1.04 months (Stine et al., 2009).

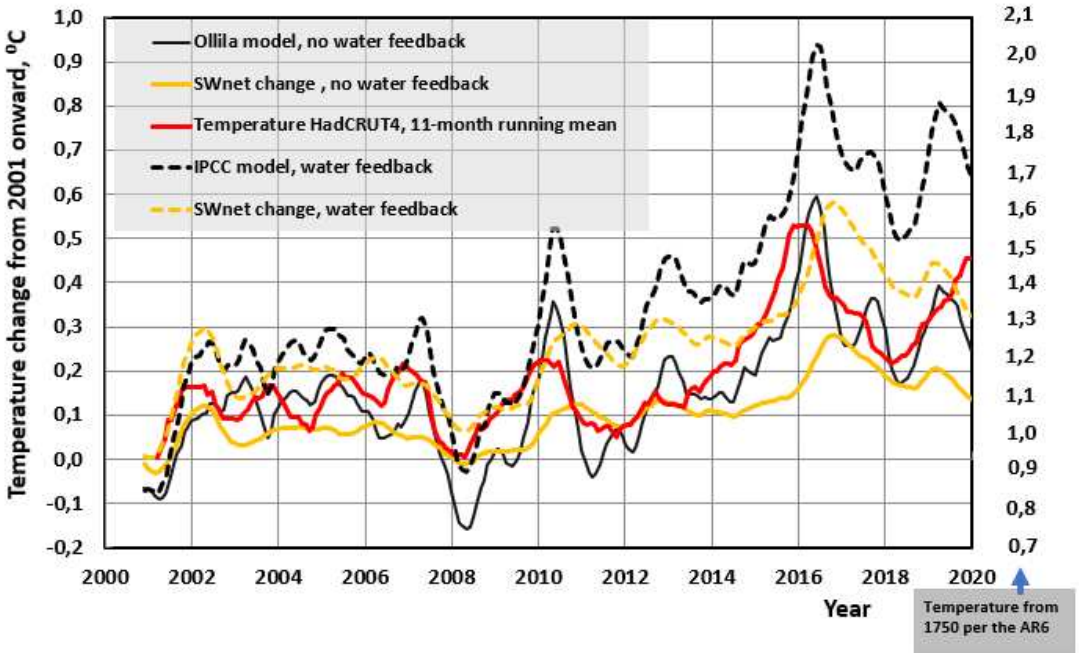

Figure 12. Calculated and observed temperature changes from 2001 to 2020. The SW_{net} changes are the same as in Fig. 11.

The SW_{net} anomaly with the magnitude of 1.75 Wm^{-2} took place under real climate conditions from January 2001 to December 2021; the observed HadCRUT4 (2021) temperature change was 0.46 °C.

The temperature change from 2001 to 2019 according to the IPCC model (Ollila, 2021) is the sum of the SW_{net} change, 0.78 °C, anthropogenic drivers, 0.30 °C, and the ENSO effect, 0.03 °C, to give a total of 1.11 °C, meaning an error of +0.65 °C in the HadCRUT4 temperature. The Ollila model (Ollila, 2021) is the sum of a SW_{net} change of 0.40 °C, CO_2 forcing of 0.10 °C, an ENSO effect of 0.03 °C, and cloud effects of -0.01 °C, for a total of 0.52 °C, meaning an error of +0.06°C in respect of HadCRUT4.

Both model-calculated temperatures follow the ups and downs of the global observations very well indicating that the dynamical time constants are correct. The temperature errors of the IPCC's model are due to the positive water feedback and strong RF value of CO_2.

It is also interesting to note that during the period from 1979 to 2016, the average error of 102 CMIP5 test runs by Christy (2017) to the observed temperature was 0.55 °C, which is close to the temperature impact of the SW anomaly of 0.43 °C as calculated by Ollila (2021) from 2001 to 2019 applying simple models.

The IPCC dropped out this change in AR6 model-based temperature calculations since the solar impact has been -0.01°C. If the real change according to the IPCC science would has been used, the model-calculated temperature change would have been 1.27 + 0.76 = 2.03 °C exceeding the Paris agreed temperature limit.

3.12 The summary of anthropogenic and natural drivers

The summary of climate drivers has been summarized in Table 4.

Table 4. The main anthropogenic and natural drivers of surface temperature changes according to IPCC (2013), IPCC (2021), and this study (=NAGW) from 1750 to 2019. The values in parentheses are calculated according to the IPCC science if the SW anomaly of the 2000s is included.

Driver	IPCC/AR5, °C	IPCC/AR6, °C	NAGW, °C
Carbon dioxide	0.84	1.01	0.36
Methane	0.49	0.28	0.14
Nitrogen oxide	0.09	0.10	0.04
Other anthropogenic gases	0.18	0.44	-
Greenhouse gases	1.59	1.83	0.54
Albedo, volcanic	-0.08	-0.09	-
Aerosols, clouds, and contrails	-0.42	-0.49	-
Anthropogenic totally	1.11	1.28	0.54
Solar	0.03	-0.01	0.32
SW radiation anomaly	-	0.00 (0.78)	0.43
Drivers totally	1.17	1.27 (2.03)	1.29
Observed temperature change	0.85°C	1.29°C	1.29°C
Error, %	+37.7%	-1.6% (57%)	0.0%

The most essential result is that according to AR6 (IPCC, 2021), the contribution of CO_2 during the industrial era has been 1.1 °C but according to this study it is 0.36 °C and according to Harde (2022) it is 0.34 °C.

The trend in climate driver magnitudes from AR4 to AR6 is consistent. The most striking feature is the temperature error percentage change from +37.7% in 2011 to -1.6% in 2019 (material years of AR5 and AR6). This change cannot be explained by the abrupt decrease of anthropogenic drivers as noticed in Table 4 figures. A possible reason could be that the surface temperature has paused as it did in the period from 2000 to 2014 but the temperature increase rate has been greater than normal since 2014. The most probable reason is the emerging SW radiation anomaly of 0.43 °C from 2001 to 2019 as indicated in the last column.

3.13 The GH effect and contribution of GH gases

The temperature effect of the GH effect is generally accepted to be 33-34 °C but the radiative force on the Earth's surface causing this temperature increase is getting almost no attention. The cause of the GH effect can be found only in GH effect definitions. The first comprehensive scientific definition of the GH effect based on the present-day knowledge of radiation fluxes and the effects of clouds has been presented by Hartmann (2015): *"Most of this emitted infrared radiation is absorbed by trace gases and clouds in the overlying atmosphere. The atmosphere also emits radiation, primarily at infrared wavelengths, in all directions. Radiation emitted downward from the atmosphere adds to the warming of Earth's surface by sunlight. This enhanced warming is termed the greenhouse effect.*"

This has not been good enough for the IPCC, which introduced its own definition in the AR5 (2013): *"The longwave radiation (LWR, also referred to as infrared radiation) emitted from the Earth's surface is largely absorbed by certain atmospheric constituents - (greenhouse gases and clouds) - which themselves emit LWR into all directions. The downward directed component of this LWR adds heat to the lower layers of the atmosphere and to the Earth's surface (greenhouse effect)."*

They may look very similar, but there is a crucial difference. The AR5 defines that only GH gases

and clouds are responsible for the GH effect. Hartmann does not specify that they are only GH gases and clouds would reradiate downward from the atmosphere, but it is the atmosphere itself, which causes the infrared radiation. So, there might other energy sources which warm up the atmosphere as solar radiation is absorbed by the atmosphere. Hartmann is in line with Planck's law that any material, which has a temperature above absolute zero, will emit electromagnetic radiation according to its temperature.

Ollila (2019) introduced his definition in 2019 and it considers all the energy fluxes warming the atmosphere: *"The Earth's surface emits LW radiation (infrared radiation) and it transfers heat energy in the form of latent and sensible heating into the atmosphere. Most of the emitted infrared radiation is absorbed by trace gases and clouds in the atmosphere. All three energy fluxes increase the temperature of the atmosphere. The part of the infrared radiation due to these three energy sources emitted downward from the atmosphere adds to the warming of Earth's surface by sunlight and it is called the greenhouse effect."*

In AR6 the IPCC (2021) reformulated the GH effect definition and it can be found only in Glossary:

"The infrared radiative effect of all infrared-absorbing constituents in the atmosphere. Greenhouse gases (GHGs), clouds, and some aerosols absorb terrestrial radiation emitted by the Earth's surface and elsewhere in the atmosphere. These substances emit infrared radiation in all directions, but, equal, the net amount emitted to space is normally less than would have been emitted in the absence of these absorbers because of the decline of temperature with altitude in the troposphere and the consequent weakening of emission. An increase in the concentration of GHGs increases the magnitude of this effect; the difference is sometimes called the enhanced greenhouse effect."

This definition does not specify anymore that only the GH gases and clouds are responsible for the downward LW radiation to the Earth's surface like in the AR5 since this radiation has not been noticed at all: only radiation to all directions. It can be speculated that the IPCC noticed its fault in the AR5 definition that the absorption of LW radiation of about 155 Wm^{-2} cannot create the radiation of about 345 Wm^{-2} and tried to fix the problem. This time the IPCC does not show what is causing the GH effect by omitting the downward radiation which is the essence of the GH effect. If you remove the downward radiation, you remove the GH effect.

The existence of the GH effect is a generally acknowledged fact among researchers but the magnitude (the numerical value) of radiative drivers causing the GH effect has not been analyzed in the assessment reports of the IPCC. The GH effect can be illustrated by the energy budget of the Earth, Fig. 13.

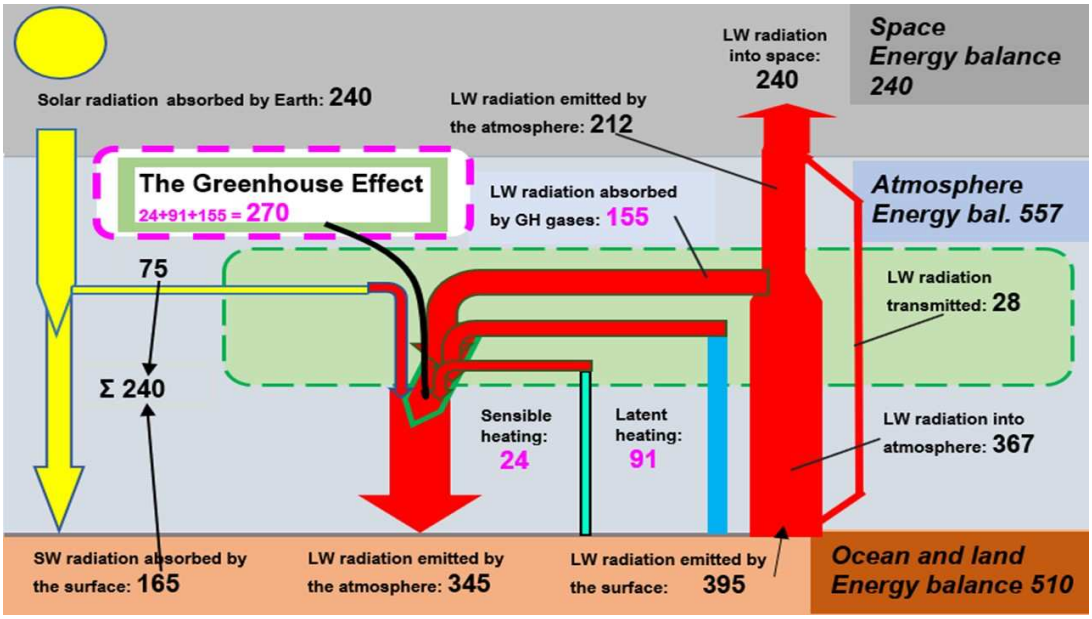

Figure 13. The Earth's energy balance (Ollila, 2019).

The energy balance presented in Fig. 13 is from Ollila (2019). Its numerical flux values are inside the accuracies of Wild et al. (2019), which has been referred to in the AR6 (IPCC, 2021).

The magnitude of the GH effect can be summarized from the flux values in Fig. 13. The reradiation LW flux of 345 Wm^{-2} to the surface is a sum of four fluxes (Wm^{-2}): the absorption of SW radiation 75, LW absorption by GH gases and clouds 155, latent heating 91, and sensible heating 24. The SW absorption flux of 75 Wm^{-2} together with the SW flux to the surface of 165 Wm^{-2} encompasses the net SW radiation of 240 Wm^{-2} to the Earth. The conclusion is that the GH effect is the sum of three energy fluxes recirculating between the surface and the atmosphere, and its magnitude is 270 Wm^{-2} (435-75 = 270).

GH effect deniers either say that the downward LW radiation flux of 345 Wm^{-2} is not real or it cannot warm the surface, since it radiates from the atmosphere being colder than the surface. This flux is real and its value can be confirmed by the worldwide measurement network (Driemel et al, 2018). Its reality and meaning are a fact since the energy budget of the surface cannot be closed without this radiation flux. The rate of radiation heat transfer from a body at temperature T_1 which is surrounded by a body at temperature T_2 is given by the Stefan-Boltzmann law

$$Q = \sigma A \varepsilon (T_1^4 - T_2^4) \ [Wm^{-2}], \quad (7)$$

where σ is the Stefan–Boltzmann constant, A is the surface area of the radiator, and ε is the emissivity. The equation means that there is also a heat transfer rate from a colder body since all material radiates electromagnetic radiation according to Planck's law. The surface temperature T_1 is a result of these two heat transfer rates. The observation based on average radiation flux values over the period 1985-1988 shows that in the clear-sky conditions, the LW radiation upward is 394.1 Wm^{-2} and downward 313.5 Wm^{-2} but in the cloudy-sky conditions LW radiation upward is 396.3 $Wm^{-2,}$ and downward 359.0 Wm^{-2}. These figures mean that during relatively short periods of a few days (about two days of three are cloudy), the surface temperature is higher in cloudy-sky conditions even though the SW radiation to the surface decreases by 68.3 Wm^{-2}. This would not be possible without the simultaneous increase of LW radiation by 45.5 Wm^{-2}.

Practical examples of the warming effect of different sky conditions and the S-B law are carports used in Scandinavian countries: the car windows below open car roofs stay clear in temperatures

from -0 °C to -25 °C when adjacent car windows under the open sky become frozen.

LW radiation excluding the SW radiation absorption radiation is the basis for calculating the contributions of GH gases and clouds to the GH effect. The most referred figure (Kiehl and Trenberth, 2009) of the CO_2 contribution is 26 %. Climate change researchers should realize that this result is calculated in the modified US Standard Atmosphere 76 (US 76) containing 50 % less water than the average global atmosphere (Ollila, 2014). The US 76 has also been called "a standard atmosphere", creating a wrong image (Liou, 1992).

Schmidt et al. (2010) have used the average atmospheric composition and the GH effect magnitude of 155 Wm^{-2} in calculating the contributions of GH gases and clouds in the GH effect. Their results and the same of Ollila (2017a) have been summarized in Table 5.

Table 5. The contributions of GH gases and clouds in the GH effect according to Kiehl & Trenberth (1997), Michell (1989), Schmidt et al. (2010), and Ollila (2017a).

GH effect element	Ollila		Kiehl & Trenberth	Michell	Schmidt et al.
LW absorption element	RF, Wm^{-2}	Contr., %	Contr., %	Contr., %	Contr., %
Water	90.9	33.6	60 (38)	65	50
Carbon dioxide	20.1	7.4	26	32	19
Ozone	6.9	2.6	8	1	
Methane & Nitrogen oxide	1.8	0.7	6	2	7
Clouds	35.9	13.3	(39)		25
LW absorption	*155.6*		*125 (155)*		*155*
Latent heating	90.8	33.6			-
Sensible heating	24.2	8.9			-
GH effect	270.6		155		155

Michell (1989) has not specified the atmosphere. The %-values in parentheses of Kiehl & Trenberth are for cloudy sky conditions. The major reason for a much lower contribution-% of CO_2 by Ollila (2017a) is the magnitude of the GH effect 270.6 Wm^{-2} versus the 155 Wm^{-2} of Schmidt et al. (2010); the absorption value of CO_2 is practically the same in both papers. A counterargument against the calculation basis of 270 Wm^{-2} could be that latent heating does not change the surface temperature, and the difference between the surface emitted radiation 395 Wm^{-2} and the net radiative flux from the Sun is 395 – 240 = 155 Wm^{-2}, which is exactly the absorption magnitude by GH gases and clouds.

The reradiation of 345 Wm^{-2} is the sum of all four energy fluxes warming the atmosphere. This radiation flux warms up evenly the surface and it has an even-handed contribution to three energy fluxes cooling the surface: the LW radiation, latent and sensible heating. We cannot conclude that the latent heating energy originates only from the latent heating part of atmospheric reradiation. In the same way, we cannot conclude that the SW absorption flux of 75 Wm^{-2} contributes only to the radiation capability of the surface, but it does not contribute the latent and sensible heating. Every component warming up the atmosphere contributes to the GH effect (LW reradiation minus SW absorption) according to its energy flux absorbed in the atmosphere. The situation in the climate zones shows that latent and sensible heating is related to the high temperatures of the tropical zone. Therefore, the real GH effect is the sum of LW absorption in the atmosphere, latent heating, and sensible heating.

5. Conclusions and discussion

The alternative climate model NAGW including natural and anthropogenic drivers can explain the long-term global warming from 1750 onward as well the short-term warming during the 2000s.

The summary of the differences between the most important key figures of the IPCC and the challenging NAGW is tabulated in Table 3. The known TSI variations have an important role in explaining the warming before 1880. There are two warming periods since 1930 and the cycling AHR effects can explain these periods of 60-year intervals. The warming mechanisms of TSI and AHR include cloudiness changes and these quantitative effects are based on empirical temperature changes. This review concludes that the NAGW has a solid theoretical background, and its warming value has better conformity with the observed temperature than the AGW. The major parameters of the AR6 (IPCC, 2021) and the parameters applied in the NAGW are collected in Table 6.

Table 6. The summary of differences between the IPCC (2021) and this study including uncertainty limits.

Parameter	AR6, IPCC	NAGW
CO_2 contribution to the GH effect	About 19 % – 26 %	7 % – 8 %
H_2O contribution in the GH effect	About 50 % – 69 %	66 % – 69 %
Water feedback	Amplifies GH gas effects by a factor from 2 to 3	Only short-term (1-2 years) positive feedback
Climate sensitivity parameter (λ)	0.47 K/(Wm^{-2}) ± 0.03	0.265 K/(Wm^{-2}) ± 0.05
RF value of 2 * CO_2	3.93 Wm^{-2} ± 0.47 Wm^{-2}	2.4 Wm^{-2} ± 0.3 Wm^{-2}
Anthrop. CO_2 in the atmosphere in 2019	265 GtC	70 GtC
The residence time of anthropogenic CO_2	From centuries to millennia	16 years ± 1 years
The residence time of total CO_2	Same as anthropogenic CO_2	70 years ± 10 years
Transient Climate Response – TCR	1.8 ºC (1.4 ºC + 2.2 ºC)	0.6 ºC ± 0.15ºC
Equilibrium climate sensitivity - ECS	3.0 ºC (2.5 ºC – 4.0 ºC)	0.6 ºC ± 0.15 ºC
Greenhouse effect	159 Wm^{-2}	270 Wm^{-2}

The differences and the reason for them are already analyzed in the former sections. The most important differences are the water feedback and the RF formula of CO_2. These two differences explain the differences in CS values. Considering the future atmospheric CO_2 concentration development, also the residence time difference is very essential. Table 6 does not show the temperature effect of the SW radiation anomaly, which is not included in GCM simulations in the AR6 calculations for 2019, and which is about 0.78 °C.

Because the Sun's activity should be decreasing and the AHR effect also declines after a few years, the global temperature according to this alternative warming theory should decline permanently after 2020 even though the warming effect of GH gases increases steadily.

Conflicts of interest/competing interests: The author has no conflicts of interest to declare that are relevant to the content of this article.

Funding: No funding was received for conducting this study.

Guest-Editor: Stein Storlie Bergsmark; Reviewers: anonymous.

References

Agnihotri R, Dutta K, Bhushan R, Somayajulu BLK, 2002: Evidence for solar forcing on the Indian monsoon during the last millennium. Earth and Planet Sci Lett, 198, 521-527. https://doi.org/10.1016/S0012-821X(02)00530-7

Attolini MR, Cecchini S, Galli M, Nanni T, 1987: The Gleissberg and 130-year periodicity in the cosmogenic isotopes in the past: The Sun as a quasi-periodic system. Proceedings of the 20th International Cosmic Ray Conference, Moscow, 4, 323, Nauka, Moscow. https://articles.adsabs.harvard.edu/pdf/1987ICRC...20d.323A

Bard E, Raisbeck G, Françoise You F, Jouzel J, 1997: *Solar modulation of cosmogenic nuclide production over the last millennium: comparison between 14C and 10Be records*. Earth & Planet Sci Lett, 150, 0–462. https://doi.org/10.1016/S0012-821X(97)00082-4

Bard E, Raisbeck G, Françoise You F, Jouzel J, 2000: *Solar irradiance during the last 1200 years based on cosmogenic nuclides.* Tellus, 52B, 985–992. https://doi.org/10.1034/j.1600-0889.2000.d01-7.x

Barrett J, Bellamy D, Hug H, 2006: *On the sensitivity of the atmosphere to the doubling of the carbon dioxide concentration and on water vapour feedback.* E&E, 17(4), 603-607. https://sci-hub.wf/10.1260/095830506778644198

Bengtsson L, Schwartz SE, 2013: *Determination of a lower bound on Earth's climate sensitivity.* Tellus B Chem Phys Meteorol, 65:1. DOI: 10.3402/tellusb.v65i0.21533

Berry EX, 2021*: The impact of human CO_2 of atmospheric CO_2.* Sci Clim Change, 1.2, 213-249. https://scienceofclimatechange.org/wp-content/uploads/Berry-2021-Impact-of-human-CO2.pdf

Briffa KR, Osborn TJ, Schweingruber FH, Harris IC, Jones PD, Shiyatov SG, Vaganov EA, 2001: *Low-frequency temperature variations from a northern tree ring density network.* J Geophys Res Atmos, 106, 2929–2941. https://doi.org/10.1029/2000JD900617

Bond G, 1997: *A Pervasive Millennial-Scale Cycle in North Atlantic Holocene and Glacial Climates*. Science, 278(5341), 1257–1266. DOI: 10.1126/science.278.5341.1257

CERES, 2021: The National Oceanic and Atmospheric Administration (NOAA), *CERES EBAF-TOA Data*: https://ceres-tool.larc.nasa.gov/ord-tool/jsp/EBAFTOA41Selection.jsp

Chen D, Wang H, Sun J, Gao Ya, 2018: *Pacific multi-decadal oscillation modulates the effect of Arctic oscillation and El Niño southern oscillation on the East Asian winter monsoon*. Int J Clim, 38, 2808-2818. https://doi.org/10.1002/joc.5461

Christy JA, 2017: Testimony. U.S. House Committee on Science, Space & Technology. https://docs.house.gov.pdf

Cini Castagnoli G, Bonino G, Serio M, Sonett CP, 1992: *Common spectral features in the 5500-year record of total carbonate in sea sediments and radiocarbon in tree rings*. Radiocarbon, 34(3), 798–805. DOI: https://doi.org/10.1017/S0033822200064109

Connolly R, Soon W, Connolly M, Baliunas S, Berglund, 2021: *How much has the Sun influenced Northern Hemisphere temperature trends? An ongoing debate* . Res Astron Astrophys, 21, 31. https://iopscience.iop.org/article/10.1088/1674-4527/21/6/131/meta

Connor C, 2013: *Statement of Professor Connor.* Ancient forest thaws from melting glacial tomb. https://www.livescience.com/39819-ancient-forest-thaws.html

Crowley TJ, Lowery TS, 2000: *How Warm Was the Medieval Warm Period?* J Hum Environ Stud, 29(1), 51–54. https://doi.org/10.1579/0044-7447-29.1.51

Dansgaard W, Johnsen SJ, Clausen HB, Dahl-Jensen D, Gundestrup N, Hammer CU, Oeschger H, 1984: *North Atlantic climatic oscillations revealed by deep Greenland ice cores.* Geophys Monogr Ser Climate Processes and Climate Sensitivity 29, 288–298. https://doi.org/10.1029/GM029p0288

Dansgaard W, Johnsen SJ, Clausen HB, Dahl-Jensen D, Gundestrup NS, Hammer CU, Hvidberg CS, Steffensen JP, Sveinbjörnsdottir AE, Jouzel J, 1993: *Evidence for general instability of past climate from a 250-kyr ice-core record*. Nature, 364(6434), 218–220. https://doi.org/10.1038/364218a0

Davis WJ, 2017: *The relationship between atmospheric carbon dioxide concentration and global temperature for the last 425 million years*. Climate *5*(4), 76. https://doi.org/10.3390/cli5040076

Davis W, Taylor P, Davis W, 2018: *The Antarctic centennial oscillation: A natural paleoclimate cycle in the southern hemisphere that influences global temperature.* Climate, 6(1), 3. https://doi.org/10.3390/cli6010003

Davis WJ, Taylor PJ, Davis WB, 2019: *The origin and propagation of the Antarctic centennial oscillation. Climate*, 7(9), 112. https://doi.org/10.3390/cli7090112

Driemel A, Augustine J, Behrens K, Colle S, Cox C, et. 2018: *Baseline Surface Radiation Network (BSRN): structure and data description (1992–2017)*. Earth Sys Sci Data, 10(3), 1491-1501. https://doi.org/10.5194/essd-10-1491-2018

Drotos G, Becker T, Mauritsen T, Stevens B, 2020: *Global variability in radiative-convective equilibrium with a slab ocean under a wide range of CO_2 concentrations.* Tellus A: Dyn Meteorol Oceanogr, 72(1), 1–1. https://sci-hub.wf/10.1080/16000870.2019.1699387

Ermakov VJ, Okhlopkov VP, Stozhkov YuI, 2009: *Influence of cosmic rays and cosmic dust on the atmosphere and Earth's climate*. Bull Russ Acad Sci: Phys, 73, 434-436. https://doi.org/10.3103/S1062873809030411

Etminan E, Myhre G, Highwood EJ, Shine KP, 2016: *Radiative forcing of carbon dioxide, methane, and nitrous oxide: A significant revision of methane radiative forcing*. Geophys Res Lett 43:12614-12636. https://doi.org/10.1002/2016GL071930

Feynman J, Fougere PF, 1984: *Eighty-eight-year periodicity in solar-terrestrial phenomena confirmed*. J Geophys Res: Space Phys, 89, 3023–3027. https://doi.org/10.1029/JA089iA05p03023

Fleming RJ, 2018: *An updated review about carbon dioxide and climate change.* Environ Earth Sci, 77(6), 262–. https://link.springer.com/article/10.1007/s12665-018-7438-y

Folland CK, Parker DE, Kates FE, 1984: *Worldwide marine temperature fluctuations 1856–1981*. Nature, 310, 670–673. https://doi.org/10.1038/310670a0

Folland CK, Parker DE, Kates FE, 1986: *Sahel rainfall and worldwide sea temperatures, 1901-85.* Nature, 320, 602-607. https://doi.org/10.1038/320602a0

Friedlingstein P, Jones MW, O'Sullivan M, Robbie MA, Hauck J, et al., 2020: *Global Carbon Budget 2020.* Earth Syst Sci Data 12:3269-3340. https://doi.org/10.5194/essd-12-3269-2020

Gats, 2014: *Spectral calculations tool*, http://www.spectralcalc.com/info/about.php

Gervais F, 2021: *Climate sensitivity and carbon footprint.* Sc Clim Change, 1.1, 70-97. https://scienceofclimatechange.org/wp-content/uploads/Gervais-2021-Climate-Sensitivity-Carbon-Footprints.pdf

Gruber N, Clement D, Carter B, Feely RA, van Heuven S, Hoppema M, Ishii M, Key RM, Kozyr A, Lauvset SK, Lo Monaco C, Mathis JT, Murata A, Olsen A, Perez FF, Sabine, CL, Tanhua T, Wanninkhof R, 2019: *The oceanic sink for anthropogenic CO_2 from 1994 to 2007.* Science, 363(6432), 1193–1199. doi: 10.1126/science.aau5153

Hale GE, 1908: *On the probable existence of a magnetic field in sunspots*. Astrophys J, 28, 315-343. 10.1086/141602

HadCRUT4, 2021: *HaDCRUT4 temperature data of Met Office Hadley Centre.* https://www.metoffice.gov.uk/hadobs/hadcrut4/

Harde H, 2013: *Radiation and heat transfer in the atmosphere: A comprehensive approach on a molecular basis.* Int J Atmos Sci, ID 503727. https://doi.org/10.1155/2013/503727

Harde H, 2017: *Radiation transfer calculations and assessment of global warming by CO2*. Int J Atmos Sci, https://downloads.hindawi.com/archive/2017/9251034.pdf

Harde H, 2022: *How Much CO2 and the Sun Contribute to Global Warming: Comparison of Simulated Temperature Trends with Last Century Observations.* Sc Clim Change, 2.2, 105-133. https://scienceofclimatechange.org/wp-content/uploads/Harde-2022-CO2-Sun-Global-Warming.pdf

Harde H, Salby ML, 2021: What Controls the Atmospheric *CO*2 Level? Sci Clim Change, 1.1, 54-69. https://scienceofclimatechange.org/wp-content/uploads/Harde-and-Salby-2021-What-Controls-CO2.pdf

Hartmann DL, 2015: *Global Physical Climatology,* Elsevier Science, USA. https://www.elsevier.com/books/global-physical-climatology/hartmann

Hauck J, Zeising M, Le Quéré C, Gruber N, Bakker DCE, Bopp L, et al., 2020: *Consistency and challenges in the ocean carbon sink estimate for the global carbon budget*. Front Mar Sci, 7, 852. https://doi.org/10.3389/fmars.2020.571720

HITRAN, 2021: *High-Resolution Transmission Molecular Absorption data base*, Harvard-Smithsonian Center for Astrophysics. https://www.cfa.harvard.edu/hitran/

Hoyt DV, Schatten KH, 1993: *A discussion of plausible solar irradiance variations, 1700-1992.* J Geophys Res, 98(A11), 18895-18906. https://doi.org/10.1029/93JA01944

Hughes AG, Jones TR, Vinther BM, Gkinis V, Stevens CM, Morris V, Vaughn BH, Holme C, Markle BR, Whiter JWC, 2020: *High-frequency climate variability in the Holocene from a coastal-dome ice core in east-central Greenland*. Clim Past, 16, 1369–1386. https://doi.org/10.5194/cp-16-1369-2020

Humlum O, Stordahl K, Solheim J-E, 2013: *The phase relation between atmospheric carbon dioxide and global temperature.* Glob Planet Change, 100, 51–69. https://www.sciencedirect.com/science/article/abs/pii/S0921818112001658?via%3Dihub

Jones PD, Briffa KR, Barnett TP, Tett SFB, 1998: *High-resolution paleoclimatic records for the last millennium: interpretation, integration, and comparison with General Circulation Model control-run temperatures*. Holocene, 8(4), 455–471. https://doi.org/10.1191/095968398667194956

IPCC, 2001: *Climate Change 2001, The Physical Science Basis, TAR*, (eds. Salomon S. et al.). Cambridge Univ. Press, UK. https://www.ipcc.ch/site/assets/uploads/2018/03/WGI_TAR_full_report.pdf

IPCC, 2007: *Climate Change 2007, The Physical Science Basis, AR4*, (eds. Salomon S. et al.). Cambridge Univ. Press, UK. https://www.ipcc.ch/report/ar4/wg1/

IPCC, 2013: *Climate Change 2011, The Physical Science Basis, AR5*, (eds. Salomon S. et al.). Cambridge Univ. Press, UK. https://www.ipcc.ch/site/assets/uploads/2017/09/WG1AR5_Frontmatter_FINAL.pdf

IPCC, 2021: *Climate Change 2021, The Physical Science Basis, AR6*, Cambridge Univ. Press, UK. https://www.ipcc.ch/report/ar6/wg1/

Joos F, Prentice IC, Sitch S, Meyer R, Hooss G, et al., 2001: *Global warming feedbacks on terrestrial carbon uptake under the Intergovernmental Panel on Climate Change (IPCC) Emission Scenarios*, Glob Biogeochem Cycles, 15, J891-908. 10.1029/2000GB001375

Joos F. Roth R, Fuglestvedt JS, Peters GP, Enting IG, 2013: *Carbon dioxide and climate impulse response functions for the computation of greenhouse gas metrics: a multi-model analysis*. Atm Chem Phys, 13(5): 2793–2825. doi:10.5194/acp-13-2793-2013

Kauppinen J, Heinonen JT, Malmi PJ, 2014: *Influence of relative humidity and clouds on the global mean surface temperature.* E&E 25(2). https://doi.org/10.1260/0958-305X.25.2.389

Kerr RA, 2000: *A North Atlantic Climate Pacemaker for the Centuries*. Science, 288,1984-1985. DOI: 10.1126/science.288.5473.1984

Kiehl JT, Trenberth KE, 1997: *Earth's annual global mean energy budget*. Bull Amer Meteor Soc 90: 311-323. https://doi.org/10.1175/1520-0477(1997)078<0197:EAGMEB>2.0.CO;2

Kissin YV, 2015: *A simple alternative model for the estimation of the carbon dioxide effect on the Earth's energy balance*. E&E, 26(8), 1319–1333. https://doi.org/10.1260/0958-305X.26.8.1319

Klyashtorin LB, Borisov V, Lyubushin A, 2009: *Cyclic changes of climate and major commercial stocks of the Barents Sea.* Mar Biol Res, 5, 4-17. https://doi.org/10.1080/17451000802512283

Lean J, 1995: *Construction of solar irradiance since 1610: Implications for climate change*. Geophys Res Lett 22: 3195-3198. https://doi.org/10.1029/95GL03093

Lean J, 2004: *Solar Irradiance Reconstruction,* IGBP PAGES/World Data Center for Paleoclimatology Data Contribution Series # 2004-035, NOAA/NGDC Paleoclimatology Program.

Lean J, 2010: *Cycles and trends in solar irradiance.* WIREs Climate Change 1: 111-122. https://doi.org/10.1002/wcc.18

Levin I, Naegler T, Kromer B, Diehl M, Francey RJ, Gomez-Pelaez AJ, Steele LP, Wagenbach D, Weller R and Worthy DE, 2010: *Observations and modelling of the global distribution and long-term trend of atmospheric* $^{14}CO_2$. Tellus 62B, 26-46. DOI: 10.1111/j.1600-0889.2009.00446.x

Lewis N, Curry JA, 2015: *The implications for climate sensitivity of AR5 forcing and heat uptake estimates.* Clim Dyn, 45(3-4), 1009–1023. https://doi.org/10.1007/s00382-014-2342-y

Li Y, Wu D, Wang T, Chen L, Chenbin Z, 2023: *Late Holocene temperature and precipitation variations in an alpine region of the northeastern Tibetan Plateau and their response to global climate change*. Palaeogeogr Palaeoclimatol Palaeoecol 615(3), 111442. https://doi.org/10.1016/j.palaeo.2023.111442

Lin YC, Fan CY, Damon PE, Wallick EI, 1975: *Long-term modulation of cosmic-ray intensity and solar activity cycles*, 14th International Cosmic Ray Conference, Germany, Munchen, 3, 995–999. Max-Planck-Institut für extraterrestrische Physik, Germany. https://adsabs.harvard.edu/full/1975ICRC....3..995L

Liou KN, 1992: *Radiation and cloud processes in the atmosphere*. Oxford Univ. Press, UK. https://www.osti.gov/biblio/7081459

LLNL, 2016: Lawrence Livermore National Laboratory, *^{14}C "Bomb Pulse" Pulse Forensics*, https://cams.llnl.gov/cams-competencies/forensics/14c-bomb-pulse-forensics

Locean, 2016: *Oceans 13C*, https://www.locean-ipsl.upmc.fr/oceans13c/indexAng.htm

Loeb NG, Johnson GC, Thorsen TJ, Lyman JM, Rose FG, Kato S, 2021: *Satellite and ocean data reveal marked increase in Earth's heating rate*. Geophys Res Lett, 48, e2021GL093047. https://doi.org/10.1029/2021GL093047

Loehle C**,** 2014: *The epistemological status of general circulation models*. Ecol Modell, 276(), 80–84. https://doi.org/10.1007/s00382-017-3717-7

Lungqvist FC, 2010: *A new reconstruction of temperature variability in the extra-tropical Northern Hemisphere during the last two millennia*. Geogr Ann, 92 A 3, 339–351. https://doi.org/10.1111/j.1468-0459.2010.00399.x

Manabe S, Wetherald R, 1967: *Thermal equilibrium of the atmosphere with a given distribution of relative humidity*. J Atmos Sci 24, 241–259. https://doi.org/10.1175/1520-0469(1967)024<0241:TEOTAW>2.0.CO;2

Mann ME, Bradley RS, Hughes MK, 1999: *Northern hemisphere temperatures during the past millennium: Inferences, uncertainties, and limitations.* Geophys Res Lett, 26(6), 759–762. https://doi.org/10.1029/1999GL900070

Marsh ND, Svensmark H, 2000: *Low cloud properties influenced by cosmic rays.* Phys Rev Lett, 85, 5004-5007. https://doi.org/10.1103/PhysRevLett.85.5004

Meinshausen M, Nicholls MRJ, Lewis J, Gidden MJ, Vogel E, et al., 2020: *The shared socioeconomic pathway (SSP) greenhouse gas concentrations and their extensions to 2500*. Geosci Model Dev 13, 3571–3605. https://doi.org/10.5194/gmd-13-3571-2020

Michell JFB, 1989: *The "greenhouse" effect and climate change*. Rev Geophys, 27(1), 115-139. https://doi.org/10.1029/RG027i001p00115

Miskolczi FM, Mlynczak MG, 2004: *The greenhouse effect and the spectral decomposition of the clear-sky terrestrial radiation*. Idöjaras 108, 209-251. http://owww.met.hu/idojaras/IDOJARAS_vol108_No4_01.pdf

Miskolczi FM, 2014: *The greenhouse effect and the infrared radiative structure of the Earth's atmosphere*. Dev Earth Sc 2, the greenhouse effect. https://www.researchgate.net/publication/268507883_The_Greenhouse_Effect_and_the_Infrared_Radiative_Structure_of_the_Earth's_Atmosphere

Myhre G, Highwood EJ, Shine KP, Stordal F, 1998: *New estimates of radiative forcing due to well mixed greenhouse gases*. Geophys. Res. Lett. 25, 2715-2718. https://doi.org/10.1029/98GL01908

Myhre G, Stordal F, Gausemel I, Nielsen CJ, Mathieu E, 2016: *Line-by-line calculation of thermal infrared radiation for global condition: CFC-12 as an example*. J Quant Spectros Radiat Transf 97, 317–331. https://doi.org/10.1016/j.jqsrt.2005.04.015

NOAA, 2021: *NCEP/NCAR Reanalysis Data*. https://www.esrl.noaa.gov/psd/cgi-bin/data/timeseries/timeseries1.pl

NOAA, 2018: *The data: What ^{13}C tells us, the global view 2018.* http://www.esrl.noaa.gov/gmd/outreach/isotopes/c13tellsus.html.

NOAA, 2022: *Atlantic Multidecadal Oscillation AMO (2022).* https://psl.noaa.gov/data/correlation/amon.us.long.data

NSDC, 2020: Six tree-ring proxy data and one temperature data set. https://www1.ncdc.noaa.gov/pub/data/paleo/tree-ring/reconstructions/n_hem_temp/briffa2001jgr3.txt

Ohmura A, 2013: *Physical basis for the temperature-based melt-index method*. J Appl Meteorol 40, 753-761. https://doi.org/10.1175/1520-0450(2001)040<0753:PBFTTB>2.0.CO;2

ONI, 2021: *Oceanic Nino Index (ONI) of NOAA*: https://ggweather.com/enso/oni.htm

Ollila A, 2012: *The roles of greenhouse gases in global warming.* Energy Environ, 23(5), 781-799. https://doi.org/10.1260/0958-305X.23.5.781

Ollila A, 2013: *Dynamics between clear, cloudy and all-sky conditions: cloud forcing effects.* J Chem Biol Phys Sc 4(1), 557-575. https://www.researchgate.net/publication/274958251_Dynamics_between_clear_cloudy_and_all-sky_conditions_Cloud_forcing_effects

Ollila A, 2014: Dev Earth Sci 2, 20-30 *The potency of carbon dioxide (CO_2) as a greenhouse gas.* https://www.researchgate.net/publication/274956207_The_potency_of_carbon_dioxide_CO2_as_a_greenhouse_gas

Ollila A, 2017a: *Warming effect reanalysis of greenhouse gases and clouds*. Phys Sci Int J 13(2), 1-13. DOI: 10.9734/PSIJ/2017/30781. DOI: 10.9734/PSIJ/2017/30781

Ollila A, 2017b: *Semi empirical model of global warming including cosmic forces, greenhouse gases, and volcanic eruptions*. Phy Sci Int J 15(2), 1-14. DOI:10.9734/PSIJ/2017/34187

Ollila A, 2019: *The greenhouse effect definition*. Phy Sci Int J 23(2), 1-5. DOI: 10.9734/PSIJ/2019/v23i230149

Ollila A, 2020a: *The pause end and major temperature impacts during super El Niños are due to shortwave radiation anomalies*. Phys Sc Int J 24(2):1-20. DOI: 10.9734/PSIJ/2020/v24i230174

Ollila A, 2020b: *The Greenhouse effect calculations by an iteration method and the issue of stratospheric cooling*. Phy Sci Int J 24(7), 1-18. DOI: 10.9734/PSIJ/2020/v24i730199

Ollila A, 2020c: *Analysis of the simulation results of three carbon dioxide (CO_2) cycle models.* Phys Sc Int J 23(4),1-19. DOI: 10.9734/PSIJ/2019/v23i430168

Ollila A, 2021: *Global Circulations Models (GCMs) simulate the current temperature only if the shortwave radiation anomaly of 2000s has been omitted*. Phys Sc Int J 40(17), 45-52. DOI:10.9734/CJAST/2021/v40i1731433

Ollila A, Timonen M, 2022a: *Two main temperature periodicities related to planetary and solar activity oscillations*. Int J Clim, https://doi.org/10.1002/joc.7912

Otto A, Otto FEL, Boucher O, Church J, Hegerl G, Forster PM, Gillett NP, Gregory J, Johnson GC, Knotty R, Lewis N, Lohmann U, Marotzke J, Myhre G, Shindell D, Stevens B, Allen MR, 2013: *Energy budget constraints on climate response.* Nat Geosci, 6(6), 415–416. https://doi.org/10.1038/ngeo1836

Quay P, Sonnerup R, Westby T, Stutsman J, McNichol A, 2003: *Changes in the $^{13}C/^{12}C$ of dissolved inorganic carbon in the ocean as a tracer of anthropogenic CO_2 uptake*. Glob Biogeochem 17(1), 4-1-4-20. https://doi.org/10.1029/2001GB001817

Patterson RT, Prokoph A, Changa A, 2004: *Late Holocene sedimentary response to solar and cosmic ray activity influenced climate variability in the NE Pacific*. Sediment Geol, 172 , 67 – 84. https://doi.org/10.1016/j.sedgeo.2004.07.007

Peristykh AN, Damon PE, 2003: *Persistence of the Gleissberg 88-year solar cycle over the last ~12,000 years: Evidence from cosmogenic isotopes*. J Geophys Res: Space Phys, 108 (A1), 1003. https://doi.org/10.1029/2002JA009390

Ramanathan V, Cicerone R, Singh H, Kiehl I, 1985: *Trace gas trends and their potential role in climate change*. J Geophys Res 90, 5547-5566. https://doi.org/10.1029/JD090iD03p05547

Revelle R, Suess HE, 1957: *Carbon dioxide exchange between atmosphere and ocean and the question of an increase of atmospheric CO_2 during the past decades*. Tellus, 9(1), 18–27. https://doi.org/10.1111/j.2153-3490.1957.tb01849.x

Sabine CL, Feely RA, Gruber, Key RM, Lee K, Bullister JL, Wanninkhof R, Wong CS, Wallace DW, Tilbrook B, Millero FJ, Peng TH, Kozyr A, Ono T and Rios AF, 2004: *The oceanic sink for the anthropogenic CO_2*. Science 305, 367–371. DOI: 10.1126/science.1097403

Santer BD, Fyfe JC, Pallotta G, Flato GM, Meehl GA, England MH, Hawkins E, Mann ME, Painter JF, Bonfils C, Cvijanovic I, Mears C, Wentz GJ, Po-Chedley S, Fu Q and Zou C-Z, 2017: *Causes of differences in model and satellite tropospheric warming rates*. Nat Geosci 10, 478-485. https://doi.org/10.1038/ngeo2973

Scafetta N, 2010: Empirical evidence for a celestial origin of the climate oscillations and its implications. J Atmos Sol-Terr Phy 72, 951-970. https://doi.org/10.1016/j.jastp.2010.04.015

Schlesinger ME, 1986: *Equilibrium and transient climatic warming induced by increased atmospheric CO_2*. Clim Dyn, 1(1), 35–51. https://doi.org/10.1007/BF01277045

Schlesinger ME, Ramankutty N, 1994: *An oscillation in the global climate system of period 65-70 years*. Nature, 367, 723-726. https://doi.org/10.1038/367723a0

Schildknecht D, 2020: *Saturation of the infrared absorption by carbon dioxide in the atmosphere*. Int J Modern Phys B. https://arxiv.org/pdf/2004.00708.pdf

Schmidt GA, Ruedy R, Miller RL , Lacis AA, 2010: *Attribution of the present-day total greenhouse effect.* J Geophys. Res. 115, D20106. https://agupubs.onlinelibrary.wiley.com/doi/full/10.1029/2010JD014287

Schwabe SH, 1843: *Sonnenbeobachtungen im Jahre 1843 (in German).* Observations of the Sun in the year 1843. Astronomische Nachrichten 21, 233–236. 10.1002/asna.18440211505

Segalstad TV, 1998: *Carbon cycle modelling and the residence time of natural and anthropogenic atmospheric CO_2: On the construction of "greenhouse effect global warming" dogma. The continuing debate*. European Science and Environmental Forum (ESEF), Cambridge, England. 184-219. https://ww.researchgate.net/publication/237706208.pdf

Shapiro AI, Schmutz W, Rozanov E; Schoell M, Haberreiter M. Shapiro AV, Nyeki S, 2011: *A new approach to the long-term reconstruction of the solar irradiance leads to large historical solar forcing*, A&A, 529, A67, 1-8. https://doi.org/10.1051/0004-6361/201016173

Smith CJ, Kramer RJ, Myhre G et al., 2018: *Understanding rapid adjustments to diverse forcing agents.* Geophys Res Lett, 45, 2023–2031. https://doi.org/10.1029/2018GL079826

Steinhilber F, Abreu JA, Beer J, Brunner I, Christl M, Fischer H, Heikkilä U, Kubik PW, Mann M, McCracken KG, Miller H, Miyahara H, Oerter H, Wilhelms F, 2012: *9,400 years of cosmic radiation and solar activity from ice cores and tree rings.* PNAS, 109(16), 5967–5971. https://www.pnas.org/doi/10.1073/pnas.1118965109

Stine AR, Huybers P, Fung IY, 2009: *Changes in the phase of annual cycle of surface temperature*. Nature, 457, 435-441. https://doi.org/10.1038/nature07675

Srivastava A, Verkouteren M, 2018: *Metrology for stable isotope reference materials: $^{13}C/^{12}C$ and $^{18}O/^{16}O$ isotope ratio value assignment of pure carbon dioxide gas samples on the Vienna PeeDee Belemnite-CO_2 scale using dual-inlet mass spectrometry*. Anal Bioanal Chem 410, 4153–4163. https://doi.org/10.1007/s00216-018-1064-0

Suess HE, 1980: *The radiocarbon record in tree rings of the last 8000 years*. Radiocarbon, 22(2), 200– 209. https://www.cambridge.org/core/journals/radiocarbon/article/radiocarbon-record-in-tree-rings-of-the-last-8000-years/EBD9056098B2151DA8027942C338F514

Trenberth KE, Fasullo JT, 2013: *An apparent hiatus in global warming*? Earth's Future, 1, 19-32. https://doi.org/10.1002/2013EF000165

UAH, 2022: *UAH MSU temperature data set of lower troposphere,* http://vortex.nsstc.uah.edu/data/msu/v6.0beta/tlt/uahncdc_lt_6.0beta5.txt

Utrecht Universiteit, 2016: *Radiocarbon dating*, http://web.science.uu.nl/AMS/radiocarbon.htm

Vedeler M, Jørgensen LB, 2013: *Out of the Norwegian glaciers: Lendbreen – a tunic from the early first millennium AD.* Antiquity 87, 788–801. https://doi.org/10.1017/S0003598X00049462

Velasco Herrera VM, Mendoza B, Velasco Herrera G, 2015: *Reconstruction and prediction of the total solar irradiance: From the Medieval Warm Period to the 21st century.* New Astron*, 34(), 221–233.* https://sci-hub.wf/10.1016/j.newast.2014.07.009

Vinther BM, Jones PD, Briffa KR, Clausen HB, Andersen KK, Dahl-Jensen D, Johnsen SJ, 2010: *Climatic signals in multiple highly resolved stable isotope records from Greenland.* Quat Sci Rev, 29(3-4), 522–538. https://doi.org/10.1016/j.quascirev.2009.11.002

Vinther BM, 2011: *The medieval climate anomaly in Greenland ice core data*. PAGES news, 19(1), 27. Vinther_2011-1_27.pdf

Wijngaarden W and Happer W, 2020: *Dependence of Earth's thermal radiation on five most abundant greenhouse gases*. https://arxiv.org/abs/2006.03098

Wild M, Hakuba MZ, Folini D, Dörig-Ott P, Schär C, Kato S, Long CN, 2019: *The cloud-free global energy balance and inferred cloud radiative effects: an assessment based on direct observations and climate models.* Clim Dyn 52, 4787–4812. https://doi.org/10.1007/s00382-018-4413-y

Zhang Y, Rossow WB, Lacis AA, Oinas V, Mishchenko MI, 2004: *Calculation of radiative fluxes from the surface to top of atmosphere based on ISCCP and other global data sets: Refinements of the radiative transfer model and the input data.* J Geophys Res*,* 109(D19), D19105– https://doi.org/10.1029/2003JD004457

Estimation of e -Time for CO_2 and Revelle Factor

Raimund Müller

Edertal, Germany

OPEN ACCESS

Klimarealistene
P.O.Box 33
3901 Porsgrunn
Norway
ISSN: 2703-9072

Correspondence to mueller.raimund@outlook.com

Vol. 3.3 (2023)
pp. 328-346

Abstract

This study develops a very simple climate model, based on the standard lagging formula. The mathematical function is derived in detail. The main purpose is to estimate the e-time of carbon dioxide in the atmosphere. Many models evaluate the inflow to the atmospheric CO_2 reservoir by rate equations describing the flow from e.g. sea to atmosphere with the weakness that not all parameters describing that flow are well known.

This paper calculates the inflow and outflow to the atmosphere from the best data material that could be obtained. The conclusions are based on data rather than estimated flow parameters. I obtain as a result for each individual year an e-time. The average over 270 years is 3.96 years and it is fairly constant over this time period.

A challenge in the compilation of the annual mass balance of CO_2 in the atmosphere is the unknown amount of additional natural CO_2 emission beyond the 1750 level. I used the amount determined by Skrable, and I add the increased emissions of the oceans due to temperature increase and the massive increase in wood burning to obtain a diagram that corresponds to the measured values of the CO_2 increase.

The conclusion is, that the anthropogenic contribution to atmospheric carbon dioxide in 2020 is only 28.9 ppmv. Including the anthropogenic burning of wood gives a total of 50.5 ppmv. I have estimated the Revelle factor (R) per year over 120 years. With an average value of 1.44, it is significantly lower than the value assumed by the IPCC. Thus, the absorptive capacity of the ocean is significantly higher than assumed in most IPCC models, where they use a Revelle factor (R) greater than 10. Also, the extent of biomass growth can be verified. All necessary data to falsify this are available in extensive databases.

Keywords: e-time τ; Global Carbon Cycle; Biomass respiration; Revelle Factor; Absorption S_{LAND} and S_{OCEAN}.

Submitted 2023-02-06, Accepted 2023-08-14. https://doi.org/10.53234/scc202308/06

1. Introducti

Status quo from the perspective of IPCC AR5 [5] Chapter 6.1.1.1 (p.470fp) Carbon Dioxide and the Global Carbon Cycle:

> "The removal of all the human-emitted CO_2 from the atmosphere by natural processes will take a few hundred to thousand years (high confidence). Based on the amount of CO_2 remaining in the atmosphere after a pulse of emissions (data from Joos et al. 2013 and on the magnitude of the historical and future emissions for each RCP scenario, we assessed that about 15% to 40% of CO_2 emitted until 2100 will remain in the atmosphere longer than 1000 years (Archer and Broukin 2008)."

AR5 Chapter 6.1.1.1 addresses the process of CO_2 accumulation in biochemical cycles:

> "The Human-Caused Perturbation in the Industrial Era CO_2 increased by 40% from 278 ppmv about 1750 to 390.5 ppmv in 2011. Anthropogenic CO_2 emissions to the

> atmosphere between 1750 and 2011 were 555 ± 85 PgC (IPCC). Of these, 375 ± 30 PgC were from fossil fuel combustion and cement production, and 180 ± 80 PgC were from land use change (including deforestation, afforestation, and reforestation). {6.3.1, Table 6.1 p. 486} It is very likely that increases in CO_2 emissions from fossil fuel combustion and those from land use change are the main drivers of the observed increase in atmospheric CO_2 concentration. The deep sea stored 155 ± 30 PgC. Vegetation biomass and soils that were not affected by land-use change stored 160 ± 90 PgC".

According to IPCC AR Chapter 6 Fig 6.1 it is presented that natural emissions have increased significantly since 1750. However, Chapter 6.1.1.1 does not explain that natural respiration has increased by 10.7%, photosynthesis by 13%, ocean absorption by 33% and ocean emissions by 29% between 1750 and 2009. But these very values lead to the interpretation that the anthropogenic share of the increase is only 24% - as noted by Berry[1] and Skrable et al.[3]
The IPCC says in Box 6.1:

> "It is very certain that emissions from fossil fuels and land use change are the main cause of the observed increase in CO_2."

This is a contradiction. I disagree with these assumptions. In particular, the idea that 15% - 40% of anthropogenic CO_2 will remain in the atmosphere for more than 1000 to 10,000 years.

The Bern model does not discriminate between anthropogenic CO_2 or natural CO_2, but the strong buffering described in the Bern model would mean, that all emissions (or increased absorptions) would have a timescale around 1000 to 10,000 years. This is contradicted by the rather rapid variations observed. Especially the rather fast decreases that has occurred in history. The anthropogenic emissions are blamed for the rise in temperature during the industrial age. (IPCC AR6 WGI TS Technical Summary p. 39). These predictions are based on the assumption that there is a strong "buffering" effect in surface sea, where the high value of the Revelle factor significantly blocks absorption of excess CO_2 in the atmosphere. IPCC use Revelle factors $R > 10$. This analysis shows that the Revell factor R is about 1.44 based on IPCC data. However, good agreement between calculations and observations is only a necessary but not a sufficient condition for reliable simulations.

The conflict in the current knowledge: The IPCC uses values of land use change E_{LUC} and fossil fuel emissions E_{FF}, while natural effects E_{NF} are supposed to have remained constant during the last 7000 years. This leads to a new time scale, the adaptation time or response time, which is quite different from the e-time, in which CO_2 molecules are the same - according to the equivalence principle - regardless of whether they result from natural emissions or fossil fuel emissions. It is assumed by IPCC that the climate is static over a period of over 170 years. Therefore, the Bern model is not adequate to describe the carbon cycle. Harde[2] has demonstrated this very well, so there is no need to discuss this further.

Skrable et al. also prove that on the basis of the ^{14}C measurements the anthropogenic share can only be very small. The same applies to the statements of Berry.

Our goal is to determine the e-time and the Revelle factor (R) based on physical principles and exclusively using the available measurement data since 1750. The determination of the correct e-time is a prerequisite for further research on the future development of the CO_2 content of the atmosphere. The Revell factor enhance the outflow of excess carbon from ocean.

This paper assumes, human carbon transferred to the carbon cycle stays in this cycle forever and caused by principle of equivalence we do have only one e-time. Likewise, the atmospheric e-time determined on an annual basis is shown do be almost constant over 270 years and thus provided evidence that no saturation phenomena occurred in the ocean and in the biomass.

This paper uses the following definitions:

- Natural Carbon is carbon from natural processes with E_{NF} emissions before 1750 and E_{DCNF} aditional annual emissions since 1750
- Human Carbon is from burning carbon fuels and producing cement E_{FF}
- Land Carbon is from human-caused land-use change E_{LUC}
- Burned Biomass E_{BMV} caused by human activity not includet in E_{LUC}
- Ocean emissions caused by temperature rise E_{OT}

2. Our proposed model

I consider the total volume of CO_2 in the atmosphere with sources and sinks. I do not distinguish between natural and anthropogenic CO_2 emissions. I calculate with a single e-time. Even though there are different absorption processes with different reaction times, there is a single e-time.

Use of a tank model (Fig. 1):
If a tank has 3 valves at the bottom, each with different mass flow rates, then when all valves are open, the time to empty the tank is essentially determined by the largest valve. The CO_2 molecule will not wait for the turn of the smallest valve, which has the longest residence time. The individual molecules do not have different priorities; the equivalence principle applies. This approach must be based on the total CO_2 mass in the atmosphere. Restricting it to the anthropogenic fraction of the CO_2 content is not reasonable. If one follows this approach, one arrives at significantly different results than the IPCC. The basic assumption of why the IPCC model with biochemically driven time scales up to several 1000 years is not proven, can be explained by a tank model. With a Revelle factor (R) of 10, IPCC obviously is closing valve S_{OCEAN}. The reason that IPCC ends up with a model where the smallest valve determines the time, is their Impulse Response Function (IRF). Their IRF comes from curve fitting of exponential functions to a curve that is not exponential. The exponentials are only curve fitting functions without physical meaning.

CO_2 Flow Diagram in 2020

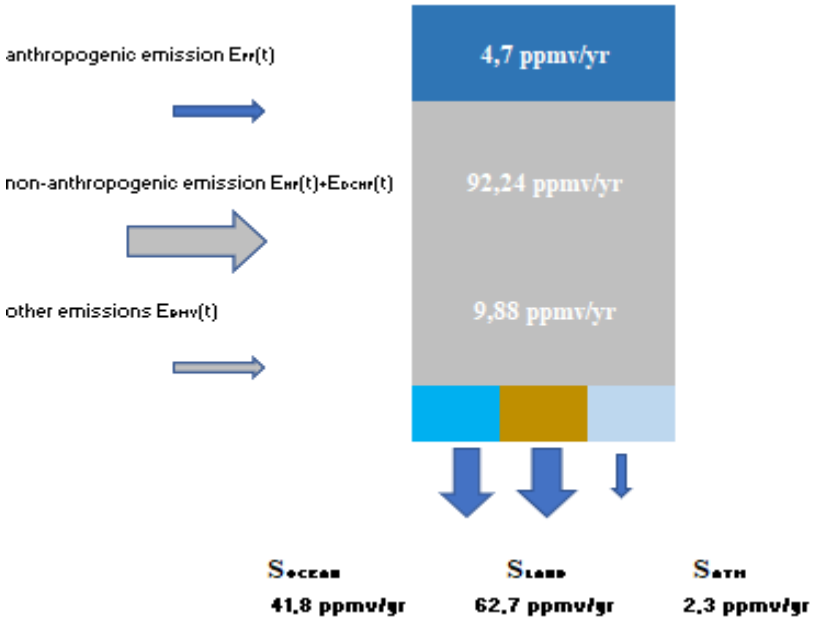

Fig. 1: Explanation of the tank model (Definitions see page 332)

In Fig. 1 emissions are inflow to the atmosphere and the outflow goes to different sources (S). It is the size of the valve that determines the total outflow of the reservoir atmosphere. The largest valve essentially determines (has the main influence on) the time until the reservoir is empty, not the smallest. The e-time τ is an essential measure for the future development of the CO_2 content of the atmosphere.

Therefore, I follow the approach:

- The historical CO_2 content based on natural CO_2 emissions/uptake follows the same physical exchange principle as anthropogenic emissions.
- There is no justification for assuming that pre-industrial emissions are constant.
- There is no justification for assuming that Airborne Fraction is constant.
- Increased CO_2 levels from 280 ppmv to 411 ppmv have been shown to increase biomass by up to 30%, see Huntingford et al.[6] and Tayler et al.[7] This also enhances the seasonal biomass cycle in the northern hemisphere.
- The increased biomass and increased CO_2 partial pressure cause an additional increase in absorption and emission.
- The results of the ^{14}C study (Skrable et al. [3]) were included in the work.
- The residence time τ can be composed of different components.
- Since there was an equilibrium between E_{LAND}+E_{OCEAN} and S_{LAND} + S_{OCEAN} before 1750, I assume that the ocean has increased absorption due to increased CO_2 partial pressure, as assumed by the IPCC in Fig. 6.1.
- The increase in E_{DCNF} (=Emissions additional non fossil, see table 1) was tabulated from Skrable et al.[3].
- The partial pressure of 1 hPas results in a *C* uptake of 3.3t/km²yr on land and 0.9 t/km²yr in the ocean. Takahashi et al.[8]. although there are large uncertainties here (Nsikak et al. [9]
- Biomass burning, which has increased sharply, especially since the 1970s, must be accounted for in the overall CO_2 budget. These are not included in E_{LUC} and E_{NF} (bp statistics[10]).

3. Physical concept to estimate the e-time

3.1 General comment:

There are many definitions of lifetime. The way we define time constants is according to Edwin X. Berry [1]

In our model I use the e-time**.**
e-time = the average time for the level to move (1 - 1/e) of the distance to its balance level. These principles are contained in an equation, the general conservation law (Harde [2]).

3.2 Our model with e-time

Mathematical model is the standard lagging formula, Tahvonen et al.´s equation [21] (which also can be derived from the Bern model formalism) is:

$$\frac{dC}{dt} = \frac{-C}{\tau} + \frac{dEa}{dt} \quad (1)$$

where

C = atmospheric concentration of CO_2, unit: ppmv
τ = e-time , unit: year
Ea = total emission into the atmosphere since starting year (in this paper we have 1750 as starting year) , unit: ppmv
dEa/dt is the change in total emission with time.
dC/dt is the change in atmospheric concentrations.
C/τ is the outflow from the atmosphere and
dEa/dt in this equation is the total influx into the atmosphere – from sea, from land and

from human emissions.

Equation(1) can be derived from basic equations used in the Bern model (Oeschger et.al[14]). The general solution to equation (1) is

$$C(t) = e^{-t/\tau} * \int_0^t e^{u/\tau} * \frac{dEa}{du}\, du + C(0) * e^{-t/\tau} \quad (2)$$

Where *t*=0 in our analysis corresponds to year 1750.

The integral on the right side cannot be solved in a general way. It is thus not possible to write down a closed analytical expression for *C(t)*.
I can obtain the following equation from the general solution (2).

$$C(t) = e^{-\frac{t}{\tau}} * \int_{t-1}^{t} e^{u/\tau} * \frac{dEa}{du}\, du + e^{-1/\tau} * C(t-1) \quad (3)$$

The equation for tau can be derived from the equation above.
If the emission during year t is uniform an equal to $\emptyset(t)$, then $\frac{dEa}{dt} = \emptyset(t)$

Eq. (3) becomes,

$$C(t) = \tau * \emptyset(t) * \left(1 - e^{-1/\tau}\right) + e^{-1/\tau} * C(t-1) \quad (3.5)$$

Since we have an approximate knowledge of τ , as the average time a CO_2 molecule stays in the atmosphere is about 4 years (can be estimated from IPCC data), we can approximate

$$\tau * \left(1 - e^{-1/\tau}\right) \approx 0.88$$

With $\emptyset(t)$ as the emission during year *t* we get the following equation.

$$C(t) = C(t-1) * e^{-\frac{1}{\tau}} + 0.88 * \emptyset(t) \quad (4)$$

Equation (4) is derived from equation (2) and is consequently general.

$$e^{-1/\tau} = \left(C(t) - 0.88 * e\emptyset(t)\right)/C(t-1)$$

$$\tau = 1/\ln\left(C(t-1)/(C(t) - 0.88 * \emptyset(t)\right) \quad (5)$$

Equation (5) is slightly approximative (since we assumed that

$$\tau * \left(1 - e^{-1/\tau}\right) \approx 0.88.$$

The important feature is to use the same approximation for all year.

E(t) is the emission of CO_2 per Year. With different sources of emissions, we define:

$$E(t) = EFF(t) + ENF(t) + EDCNF(t) + ELUC(t) + EOT(t,T) + EBMV(t)$$
$$S(t) = SN(t) + SLAND(t) + SCEMENT(t) + SDCN(t) + SOCEAN(t) + BIM$$

In equilibrium there must be *E(t) = S(t)*
In a simple model further changes in these fluxes are simply disregarded in the total balance.
In the IPCC report in 1750 the CO_2 concentration has been 589 GtC ~ 276.5 ppmV. We use the same starting point.

Table 1: Compilation of used symbols

Symbol	*Quantity*
E_{FF}	Emission fossil fuel
E_{NF}	Emission non fossil year 1750
E_{DCNF}	Emissions additional non fossil (Skrable)
E_{LUC}	Land use change, Forestry, deforestation, Dynamic global vegetation model (DGVM)
E_{OT}	Emissions by ocean temperature increase
E_{BMV}	Emissions by antropogen burning of biomass
S_N	Absorption by gross photosynthesis
S_{LAND}	Absorption by Land
S_{CEMENT}	Cement + process absorptions
S_{DCN}	Absorption by additional biomass
S_{OCEAN}	Absorption by ocean
BIM	Budget imbalance

4. Evaluation of the e-time τ of CO_2 in the atmosphere and τ per year.

The target value for *C(t)* was calculated for each year in an Excel spreadsheet using the known emission data from Global Carbon Budget with the variable Tau. To get the measured *C(t)* line to coincide with the calculated *C(t)* line in the spreadsheet there were two preconditions:
1. the total emission amount must be correct
2. the chosen value of Tau could be adjusted until there was a clear match.

I calculate the e-time by sum of emissions (Example for 2020):
ΣE_i = 226.53 GtC/yr ~ 106.3 ppmv/yr ; *C(2020)* = 414.70 ppmv; *C (2019)* = 411.43ppmv.

$$C(t) = C(t-1) * e^{-\frac{1}{\tau}} + 0.88 * \Sigma Ei(t) \quad (6)$$

follows τ = 4.0 years.

When we calculate *C(t)* using equation (6) for any single year since 1750 the new τ value, by using data from Global Carbon Budget [4], Mauna Loa Observatory MLO[13], pb[10], Scrable at al.[3] and EDGAR[16], I get a perfect match of these data and the calculated CO_2 concentrations between 1750 and 2020, as shown in Fig 2. Using these data (Table 2) in formula (6) for each individual year, we have only one variable in each case, namely τ. The result is shown in Fig. 2 and Table 2. We simulate the increase of CO_2 since 1750.

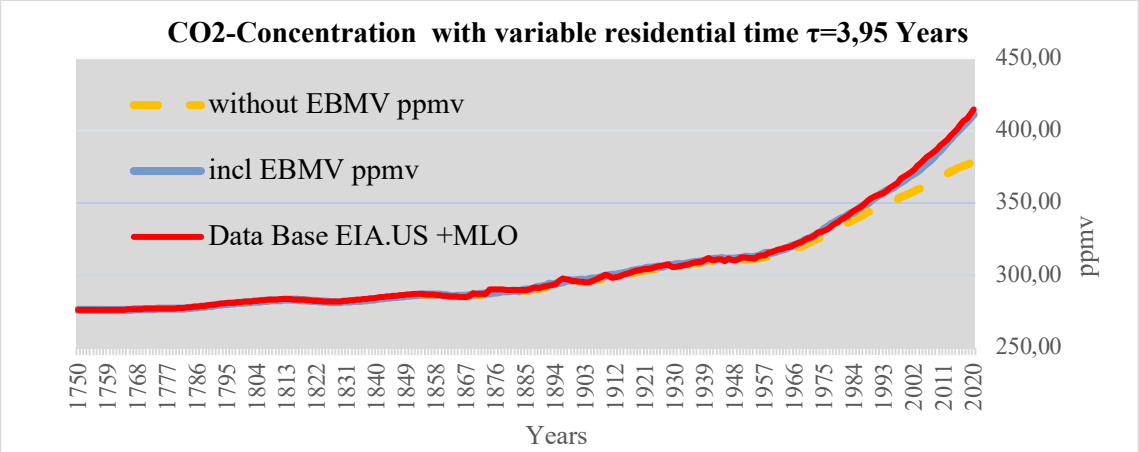

Fig 2: Measured and simulated C(t) The red line represents the database from Mauna Loa[34], EIA[15],

and Skrable[3], the blue one our calculation. The yellow one if we do not consider the biomass burning E_{BMV}. Additionally, the temperature increase is incorporated.

In the same way, it is possible to determine the tau value by means of the same data with formula (5) each year. The result is Fig 3. Analysis of the trend in τ-value on an annual basis shows a decrease since 1970 Fig.3. Further investigation of the causes is needed here. It is expected that the e-time should be constant, and despite the decrease in the data after 1970 the value is fairly constant. The fact that we obtain a rather constant value strongly support that the data used in our analysis are consistent. If the biomass increases the likelihood for being absorbed increase, thus the e-time in the atmosphere decrease if the biomass increase. We obtained with standard deviation the value of 3.92 +/-0.03.

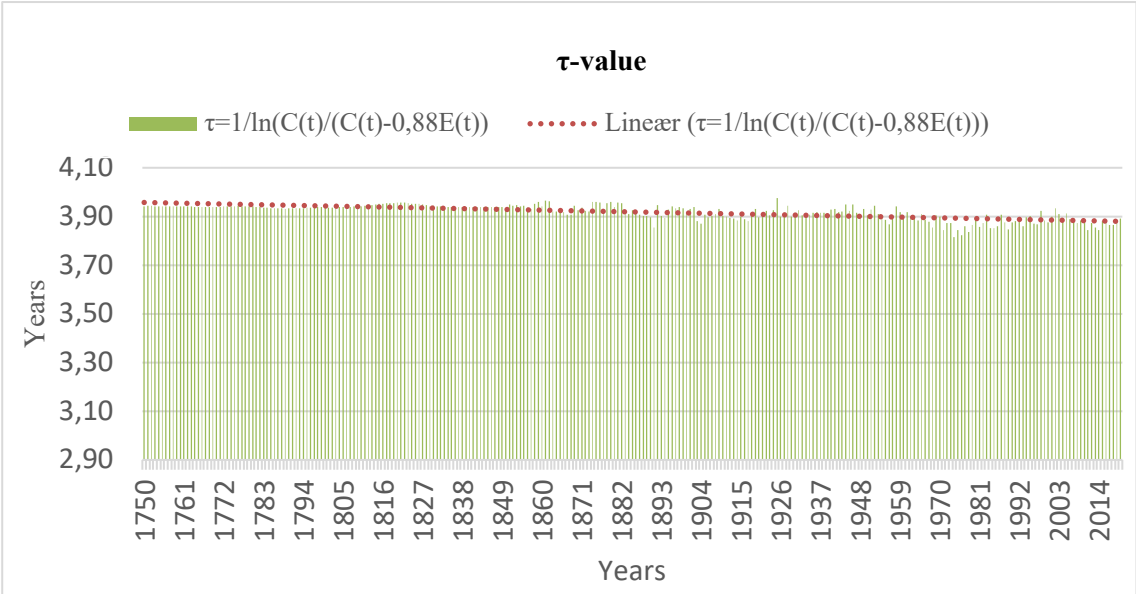

Fig 3: Calculation of τ-value

According to Skrable at al.[3]:
In 1750 was the end of the little ice age. From 1750 *C(t)* increased from 276.44 ppmv to 287.06 ppmv in 1850 due to natural warming. This process did not stop, but increased according to the magnitude of the relation *R* of $^{14}C/\ ^{12}C$ to 359.0 ppmv (without E_{FF}, E_{LUC}, E_{BMV}, S_{OT} see page 341 our Discussions) in 2018. The observed exponential decay of ^{14}C in the atmosphere after the dropping of the atomic bomb gives an e-time of about 9.5 years (calculated by data Table 2a from Skrable). The impact of E_{FF}, E_{LUC}, E_{BMV}, S_{OT} is only 47 ppmv in 2018. This has to be added, Skrable did not implement E_{BMV} and S_{OT}. But in his revision of May 11, 2022 [22], he enlarged E_{DCNF} from 82 to 88. His result is 405.4 ppmv. See Table 2a page 300 in Skrable et al.[3]. This is close to our results, but using a different method.

Table. 2: This is shown in the excerpt from the Excel spreadsheet.

Year	antropogen EFF kum.	Skrable EDCNF kum.	C(1750)= ENF kum	ELUC kum	Temp.cor. SOT	EBMV kum	C(t) incl EBMV	C(t) Measurement
	ppmv	ppmv	ppmv	ppmv	2.4ppmv/K	ppmv	ppmv	EIA.US +SPO+MLO
1750	0	0	276,48	0	0	0	276,48	276,44
2010	15,0677	76,4758	276,48	4,99	2,30	11,20	386,51	389,9
2011	15,4637	77,2816	276,48	5,16	2,51	12,09	388,98	391,65
2012	15,8981	78,0940	276,48	5,63	2,73	13,05	391,89	393,85
2013	16,2926	78,8961	276,48	5,36	2,97	14,11	394,11	396,52
2014	16,6338	79,7057	276,48	5,51	3,24	15,21	396,78	398,65
2015	16,9273	80,4968	276,48	5,77	3,53	16,17	399,37	400,83
2016	17,1510	81,2692	276,48	5,37	3,84	17,18	401,29	404,24
2017	17,3198	82,0223	276,48	5,33	4,18	18,26	403,59	406,55
2018	17,5042	82,7120	276,48	5,59	4,55	19,34	406,18	408,52

5. Calculation of the total balance $E(t) = E_{NF} + E_{DCNF} + E_{FF} + E_{LUC} + E_{BMV} + E_{OT}$

Here I explain the evaluation of the data in the Excel table. Determination of the values using the example of the year 2020. All data were obtained from the sources according to the reference annexes. The determination of these values in sections 5.1a to 5.1d is the prerequisite for the successful determination of tau and the Revelle factor (*R)*.

The finding for year 2020:
Natural emissions E_{NF} released about 150 GtC (1750). E_{NF} was assumed to be constant over 270 years. The additional natural emissions are referred to as E_{DCNF} (Skrable Table 2[3]).

5.1a. Additional non-fossil fuel emissions E_{DCNF} growth according to Skrable et al.[3]

E_{DCNF} is the sum of additional emissions caused by partial pressure increase on ocean surface and biomass respirations due to growth of biomass. I consider here the growth of biomass as shown in Figure 4. Another method would be to use the annual variation of the Mauna Loa Observatory measurements. I explain this in a separate chapter 6.

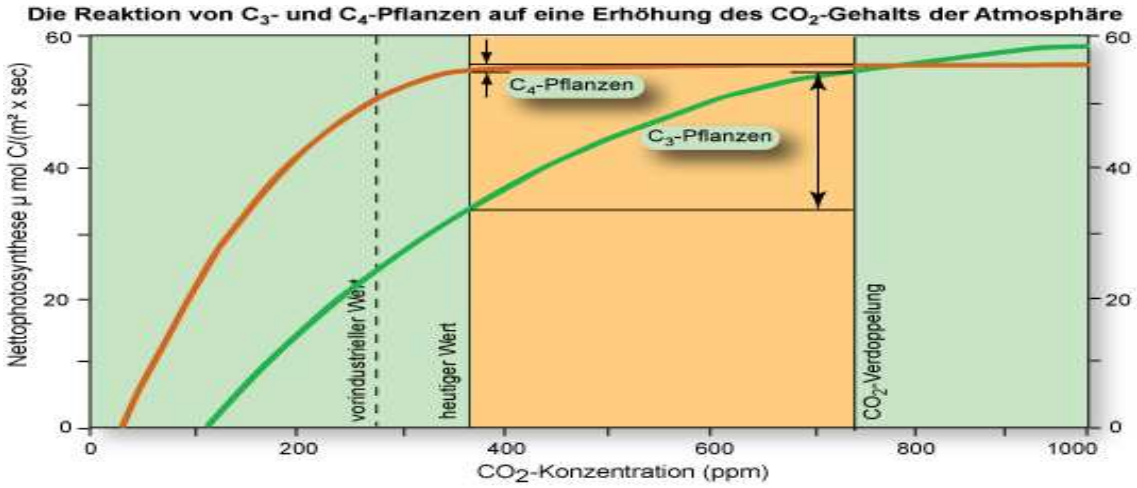

Fig 4: Hamburger Bildungsserver[12]: photosynthesis at higher CO_2 concentrations

According to Fig 4 the increase of C3-plants for 280 ppmv to 400 ppmv is up to 30% , proofed by Taylor et al.[7]
The total increase in 2020 is E_{DCNF} = 47.13 GtC

5.1b E_{FF} in 2020 is 9.5 GtC and E_{LUC} is 2.92 GtC according Global Carbon Budget

5.1c Emission by temperature increase of ocean E_{OT}

The CO_2 emission of the ocean was stable until 1975. With the temperature increase until 2020 there is an increase in CO_2 emission, but we do not get Becks estimations. Increase in sea temperature by 0.8°C see Fig 5:
According to Takahashi [8], the Ocean balance:

$$P(CO2)sw = (pCO2)sw * (To) * exp(0.0433 * (T - To)$$

for 1°C Results 18µatm, for 0.8°C 14.4 µatm
With 1 µatm = 0.9 g/m²yr that is 2.4 ppmv/yr at 1°C For 0.8°C follows
$S_{OT}=E_{OT}(t,T)$=1.905ppmv/yr equal to 4 GtC/yr.

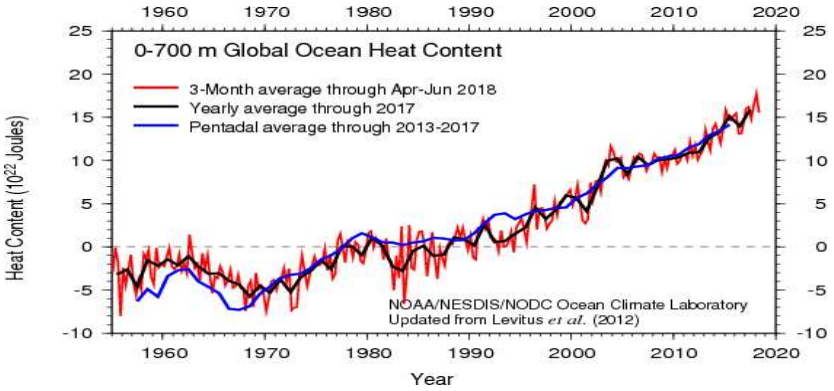

Fig 5: Increase of global ocean heat content [24]

5.1d Emissions from biomass combustion E_{BMV} are 13.9 GtC/yr

CO_2 emissions from biomass burning have increased dramatically, especially since 1970. The data was provided by the bp study [10]. See Fig 6. Until 2000, there is a good agreement without E_{BMV}. Since 2000, the measured CO_2 levels have increased much more. If I add the CO_2 from annual biomass production, from geothermal and biomass according to the bp study [10], we get over 700 TWh in 2019, especially due to the strong increase since 1970 with 27.9 TWh. The calorific value when burning biomass can be converted directly. 1 TWh ~ 0.069 $MtCO_2$. If we do not take this into account in our overall balance, the CO_2 balance does not fit the theory and the measurement. Geothermal and other values can be neglected. They are very small.

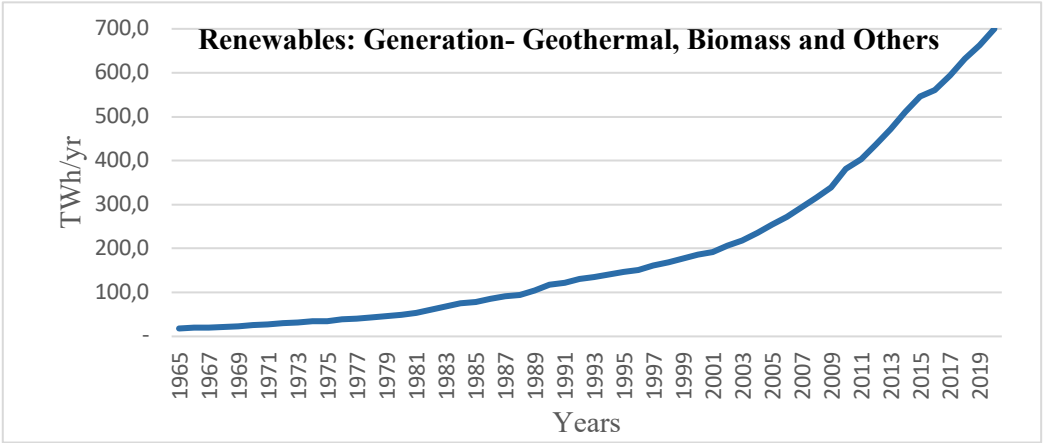

Fig 6: Energy production by Geothermal and Biomass according bp study[10]

Recently, Yatang Cheng et al. [23] from MPIC published a study looking at biomass burning leading to an increase in aerosol particles that enhance cloud cover at low altitudes, causing a decrease in temperature in Asia.

5.2 Summary of individual emissions

We have a total emission of 227.53 GtC/yr in 2020. We can split the absorption of this emission with 39.7% =90 GtC to the ocean and 133 GtC remain for the land+cement. 4.2 GtC =1.98 ppmv remain in the atmosphere. With Formula (5) we receive $\tau = 3.95$ years.

In the calculation, I used the Global Carbon Budget 2021 data[4] for E_{FF} and E_{LUC}. The data for E_{NF} and E_{DCNF} were used from Skrable et al. [3]. The Data for E_{BMV} from bp [10]. Using these data, we obtained an increase in 2020 of E_{DCNF} = 47.13 GtC/yr ~ 21.8 ppmv/yr. E_{FF}+E_{LUC} in 2020 is 12.4 GtC/yr.

Thus, the anthropogenic increase in CO_2 emissions in 2020 is only 5.5% +/- 0.5% of 227 GtC/yr. Summed up since 1750, the anthropogenic share is 23.3ppmv +/- 1.14 ppmv Using the best available data for emissions since 1750, we thus calculate an anthropogenic influence of the increased

CO_2 content of only 17.4% (23.3 ppmv of 135 ppmv). If E_{BMV} should be defined as part of anthropogenic emissions we have different values: 50.5 ppmv +/- 6.4 ppmv.

There is no evidence of constant AF, no evidence that out of the mass flow the emitted, absorbed and remaining amounts are from the same source. The air born fraction makes no sense.

6. The monthly mean CO_2 at Mauna Loa Observatory

Rough estimate:
The annual variations caused by absorption and emission from plants depend on the northern and southern global land area. In the Northern Hemisphere we have 66% of the land mass and of that 25% is desert and ice. This is 70% of the total biologically active land area on Earth. In 2020, a total of 226.8 GtC will be emitted. In the Northern Hemisphere it was 158.8 GtC, an estimated 58% was in winter = 92.1 GtC.

In the Southern Hemisphere it was 68 GtC with 42% in October through March. Total emissions were thus 120.7 GtC in winter and 106.1 GtC in summer. The difference between winter and summer is 14.6 GtC, which is about 6.9 ppmv and corresponds to the measurement at Mauna Loa.

As can be verified in Fig 7 the amplitude in 1958 to 1960 was a 3-year average of 6.0 ppmv. In 2019 to 2021, it averaged 7.1 ppmv, a 19% increase. This is equivalent to the increase in the entire biomass cycle of CO_2 emissions. In the calculation, we had total emissions of 81.3 ppm in 1960 and 106.6ppm in 2020, an increase of 31.1%. 40% of this was emitted from the ocean. So, for the CO_2 biomass cycle, the increase is 18.6%. This fits our rough approximation.

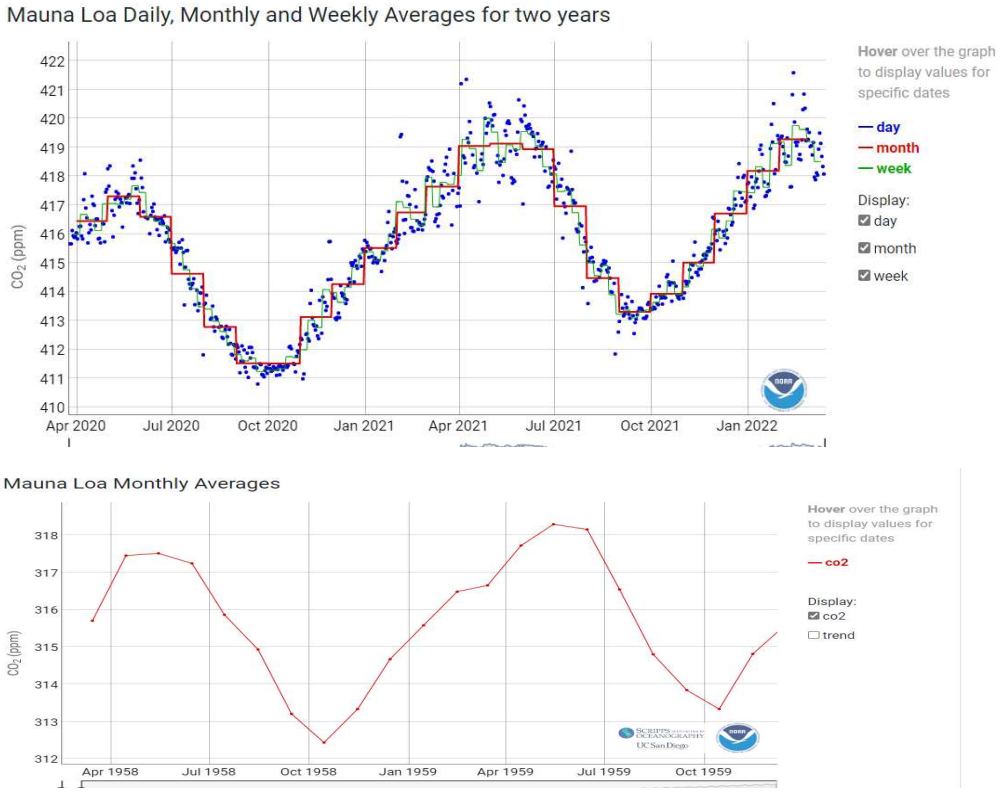

Fig 7: CO_2 values from Mauna Loa in 2021 and 1958[13]

Massen [18] and Beck [17] just showed the difference during the year in the northern latitudes. According to Beck in start of the Year SOY and mid of the Year MOY by sea stations is about 7

ppm and on land stations about 10 ppm during 1985 until 2005. This confirms the influence of biomass. The magnitude of negative MOY gradients of the sea stations remains more or less constant with time (Table 5 in [18]), whereas the latitudinal gradients of land stations change remarkably (trend is - 0.0032 per year) and suggest a rising summertime CO_2 uptake in the more northern regions, possibly due to an ongoing greening of the NH land-masses (Fig. 5 in [18]).

7. The absorption process and the constancy of S_{LAND} and S_{OCEAN}

Henry´s Law states:
C_i = concentration in liquid mol/dm³; P = partial pressure of gas in atm = 102325Pa, and H_{cp} in mol/m³Pa

According to Wikipeda:
*"*Atmospheric chemists often define the Henry solubility as $H_{cp} = c_a/P$. c_a is the concentration of a species in the aqueous phase, and P is the partial pressure of that species in the gas phase under equilibrium conditions. The Henry solubility can also be expressed as the dimensionless ratio between the aqueous-phase concentrations of a species and its gas-phase concentration c_g: $H_{cc} = c_a/c_g$. For an ideal gas, the conversion is: $H_{cc} = H_{cp} * R*T$ with H_{cc} constant of solubility and R the gas constant. C_i is proportional to P and revers proportional to T.*"*

So, we find:

$$Ci = P * Hcc/(R * T) = P/T * Hcc/R$$

and H_{cc}/R is constant. As colder the ocean as larger C_i at constant partial pressure.

1750 we had

$$Ci = 27{,}6\ \text{Pa}/287.5\ \text{K} * Hcc/R = 0.0960 * Hcc/R$$

2020 we had

$$Ci = 42\ \text{Pa}/\ 289.1\text{K} * Hcc/R = 0.1453 * Hcc/R$$

C_i increased about 51%. ((Relation 0.1453 to 0.0960)**.**

7.1 S_{LAND} and S_{OCEAN} in relation to C(t):

The annual absorption of S_{OCEAN} and S_{LAND} seems to be constant in the last 270 years in relation to $C(t)$. Table 3 and Fig 8 confirms there is no saturation in S_{OCEAN} and S_{LAND}.

Table 3: This is shown in the excerpt from the Excel spreadsheet for each single year. The ratio of $E(t)$ - divided into shares of land (61.5%) and Ocean (36.59%) in relation to $C(t)$. $E(t) = E_{NF} + E_{DCNF} + E_{FF} + E_{LUC} + E_{OT} + E_{BMV}$

Year	Sum E(t) in ppmv ENF+EDCNF+EFF+ELUC+EOT+	C(t) Measurement EIA.US +SPO+MLO	61,50% SLAND/c(t) in %	36,65% SOCEAN/c(t) in %
1750	70,4	276,44	15,37%	9,16%
2012	101,9	393,85	15,61%	9,30%
2013	103,0	396,52	15,67%	9,34%
2014	103,7	398,65	15,71%	9,36%
2015	103,5	400,83	15,58%	9,28%
2016	104,3	404,24	15,58%	9,28%
2017	105,3	406,55	15,64%	9,32%
2018	105,8	408,52	15,64%	9,32%
2019	106,2	411,43	15,59%	9,29%

From Table 3, we obtain the diagram Fig 8 for all years.

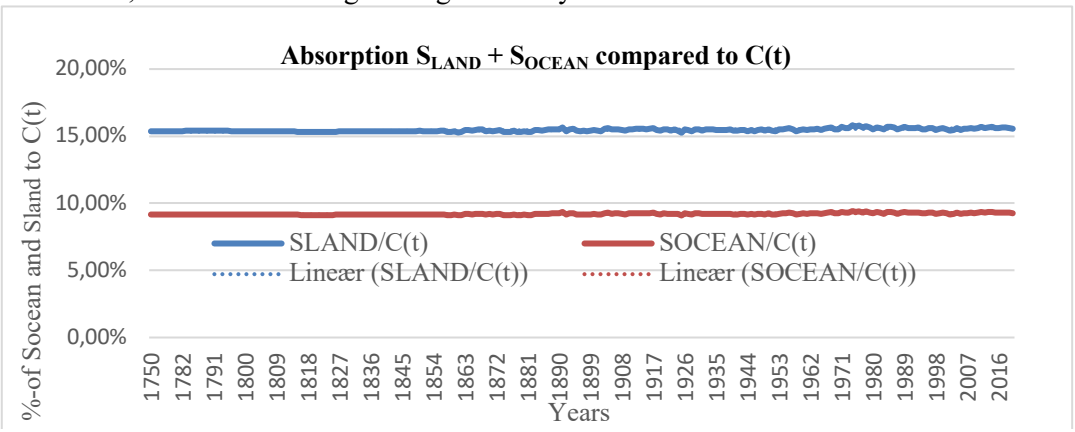

Fig 8: The relative total absorption on ocean and on land stays constant over 270 Years

Absorption by ocean S_{OT}+$S_{\Delta p}$:
In contrast, Nsikak et al. [9] give measured values of 1.84 to 2.96 mol/ m² CO_2/yr. That would be 105.6 t/km²yr!
The North Atlantic does have a very strong CO_2 sink capacity. Measurements from 2005 with CO_2 = 380ppmv shows a very high fluctuation depending on weather conditions and temperature. With high standard deviation there is a significant and consistent undersaturation of the process of absorption.
Our focus: The absorption of CO_2 by Ocean is linear to partial pressure. Between 2011 and 2020 we have 411.7ppmv-391.65ppmv=20.05ppmv. This gives a higher CO_2 emission of 4 GtC/yr (Henry´s Law).
S_{OT} = E_{OT} = see list 5c above = 4 GtC/yr.
The total absorption by Ocean in 2020 is 80.0 GtC +4 GtC +4 GtC = 88.0 GtC/yr = 41.3 ppmv/yr or 39.5% of all absorptions.

8. Estimation of the Revelle factor (*R*) with the Bern Model

In this section I will estimate the Revelle factor based on the Global Carbon Budget data[4]. and values from IPCC AR5 Chapter 6 Fig. 6.1. The analysis will be based on the Box-Diffusion model (BDM) developed by Oeschger[14]. The BDM is also called the Bern Model. Following Oeschger we have a three-box model – the atmosphere, the mixed layer and land. In addition there is the "Deep Sea". The mixed layer is the surface layer of the oceans, and it is assumed that the carbon concentration is uniform within the mixed layer. It is also assumed that the depth of the mixed layer is 75 meters. Carbon is flowing from the atmosphere into the mixed layer. Carbon is transported away from the mixed layer in two ways:

- direct flow from the mixed layer into the atmosphere
- by eddy diffusion from the mixed layer into the Deep Sea

Using the same notations and values as Oeschger et al.[14] (but without division by area which is irrelevant).

$N_i + n_i\,(t)$ = total amount of C in reservoir i
$i = a$ (atmosphere), m (mixed layer), d (deep sea)
N_i is the preindustrial equlibrium value (constant) and
n_i is the deviation from the preindustrial equilibrium
h_m = depth of mixed layer = 75 meters

h_d = depth of deep sea = 3725 meters

k_{am} = exchange rate atmosphere − mixed layer $= \frac{1}{7.53 \text{ years}} = 1/\tau am$

k_{ma} = exchange rate mixed layer − atmosphere $= \frac{1}{9.73 \text{ years}}$ = 1/τma

The effect of the Revelle factor (as defined by Suess and Revelle) is that the outflow from the surface sea to the atmosphere is given by:

$$\emptyset = k_{ma}(N_m + R * n_m) \quad (7)$$

Where

N_m is the preindustrial level of carbon in surface sea
n_m is excess carbon in surface sea
k_{ma} is a rate constant (inverse of the preindustrial residence time)

The Revelle factor enhance the outflow of excess carbon. The background to the Revelle factor is that the effective solubility of CO_2 in sea water is pH dependent. The solubility decreases when the pH decrease. Atmospheric CO_2 increases -> carbon in surface sea increases -> pH decreases -> solubility decreases

$$R = Revell\ factor \approx 10$$

at pre − industrial equilibrium: $k_{am} * N_a = k_{ma} * N_m$ (8)

Comment: $1/k_{am}$ is equivalent to τ between atmosphere and mixed layer. Oeschger et al. used the value 7.53 years. The outflow from the mixed layer into the atmosphere is given by the expression:

$$k_{ma}(N_m + R * n_m) \quad (9)$$

Where $N_m + n_m$ is the total carbon content in the mixed layer. The outflow from the atmosphere into the mixed layer is:

$$k_{am}(N_a + n_a) \quad (10)$$

As can be seen from the above equations, the Revelle factor *R* increases the outflow from the mixed layer faster than the content increases. If for example the carbon content in the mixed layer increases with 10% above equilibrium, $n_m = 0.1 * N_m$, the ouflow increases from the equilibrium $k_{ma} * N_m$ to $k_{ma} * (N_m + R * 0.1 * N_m) = 2 * k_{ma} * N_m$ (using the BDM value *R*=10), which is an 100% increases (doubling).

The outflow is strongly dependent on the concentration (Revelle effect). How much carbon that can be absorbed by the surface sea, without significantly changing pH (and consequently the outflow) is dependent on the absorption volume.

I do not see any significant increase from surface sea to atmosphere in data. At the same time, we know that surface sea has absorbed certain amount of carbon. If the surface sea is only 45 meters it means that it has a rather high additional carbon concentration, but a rather moderate increase in outflow. That leads to a lower *R* value in the data analysis. If surface sea is 90 meters, the concentration increase is only half and there is still room for an amplification.

The Revelle factor can be calculated from the following equations:
If we know the equilibrium flux, $\emptyset_{eq}[ppmv/a] = k_{ma} * N_m$, and we know the additional flux,

$$\emptyset_{add} = k_{ma} * R * \text{nm},$$

then we can calculate the *R*-value from data.

$$R = {}^{\emptyset_{add}}\!/_{\emptyset_{eq}} * {}^{N_m}\!/_{n_m} = \text{ relative flux increase/relative carbon increase in mixed layer}$$

With

$$N_m = 900 \; and \; \emptyset_{eq} = 60.7 \; we \; get \; R = 14.8 * {}^{\emptyset_{add}}\!/_{n_m}$$

(11)

Unfortunately, the values given in the literature and IPCC that are needed to determine the Revelle factor with certainty are all inconsistent or not available. I will therefore estimate the values of the Revelle factor using different parameters from the literature. The percentage of land and ocean in emission and absorption together with the IPCC data are crucial for the value of *R*. Small changes affect large swings.

I assume that the following data from IPCC (Fig 6.1) are correct:

ϕ_{am} = 60 GtC; ϕ_{ma} = 60.7 GtC;
N_m = 900 GtC; N_a = 589 GtC;
n_a = 240 GtC; n_d = 155 GtC;

The data for k_{ma} and k_{ma} from Oeschger cannot be correct.
In the calculation I assume:

1. k_{ma}=14.49 and not 9.73 as given by Oeschger
2. absorption fraction Ocean 1750-2020: 37.6% up to 38.7%
3. emission fraction Ocean 1750-2020: 36.7% up to 40.0%
4. deep sea ϕ_{md} is proportional to ϕ_{am}

Brief procedural description of our considerations for determining ϕ_{add} and n_m:

$$\phi add = \phi ma - \phi eq \tag{12}$$

ϕ_{ma} can be determined from the sum of emissions according to Global Carbon Budget GCB [4] for each year. The proportion of CO_2 emitted by the Ocean is known. It is between 36.7% and 40%. According to IPCC the share in 1750 is 60.7/169 = 35.9% in 2006 it is 39.6%. With this data we do have $\phi_{add.}$

To obtain n_m, we need the *C* uptake of the Ocean. The total absorption ϕ_{am} is the sum of all emissions per year ϕ_{ma} minus the fraction that remained in the atmosphere. According to IPCC 1750, the fraction of the ocean is: 60/169.2 = 35.46%, in 2006 39.4%.

Now the values of the CO_2 absorbed in Deep Sea are missing. With a residence time of 2000 years and a content of 37100 GtC, the following is obtained:

$$\phi md = 37100 \; (1 - EXP(-1/\tau)) = 18.45 \text{ GtC} \tag{13}$$

An annual exchange of 18.45 GtC at equilibrium. This can only be an estimate, since we would actually have to use the diffusion equation. On the other hand, with the method we reach the IPCC value of 155 GtC in 2008, which justifies the estimate. I assume that the value $\phi_{md}(t)$ is proportional to the value $\phi_{am}(t)$. From this, equation (4) can again be used to determine the $C_{deepsea}(t)$. In 2006 we obtain in this way the value of 37255 GtC and are thus in agreement with IPCC Fig 6.1. It follows, there will be about 30% of the absorbed *C* from ϕ_{am} diffusing into Deep sea.

If we now determine $C_{ocean}(t)$ with equation (4) and annually subtract the fraction diffused into Deep sea:

$$C_{OCEAN}(t) = C_{OCEAN}(t\text{-}1)/EXP(1/\tau_m) + \phi_{am} + \phi_{md}(1750) - \phi_{md}(t) \tag{14}$$

we obtain a reasonably correct value for $C_{ocean}(t)$. This procedure then yields

$$nm(t) = Cocean(t) - Nm \tag{15}$$

the annual values. From this follows $n_m(t)$ with which we calculate the Revelle factor R.

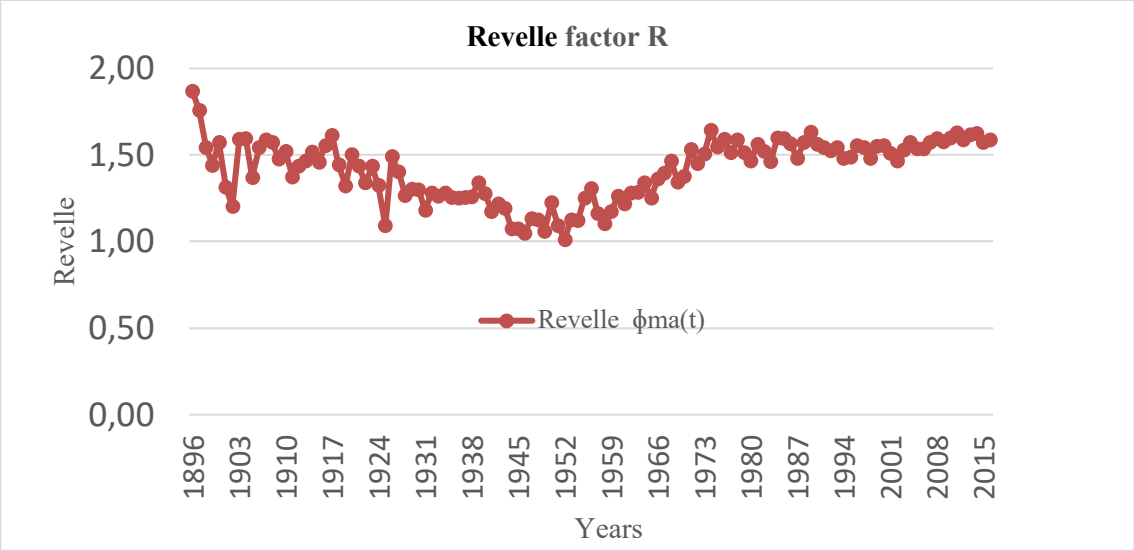

Fig 9: Revelle factor R

The average value with standard deviation is 1.44 +/- 0.2 which proves the high absorption capacity of the ocean.

9. Discussion:

The results can only be as good as the data used, since I did not use freely selectable parameters or make other corrections. I have tried to get the best possible data. In the calculation, I used the Global Carbon Budget 2021 data[4] for E_{FF} and E_{LUC}. The data for E_{NF} and E_{DCNF} were used from Skrable et al. [3]. The Data for E_{BMV} from bp [10].

An essential question is the determination of the biomass. In the reports of IPCC_AR6_WGII as well as IPCC_AR5_WGII, biomass is given as 450 PgC and 450 to 550 PgC, respectively, as constant values since 1750. In contrast, Erb et al. [19] assumes an increase of 100 GtC since 1750, as does Zaichun Thu et al. [20]. He observed a widespread increase of growing season integrated leaf area index (LAI) (greening) over 25% to 50% of the global vegetated area, since 1982 using NASA data. The importance of this question lies in the short e-time. If this is constant, then a 30% increase in photosynthesis means an equal 30% increase in CO_2. At 450 GtC biomass, 30% is 135 GtC. This would correspond to an increase from 280 ppmv to 364 ppmv.
The increase of C_i of 51% must have consequences in the carbon content of the surface ocean. With a stable residence time we have equilibrium between CO_2 content in the atmosphere and the carbon reservoir biomass and ocean. If the carbon content of the atmosphere changes, the carbon content of the biomass and the oceans must change in the same proportion.

My view (today) is that the absolute best way to estimate the effective Revelle factor R is the way I did it. All parameters are in the data (even the ones that we do not know of).

I believe that the calculation of the residence time is simple, straightforward and completely understandable. There is no significant increase in residence time. My understanding is that scientists have observed rather fast increases AND decreases over the last 100´s of years (e.g. Beck). Fast decreases strongly contradict the IPCC model.
What I have newly introduced are the values of Skrable E_{DCNF} for additional natural CO_2 emissions as well as the values of bp-study about the extent of wood burning, which are not included in the E_{LUC}! Without these, at least since 1970, the reconciliation would be difficult. An important

criterion is the data used by Skrable. From the ^{14}C method, it should be expected to obtain a correct additional natural CO_2 emission. However, I had to supplement this via E_{OT} and E_{BMV}. Here, a review of the linearized interpolated data used by Skrable from the very small volume of measured data would be beneficial. The variation of specific activity of 14C *S(0)* in year 1750 in Skrable's paper is 16.33 +/- 2.7 dpm $(gC)^{-1}$. This is +/-16,3%. By using the value of *S(0)* = 14.9, which is only 9% less, it would not be necessary to implement E_{BMV} and E_{OT}. They would be part of E_{DCNF}.

In contrast to this, I have calculated the equation for the CO_2 content of the atmosphere from the data of Global Carbon Budget 2021 using the e-time formula for every single year since 1750 with only one parameter, namely the tau value. This was presented in Fig 3 and compared with the measured CO_2 values contained therein. By iterative procedure the Tau value could be determined in such a way that the graph agrees with the calculated one. The result from this is the tau value of 3.92, while Berry obtains the value 3.5. I was also able to determine the tau value per year since 1750 by means of the measured values and thus confirm its constancy, which Berry assumed as an assumption. With Berry's work it can be confirmed retrospectively that the premises of IPCC Fig 6.1 are correct.

Of course, it would be interesting to obtain the tau values for the individual reservoirs. There is also a need for more research here. Also, the effects of the temperature increase of 3.5K and the calculated increase of the CO_2 content by 100 ppmv (Harde) is very exciting.

If the fixed tau value is a proof that the concentration is proportional to the outflow, then, if *C(t)* of the atmosphere increases the *C* fraction of the biomass must increase in the same measure. In the case of the ocean, the temperature dependence is added. For residence time the direction of the flux does not matter, but for relaxation time, the direction is essential. Moreover, since most natural fluxes are temperature dependent, the absorption of some additional CO_2 above the dynamic equilibrium acts as a pressure dependent process that is essentially temperature independent. So far there is no assumptions on relation between outflow and pressure. If the outflow is proportional to the pressure - then tau will be a constant. The fact that tau is rather constant (using equation 1) is a very strong indication that the outflow in fact is proportional to the pressure.
I do NOT assume that the outflow is proportional to the pressure. It is the other way around. Analysis of the data leads to the conclusion that the outflow is nearly proportional to the pressure (since tau is nearly constant).I show that the outflow is almost proportional to the pressure - I do not assume that.

Indeed, a decreasing tau value shows that the outflow is increasing faster than the pressure. In the Bern model - which is used by the IPCC - emissions in addition to natural emissions are predicted to remain in the atmosphere for a long time. This is because the natural sinks are saturated (due to ocean acidification and limited biomass increase).

In addition, I could confirm that the sinks S_{OCEAN} and S_{LAND} remained constant in relation to *C(t)* over 270 years, i.e. no saturation can have occurred.

9.1 A future task
It is difficult to do a *C* mass balance. The carbon balance in 1750 differs significantly from that in 2020. This should be investigated further, considering the carbon content of soil (1500 GtC) and permafrost (1200 GtC). According to Schrumpf et al. (2011) [25] the carbon emissions from the soil should be 10 times the anthropogenic emissions! This is not included in any carbon balance so far.

Emission and absorption from biomass and ocean are currently about 210 GtC/yr and about 100 ppmv/a, respectively. According to Mauna Loa data, CO_2 concentration varies by 9 ppmv between northern summer and winter. This is equivalent to 9% of total natural emissions. Thus, absorption and emission occur simultaneously across the planet with a variation of 9%.

Anthropogenic emissions are smaller than the natural fluctuation between summer and winter with about 5 ppm. So it makes no sense to consider them as separate superpositions with their own residence time as suggested by the Bern model.

Within the last 10 years we had a certain stagnation with E_{FF} but not with E_{BMV}:

> In 2010 the emissions of E_{FF}+E_{LUC} has been 12.21 GtC. included E_{BMV}: 19.78 GtC*
> In 2020 the emissions of E_{FF}+E_{LUC} has been 12.42 GtC included E_{BMV}: 26.31 GtC*
> In 2010 the absorption of S_{LAND}+S_{OCEAN}+S_{CEMENT} has been 5.71 GtC.
> In 2020 the absorption of S_{LAND}+S_{OCEAN}+S_{CEMENT} has been 6.14 GtC, an increase of almost 0.7%/a. * Data from [4], [10]

Although the emissions E_{FF} stalled, the sinks grew further. The partial atmospheric pressure increased an average of 2 ppmv/yr from 2000-2010, and an average of 2.4 ppmv/yr in 2010-2020. We conclude that any reduction of emissions from 12 GtC/yr to 6 GtC/yr would not change the rate of absorption, the force of absorption caused by partial pressure of CO_2 keeps it constant. There is a constant relation between partial pressure of CO_2 and absorption. Hence there will be no further increase of $C(t)$. At 6 GtC/yr of emissions and 6 GtC/yr of absorption we reach a new equilibrium. Even if E_{FF} emissions remained constant in the last decade, this does not lead to a stagnation of the increase in CO_2 concentration. This is not due to saturation of the sinks. On the contrary, their absorption capacity is steadily increasing. The cause is the very strong increase in emissions of E_{BMV}. This has not been sufficiently considered so far. See Fig 6.

A look into the future: The tau value of 3.92 years makes the CO_2 level hardly exceed the Scenario SSP2-4,5 even if the remaining reserves of 918 GtC of E_{FF} available according to IPCC are burned.

Summary

I was able to determine the e-time, based on Global Carbon Budget [4] and bp [10] data, annually from 1750 to 2020. The result of 3.92 +/- 0.03 years (standard deviation) is relatively constant over 270 years. This is also a requirement for a stable Revelle factor R determined using the Oeschger Box Diffusion Model. It is 1.44 +/- 0.2, which proves the high absorption capacity of the ocean. This also shows the constancy of S_{OCEAN} and S_{LAND} in relation to $C(t)$. Thus, no saturation phenomenon can be detected.

In the context of the CO_2 balance, it was checked how the absorption capacity of the oceans changes due to the increased CO_2 content. The concentration Ci in liquid mol/dm³ from Henry Law increased by 50%. Likewise, the Mauna Loa data and the photosynthesis of the biomass [6], [7], [12] showed that the biomass grew in the same order of magnitude and thus its absorption and emission capacity increased in the same proportion as the CO_2 content of the atmosphere. The value for E_{DCNF} given by Skrable had to be supplemented with the values of E_{BMV} and E_{OT}. Only in this way was it possible to compare the measured $C(t)$ values with those determined on the available data basis. Finally, from these results the conclusion can be drawn that the anthropogenic fraction of the CO_2 content of the atmosphere is 28.9 ppmv (as for Berry), with the inclusion of E_{BMV} it is 50.5 ppmv +/- 6.4 ppmv (as for Skrable).

Funding

This research did not receive any specific grant from funding agencies in the public, commercial, or not-for-profit sectors.

Guest-Editor: Stein Storlie Bergsmark; Reviewers: anonymous

Acknowledgments

I thank Prof. F. Vahrenholt, Jonas Rosén, Ferdinand. Engelbeen and Prof . H. Harde for many helpful discussions when preparing the paper. I also thank the editor as well as the reviewers for critical reading the manuscript and important advices.

References

1. Berry, Edwin X., 2019: *Human CO_2 Emissions Have Little Effect on Atmospheric CO_2*. International Journal of Atmospheric and Oceanic Sciences 3(1): 13-26. https://doi.org/10.53234/scc202301/21

2. Harde, Hermann, 2019: *What Humans Contribute to Atmospheric CO_2: Comparison of Carbon Cycle Models with Observations,* International Journal of Earth Sciences; Vol8 No3: 1-20. https://doi.org/10.11648/j.earth.20190803.13

3. Skrable, Kenneth, et al.: 2022: *World Atmosperic CO_2, its 14C Specific Activity, Non-Fossil Component, Anthropogenic Fossil Component and Emissions (1750 -2018),* Health Physics Society. https://doi.org/10.1097/HP.0000000000001485

4. Global Carbon Budget, 2021, https://www.globalcarbonproject.org/carbonbudget/21/highlights.htm.

5. IPPC AR6 WGI, chapter5.P.6, 2021: Carbon and Other Biogeochemical Cycles — IPCC

6. Huntingford, C., et al., 2017: I*mplications of improved representations of plant respiration in a changing climate*, NATURE COMMUNICATIONS 8. https://rdcu.be/dceT7

7. Taylor, Charles, Schlenker, 2021: *Environmental drivers of agricultural productivity growth: CO2 fertilisation of US field crops*, NATIONAL BUREAU OF ECONOMIC RESEARCH 1050 Massachusetts Avenue Cambridge, MA 02138. Environmental Drivers of Agricultural Productivity Growth: CO_2 Fertilization of US Field Crops | NBER

8. Takahashi et al., 2009: *Climatological mean and decadal change in surface ocean pCO2 and sea-air CO2 flux over the global oceans,* Deep-Sea Res.II. https://www.researchgate.net/publication/313396016

9. Nsikak et al., 2014: *Observed trend of pCO2 and Air-sea CO_2 fluxes in the North Atlantic Ocean*, International Journal of Marine Science, Vol4 No72, 1-7 https://www.researchgate.net/publication/304658632_Observed_trends_of_pCO_2_and_air-sea_CO_2_fluxes_in_the_North_Atlantic_Ocean

10. bp, July 2021: *Statistical Review of World Energy* Statistical Review of World Energy | Energy economics | Home (bp.com)

11. CISRO: iTWire - Rising CO2 level making Earth's deserts bloom: CSIRO study

12. Hamburger Bildungsserver: *Die zentrale Plattform für Lehrende und Lernende.* (hamburg.de)

https://bildungsserver.hamburg.de/resource/blob/265480/01e4f121413e4a2949efa062dd85ca65/2007-vegetation-data.pdf

13. N(t) from the Mauna Loa database, 2022: https://www.esrl.noaa.gov/gmd/ccgg/trends/data.html

14. Oeschger, H., et al., 1975: *A box diffusion model to study the carbon dioxide exchange in nature*, Physics Institute, University of Bern, Switzerland (Manuscript received May 2; revised version July 29, 1974) A box diffusion model to study the carbon dioxide exchange in nature - Tellus A: Dynamic Meteorology and Oceanography (tellusjournals.se)

15. EIA-US Greenhouse gases' effect on climate - U.S. Energy Information Administration (EIA)

16. EDGAR v.5.0 EDGAR - The Emissions Database for Global Atmospheric Research (europa.eu)

17. Beck, Ernst Georg, 2022 :*Reconstruction of Atmospheric CO2 Background Levels since 1826 from Direct Measurements near Ground*; SCC Vol 2.2 (2022) pp. 148-211. https://doi.org/10.53234/scc202112/16

18. Massen, Francis et al. 2022 *Observed Temporal and Spatial CO2 Variations Useful for the Evaluation of Regionally Observed CO2 Data*: SCC Vol 2.3 (2022) pp. 137- 147. Fig 3+4 https://doi.org/10.53234/scc202112/xxx

19. Karl-Heinz Erb et al. 2018 *Unexpectedly large impact of forest management and grazing on global vegetation biomass;* Nature Volume 5563, page 73-76 https://pubmed.ncbi.nlm.nih.gov/29258288/

20. Zaichun Zhu (Chinese Academy of Sciences, Beijing) et al., Nature Climate Change, doi: 10.1038/nclimate3004

21. Tahvonen, OI, von Storch, H & von Storch, J 1993, *'Economic efficiency of CO2 abatement programs'*, Climate Research*, vol. 4, pp. 66-90*. Economic efficiency of CO2 abatement programs — University of Helsinki

22. Skrable revision hp_2022_05_31_skrable_22-00080_sdc1.pdf (lww.com)

23. Yatang Cheng biomass burning south east asia | Max Planck Institute for Chemistry mpic.de)

24. NOAA/NESDIS/NODC Ocean Climate Laboratory Global Ocean Heat Content CDR | National Centers for Environmental Information (NCEI) (noaa.gov)

25. Schrumpf et al. MPI 2011 Unser wichtigster Kohlenstoffspeicher: Wie der Boden als dünne Haut der Erde globale Stoffkreisläufe und das Klima beeinflusst | Max-Planck-Gesellschaft (mpg.de)

OPEN ACCESS

Klimarealistene
P.O. Box 33,
3901 Porsgrunn
Norway
ISSN: 2703-9072

Correspondence:
janesol@online.nol

Vol. 3.3(2023)

pp. 347-352

False Alarm

Book Review

Jan-Erik Solheim

Independent Scientist, Bærum, Norway

Gösta Petterson: False Alarm The Climate Issue from a Scientific Aspect,
Published by Elsa Widding AB, Sweden

Submitted 2023-09-21; Accepted 2023-09-22. https://doi.org/10.53234/scc202310/11

Gösta Petterson is a professor emeritus in biochemistry at Lund University, Sweden. He has used reaction kinetics modeling as tools in his studies of mechanisms of catalysis for central metabolic enzymes, as well as interaction of enzymes in complex biological systems. Several of his studies have dealt with plants' fixation of atmospheric CO_2. He is therefore an expert in one of the most important and controversial questions, the carbon cycle and modeling the human contribution of carbon to the Earth's atmosphere. The book has 298 pages and covers all scientific aspects of the current climate discussion plus how the scientific discussion has become political. One third of the book covers the carbon cycle, the carbon dioxide sources, and the carbon cycle models.

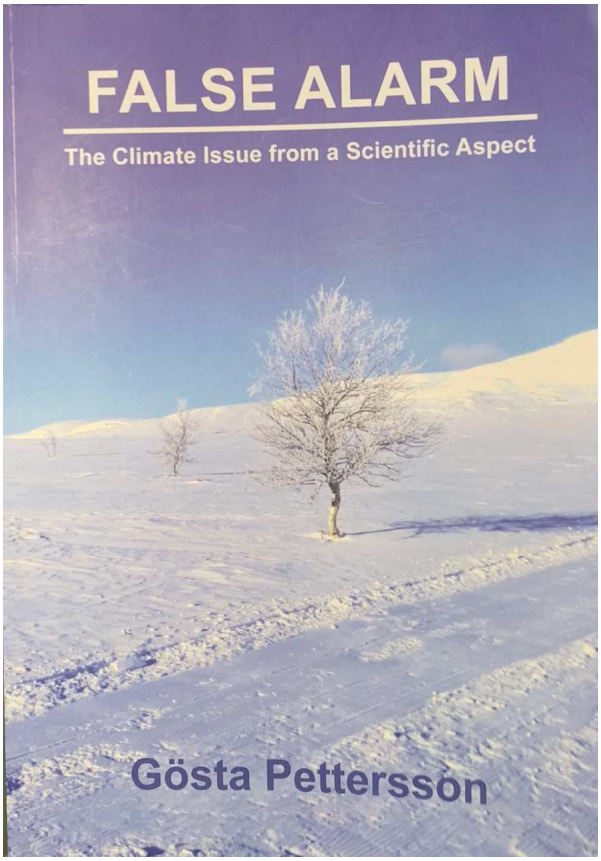

1. The Swedish tiger

The author writes that he learned to read during World War II, and at that time posters with the words "A Swedish tiger" were everywhere. The meaning was that a Swede should be strong but quiet. As a researcher he kept quiet, even when he as an expert in modeling the carbon cycle and nature's uptake of CO_2, discovered that essential parts of the alarmist messages conflicted with experimental findings concerning the relaxation time of atmospheric excesses of CO_2. But he kept quiet. He did not mention this to anybody, at least not in public. *Perhaps I should*, he writes, *when alarmists started using the. Bern model to calculate future atmospheric CO_2 levels"* and he knew how poor the Bern model was for its purpose.

However, as media started feeding us almost daily with alarming messages about a global catastrophe because of our use of fossil fuel referring to consensus between almost all climate scientists, he noticed that scientists from many fields protested. Not only climatologists, but many geologists, chemists, physicists, astronomers, statisticians and mathematicians had different opinions. He then decided to form his own his own opinion about the issue. The result is this book.

He started with the title "False Alarm?". As he became convinced that the current state of knowledge does not provide any reason to be afraid of a catastrophic climate change due to our emissions of greenhouse gases, he removed the question mark. The result is a very sober and straight forward presentation of the scientific aspects of the climate discussions. The book was first published in 2020, and gives a good overview of the climate controversy, without complicated equations. For all topics, he presents both the view of the alarmists and the sceptics. He compare these with the existing scientific evidence. In some cases, they agree, but in most cases they disagree. Usually, Petterson sides with the sceptics, but in some cases, he also finds that the sceptics too are exaggerating.

2. The alarmist message

The book opens with a chapter on how researchers may look at a problem from different angles and arrive at different conclusions, depending on their field and specialty. In the following chapter he describes the alarmist's message, and how this was brought into the political agenda. He accepts that the global temperature has increased during the last hundred years, and how radiative equilibrium leads to different temperatures on the surface of the Earth.

The author explains that the earth is a rocky planet with an atmosphere, and this atmosphere is vital for our climate. The temperature varies with height, completely governed by the earth's gravity, making the top of the atmosphere approximately 33 K colder than average ground temperature. The *gravitational effect* as explanation of a warmer surface, was taught until the 1950'ies. Present days climatologists, however, have abandoned this explanation, in favor of the warming being the result *of the greenhouse effect.* They claim that the Earth is heated by back radiation from an atmosphere heated by infrared emissions from the Earth. In the 1930'ies physicists did experimental studies of absorption in air and concluded that the possible greenhouse effect of CO_2 must be negligible compared with the warming due to water in the oceans or in the atmosphere.

The alarmist message is built on a few separate, independent hypotheses:

- *That a global warming is going on*
- *That the warming is caused primarily by the increase of atmospheric CO_2 content*
- *That the increase in atmospheric CO_2 content is primarily caused by human activities*
- *That the warming caused up to now will continue through the 21st Century and beyond, since CO_2 remains a long time in the atmosphere*
- *That the warming has, or will have, catastrophic consequences*

It is the last hypothesis that determines if one is an alarmist or not. A researcher may support some of the other statements without being an alarmist. But normally an alarmist supports all of them. The message from the alarmists gained support from environmental movements and it was put on the political agenda after a series of international conferences, which ended up with the creation of IPCC in 1988.

The role of the IPCC is to provide policy makers with policy relevant facts relating to anthropogenic climate change. IPCC is described as a non-political organization, with decisions made solely on scientific matters. This is, according to the author, a contradiction, in his definition of politics: *Scientific issues are not determined through decisions, certainly not through decisions made by representatives for national governments*. *I have dedicated my own life to science, and to me it is important that the boundary be kept clear between science and politics. The IPCC reports are contributions to the political debate, not the scientific one. This does not rule out, of course, that the IPCC reports may contain scientifically interesting information.*

He then explains how the IPCC was captured by the alarmists, and how the Rio Declaration opened for faith to replace knowledge for important environmental decisions:

> *In order to protect the environment, the precautionary principle should be widely applied by States according to their capabilities. Where there are threats of serious or irreversible damage on the environment, lack of full scientific certainty should not be used as a reason for postponing cost-effective measures to prevent environmental degradation.*

He then asks: What shall we do if the suggested measure to avert one threat increases another threat? *Myself*, he writes, *I am convinced that biodiversity is far more threatened by CO_2 deficiency than by CO_2 surplus.*

3. The catastrophic scenarios

In this section he explains the dangers the alarmists fear that a global warming will lead to, and how the sceptics argue against this. He respects the activists for expressing their opinion but is strongly against their behavior in scaring people.

He points to the climatologist Stephen Schneider as the driving force in scaremongering, as he cried year after year "*... that we have to offer up scary scenarios."* And the IPCC lead editor John Houghton who wrote a debate article with the title "*Global Warming is now a weapon of mass destruction – It kills more people than terrorism."* Today we are bombarded by tales of scary futures by Greta Thunberg and the UN Secretary General António Guterres.

Gösta Petterson then gives short reviews of the most catastrophic threats presented by the alarmists as heat waves, health effects, desertification, tropical diseases, extinction of plants and animals, acidification of lakes and oceans, floods, storms and hurricanes, extreme weather, melting glaciers, melting polar ice, swallowed coral islands, rising sea level etc. He compares the IPCC reports with the reports from NIPCC[1] and finds that the latter have a more realistic view.

One topic which Al Gore and other politicians have used in their agitation, is the melting of glaciers. Often huge rivers come from glaciers, signaling huge melt-off. He gives an example from the Nigars-glacier in western Norway. This glacier is growing – and it still has a strong river starting from the glacier. The water must be from melting snow accumulated the previous winter, not from the glacier itself. Even if the glacier were gone, the water from last winter snow will supply the river. This is evident in Norway with huge lakes in the high mountains behind moraine ridges created by melted glaciers.

[1] http://climatechangereconsidered.org/

He then presents a short history of the infamous hockey stick graph, which erased the Medieval Warm Period, and then he describes the natural causes for climate change. He shows the phase relation between temperature and CO_2 and concludes this part of the book with thermal outgassing as a most likely source for the increasing CO_2 level.

4. The missing CO_2 source and kinetic carbon cycle models

This topic is covered in three chapters which are the very core of the book. Here he discusses carbon reservoirs, the carbon circulation, and nature's uptake of anthropogenic CO_2 emissions. He shows that the IPCC budget for the 1990's is not in balance. By IPCC, a missing sink of 2.6 GtC/yr is given the name of *residual terrestrial sink* or *hypothetical land sink* (AR4) and *fertilizing effect on land plants* (AR5).

After explaining the basic concepts in reaction kinetics, he shows how a mono-exponential relaxation process can be characterized by its relaxation time (*1/e* -time r or half-life $t_{1/2}$) and concludes that there is at least one non-anthropogenic CO_2 source missing in the carbon cycle budget of the IPCC. He identifies the source as thermal outgassing and arrives at a conclusion that the hydrosphere and biosphere have thermal outgassing at the same time.

He presents a simple model, based on the rapid change in CO_2 in the 1998 El Nino, and the bomb ^{14}C uptake in the hydrosphere and the biosphere, and ends up with 60 % uptake in hydrosphere, 21 % in biosphere and only 19 % of anthropogenic CO_2 remaining in the atmosphere. His relaxation time becomes 14 years, like Olilla (2023), but longer than that of Harde and Salby (2021) and Müller (2023). He writes that the Bern model used by IPCC, assumes that 100 % of the increase of CO_2 since industrialization is due to anthropogenic emissions. Since this is wrong, also the climate models, which all use the Bern model, must be wrong.

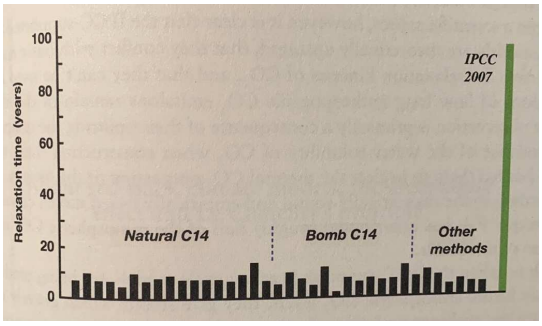

Figure 1. Experimental estimates of the relaxation time of atmospheric CO_2 compared to the approximate relaxation time used by the IPCC based on the Bern model (green bar) (Figure 47 in the book).

5. Some treacherous errors

Gösta Petterson gives many examples of errors in the IPCC arguments. One example is gas diffusion in ice. Since ice core analyses are important for estimates of temperature and CO_2 before the time of thermometers, it is necessary to find out how gas bubbles with trapped CO_2 behave. Petterson writes that he has not found any relevant data for diffusion rates in ice in the literature.

The radiologist and glaciologist Sbigniew Jaworoski has written several papers about what happens in ice. He has found small cracks, large cracks, bubbles of water and even lakes of water in the interior of glaciers. He claims that CO_2 inside glaciers become diluted and averaged over long periods, and this leads to lower values than those in the open air when the snow accumulated.

The Siple (Antarctica) ice core data have been used as a proxy for the pre-Mauna Loa CO_2 data. It was a big surprise when CO_2 data in the Siple ice core dated up to 1890 showed higher values

than Mauna Loa in the 1960'es. Based on the assumption that all rise of CO_2 during industrial time is due to human emissions, this could not be right. It was then assumed that the ice bubbles stayed open in about 80 years before they closed, so the data from 1890 was labelled 1970 – and a 'bandy stick' curve for CO_2 was created. This bandy stick was broken by botanists that presented stomata evidence for higher CO_2 levels both in the Middle Age and in the middle of the 20th century. Petterson also agreed with Ernst-Georg Beck (2010, 2022) that a large number of chemical observations of CO_2 in the 1940'ies showed almost as high level of CO_2 as around 2010. This obviously was the result of thermal outgassing from warmer oceans also observed around 1940. Strong evidence for the 1940 peak, writes Petterson, is that between 1950 and 1960, when the oceans had cooled, the Mauna Loa and Beck's estimates were almost the same.

In the following chapters Petterson discusses the difference between weather, which can be fairly well predicted a few days in advance, and long-time climate prediction based on models, all based on a greenhouse warming effect, which has never been experimentally proved.

Le Chatelier's principle, that nature seems to correct small perturbations, bringing variables back to the equilibrium state, is well known in chemistry. This has given us a stable climate for millions of years, with only the Sun and internal oscillations forcing climate change.

He explains how the Earth's atmosphere got its oxygen from the photosynthesis of CO_2, and how the oxygen became is 21% and will stay at 21% for a long time. The photosynthesis produces carbon for the plants and oxygen for combustion. As long as CO_2 is fossilized and taken out of the cycle, the oxygen level will increase, and the CO_2 level diminish. The level of CO_2 is now so small that there is little left to fossilize. We should be extremely happy that the increased temperature for a short period has increased the CO_2 level from 0.03 to 0.04 %.

In the following sections, we are confronted with the construction of global mean temperatures, based on a highly variable number of stations, dominated by heated-up cities. He explains how temperature anomalies are created and how observed flat temperature trends are 'corrected' to show increasing temperatures towards the end of the last millennium. He claims that large parts of the world like Antarctica, Australia, New Zealand and Russia have neither warmed nor cooled during the 1900s. For the Arctic, the Nordic, and the rural US, the temperature peaked in 1940 followed by a decline until 1970 and then warming to about the same level as in the 1940'ies. A longer temperature series is shown in the trendless temperature graph of Uppsala 1722-2020 below.

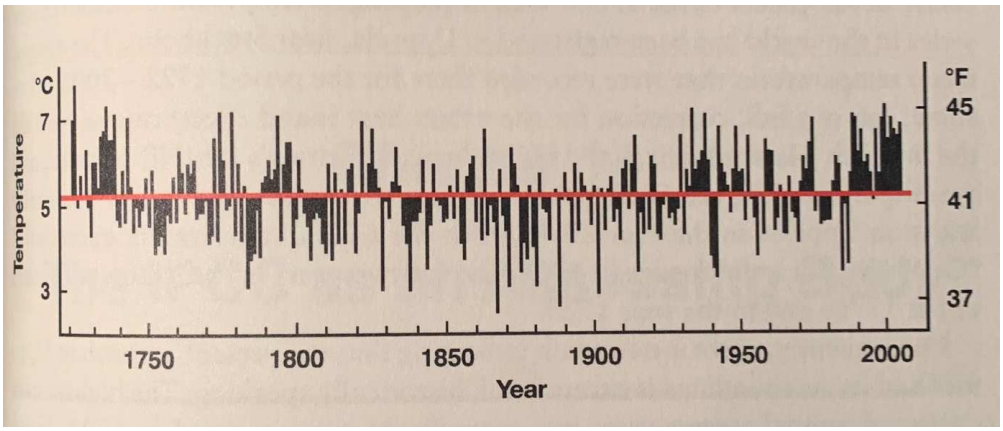

Figure 2. Annual temperatures in Uppsala, Sweden since 1722. A slight urban warming is observed the last years. (Figure 58 in the book)

The final chapters discuss how IPCC as an assessing body, with the aim to produce convincing proof that our use of fossil fuels leads us to catastrophic global warming, has produced lie after lie to hide that the climate behaves in a normal way, only perturbed at a few locations by human activities. The author tells how they allow hypothesis to precede observation, how

counterarguments are overlooked and silenced, and how fake observations or 'corrections' are introduced to bolster the warming narrative. For a long time, the political establishment and media have refused to believe that IPCC is a political body. The Climategate with the leakage of many thousand e-mails from the inner circles of IPCC changed that. The short list of the most well-known e-mails is an interesting reading.

6. Concluding remarks

It has been increasingly clear that IPCC is an agitating body influenced by strong environmental organizations such as WWF and Greenpeace, the Solar and Wind Power lobbies, and by Governments who decide what IPCC has to conclude in their summary reports. The author concludes this way:

Is the debate over? No, the scientific debate never ends. But the bases for the alarmist message is in an advanced state of crumbling to dust, by the collection of knowledge that has been done, and is still being done. Prominent alarmists like Al Gore and James Hansen these days refuse to take part in scientific debates. Alarmists' handbooks nowadays advise their readers not to engage in discussions about the scientific aspects of the climate issue. There is no interest in continued participation in a debate that, on one point after the next has illustrated how scientifically invalid the alarmist message is. They settle for continuing to scare us.

In this book we have learned that a hard-working professor of chemistry has kept silent for years with the errors he discovered in the IPCC treatment of his own special field. He kept quiet, thinking it was not his business. But when he retired, he started a general investigation of all the claims made by climate activists and IPCC. In the beginning it looked like an ordinary scientific discussion, but as he moves closer and closer to the IPCC – he becomes more and more surprised over the errors, cover ups and manipulation of data and people. Today we witness hysterical media and loud speaking politicians, all trying to save the world from a non-existing catastrophe. It is the hope of the author – that this book can bring some rationality into the discussion and save the world from a completely unnecessary policy-made disaster.

At least it has convinced the book reviewer that a journal like Science of Climate Change, with open doors to both sceptics and activists, is a necessity to bring the world back to rational scientific discussion. This is a book worth reading.

Guest-Editor: Stein Storlie Bergsmark.

References

Beck, E.-G., 2010, 2022: *Reconstruction of Atmospheric CO_2 Background Levels since 1826 from Direct Measurements near Ground,* Science of Climate Change, V2.2, 148-211. https://doi.org/10.53234/scc202112/16

Harde, H. and Salby, M., 2021: *What controls the atmospheric CO_2 level*, Science of Climate Change, V1.1, 54-69. https://doi.org/10.53234/scc202106/22

Ollila, A., 2023: *Natural Climate Drivers Dominates in the Current Warming*, Science of Climate Change, V3.3, 290-327. https://doi.org/10.53234/scc202304/03

Müller, R., 2023: *Estimation of e-Time for CO_2 and Revelle Factor*, Science of Climate Change, V3.3, 328-346. https://doi.org/10.53234/scc202308/06